

**Copper and Tin Electrodeposition from Deep
Eutectic Solvents using Pulse Current**

Xiaomeng Su

**Thesis submitted to the University of Strathclyde
for the degree of Doctor of Philosophy**

Department of Chemical and Process Engineering
University of Strathclyde

June 2019

Declaration of Authenticity and Author's Rights

This thesis is the result of the author's original research. It has been composed by the author and has not been previously submitted for examination, which has led to the award of a degree.

The copyright of this thesis belongs to the author under the terms of the United Kingdom Copyright Acts as qualified by University of Strathclyde Regulation 3.50. Due acknowledgement must always be made of the use of any material contained in or derived from this thesis.

Signed:

Date: 21th June, 2019

ABSTRACT

In the past, metal electrodeposition has mainly been performed using aqueous electrolytes. However, such system often suffers from performance limitations and environmental concerns. Deep eutectic solvents (DES) are a type of ionic melt that has recently being proposed for electrodeposition metals and alloys. In addition, most electrodeposition studies are performed using direct current (DC) plating method. However, metal plated using this method often suffers from issues such as poor deposit quality and low Faradaic efficiency, which lead to the adoption of pulse plating method as an alternative. Currently, most studies of metal plating from DES have been carried out using DC plating and there have been relatively few studies of pulse plating. Therefore, the main objective of this study is to investigate aspects of pulse deposition from DES.

Copper and tin were studied in this piece of research. The plating experiments of both metals were conducted in the ethaline-based DES using pulse current. The electrochemical characteristics were studied first, followed by the examination of the effects of pulse parameters on various aspects. Material characterization were also performed.

It was found that copper reduction reaction in ethaline is a two-step single electron transfer process. While acceptable deposits were obtained, the current efficiency for pulse-plated copper was low in many cases. The

occurrence of comproportionation (corrosion) reaction between cupric ions and copper: $\text{CuCl}_4^{2-} + \text{Cu} \rightarrow 2\text{CuCl}_2^-$ was proposed and further tested via independent metal dissolution experiments. Two mathematical models were proposed to explain the relationship between the metal deposition and dissolution effect qualitatively, yet a more complex model needs to be developed to account for the results. Benzotriazole (BTA) was also tested and it was found the corrosion behaviour was suppressed to some extent.

In the study of tin plating, the reduction of Sn^{2+} species takes place in a single two-electron transfer process. Pulse deposition experiments were carried out and the deposits showed high current efficiency with acceptable deposit properties and no corrosion behaviour was observed. However, no direct relationship was found between the deposit properties with the pulse parameters. The grain size ranged between 2.9 μm to 6.2 μm and oxygen was incorporated in some pulse conditions.

In conclusion, this study has shown that it is possible to deposit both copper and tin from DES using pulse plating methods. Corrosion behaviour was observed in copper but not in tin. Collectively, the results showed that combining the technique of pulse plating and the use of DES solution can be a novel way to plate copper and tin. Currently, they do not offer superior advantages in terms of deposit quality and microstructure compared to the conventional methods, and it is clear that further optimisation of the process is required.

ACKNOWLEDGEMENT

I would like to express my deepest gratitude to the following people during this piece of research until completion:

- My primary supervisor Prof. Sudipta Roy for her guidance and support with invaluable advices throughout the research project
- My secondary supervisor Dr. Todd Green for his guidance and support with his invaluable knowledge during my PhD study
- The scholarship offered by the Faculty of Engineering of the University of Strathclyde for providing financial support for the research
- Mr. Jim Murphy, Mr Christopher Jones and all the technical staff in the Department of Chemical and Process Engineering for their assistance in my experiments
- All administration staff at the Department of Chemical and Process for their support and assistance in my study
- Mr. Jim Gallagher in the University of Glasgow with his help and guidance on the SEM and EDX analysis of my samples
- The members of our research group especially Dr. Priscila Estefania Valverde Armas and Dr. Eden May B. Dela Pena for sharing their research experience
- My parents Ying Su and Ji Chen for their financial and emotional supports

- Mr. Zhuge Yan for his invaluable knowledge and experience on the Matlab coding as well as friendship and encouragement
- Mr. Wenhan Cao for his invaluable advice and experience in research as well as friendship.

LIST OF CONTENTS

ABSTRACT	i
ACKNOWLEDGEMENTS	iii
LIST OF FIGURES	x
LIST OF TABLES	xiv
LIST OF SYMBOLS	xv
LIST OF ABBREVIATIONS	xix
Chapter 1. Introduction	1
1.1 Aqueous electrolyte in metal plating industry	2
1.1.1 Copper deposition	2
1.1.2 Tin deposition	6
1.2 Ionic liquids and deep eutectic solvents (DES)	7
1.3 Direct current plating and pulse current plating	10
1.4 Problem statement and importance of this work	11
1.4.1 Electrolyte	11
1.4.2 Plating current	12
1.4.3 Research gap	13
1.5 Project aim and research objectives	14
Reference List	17
Chapter 2. Literature Review	22
2.1 Ionic liquids	22
2.1.1 Traditional ionic liquids	22
2.1.1.1 Haloaluminate-based ionic liquids	22
2.1.1.2 Air and water stable ionic liquids	28
2.1.2 Eutectic based ionic liquids	34
2.1.2.1 Type I eutectics	37

2.1.2.2 Type II eutectics	39
2.1.2.3 Type III eutectics	41
2.1.2.4 Type IV eutectics	44
2.2 Summary of studies of metal electrodeposition from ionic liquids in DC plating	45
2.2.1 Tin	45
2.2.2 Copper	53
2.2.2.1 Haloaluminate-based ionic liquids	53
2.2.2.2 Air and water stable ionic liquids	55
2.2.2.3 Deep eutectic solvent	58
2.3 Summary of studies of metal electrodeposition from aqueous solutions using pulse current	63
2.3.1 Tin	63
2.3.2 Copper	68
Reference List	77
Chapter 3. Fundamentals of Electrochemistry and Electrodeposition	93
3.1 Electrodeposition process	94
3.2 Electrodeposition thermodynamics	96
3.2.1 Nernst equation	96
3.2.2 Plating overpotential	98
3.3 Electrodeposition kinetics	100
3.3.1 Faradaic and capacitive currents	101
3.3.2 Overpotential and Butler-Volmer equation	104
3.3.3 Effect of mass transport limitation in DC plating	106
3.4 Electrodeposition by pulse current	110
3.4.1 Definitions of pulse plating and pulse parameters	110
3.4.1.1 Pulse waveform	111
3.4.1.2 Duty cycle	112
3.4.1.3 Current density	112

3.4.2 Pulse plating kinetics	113
3.4.2.1 Electrical double layer charging and discharging	113
3.4.2.2 Capacitive damping effect of Faradaic current	116
3.4.3 Effect of mass transport limitations on pulse plating	118
3.4.3.1 Concentration profiles and dual diffusion layers	118
3.4.3.2 Maximum plating rate in pulse plating	121
3.5 Nucleation mechanism of metal deposit	123
3.6 Current distribution	125
Reference List	128
Chapter 4. Experimental Procedure	133
4.1 Determination of pulse parameters	133
4.1.1 DC and pulse limiting current densities	133
4.1.2 Electrical double layer capacitive effect	137
4.2 Material preparation	140
4.2.1 Electrolyte formulation	140
4.2.2 Electrode preparation	141
4.3 Electrochemical cell	143
4.4 Metal plating experiments	145
4.5 Metal dissolution experiment	145
4.5.1 Stagnant metal immersion experiment	146
4.5.2 Agitated metal dissolution experiment using RDE	146
4.6 Deposit appearance observation and gravimetric Measurement	147
4.7 Material characterization	148
4.7.1 Scanning electron microscopy (SEM)	148
4.7.2 Energy-dispersive X-ray spectroscopy (EDX)	149
4.8 Microstructural classification	151

Reference List	154
Chapter 5. Results and Discussions: Electrodeposition of Copper and the Investigation of Metal Dissolution Behaviour	156
5.1 Electrochemical study of DES electrolyte	156
5.2 Electrochemical characterization of Cu deposition	162
5.2.1 Visual appearance	163
5.2.2 Faradaic (current) efficiency	163
5.2.3 Potential profiles	166
5.3 Examination of metal dissolution behaviour	170
5.3.1 Metal dissolution under stagnant and agitation condition	170
5.3.2 Further investigation of metal dissolution process	174
5.3.3 Determination of dissolution rate and current density	177
5.3.4 Dissolution potential	179
5.3.5 Examination of solution aging effect	184
5.4 Mathematical model for pulse deposition and dissolution	186
5.4.1 Constant dissolution current density model	189
5.4.2 Varying dissolution current density model	191
5.5 Study of the effect of benzotriazole additive (BTA)	195
5.5.1 Voltammetry of Cu ethaline DES electrolyte with BTA	197
5.5.2 The effect of BTA on Cu pulse electrodeposition in DES	199
5.5.3 The effect of BTA on Cu dissolution in DES electrolyte	202
5.5.4 The effect of BTA on the mathematical model	206
Reference List	211
Chapter 6. Results and Discussions: Electrodeposition of Tin	218
6.1 Electrochemical study of Sn ethaline DES	218

6.1.1 Cyclic voltammetry of Sn ethaline DES	219
6.1.2 Linear sweep voltammetry of Sn ethaline DES	222
6.2 Electrochemical characterization of Sn deposition	224
6.2.1 Visual appearance	225
6.2.2 Faradaic (current) efficiency	226
6.2.3 Potential profiles	227
6.3 Material characterization of Sn deposit	232
6.3.1 SEM analysis	232
6.3.2 EDX analysis	237
Reference List	241
Chapter 7. Conclusions and Future Studies	245
7.1 Conclusions	245
7.2 Future studies	251
Appendix	254

LIST OF FIGURES

Figure 1-1 Schematic phase diagram of eutectic melting point	10
Figure 1-2 Schematic diagram of DC and unipolar PC	11
Figure 2-1 Schematic diagram of formation of [C ₄ py] and [EMIM] chloroaluminate ionic liquids	25
Figure 2-2 Example of discrete ion in the second generation of ionic liquid (from left to right: bis-trifluoromethanesulphonyl, trifluoromethanesulfonate, tetrafluoroborate and hexafluorophosphate)	34
Figure 2-3 Schematic phase diagram of eutectic compounds	35
Figure 2-4 Example of choline chloride (top left) and widely used HBD (urea, ethylene glycol, glycerol)	41
Figure 3-1 Schematic diagram of electrochemical cell in plating process	95
Figure 3-2 Schematic diagram of electrical double layer by Stern model	101
Figure 3-3 Equivalent circuit in the electrodeposition system	102
Figure 3-4 Profiles of Faradaic and capacitive current densities in the galvanostatic DC plating	103
Figure 3-5 Development of concentration profiles and diffusion layer in DC plating	107
Figure 3-6 Schematic diagram of pulse plating sequence: unipolar (left) and bipolar (right)	111
Figure 3-7 Faradaic and capacitive currents profiles in galvanostatic pulse plating	114
Figure 3-8 Damping effect of Faradaic current due to electrical double layer charging (a) small damping effect with $t_{on} > t_c$ and $t_{off} > t_d$ (b) large damping effect with $t_{on} < t_c$ and $t_{off} < t_d$	117
Figure 3-9 Schematic diagram of concentration profiles in pulse plating (a) pulse on-time ($t_1 < t_2 < t_3$) (b) pulse off-time ($t_3 < t_4 < t_5 < t_6$)	120
Figure 3-10 Schematic diagram of nucleation mechanism (a) charge transfer with surface diffusion (b) charge transfer without surface diffusion (c) charge transfer forming a new nucleus	124
Figure 4-1 Virgin cupric ethaline melt DES electrolyte (left) and tin ethaline melt DES electrolyte (right)	141

Figure 4-2 Working electrode (left), counter electrode (middle) and reference electrode (right)	142
Figure 4-3 Working electrode tip holder assembly and components	143
Figure 4-4 Schematic diagram of electrochemical cell in metal electrodeposition experiment	144
Figure 4-5 Schematic diagram of working principle of SEM	150
Figure 4-6 Schematic diagram of working principle of EDX	151
Figure 4-7 Deposit microstructure classification based on steady state and transient mass transfer limitations	152
Figure 5-1 Cyclic voltammetry of ethaline melt containing 0.2 M CuCl ₂ on Pt electrode under 700 rpm RDE rotation speed at 25°C temperature with various scan rates (—) 10 mV/s (—) 20 mV/s (—) 30 mV/s (—) 40 mV/s (—) 50 mV/s	158
Figure 5-2 Linear sweep voltammetry of ethaline melt containing 0.2 M CuCl ₂ on Pt electrode 25°C temperature with 5 mV/s at various RDE rotation speed (—) 300 rpm (—) 500 rpm (—) 700 rpm (—) 900 rpm (—) 1200 rpm	161
Figure 5-3 Results from pulse deposition of Cu in 0.2 M Cu ethaline under various pulse conditions	164
Figure 5-4 Potential profile in single pulse in pulse electrodeposition of Cu with the condition of $t_{on} = 200$ ms and $\theta = 0.5$	167
Figure 5-5 Potential profile of single pulse in pulse plating of Cu, $t_{on} = 200$ ms (—) $\theta = 0.2$ with no Cu coverage (—) $\theta = 0.5$ with partial Cu coverage (—) $\theta = 0.67$ with full Cu coverage	169
Figure 5-6 Appearance of ethaline DES after 410 hours soaking experiment with Cu sheet (left) and steel disc (right)	171
Figure 5-7 Appearance of CuCl ₂ ethaline DES after 410 hours soaking experiment with Cu sheet (left) and steel disc (right)	172
Figure 5-8 Plated Cu deposit on steel substrate before (left) and after (right) 15 minutes dissolution experiment in 0.2 M Cu ethaline under 700 rpm RDE rotation speed	174
Figure 5-9 Relationship between dissolution current density and square root of RDE rotation speed (regression equation $y = 0.81x$ with $R = 0.99$)	180
Figure 5-10 Dissolution potential profiles of Cu substrate under various RDE rotation speeds (—) 300 rpm (—) 500 rpm (—) 700	

rpm (—) 900 rpm (—) 1200 rpm	180
Figure 5-11 Visual appearance of Cu disc before (left) and after the dissolution experiment (right)	181
Figure 5-12 Dissolution potential of Cu disc with varying RDE rotation speeds	182
Figure 5-13 Polarization diagram of 0.2 M CuCl ₂ ethaline DES on Pt electrode under 700 rpm at 25°C	184
Figure 5-14 Dark red precipitate in the aging DES solution (left) and its dissolution in water (right)	185
Figure 5-15 Faradaic efficiency of consistent repeated pulse deposition of Cu under the pulse condition of 10 ms pulse on-time and 0.67 duty cycle	186
Figure 5-16 Relationship of ϵ_f vs $[2(1-\theta)/j_p\theta]$ derived from pulse plating of Cu experiment (•) 10 ms pulse on-time (◐) 50 ms pulse on-time (◑) 100 ms pulse on-time (◒) 200 ms pulse on-time (◓) j_{dis}	190
Figure 5-17 Relationship between dissolution current density and potential derived from the polarization curve (0.2 M CuCl ₂ ethaline DES, 700 rpm RDE rotation speed, Pt electrode)	192
Figure 5-18 Schematic diagram of BTA structure	196
Figure 5-19 CV diagram of 0.2M Cu ethaline containing on Pt electrode under 700 rpm RDE rotation speed (—) No BTA (—) 10 mM BTA	198
Figure 5-20 Appearance of 0.2 M CuCl ₂ ethaline DES and 10 mM BTA after 410 hours soaking experiment with Cu sheet (left) and steel disc (right)	202
Figure 5-21 Dissolution potential with varying RDE rotation speeds in 0.2 M CuCl ₂ ethaline DES electrolyte (•) without BTA (◐) 5 mM BTA (◑) 10 mM BTA	205
Figure 5-22 Polarization diagrams of 0.2 M CuCl ₂ ethaline DES on Pt electrode under 700 rpm at 25°C (—) No BTA (—) 10 mM BTA	206
Figure 5-23 Relationship of ϵ_f vs $[2(1-\theta)/j_p\theta]$ derived from pulse plating of Cu experiment (•) 10 ms pulse on-time (◐) 50 ms pulse on-time (◑) 10 ms pulse on-time with BTA (◒) 100 ms pulse on-time with BTA (◓) j_{dis} (◔) $j_{dis(BTA)}$	207
Figure 6-1 Cyclic voltammetry of 0.1 M SnCl ₂ ethaline melt containing	

on Pt electrode under 700 rpm RDE rotation speed at 25°C temperature with various scan rates (—) 10 mV/s (—) 20 mV/s (—) 30 mV/s (—) 40 mV/s (—) 50 mV/s	220
Figure 6-2 Linear sweep voltammetry of 0.1 M SnCl ₂ ethaline DES electrolyte on Pt electrode 25°C temperature with 5 mV/s at various RDE rotation speed (—) 300 rpm (—) 500 rpm (—) 700 rpm (—) 900 rpm	223
Figure 6-3 Visual appearance and Faradaic efficiency from Sn pulse electrodeposition in 0.1 M SnCl ₂ ethaline DES under various pulse conditions	226
Figure 6-4 Potential profile in a single pulse in pulse electrodeposition of Sn with the pulse condition of $t_{on} = 50$ ms and $\theta = 0.5$	229
Figure 6-5 Potential profiles comparison of Sn deposition with 10 ms t_{on} with (—) $\theta = 0.1$ (—) $\theta = 0.2$ (—) $\theta = 0.5$ (—) $\theta = 0.67$	230
Figure 6-6 Potential profiles comparison of Sn deposition with 0.1 duty cycle θ with (—) $t_{on} = 10$ ms (—) $t_{on} = 50$ ms (—) $t_{on} = 100$ ms	231
Figure 6-7 The microstructure and grain size of Sn deposit from pulse plating and DC plating in 1000x magnification from SEM characterization	233
Figure 6-8 The microstructure of Sn deposit from pulse plating at the edge and centre of substrate under 5000x magnification from SEM characterization	235

LIST OF TABLES

Table 1-1 Summary of electrolytes used in commercial copper plating industry	5
Table 1-2 Summary of electrolytes used in commercial tin plating industry	8
Table 5-1 Faradaic efficiency from pulse deposition of Cu in 0.2 M Cu ethaline DES under various pulse conditions	165
Table 5-2 List of weight change and rate of change of Cu sheet and steel disc in ethaline with and without CuCl ₂	173
Table 5-3 Wagner number of each pulse condition for copper deposition	176
Table 5-4 Dissolution rate and current density with varying RDE rotation speed for Cu disc	179
Table 5-5 List of dissolution current density determined from different approaches	193
Table 5-6 Plating results from pulse deposition of Cu in 0.2 M CuCl ₂ ethaline DES containing 10 mM BTA under various pulse conditions	200
Table 5-7 N_m and N_p values for pulse condition with BTA addition	200
Table 5-8 Faradaic efficiencies from Cu pulse deposition in 0.2 M CuCl ₂ ethaline DES with (black font) and without 10 mM BTA (red font) under various pulse conditions	201
Table 5-9 List of weight change and rate of change of Cu sheet and steel disc in CuCl ₂ ethaline DES with and without BTA	203
Table 5-10 Dissolution rate and current density with varying RDE rotation speeds Cu disc with 5 mM and 10 mM BTA addition	204
Table 5-11 List of dissolution current density determined from different approaches with and without BTA	208
Table 6-1 Elemental composition of Sn deposits characterized by EDX analysis	237

LIST OF SYMBOLS

Latin symbols

a	Thermodynamic activity	--
A	Surface area	cm ²
c	Concentration	mol L ⁻¹
C	Capacitance	Farad, F
D	Diffusion coefficient	cm ² s ⁻¹
E	Electrode potential	Volt, V
F	Faraday constant	Coulomb mol ⁻¹
h	Thickness of metal deposit	cm
i	Current	A
j	Current density	A cm ⁻²
L	Length	cm
m	Mass	g
M	Molar mass	g mol ⁻¹
Q	Charge	Coulomb, C
R	Gas constant	J K ⁻¹ mol ⁻¹
t	Time	s
T	Absolute temperature	K
z	Ionic charge	--

Latin symbols for subscripts and superscripts

a _{ox}	Thermodynamic activity of oxidized species	--
a _{red}	Thermodynamic activity of reduced species	--
c _b	Ion concentration in bulk solution	mol L ⁻¹
c _s	Ion concentration at the electrode surface	mol L ⁻¹
C _{EDL}	Capacitance of electrical double layer	Farad, F
E ⁰	Standard electrode potential	Volt, V

E_{dis}	Dissolution potential	Volt, V
$E_{\text{dis(B)}}$	Dissolution potential with BTA	Volt, V
E_{off}	Potential at the end of pulse off-time	Volt, V
E_r	Reversible electrode potential	Volt, V
j_{anodic}	Anodic current density	A cm ⁻²
j_{av}	Average current density	A cm ⁻²
j_c	Capacitive current density	A cm ⁻²
j_{cathodic}	Cathodic current density	A cm ⁻²
j_{dis}	Dissolution current density	A cm ⁻²
$j_{\text{dis(B)}}$	Dissolution current density with BTA	A cm ⁻²
$j_{\text{dis(c)}}$	Dissolution current density determined by calculation	A cm ⁻²
$j_{\text{dis(cr)}}$	Dissolution current density determined by constant corrosion rate model	A cm ⁻²
$j_{\text{dis(vr)}}$	Dissolution current density determined by varying j_{dis} model	A cm ⁻²
j_f	Faradaic current density	A cm ⁻²
j_{lim}	DC limiting current density	A cm ⁻²
j_o	Exchange current density	A cm ⁻²
j_p	Peak current density	A cm ⁻²
j_{plim}	Pulse limiting current density	A cm ⁻²
L_c	Characteristic length	cm
m_a	Mass measured after dissolution experiment	g
m_{actual}	Actual mass gain in plating process	g
m_b	Mass measured before dissolution experiment	g
m_{dis}	Metal mass loss from dissolution	g
$m_{\text{theoretical}}$	Theoretical mass gain in plating process	g
N_m	Steady state mass transfer limitation number $N_m = j_{\text{av}} / j_{\text{lim}}$	--
N_p	Transient mass transfer limitation number $N_p = j_p / j_{\text{plim}}$	--
Q_{dep}	Deposition charge	Coulomb, C

Q_{dis}	Dissolution charge	Coulomb, C
Q_{EDL}	Charge of electrical double layer	Coulomb, C
r_{dis}	Rate of metal dissolution	g s^{-1}
R_{CT}	Resistance of charge transfer reaction	Ω
R_{Ω}	Resistance of ohmic overpotential	Ω
t^*	Dimensionless time	--
t_{anodic}	Pulse time for anodic current density	s
t_{cathodic}	Pulse time for cathodic current density	s
t_{c}	Electrical double layer charging time	s
t_{d}	Electrical double layer discharging time	s
t_{dep}	Deposition time	s
t_{off}	Pulse off-time	s
t_{on}	Pulse on-time	s
t_{total}	Total pulse time	s
W_{a}	Wagner number	--
Z_{dis}	Ionic charge in dissolution process	--
Z_{p}	Ionic charge in deposition process	--

Greek symbols

α	Charge transfer coefficient	--
δ	Thickness of mass transfer diffusion layer	cm
Δ	Capacitive damping effect	--
ε	Faradaic efficiency	--
η	Overpotential	Volt, V
θ	Pulse duty cycle	--
κ	Specific conductivity	S m^{-1}
ν	Kinematic viscosity	$\text{cm}^2 \text{s}^{-1}$
ρ	Density	g cm^{-3}
ω	Rotation disc electrode rotation speed	rad s^{-1}

Greek symbols for subscripts and superscripts

α_a	Anodic charge transfer coefficient	--
α_c	Cathodic charge transfer coefficient	--
δ_d	Thickness of diffusion layer in DC system	cm
δ_p	Thickness of inner diffusion layer in pulse system	cm
δ_s	Thickness of outer diffusion layer in pulse system	cm
ϵ_d	Deposition efficiency	--
ϵ_f	Observed Faradaic efficiency	--
η_c	Concentration overpotential	Volt, V
η_s	Surface overpotential	Volt, V
η_Ω	Ohmic overpotential	Volt, V

LIST OF ABBREVIATIONS

AFM	Atomic force microscopy
ATF	Trifluoroacetate
BMIM	1-butyl-3-methylimidazolium
BMP	1-butyl-1-methylpyrrolidinium
BTA	Benzotriazole
BuPyCl	N-butylpyridinium chloride
C ₄ mpyrr	N-butyl-N-methylpyrrolidinium
C ₄ py	1-butylpyridinium
ChCl	Choline chloride
ChCl: 2EG	Choline chloride: 2 ethylene glycol
CV	Cyclic voltammetry
DC	Direct current
DCA	Dicyanamide
DES	Deep eutectic solvent
EBSD	Electron backscatter diffraction
EDL	Electrical double layer
EDX	Energy dispersive X-ray spectroscopy
EG	Ethylene glycol
EMIM	1-ethyl-3-methylimidazolium
EtIm	1-ethylimidazole
EtPyBr	N-ethylpyridinium bromide
FAP	Tris(pentafluoroethyl)trifluorophosphate
GE	Gelatine
HBD	Hydrogen bond donor
IL	Ionic liquid
LSV	Linear sweep voltammetry
MeCN	Acetonitrile

NTF	Bistriflamide
OCP	Open circuit potential
OTF	Triflate
PC	Pulse current
PCB	Printed circuit board
PEG	Polyethylene glycol
PhCN	Benzonitrile
PRC	Pulse reverse current
RDE	Rotating disc electrode
SCN	Thiocyanate
SEM	Scanning electron microscopy
SHE	Standard hydrogen electrode
SSP	Sulphopropyl sulphides
STM	Scanning tunnelling microscopy
TCB	Tetracyanoborate
TCM	Tricyanomethide
Tf ₂ N	Bis(trifluoromethylsulfonyl)imide
TMHA	Trimethyl- <i>n</i> -hexylammonium
TOMAC	Tri- <i>n</i> -octylmethylammonium chloride
TU	Thiourea
UV-Vis	Ultraviolet-visible spectroscopy
XRD	X-ray diffraction

Chapter 1. Introduction

Electroplating is a process which enables the formation of metallic film by using electrical current through electrochemical reactions [1]. It allows the surface properties of specific product to be modified for the purpose of corrosion protection, aesthetic improvement, abrasion resistance or mechanical properties enhancement. The technique was first invented by Italian chemist Luigi Valentino Brugnatelli at the beginning of 19 century when he performed gold deposition using voltaic pile. In 1840, metal deposition industry was founded by the Elkington cousins after the first patents in the electroplating domain were awarded to them. The plating processes of other metals, such as Ni, Sn and Zn, were also developed in the following decade. Plating industry achieved significant progress after electric generators were introduced in the late 19th century. Nowadays the technique has been broadly used in various industries such as electronics, sensors, optics, jewellery, automobile and aeroplane manufacturing. Copper and tin are the two types of metals that have been commonly plated worldwide [2].

The choice of electrolyte and type of deposition mode are two important aspects in the plating system. This chapter will firstly describe the traditional aqueous electrolytes applied in the copper and tin electroplating industry, followed by a brief introduction of ionic liquid which is considered as a reasonable candidate to replace the aqueous solution. The difference

between direct current (DC) and pulse current (PC) will be described. Finally the electroplating issues, current research gap and project objectives of this piece of research would be mentioned.

1.1 Aqueous electrolyte in metal plating industry

1.1.1 Copper deposition

Copper is a sort of ductile and malleable reddish metal with a high electrical and thermal conductivity [3]. It was extracted and used since the advent of human civilization [4]. Now the electroplated copper has been widely used in electroforming, electrorefining, automotive industry, plastics and printed circuit boards [5]. There are four types of aqueous electrolyte used for commercial purpose: acid, cyanide, alkaline and pyrophosphate ions systems.

The acid electrolyte solution was first referred in copper deposition in 1810 [6]. Decades later it was used in the commercial copper electroplating process. A number of acid copper plating system such as copper fluoborate, sulphate, nitrate and chloride have been developed and evaluated [2]. Currently only acid copper sulphate electrolyte is widely used. Although copper fluoborate has a higher solubility and can plate copper at a higher current density compared to sulphate system, the fluoborate is very expensive and its price is nearly double to sulphate. Sulphate solution is cheap, easy to

control and could produce high purity copper. Copper plated from acid solution is mainly used in electroplating, electroforming and electrorefining. It is also widely used in printed wiring boards and semiconductor wafers. Additive agents such as benzotriazole and some organic compounds are needed in the acid copper plating to improve the deposit morphology [7, 8].

The introduction of copper cyanide solution was in 1915 [2]. It was applied successfully in commercial copper plating in 1938 and mainly used in automotive industry in the following years. Cyanide electrolyte offers high deposition rate and achieves smooth and bright deposits. Additives containing metalloids and organic compounds such as saccharin and unsaturated alcohols are necessary during the plating process. The biggest issue of such electrolyte is the toxicity, which can pose a serious environmental hazard. Site contamination is also a serious safety concern to the workers. Moreover, waste treatment is much more expensive and the process is complicated.

The third type of electrolyte used in copper plating industry is alkaline solution [2]. It was developed to replace the cyanide electrolyte due to the environmental issue and high disposal cost in the mid-1980s. The alkaline solution has a high plating rate, high throwing power and much safer to work with [9]. The drawbacks of such electrolytes are high operating cost and they are very susceptible to impurities.

Pyrophosphate solution was discovered by Roseleur in 1847 and the commercial use was in 1941 [10]. Copper plated by pyrophosphate electrolyte

was extensively used in the production of waveguides, heat exchangers, toy making molds, helical antennae and paint spray masks [2]. Except for the main component copper pyrophosphate ($\text{Cu}_2\text{P}_2\text{O}_7 \cdot 3\text{H}_2\text{O}$), nitrate, ammonia and sodium salt ($\text{Na}_4\text{P}_2\text{O}_7$) are also present in the electrolyte to improve deposit quality. Organic additives such as pyrimidines and glycol could refine the grain structure. Some chlorides and alkaline metals are used as brighteners for thick copper deposition in electroforming industry. However, pyrophosphate solution is much more expensive than those acid electrolytes. A brief summary of the electrolytes used in copper plating industry are listed in Table 1-1.

Apart from electroplating, vapour deposition process is also used in Cu fabrication. Metal film can be deposited on the substrate either from condensation of vapour (physically) or using volatile precursors (chemically) [11]. This method is named as dry process as it was performed in vacuum. However, this technique can cause a variety of deposit contaminations [12]. The operation cost is very high since vacuum or inert condition must be maintained throughout the coating process, which leads to high power consumption.

In addition, Cu can also be plated by using electroless deposition process, where no external electrical current is applied. Metal reduction reaction is initiated with the presence of catalyst. However, one of the issues with this technique is the operating condition to initiate the reaction. For instance, high temperature is required for Ni electrodeposition. Moreover, the

deposition microstructure is difficult to be controlled therefore the desired deposit property is difficult to achieve.

	Acid	Cyanide	Alkaline	Pyrophosphate
Main Components	copper sulphate (fluoborate), sulphuric (fluoboric) acid, chloride (boric acid)	Copper cyanide, sodium (potassium) cyanide, sodium carbonate	sodium hydroxide, copper sulphate, sodium carbonate	Copper pyrophosphate, potassium (sodium) phosphate, nitrate, ammonia
Additives	benzotriazole, cadmium, cobalt, gulac	Selenium, lead, saccharin, unsaturated alcohols	-	Pyrimidines, glycerol, sodium sulphite, potassium bromide, lead, citric
Usage	Electroforming, electrorefining, electroplating, printed circuit boards	Surface improvement in soldering, undercoat for other deposits, decoration	Heat treat masking barrier	Heat exchangers, toy making mods, waveguides, paint spray masks
Property	Cheap, process easy to control, high purity plating	High rate of deposition, can achieve bright and smooth deposit, toxic and high disposal cost	High plating rate, high throwing power, high operation cost, sensitive to impurities	Good mechanical copper deposit, very expensive electrolyte Low stress

Table 1-1 Summary of electrolytes used in commercial copper plating industry

1.1.2 Tin deposition

Tin is a ductile, malleable and soft silver-white metal. The extraction and use of Sn can be traced back to 3000 B.C. Nowadays the plated tin has a number of applications. It plays a vital role in the production of printed circuit boards and microelectronics components [14]. Tin is also used in automotive industry to improve the corrosion resistance. Jewellery industry uses tin for coating to reduce the cost. In addition, tin is considered as good anode material in the rechargeable lithium ion battery. There are two primary baths in the commercial tin plating: acid and alkaline. The choice of electrolyte depends on the applications.

The alkaline solution used for tin plating was introduced by Wernlund and Oplinges in 1933 [15]. The bath contains either sodium or potassium stannate (Sn^{4+}) and hydroxide. It offers high throwing power and achieves quality deposit. Potassium stannate solution has a higher plating rate, conductivity and salt solubility compared to sodium stannate, but the operation cost is also higher. Tin deposit plated by alkaline bath generally has a finer grain microstructure without any additive agents. However, the alkaline plating system has a higher power consumption and slower plating rate than the acidic electrolyte.

There are three types of acidic solution commercially available in tin electrodeposition: sulphate, fluoborate and halogen [15]. In the acid solution tin ions are in divalent status (Sn^{2+}) rather than tetravalent (Sn^{4+}) in the

alkaline electrolyte. In the sulphate system, additive agents are essential to prevent tin oxidation, minimize the dendritic growth of deposit or achieve specific grain microstructure. For instance, cresol is added into sulphate bath as an antioxidant in plating process. Animal glue and gelatin are used to improve the deposit quality. The main issue for sulphate system is the precise control of the amount of additive.

Fluoborate salt has higher solubility in water so tin can be deposited in a faster rate with excellent throwing power under high current density [15]. Similar to sulphate bath, additive agents such as β -naphthol and gelatin are also necessary if a satisfactory deposit quality to be achieved.

Tin plated by halogen bath shows a very smooth grain structure [12]. The solution also offers high conductivity and deposition rate. It was developed in the electroplating process of steel strips. The halogen bath is mainly composed of stannous chloride or fluoride. Inhibitors are needed to suppress tin oxidation under atmospheric condition. The summary of various baths used in tin plating industry is listed in Table 1-2.

1.2 Ionic liquids and deep eutectic solvents (DES)

The ionic liquid is a type of fluid which is generally in a liquid state below 100°C. The solvent is composed of only cations and anions and has a low melting point due to its low lattice energy [16]. The first advent of ionic

	Alkaline	Sulphate	Fluoborate	Halogen
Main Components	Potassium (sodium) stannate, hydroxide	Stannous sulphate	Stannous fluoborate	Stannous chloride (fluoride)
Additives	-	Cresol, gelatin, animal glue, β -naphthol	β -naphthol, gelatin	Gelatin, polyalkylene oxide
Usage	-	Barrel plating	Barrel plating	Electroplating process of steel strips
Property	Fine grain deposit structure, high power consumption, slow plating speed	Smooth grain structure, high conductivity and moderate plating speed, hard to control the additive amount	Fine – grained and smooth grain structure, high conductivity and high deposition rate,	Smooth grain structure, high conductivity and high deposition rate

Table 1-2 Summary of electrolytes used in commercial tin plating industry

liquids was in 1888 when S. Gabriel and J. Weiner discovered ethanalammonium nitrate, which has a melting point of 52°C to 55°C [17]. Ethylammonium nitrate, which has a melting point of 12°C, was reported as the earliest room temperature ionic liquid by P. Walden in 1914 [18]. A series of ionic liquids, which contain imidazolium and pyridinium cations combined with halides and $AlCl_4^-$ ion, were developed during 1970s by Osteryoung and Hussey research groups [19, 20]. The research on ionic liquid has become more intensive since the potential of such new solvents was realized [21].

Ionic liquid offers a number of promising properties such as wide potential windows, high solubilities of metal salts and high conductivities. The application of ionic liquids includes super capacitors, batteries, gas storage and cleaning agents.

By convention, there are two types of ionic liquid. The first generation of ionic liquids primarily describes the chloroaluminate or chlorozincate based eutectics. The ionic mixtures containing discrete anions are considered as the second generation of ionic liquids. Deep eutectic solvents (DES) form a new class of ionic liquid [21]. This type of ionic melt had a melting point close to room temperature and was firstly discovered by Abbott and Sun [22, 23]. DES shares a number of similar physical properties to traditional ionic liquid, but they have many differences in terms of chemical properties. DESs are composed of Lewis or Bronsted acids and bases. They have a very low melting point due to the low lattice energy from the ions. The melting point of mixing compound is much lower than any single original components, since the freezing point is significantly depressed due to the weakened strength of interaction between the compounds [22], as shown in Figure 1-1.

DES is classified into four main categories based on the complexing agent used: type I and type II DESs are synthesized from anhydrous and hydrated metal halides, respectively; type III DESs are formed by hydrogen bond donors [21]. The last type of DESs are those ambient temperature non quaternary ammonium or pyridinium eutectic mixtures.

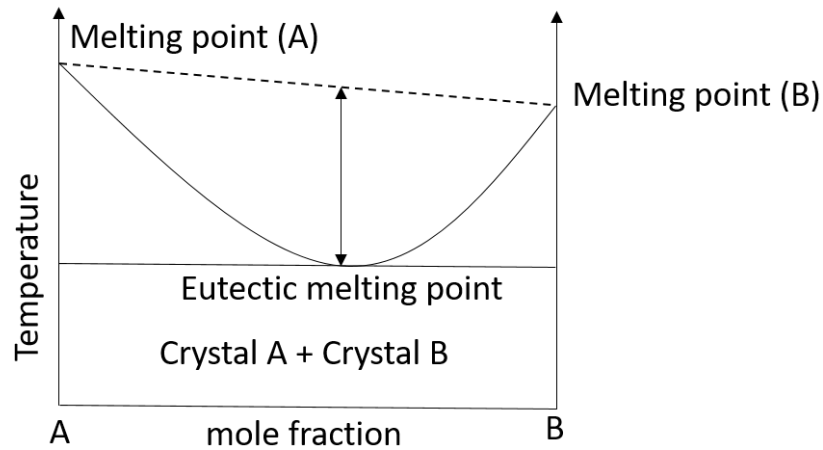


Figure 1-1 Schematic phase diagram of eutectic melting point

1.3 Direct current plating and pulse current plating

Metal electrodeposition is driven by the external electrical current. Primarily there are two modes of current application: direct current and pulse current. Conventionally the electroplating industry adopted DC technique, where a unidirectional current with fixed magnitude is applied throughout the entire plating process. The magnitude of current is the only parameter which can be controlled. The application of pulse plating technique started from the late 19th century [24]. This technique allows the electricity current to change periodically in sequence [25]. There are two types of pulse current: one is unipolar pulse mode, where unidirectional current is applied for certain duration of time before switching off. The other one is bipolar pulse mode, where two opposite directional currents are applied in sequence [26, 27]. In the unipolar pulse system, there are four main operating parameters: the

magnitude of applied current density (j_p), pulse on-time which current is applied (t_{on}), pulse off-time which current is switched off (t_{off}) and duty cycle (θ), which is the proportion of pulse on-time to the total pulse time in one single period. In bipolar pulse system, there are five operating parameters: the magnitude of cathodic current density ($j_{cathodic}$) and anodic current density (j_{anodic}), with their corresponding pulse time ($t_{cathodic}$ and t_{anodic}) and duty cycle. The unipolar pulse mode is applied in most of the electroplating processes. The schematic diagrams of DC and unipolar PC are shown in Figure 1-2. t_{on} and t_{off} usually are in the range of millisecond or second.

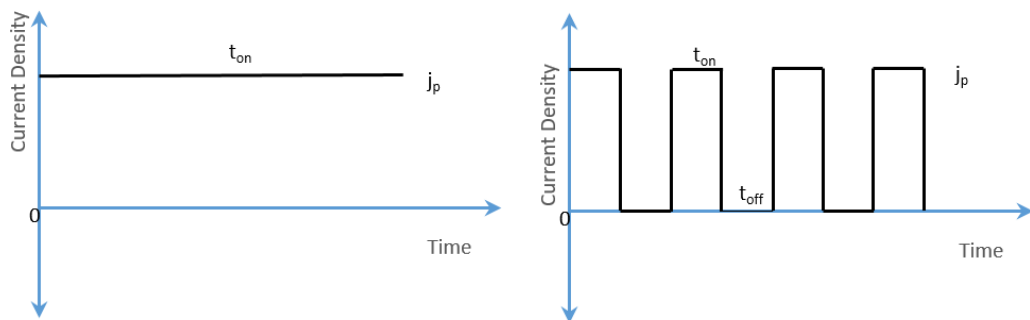


Figure 1-2 Schematic diagram of DC and unipolar PC

1.4 Problem statement and importance of this work

1.4.1 Electrolyte

Traditionally the aqueous solution has been widely used in electroplating industry. However, the water-based system has a variety of

drawbacks. Safety concerns are raised due to the toxicity from the plating electrolyte, especially cyanide solution [28]. Spillage of those electrolytes can give rise to serious health and environmental hazards. The process of waste treatment and disposal of cyanide and heavy metals is expensive [29]. In addition, metals which have very negative reduction potentials, such as Cr and Mg, are either plated with poor deposit quality or impossible to be plated by using aqueous electrolytes [26]. Moreover, the electrode substrate suffers from passivation due to the limited electrochemical window of water-based solution [21]. Hydrogen evolution often occurs during the plating process and lead to poor deposit quality. Industry uses different types of additives to tackle these issues. However, the introduction of additives causes complex deposition mechanism with increased operational cost. These issues could be solved by replacing the aqueous bath to ionic liquid.

1.4.2 Plating current

As been described, traditionally DC was applied in plating industry since it is cheap, easy to operate and has few equipment requirements. However such technique has two major limitations. The deposits produced by DC plating often suffers from poor deposit quality and low deposition efficiency [30]. Moreover, there is little room for improvement on the deposit quality due to few parameters that can be operated in the DC plating system. These issues can be solved by applying PC and pulse plating offers a variety

of advantages [31, 32]. The quality of metal deposit can be improved by achieving smaller and finer grains because the nucleation and mass transport process are very different from DC plating [33]. The details will be described in later sections. Secondly, more parameters such as the magnitude of applied current and time periods can be regulated to improve the morphology of deposit. Pulse plating can also enhance alloy deposition process and control elemental composition [27]. In addition, the additive usage can be reduced in comparison to DC plating. Nevertheless, the operation of many variables and expensive pulse rectifiers are the main drawbacks of pulse plating.

1.4.3 Research gap

At present, there has been a number of studies focusing on the electrodeposition of copper and tin by using ionic liquid under DC conditions. In addition, various studies have shown the advantages of applying PC in the copper and tin plating. However, few sources are available to discuss the effect of incorporating pulse plating technique into electrodeposition using ionic liquid electrolyte except that Xing has performed preliminary research work on investigating the microstructure of copper deposit under various pulse parameters [34]. This piece of work will test the hypothesis if both Cu and Sn electroplating process and metal deposit could be further improved by combining both the advantages from ionic liquid and pulse plating method. In addition, this research would conduct more intensive studies and provide an

in-depth understanding compared to Xing's work. Not only it includes the thorough examination of how pulse parameters could affect the mechanism of plating process and deposit microstructures, but also the further investigation of occurrence of metal dissolution reaction and mathematical relationship between plating and dissolution process. These unique aspects of my research work could be contributed to the indispensable knowledge to the process improvement in electroplating.

1.5 Project aim and research objectives

As mentioned in the previous section, there are distinct advantages of using deep eutectic solvent and pulse current in the electroplating process, yet little research has been carried out on combining both methods. This PhD study will provide a fundamental understanding of the combination effects of using deep eutectic solvents in copper and tin electrodeposition by applying pulse current. The plating results can also be compared to those either using ionic liquid or pulse current individually. This piece of research is divided into two sections: copper plating (phase 1) and tin plating (phase 2). Both phases mainly focus on the following objectives:

- Conduct the voltammetric study of the deep eutectic solvents to ascertain the electrochemical properties

- Study and compare the general appearance and microstructure of metal deposit
- Determine the Faradaic efficiency and potential transient of pulse plating with all pulse conditions
- Perform the material characterization to examine the effects of pulse conditions

Significant amount of metal dissolution was observed during the pulse plating of copper experiment. Therefore, an additional objective was set to investigate the corrosion behaviour. Benzotriazole (BTA) was used as a corrosion inhibitor and was tested later.

- Determine the corrosion current densities and potentials under various agitation conditions
- Conduct the voltammetric study and examine the corrosion inhibition by BTA in copper pulse plating experiments
- Establish mathematical models relating to corrosion reaction and plating process

This chapter has summarized various types of electrolyte utilized in the industrial electroplating process of copper and tin. The concepts of ionic liquid, deep eutectic solvents as well as direct and pulse plating techniques

were also introduced, followed by the discussion of the significance of this piece of research work with its objectives. Prior to the investigation of pulse electrodeposition in DES, a literature review will be presented to elaborate the relevant research work which have been conducted.

Reference List

1. Nasser K. (2004). Electroplating - Basic principles, Processes and Practice. Elsevier Ltd. Berlin
2. Mordechay S, Milan, P. (2010). Modern Electroplating. Wiley. New York
3. Chemical properties of copper - Health effects of copper – Environmental effects of copper, Lenntech, viewed 26/02/2018.
<<https://www.lenntech.com/periodic/elements/cu.htm>>
4. Copper – A metal for the ages, USGS, viewed 26/02/2018,
<<http://pubs.usgs.gov/fs/2009/3031/FS2009-3031.pdf>>
5. Sard R. (1986). Encyclopedia of Materials Science and Engineering. Vol. 2. M. B. Bever ed. Wiley. New York
6. Smee A. (1843). Elements of Electrometallurgy. 2nd ed. Longmans & Green. E. Palmer
7. Farndon, E.E., Walsh, F.C., Campbell S. A. (1995). Effect of thiourea, benzotriazole and 4,5-dithiaoctane-1,8-disulphonic acid on the kinetics of copper deposition from dilute acid sulphate solutions. Journal of Applied Electrochemistry. 25 (6) pp 574-583
8. Rashkov R, Nanev C. (1995). Effect of surface active agents on the initial formation of electrodeposited copper layers, Journal of Applied Electrochemistry. 25 (6) pp 603-608

9. Uceda D.A., O'keefe T.J. (1990). Electrochemical evaluation of copper deposition with gas sparging, *Journal of Applied Electrochemistry*. 20 (2), pp 327-334
10. Roseleur A. (1855). *Manipulations hydroplastiques – guide pratique du doreur, de L' Argenteur et de Galvanoplaste*, 1st ed., Roseleur. Paris
11. Mattox D. M. and Andrew W. (1998). *Handbook of physical vapor deposition (PVD) processing: film formation, adhesion, surface preparation and contamination control*. Noyes publication: New Jersey
12. Tanaka Y., Oikawa K., Sutou Y., Omori T., Kainuma R. and Ishida K. (2006). Martensitic transition and superelasticity of Co-Ni-Al ferromagnetic shape memory alloy with $\beta + \gamma$ two – phase structure. *Materials Science and Engineering*. 439-440, pp 1054-1060
13. Mallory G.O., and Hajdu J.B., (ed.) (1990) *Electroless Plating Fundamentals and Applications*. Noyes Publications/William Andrew Publication. New York
14. Walsh F.C., Low C.T.J. (2016). A review of developments in the electrodeposition of tin, *Surface & Coatings Technology*. 288, pp 79-94
15. Samel M.A.F. (1993). *The Electrodeposition of Tin and Lead-tin Based Alloys*. PhD thesis, Loughborough University Institutional Repository. Loughborough

16. Endres F., Abbott A., Macfarlane D. (2017). Electrodeposition from ionic liquids. 2nd ed. Wiley-VCH. Germany
17. Gabriel S., Weiner J. (1888). Ueber einige Abkömmlinge des Propylamins. *European Journal of Inorganic Chemistry*. 21 (2) pp 2669-2679
18. Walden P. (1914). Molecular weights and electrical conductivity of several fused salts. *Bulletin de l'Académie Impériale des Sciences de Saint-Pétersbourg*.
19. Chum H.L., Koch V.R., Miller L.L., Osteryoung R.A. (1975). Electrochemical scrutiny of organometallic iron complexes and hexamethylbenzene in a room temperature molten salt. *Journal of the American Chemical Society*. 97 (11) pp 3264-3265
20. Wilkes J.S., Levisky J.A., Wilson R.A. Hussey C.L. (1982). Dialkylimidazolium chloroaluminate melts: a new class of room-temperature ionic liquids for electrochemistry, spectroscopy and synthesis. *Inorganic Chemistry*. 21 (3) pp 1263-1264
21. Smith E.L., Abbot A.P., Ryder K.S. (2014). Deep eutectic solvents (DESs) and their applications. *Chemical Reviews*. 114 pp 11060-11082
22. Abbott A.P., Boothby D. Capper G. Davies D.L., Rasheed R.K. (2004). Deep eutectic solvents formed between choline chloride and carboxylic

- acids: versatile alternatives to ionic liquids. *Journal of the American Chemical Society*. 126 (28) pp 9142-9147
23. Hsiu S.I., Huang J.F., Sun I.W., Yuan C.H., Shiea J. (2002). Lewis acidity dependency of the electrochemical window of zinc chloride 1-ethyl-3-methylimidazolium chloride ionic liquids. *Electrochimica Acta*. 47 (27) pp 4367-4372
 24. Montgomery A. (1989). Pulse plating of electrolytic copper. *Circuit World*. 15 (2) pp 33-35
 25. Yin K.M., Jan S.L., Lee C.C. (1997). Current pulse with reverse plating of nickel-iron alloys in a sulphate bath. *Surface and Coatings Technology*. 88 (1-3) pp 219-225
 26. Ispas A., Bund A. (2014). Electrodeposition in ionic liquids. *The Electrochemical Society Interface*. 23 (1) pp 47-51
 27. Chandrasekar M.S., Pushpavanam M. (2008). Pulse and pulse reverse plating – conceptual, advantages and applications. *Electrochimica Acta*. 53 (8) pp 3313-3322
 28. Jordan M. (1995). *The electrodeposition of tin and its alloys*. Leuze, Germany
 29. Plieth W. (2008). *Electrochemistry for Materials Science*. Elsevier, Netherlands

30. Shanthi C., Barathan S., Jaiswal R., Arunachalam R.M. (2009). Study of surface morphology in DC and pulse plating of silver alloy. *Indian Journal of Engineering and Materials Sciences*. 16 (2) pp 128-132
31. Cha S.H., Kim S.S., Cho S.K., Kim J.J. (2007). Copper bottom-up filling by electroplating without any additives on patterned wafer. *Electrochemical and Solid-State Letters*. 10 (2) pp 22-24
32. Roy S. (2008). Mass transfer considerations during pulse plating. *Transactions of the IMF*. 86 (2) pp 87-91
33. Ibl N. (1980). Some theoretical aspects of pulse electrolysis. *Surface Technology*. 10 pp 81-104
34. Xing S.J. (2014). Environmentally Friendly Baths for Cu-Sn Co-electrodeposition: Cyanide-free Aqueous Bath and Deep Eutectic Solvents. Department of Industrial Engineering, Università DeGlia Studi Di Trento. Trento

Chapter 2. Literature Review

2.1 Ionic liquids

2.1.1 Traditional ionic liquids

2.1.1.1 Haloaluminate-based ionic liquids

One alternative to the aqueous system in electrodeposition process is the ionic melts [1]. The molten salts, which melt at elevated temperature due to their large lattice energies, are known for one hundred years for aluminium deposition. Compared to the aqueous system, they have higher conductivities, higher solubilities for metal salts and wider electrochemical potential windows. Since these salts can deposit a metal at high temperature and there is no water present in the melt, most of the limitations encountered in aqueous solutions due to the breakdown of water can be overcome. Therefore, these melts have been widely used in electroextraction of metals like Ti, Al and Na [2, 3, 4].

However, the range of substrates suitable for deposition from high temperature molten salts is limited. In addition, the operation conditions for high temperature molten salts are difficult to achieve. Metal plating from ionic melts radically changed when the melting point was reduced. High temperature molten salts were replaced by the use of ionic material which melted at a lower temperature [1]. This was achieved when the lattice energy

was significantly reduced due to the delocalization of the charge on the ions, resulting in a much lower melting point.

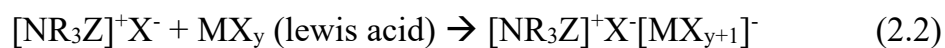
Traditionally there are two types of ionic liquids developed depending on the ion species. The first generation of ionic liquids are the room temperature haloaluminate-based ionic liquids. The haloaluminate-based ionic system was first developed in the mid twentieth century. Hurley and Wier found that the eutectic mixture of AlCl_3 and N-ethylpyridinium bromide (EtPyBr) with a composition ratio of 2:1 had a melting point as low as -40°C [5]. They also reported that aluminium could be plated by using such ionic mixture [6]. However the use of such mixture was limited. The reasons were that, it was only in liquid state when the mole fraction of AlCl_3 was exactly at 0.66. Moreover, the electrochemical stability was an issue since the bromide ion could be easily oxidized.

In 1978, Osteryoung and his colleagues reported that the properties of ionic liquid could be improved by replacing EtPyBr with N-butylpyridinium chloride (BuPyCl) [7, 8]. The mixture had a melting point of 40°C and became liquid in ambient condition with a broader mole fraction range of AlCl_3 from 0.43 to 0.66. In addition, the anodic breakdown limit was improved by the replacement of bromide to chloride. The main drawback of such system was that the butylpyridinium cation could be easily reduced [9].

In the 1980s, Wilkes and his co-workers investigated a number of organic cations. They found that N,N'- dialkylimidazolium cations had higher

electrochemical stability than the N-butylpyridinium because of their higher electron affinities [10]. In fact, the ionic melts consisting of AlCl₃ with N,N'-dialkylimidazolium had lower melting points than the N-butylpyridinium based systems. They were in liquid state under room temperature with an extended mole fraction range of AlCl₃ from 0.30 to 0.66 [11]. Compared to the butylpyridinium melts, they also had wider electrochemical potential windows and higher reactivities with aluminium. Such mixture was similar to the alkylpyridinium ionic liquid in terms of viscosity, conductivity, Lewis acidity and solubility for both inorganic and organic compounds [11].

The haloaluminate-based ionic liquids are synthesized from Lewis acids and halide salts by two steps: firstly, the cation is formed by the reaction between haloalkane and trialkylamine, dialkylsulfide or trialkylphosphine. This is followed by the synthesis of anion by adding the metal halides into the salt [1]. Nowadays a number of halides can be purchased directly from the suppliers, therefore the procedure of cation synthesis usually is neglected. The general synthesis reactions are illustrated in equation (2.1) and (2.2).



In the equation (2.1) and (2.2), M and Z are the metal species, X is the halogen element (such as Br or Cl), NR_3 is the alkyl methyl compound (such as dialkylsulfide, trialkylphosphine or trialkylamine), y is the number of halogen atoms present [1]. Not only the chloroaluminate ionic liquids are produced by this method, other ionic mixtures containing CuCl , FeCl_3 and SnCl_2 can also be synthesized similarly. The procedure is exemplified by the formation of 1-butylpyridinium $[\text{C}_4\text{py}]$ and 1-ethyl-3-methylimidazolium $[\text{EMIM}]$ chloroaluminate ionic liquids, as shown in Figure 2-1.

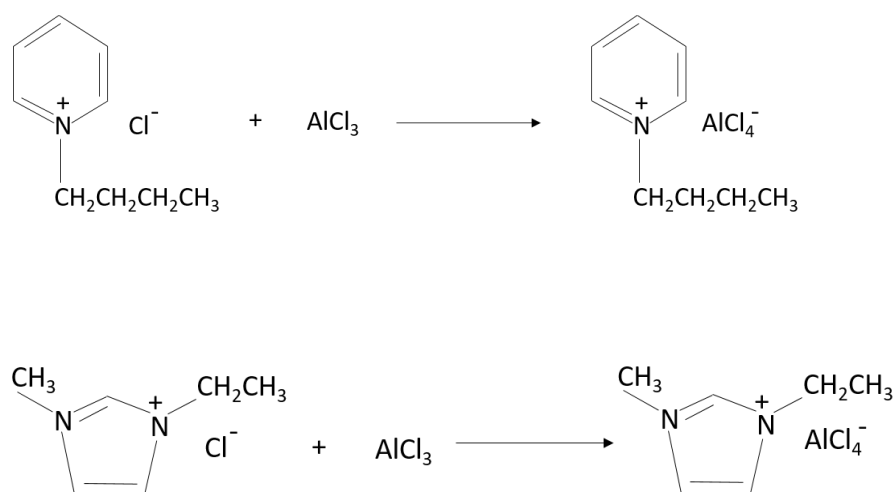
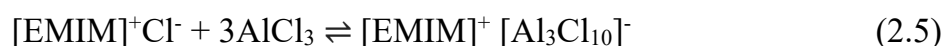
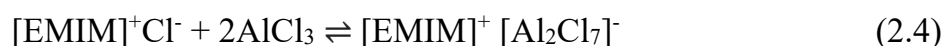


Figure 2-1 Schematic diagram of formation of $[\text{C}_4\text{py}]$ and $[\text{EMIM}]$ chloroaluminate ionic liquids

During the reaction between Lewis acid and quaternary halide salt, different types of anionic species can be formed based on the proportion of metal halides MX_y and the halide salt $[\text{NR}_3\text{Z}]^+\text{X}^-$ [1]. Take the $[\text{EMIM}]$

chloroaluminate ionic liquid as an example: $[\text{AlCl}_4]^-$, $[\text{Al}_2\text{Cl}_7]^-$ and $[\text{Al}_3\text{Cl}_{10}]^-$ anionic complex can be present in the electrolyte, depending on the moles of aluminium chloride added. The corresponding reactions are shown in equations (2.3) to (2.6).



The pH of ionic liquid can be affected by the species of anionic complex [12]. For instance, if the mole fraction of aluminium chloride does not exceed 0.5 in the final product, the solution pH is basic because the chloride ions are not bound to aluminium and act as Lewis bases. When the mole fraction of aluminium chloride equals to 0.5, the anionic species present in the electrolyte is only $[\text{AlCl}_4]^-$ because all chloride ions are bound to aluminium. Therefore the ionic liquid becomes neutral. The Cl^- and $[\text{Al}_2\text{Cl}_7]^-$ species also exist in the solution due to the auto-solvolysis of $[\text{AlCl}_4]^-$ ions, as shown in equation 2.6. The electrolyte becomes acidic if the mole fraction of aluminium chloride exceeds 0.5, since an excess of AlCl_3 is present.

A number of haloaluminate-based ionic liquids system have been examined for metal deposition. However, only aluminium and its alloys have been plated successfully. The majority of other metals, which their electrochemical behaviours were investigated, show that plating as a pure metal is not feasible [13].

As previously mentioned, Hurley and Wier conducted aluminium deposition at room temperature in 1950s [6]. They used aluminium and brass as the anode and cathode substrate respectively. Benzene was also added into the electrolyte as an additive. The microstructure of deposit was found to be related to the applied current density. A smooth, shiny and uniform deposit could be obtained if the current density applied was appropriate. If the current density was low, the deposit became white or grey in colour and the grains were very coarse and incoherent. If the current density was high, the deposit became black and non-adherent. Other factors, such as the preliminary treatment of substrate, thickness and types of cathode substrates, were also found to affect the quality and microstructure of metal deposit.

Endres and his co-workers plated Al/Au alloys by using aluminium chloride-1-methyl-3-butylimidazolium chloride ionic liquid [14]. Similar mechanisms of deposit layer formation were found compared to the aqueous solution. They also observed nanostructuring during the plating process by using *in situ* STM analytic method.

The first generation ionic liquid suffers from several drawbacks. Generally they are very sensitive to moisture. Hurley's research group found that the electrodeposition of aluminium could not be achieved if the ionic electrolyte absorbs moisture [5]. Therefore, a piece of metallic aluminium was needed to react with electrolyte before using the bath to remove the moisture. Another issue is these ionic liquids are sensitive to metallic contamination. It was found that the aluminium deposit became black and incoherent if small amounts of metallic iron or copper ions were added into the electrolyte. Furthermore, the handling condition of these ionic liquids must be strictly controlled. For instance, the ionic bath needed to be operated under inert and dry atmosphere in the aluminium plating process, since the deposit quality deteriorated with time due to the oxidation of electrolyte. Therefore, the commercial applications of these ionic liquids were very limited.

2.1.1.2 Air and water stable ionic liquids

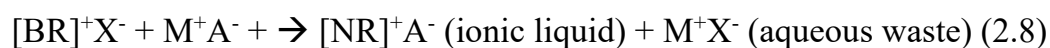
Aware of the limitations of chloroaluminate-based ionic liquids, Wilkes and his co-workers tried to search for alternative anion species to replace the reactive haloaluminate anionic system [15]. They discovered a new class of ionic liquid by replacing the AlCl_3 with discrete anions such as hexafluorophosphate and tetrafluoroborate. Two ionic melts $[\text{EMIM}]\text{BF}_4$ and $[\text{EMIM}]\text{MeCO}_2$, which were found in liquid state under ambient conditions, were prepared and characterized. They suggested that $[\text{EMIM}]$ based ionic

liquids were electrochemically and chemically stable, inexpensive to prepare and facile in handling.

Later the US Air Force Academy reported that discrete water stable anions, such as nitrate, sulphate and acetate salts, could also form similar type of ionic liquid with dialkylimidazolium cation through metathesis reactions [16]. They also developed a number of ionic melts from monoalkylimidazoliums and trialkylimidazoliums combined with those discrete anions as a candidate of high-energy batteries electrolyte.

These non-chloroaluminate melts are recognized as the second generation of ionic liquids, which usually has discrete anion [17]. In general speaking they have higher electrochemical and thermal stability as well as easier handling in humid conditions compared to the first generation of ionic liquids [1].

The synthesis route of these air and water stable ionic liquids is similar to those chloroaluminate-based melts. Firstly the organic base compound, such as pyridine or N-methylimidazole, reacts with haloalkane to generate a cation, which then further reacts with acid or metal salt in the aqueous environment to form desired ionic liquids via anion exchange process [1]. The procedure is illustrated in equation (2.7) and (2.8).



In the above equations, N is the organic base compound, R is the alkyl group, X is the halogen, M is protons (H⁺) or metal (Li, Na, etc). A is the discrete anion ([PF₆], [BF₄], etc).

A number of various air and water stable ionic liquids have been developed and they have shown different properties depending on the anionic species. The tetrafluoroborate ([BF₄]) and hexafluorophosphate ([PF₆]) based melts were the most commonly used ionic liquids in the early days. In 1997, [EMIM][BF₄] was first reported to be used as an electrolyte in the lithium electrodeposition process during the study of electrochemical behaviours of [EMIM][BF₄] in lithium ion reduction process by Osteryoung and his colleagues [1, 18]. They claimed that such ionic compound could be an ideal candidate electrolyte for using in lithium ion battery, rather than in metal deposition.

Olivier's research group developed two ionic melts, which were [BMIM][PF₆] and [BMIM][BF₄], in 1995 [19]. Compared to [EMIM][BF₄], [BMIM][BF₄], the synthesis procedure was easier and it is completely miscible with water. Therefore, both ionic melts were reported to have much potential to be studied and developed further.

The [BF₄] and [PF₆] anion based ionic melt that combined with other types of cations became less attractive for electrochemical application, since they were shown to have some issues and drawbacks. For instance, research found that [C₄py][BF₄] was less electrochemically stable than their imidazolium counterpart [20]. Huang and his co-workers found such ionic liquid was in solid state at room temperature [21]. Overall, [BF₄] and [PF₆] based ionic liquids were easy to prepare with low cost, and they showed superior performance for certain applications compared to other types of ionic liquid [22].

Triflate ([OTF]) and trifluoroacetate ([ATF]) anions were considered as alternatives to fluorinated borates and phosphates [1]. The ionic melts based on these anions generally had low viscosities and large electrochemical windows, whereas they were not very electrochemically stable [23]. Calin's research group was the first to investigate the electrochemical behaviour of 1-ethyl-3-methylimidazolium triflate [EMIM][OTF] during developing the dual intercalating molten electrolyte batteries [24]. Gratzel and his colleagues developed 1-ethyl-3-methylimidazolium trifluoroacetate [EMIM][ATF] ionic melt [25]. They showed that [ATF] anion had lower viscosity and higher conductivity compared to other anions such as [OTF] and [Tf₂N]. However it was less stable in air or N₂ environment and could decompose above 150°C.

Bistriflamide ([NTF]) based ionic liquids offer several advantages over [BF₄] or [PF₆] based melts, such as lower viscosity, higher conductivity, better

thermal and electrochemical stability [1]. Li[NTF] was found to have good potential in the use of photo-electrochemical solar energy conversion devices based on its physical and electrochemical properties [26]. However the assumed stability of [NTF] based ionic liquids raised some concerns. Li[NTF] ionic liquid decomposed in lithium metal battery due to either reactions between metal and electrolyte or electrochemical reduction of anion [27]. In addition, [NTF] based ionic liquids were actually soluble in water and not economical friendly, which limited their commercial applications [1].

The trispentafluoroethyltrifluorophosphate [FAP] anion based ionic liquids were first synthesized and reported by Chan and his co-workers in the 1960s [28]. A number of anionic complexes such as $[\text{CF}_3\text{PF}_5]^-$, $[(\text{CF}_3)_3\text{AsF}_3]^-$ and $[(\text{CF}_3)_2\text{PF}_4]^-$ were developed. They also found that trimethyltrifluoromethyltin $(\text{CF}_3)_3\text{SnF}_3$ could form ionic complexes with $(\text{CF}_3)_3\text{PF}_2$ and PF_5 in 1:1 molar ratio. In 2001, Merck KgaA studied Li[FAP] electrolyte and tried to replace the original LiPF_6 in high energy lithium-ion batteries, since LiPF_6 had low thermal and chemical stability [29]. They showed that Li[FAP] had improved hydrolytic stability and superior discharge efficiency. Later, they developed a more convenient and simple procedure for the synthesis of [FAP] based ionic melts [30]. Generally these ionic liquids are more electrochemically stable than the $[\text{BF}_4]$, $[\text{PF}_6]$ or [NTF] based ionic compounds [1].

Another type of second generation of ionic liquid is consist of cyano anion $[\text{SCN}]^-$ [1]. Pringle and his co-workers reported that $[\text{EMIM}][\text{SCN}]$ showed good electrochemical and thermal stability [31]. Therefore it could be used as electrolyte in dye-sensitized solid-state solar cells [32, 33]. In addition, Nockemann's research group reported that such ionic liquid also had high solubility of metal salt [34]. Dicyanamide anion $[\text{DCA}]^-$ has also been studied as the anionic species. MaFarlane and his co-workers found that $[\text{EMIM}][\text{DCA}]$ had extremely low viscosity [35]. They also revealed that a number of ionic liquids could be formed by $[\text{DCA}]^-$ anion with electrochemically stable cations such as pyrrolidiniums, imidazoliums and ammoniums [36]. Therefore, $[\text{DCA}]$ based ionic liquids have been widely used in various electrochemical applications due to their superior transport properties. Other types of cyano anions such as tricyanomethide $[\text{TCM}]^-$ and tetracyanoborate $[\text{TCB}]^-$ were also developed [37, 38]. Figure 2-2 illustrates some of the anion used in the second generation of ionic liquids.

The second generation ionic liquid generally suffer from several disadvantages [1]. Firstly, much concerns were raised due to their toxicity and the negative impacts on the environment. Secondly, these newly developed chemicals need to be registered with regulatory bodies. In addition, some of the anionic species are not electrochemically stable, which limits their application in electrodeposition industry.

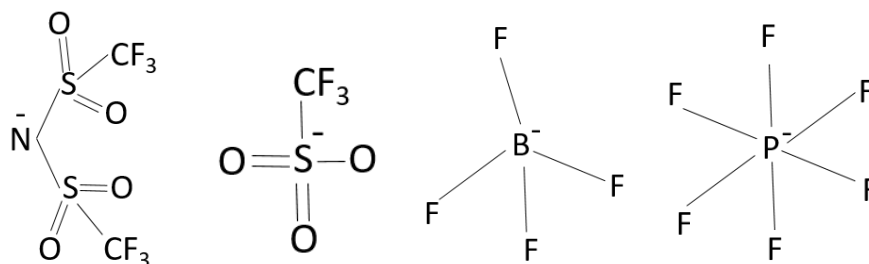


Figure 2-2 Example of discrete ion in the second generation of ionic liquid (from left to right: bis-trifluoromethanesulfonyl, trifluoromethanesulfonate, tetrafluoroborate and hexafluorophosphate)

2.1.2 Eutectic based ionic liquids

Ionic liquids based on eutectic mixtures from two components which interact with each other are named as eutectics. For mixtures with non-interacting components, the melting point and mole fraction of component generally is in linear relationship. For mixtures with interacting components, the melting point can largely deviate with the composition of component [1]. As shown in Figure 2-3, the minimum melting point is achieved at the eutectic melting point with specific mole fraction of component. The melting point of eutectic mixture is much lower than the one of either component.

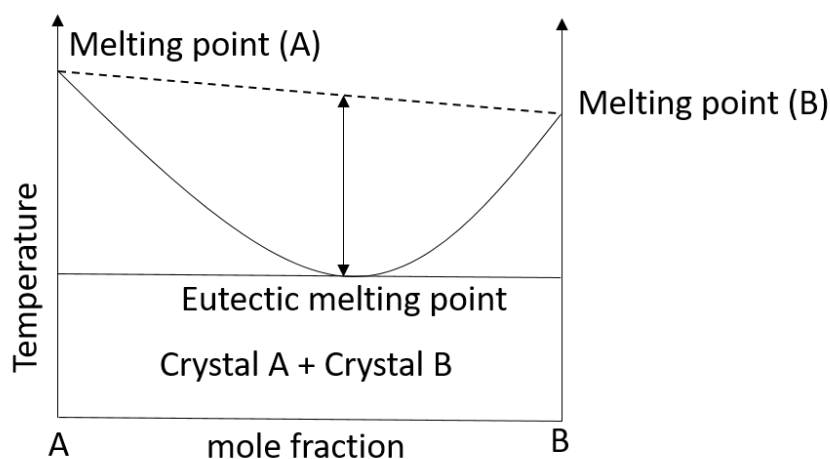


Figure 2-3 Schematic phase diagram of eutectic compounds

The eutectic compounds have been predominantly used to meet the requirement of reducing the operating temperature in the industrial production process [1]. Aluminium based ionic liquids were first developed in the mid-20th century, as mentioned in the previous section [6]. In the late 1990s both research groups of Abbott and Sun discovered that the melting points of eutectic mixtures consisting of quaternary ammonium halides and zinc halides were close to the ambient temperature [39, 40]. These eutectic systems could be expressed in the general formula as $[\text{Cat}]\text{XzY}$, where $[\text{Cat}]$ is the cation, X is the halide anion and z is the number of Y molecules. The eutectic mixtures can be subdivided into four categories, mainly depending on the type of Y molecules, which are the complexing agents:

Type I eutectics: $\text{Y} = \text{MCl}_x$, $\text{M} = \text{Fe}, \text{Zn}, \text{Sn}$, etc.

Type II eutectics $Y = MCl_x \cdot yH_2O$, $M = Cu, Cr, Co$, etc.

Type III eutectics $Y = RZ$, $Z = OH, COOH, CONH_2$, etc.

Type IV eutectics $MCl_x + RZ \rightarrow MCl_{x-1} \cdot RZ + MCl_{x+1}$, $M = Zn, Al$ and $Z = OH, CONH_2$

In the above list, R stands for the alkyl group, M is the metal, Z is the functional group. The cation species usually refer to quaternary ammonium, imidazolium, or pyridinium moieties.

There are a number of advantages of eutectic mixtures compared to those traditional ionic liquids. Firstly the synthesis process is not complicated. Normally these eutectics are formed by mixing two components with gentle heating, since the formation process is mildly endothermic [1]. Secondly, they are insensitive to water and the electrochemistry remains unaffected even when large concentrations of water are added. This can be beneficial in the industrial electroplating process. Finally, the mixing components are known chemicals and the registration as new entities with regulatory bodies is not needed.

2.1.2.1 Type I eutectics

Type I eutectic based ionic liquids were obtained using an extensive range of metal halides [4]. It was found that the melting point of such ionic liquids was related to the melting point of its metal salts. For instance, quaternary ammonium salts can only form an ionic liquid with certain species of metal salts such as SnCl_2 , FeCl_3 and ZnCl_2 , since they have very low melting point [1]. Other metal salts with higher melting point can not form ionic liquid with quaternary ammonium salts due to their large lattice energies.

Research showed that some physical properties could also be affected by the anionic species in the melt, which depends on the composition [1]. For instance in the zinc system, ZnCl_3^- , Zn_2Cl_5^- and Zn_3Cl_7^- were all present in the ZnCl_2 based eutectics system. If the mole fraction of ZnCl_2 increased from 50% up to 66%, the freezing point of ionic liquid decreased since more Zn_2Cl_5^- formed. If the mole fraction of ZnCl_2 is higher than 66%, the freezing point increased due to the formation of Zn_3Cl_7^- .

Abbott's research group studied the physical and electrochemical properties of ionic mixture from choline chloride and ZnCl_2 , SnCl_2 and FeCl_3 metal salts [39]. They found the major zinc anion species were Zn_3Cl_7^- and Zn_2Cl_5^- in Lewis basic solutions, similar results were obtained in the $\text{SnCl}_2/\text{ChCl}$ system. It was also observed that cation had little effect on the freezing point of ionic liquids. In addition, these ionic liquids were less reactive to water and suitable for large scale metal deposition.

Eutectic mixtures containing iron metal salts were also examined by a number of studies. Abbott and his colleagues found that there were two eutectic points which occurred in 33% and 67% molar ratio of metal salts in FeCl₃/ChCl system [39]. Sitze *et al.* discovered that ionic melt could be formed using [BMIM]Cl and FeCl₂ when the mole fraction of FeCl₂ was in the range of 0.25 to 0.5 [41]. [BMIM]Cl can also form liquid mixture with FeCl₃ when the molar ratio of FeCl₃ ranged from 0.53 to 1.7. They also showed that FeCl₄²⁻ was the primary anionic species in the FeCl₂ ionic liquid, whereas FeCl₄⁻ and Fe₂Cl₇²⁻ were the prevalent anions present in the FeCl₃ system. Similar results were obtained from Zhang's research group when they investigated the ionic melts prepared from [BMIM]Cl and FeCl₃ in 1:1 molar ratio [42].

Xu and his co-workers reported that the ionic melt could be made from [BMIM]Cl and GaCl₃ with 1:1 molar ratio. GaCl₄⁻ was reported as the only anionic species containing Ga using Raman scattering and ab initio calculations [43]. Tian's research group formed ionic liquid from [BMIM]Cl with InCl₃ and confirmed that InCl₄⁻ was the primary anionic species containing In using similar technique [44]. Ionic liquids were also produced from TaF₅ and NbF₅ using [EMIM] F • 2.3HF by Matsumoto *et al* [45].

Although most of the studies were focused on halide salts, only few researches have been performed on metal oxides [1]. Noguera and his co-workers formed the ionic liquid from [BMIM]Cl with both CrO₃ and

Na_2MoO_4 oxides respectively during the study of self-supported oxidants of alcohols [46]. However, little information in terms of properties, melting points and eutectic behaviours was revealed from their report.

2.1.2.2 Type II eutectics

These eutectic mixtures were developed to expand the range of metal salts from the type I eutectic [1]. In these systems, the melting point decreases due to the reduction of lattice energy by the presence of water molecules in the metal salt. Therefore, the hydrated salts tend to form liquid mixture with cations at ambient temperature compared to the anhydrous salts. Among these, the eutectic melt containing Cr salt was studied in detail.

Abbott *et al.* found that a dark green and viscous liquid could be formed from choline chloride and $\text{CrCl}_3 \cdot 6\text{H}_2\text{O}$ in a molar ratio of 1:2 [47]. The main ionic species in the liquid was $[\text{Choline}]^+$ and $[\text{Cl} \cdot 3\text{H}_2\text{O}]^-$, which accounted for the high conductivity compared to the ionic liquid prepared from anhydrous salt. Metal electrodeposition was also carried out by using such eutectic electrolyte at 60°C and a layer of crack-free, thick and adherent Cr film was obtained. In addition, over 90% Faradaic efficiency was achieved, compared to only 10% to 20% in the aqueous chromic acid solution. The absence of hydrogen production due to nearly water-free electrolyte eliminated the hydrogen evolution reaction that would damage the electrolyte.

These ionic liquids made from hydrous Cr salts were found to be very sensitive to moisture and temperature fluctuations [1]. They were highly hygroscopic and could absorb large concentration of water at ambient temperature. The liquids lost water above 70°C with a colour change from dark green to purple. Thermogravimetry revealed that the hydration release of hydrous Cr salt undergoes by two steps: three water molecules are lost at approximately 85°C and another three water molecules at nearly 180°C [47]. No significant alteration in the composition of ionic liquid was found between 50°C and 60°C.

Wang and his colleagues reported and investigated the ionic liquid system produced from choline chloride and $\text{MgCl}_2 \cdot 2\text{H}_2\text{O}$ [48]. They found that the physical properties such as viscosity, melting point, conductivity and density were a function of temperature and metal salt composition, which was similar to the other types of ionic liquid. The Mg ionic liquid exhibited high conductivity and low viscosity.

Overall, the studies on type II eutectic are limited and only Cr was successfully plated from these ionic liquids. In addition, their electrochemical potential windows are narrower and therefore metals like Ca and Al can not be plated from these melts [1].

2.1.2.3 Type III eutectics

These ionic liquids are composed of halide salts with a series of hydrogen bond donors (HBD) such as urea, ethylene glycol (EG) and glycerol, as shown in Figure 2-4 [1]. The depression of melting point is extremely large due to the interaction between halide anion and the function groups. For instance, the depression of melting point for choline chloride-urea system is 178°C, for oxalic acid-choline chloride system it is 212°C. It was reported that such large depression of freezing point by 212°C was also achieved in the choline chloride-zinc chloride system due to the formation of covalent bonds [39]. Therefore, these eutectics are named as deep eutectic solvents (DES) to differentiate from other types of ionic liquids. The freezing points of these eutectics depend on both lattice energies of HBD and salt as well as the HBD-anion interaction [1]. Compared to other room temperature ionic liquids, DES are easy to prepare, nonreactive, less expensive, chemically stable and many are biodegradable [1, 17].

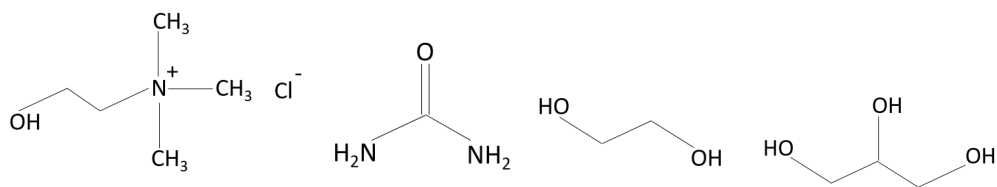


Figure 2-4 Example of choline chloride (top left) and widely used HBD (urea, ethylene glycol, glycerol)

It was found that highest conductivities and lowest viscosities were obtained from the glycol based DES system [1]. They also had large electrochemical potential windows. Therefore, several metal and alloy electrodeposition systems have been studied. Abbott and his co-workers plated Zn, Sn and Zn/Sn alloys from choline chloride-ethylene glycol and choline chloride-urea systems [49]. The species containing zinc in the two melts were different due to the ligand properties of the complexing agents. In ethylene glycol melt $ZnCl_3^-$, $Zn_2Cl_5^-$ and $Zn_3Cl_7^-$ species were found, while in urea only the $ZnCl_3^-$ species was detected.

A layer of dull and silver coloured zinc film was plated from ChCl: EG system in 1:2 molar ratio containing 0.5 M $ZnCl_2$ and 0.05 M $SnCl_2$ for one hour at 10 mA/cm² current density [49]. Although a layer of white zinc deposit could be achieved by using Type I ChCl: $ZnCl_2$ ionic liquid, it was found that the conductivity of such electrolyte was much smaller (36 μ S/cm at 40°C) compared to the one of choline chloride based systems (ChCl: urea is 1.8 mS/cm, ChCl: EG is 11 mS/cm at 40°C) [50]. This showed much better exploitation prospects for the latter ones.

Dendritic Sn was plated from ChCl-urea system containing 0.05M $SnCl_2$ for thirty minutes at 10 mA/cm² current density [49]. The morphology of Sn/Zn alloys were different and depends on the HBD of ionic liquid. In the urea based system, the deposit exhibited in cubic crystals and both metal grains were evenly distributed. Approximately 150 μ m diameter macroscopic

pores were found in the thick alloy deposit plated from such DES containing 0.5M ZnCl₂ and 0.05M SnCl₂ metal salts for 2 hours at 10 mA/cm² current density. In comparison, the top of alloy deposit exhibited dendritic microstructure and higher tin composition was found when plated by the ethylene glycol based DES.

An interesting application was demonstrated by Abbot *et al.* that the electropolishing of stainless steel could be carried out using choline chloride-ethylene glycol DES, which aims to replace the conventional corrosive and inefficient aqueous liquids [51]. A 92% current efficiency was achieved by using such electrolyte, whereas only approximately 30% current efficiency was obtained using an aqueous bath. The surface roughness achieved using DES was comparable to aqueous electrolyte. The solution did not suffer any deleterious effect when exposing to the open atmosphere and moisture was absorbed. In the aqueous systems, iron needed to be added into a fresh aqueous solution to maintain the surface finish. In addition, the quality of surface finish polished in DES was never affected without the iron addition.

In summary, the DES are highly conductive, less viscous and non-toxic and much cheaper than the other types of ionic liquids. Currently they have attracted much attention in the electrodeposition process.

2.1.2.4 Type IV eutectics

Most of these eutectics consist of quaternary ammonium, pyridinium or ammonium cations [17]. Eutectics mixtures can also be formed by using metal containing cations and anions with metal salts and organic groups such as amides or alcohols [52]. Abood and his co-workers formed the ionic melt by simply adding acetamide to AlCl_3 in 1:1 molar ratio without any introduction of quaternary ammonium cations. They claimed that low melting point could be obtained due to the coordination geometry of cationic and anionic complexes. In addition, this type of eutectic was reported to be insensitive to water.

The synthesis procedure of type IV eutectics is similar to the other eutectics [1]. Normally these mixtures have lower conductivities and are quite viscous. Abbott reported that aluminium could be plated by using a eutectic mixture of urea and AlCl_3 [53]. An alkane hydrophobic barrier was placed above the electrolyte to isolate the system from moisture so that aluminium could be plated from this solution.

Brooks and his colleagues synthesized several novel silver complexes such as $[\text{Ag}(\text{MeCn})_4]_2[\text{Ag}(\text{Tf}_2\text{N})_3]$, $[\text{Ag}(\text{EtIm})_2][\text{Tf}_2\text{N}]$ and $[\text{Ag}(\text{MeCn})_4][\text{Tf}_2\text{N}]$, which were also known as liquid metal salts [54]. Metal silver was reported to be plated using these eutectic melts. It was found that the microstructure of metal plated from $[\text{Ag}(\text{MeCn})_4]_2[\text{Ag}(\text{Tf}_2\text{N})_3]$ electrolyte was much smoother and adherent under high applied current efficiency.

However, opposite results were achieved for the deposit plated from $[\text{Ag}(\text{EtIm})_2][\text{Tf}_2\text{N}]$ solution. The smoothest morphology was obtained using the lowest current density. Dendritic grain was observed if the silver was plated using higher current density.

Although some studies were carried out to investigate the properties and applications of type IV eutectics. This area is relatively new and very few systems have been studied until now [1].

2.2 Summary of studies of metal electrodeposition from ionic liquids in DC plating

2.2.1 Tin

Electrodeposition of Sn from traditional ionic liquid has been carried out by a number of researches. The electrochemistry of Sn in haloaluminate-based ionic liquid was reported by Hussey and Xu [55], who performed the study of Sn (II) reduction in an ionic melt containing AlCl_3 with 1-methyl-3-ethylimidazolium chloride $[\text{EMIM}]\text{Cl}$ electrolyte. The voltammograms showed one reduction and one oxidation peak respectively between Sn (II) to Sn (IV) using Pt electrode in both acidic and basic conditions, although the peak potentials were separated. The formal reduction potential of Sn (II) to Sn was determined as approximately 0.55 V against Al reference electrode with 66.7% mole fraction of AlCl_3 , and -0.85 V with 44.4% mole fraction of AlCl_3

under standard conditions. In addition, the diffusion coefficient of Sn (II) was also measured as $5.3 \times 10^{-7} \text{ cm}^2/\text{s}$ and $5.1 \times 10^{-7} \text{ cm}^2/\text{s}$ for the 66.7% and 44.4% mole fraction of AlCl_3 respectively. However, there was no information available on the practical Sn deposit plated from haloaluminate-based ionic liquid.

Several other electrochemical studies of Sn from air and water stable ionic liquids were performed. Miura *et al.* investigated the electrochemical behaviours of Sn (II)/Sn in 1-n-butyl-1-methylpyrrolidinium bis(trifluoromethylsulfonyl)imide ([BMP-TFSI]) ionic melt [56]. The voltammogram showed one single reduction and one oxidation peak at -0.6 V and -0.4 V against silver reference electrode respectively. Both anodic and cathodic reactions were interpreted to be a two-electron transfer reaction through calculations by the Faraday's laws of electrolysis. Galvanostatic electrodeposition was also carried out by applying a -0.05 mA/cm² current density in 0.05 mol/dm³ Sn [BMP-TFSI] electrolyte. Smooth, dense and adhesive Sn deposit was achieved and particle size ranged between 2 μm and 5 μm . Moreover, oxidation of Sn (II) to Sn (IV) was not observed.

Sun and Huang investigated the electrochemistry of Sn in zinc chloride-1-ethyl-3-methylimidazolium chloride ionic liquid ([ZnCl₂-EMIM]) at 90°C [57]. The reduction potential of Sn (II) was measured as 0.25 V in acidic (40-60 mole fraction of ZnCl₂) and -0.24 V in basic (25-75 mole fraction of ZnCl₂) melts, respectively against Zn reference electrode. The results were similar to

the [AlCl₃-EMIM] ionic system. The voltammogram of Sn (II) in both melts using glassy carbon and tungsten electrodes illustrated the existence of Sn (IV)/Sn (II) and Sn (II)/Sn metal redox reactions. They found that the adsorption of Sn (II) ions was hindered by the presence of chloride ions in the basic melt. This inhibition effect was similar to the one in an aqueous solution.

Chen and co-workers reported the deposition of nanostructured tin deposit from a 1-ethyl-3-methylimidazolium dicyanamide ([EMIM-DCA]) ionic system [58]. Their CV data showed one anodic and one cathodic peak between -0.68 V and -0.75 V in 0.05 M Sn (II) ionic liquid at 40°C against Pt reference electrode. Potentiostatic depositions of Sn on Cu substrate were carried out at -0.74 V and -0.84 V respectively. SEM results showed that sponge like Sn deposit was plated in reticulate nanowires, of which the diameter ranged between 100 nm and 200 nm using -0.74 V applied voltage. When the voltage increased by 0.1 V the electrode surface was covered by Sn dendrites. Therefore, it was concluded that the morphology of Sn deposit depends on the applied potential. In addition, galvanostatic plating of Sn was performed using 0.6 mA/cm² and 1.2 mA/cm² current densities. Smooth, uniform and sponge Sn deposit with nanowires was formed under low applied current density. The microstructure became less uniform when higher current density was applied.

Yang *et al.* plated Sn from 1-ethyl-3-methylimidazolium tetrafluoroborate ([EMIM]BF₄) ionic liquid at ambient temperature [59]. The

voltammogram using Pt electrode versus Ag reference electrode showed that the electrochemical window of such ionic melt was 4.3 V ranging from 2.7 V to -1.6 V. CV data also showed a reduction and an oxidation peak at approximately -0.78 V and -0.69 V respectively. The linear sweep voltammetry revealed that the reduction process of Sn (II) on the Pt electrode was electrochemically irreversible. The diffusion coefficients of Sn (II) was determined as $6.07 \times 10^{-7} \text{ cm}^2/\text{s}$. Metal electrodeposition was also carried out in [EMIM]BF₄ containing 25 mM Sn (II) species on the Pt substrate. Sn was plated in isolated needle-type islands rather than a uniform layer on the substrate surface. The deposit was pure Sn without any other elemental contaminants such as boron, fluoride and chloride based on EDX analysis.

Matsunaga and his colleague studied the electrochemical behaviours of [EMIM]BF₄Cl ionic liquid system [60]. Cyclic voltammogram exhibited a reduction peak and an oxidation peak at -1.4 V and -1.3 V versus Ag reference electrode, respectively. The reversibility of both plating and stripping process was also evaluated by continuous cyclic voltammetry. The voltammograms overlapped completely after ten cycles of CV, suggesting a reasonable reproducibility. They also demonstrated that tin plating was a quasi-reversible process and deposition potential was measured as -1.38 V versus Ag reference electrode. In addition, the Faradaic efficiencies for both stripping and plating process were reported to be close to 100%.

The electrochemistry of Sn (II)/Sn in N-butyl-N-methylpyrrolidinium dicyanamide ([C₄mpyrr-DCA]) and N-butyl-N-methylpyrrolidinium bis(trifluoromethylsulfonyl)imide ([C₄mpyrr-Tf₂N]) under room temperature was reported by the Compton's research group [61]. Cyclic voltammogram of 0.01 M SnCl₂ in [C₄mpyrr-DCA] melt showed a reduction peak of at -0.425 V and an oxidation peak at -0.234 V on Pt electrode versus Ag wire reference electrode. The diffusion coefficient of Sn (II) ions was calculated to be approximately 3.0×10^{-7} cm²/s. The cyclic voltammogram of 0.01 M SnCl₂ in [C₄mpyrr- Tf₂N] melt exhibited a reduction peak at -1.0 V and an oxidation peak at -0.13 V. The corresponding diffusion coefficient was measured as approximately 3.5×10^{-8} cm²/s. The difference on diffusion coefficient was ascribed to the viscosity of ionic liquid. Additionally, the continuous CV indicated a slow decrease for both deposition and stripping currents, suggesting the breakdown of electrolyte. It was also found that the Sn (II) species present in the electrolyte could affect the morphology of tin deposit.

A few studies on electroplating and electrochemical study of Sn from deep eutectic solvents have also been reported. Voltammetry studies of Sn in urea and glycol choline chloride-based DES were carried out by Abbott and co-workers [49]. The Sn reduction peaks were found to be -0.36 V versus silver reference electrode in both urea and glycol-based liquids. Dendritic Sn deposit was obtained from the electrolysis of 0.05 M SnCl₂ in urea and choline

chloride melt in 2:1 molar ratio electrolyte using a current density of 10 mA/cm².

The electrochemistry of Sn in ethaline melt (ethylene glycol choline chloride system in 2:1 molar ratio) DES was performed and examined in detail by Roy's research group [62]. The main Sn (II) species existing in the ionic liquid was SnCl₃⁻ and the reduction potential of Sn (II)/Sn was 0.45 V against Ag reference electrode. The voltammogram of 0.05 M SnCl₂ • 2H₂O in ethaline melt revealed a reduction peak at -0.36 V and an oxidation peak at -0.25 V on the Pt substrate with 10 mV/s scan rate. The reduction of Sn (II) was found to be an irreversible electron transfer reaction. These results were in agreement with the CV data from other types of ionic liquid which have been mentioned earlier.

The diffusion coefficient of Sn (II) in ethaline melt was calculated to be 1.96×10^{-7} cm²/s by Randles-Sevcik equation and 1.4×10^{-7} cm²/s by Levich equation in stagnant and agitated systems, respectively [62]. The limiting current density for deposition was determined to be approximately -15 mA/cm² based on the polarization data of an ethaline melt containing 0.01 M SnCl₂ • 2H₂O using 2000 rpm RDE rotation speed on the Pt substrate at 35°C. The limiting current density decreased with a decrease of temperature, RDE rotation speed or Sn (II) concentration. The Faradaic efficiency for deposition was found to be in the range between 86% and 93% in the electrolyte with Sn (II) ions concentration range from 0.01 M to 0.025 M with a temperature

range from 25°C to 55°C. The Faradaic efficiency increased with an increase of Sn (II) species concentration in the electrolyte.

Roy's research group also investigated the electrodeposition of Sn from ethaline based ionic liquid [62]. Potentiostatic deposition was conducted using 0.05 M Sn ethaline melt with -0.6V applied potential under 700 rpm RDE rotation speed and 25°C conditions. A layer of smooth silver white Sn deposit was obtained after plated by 600 seconds. However, rough Sn deposit was formed when the plating time increased to 3600 seconds while keeping other parameters unchanged, indicating that the deposit quality deteriorated with the increase of plating time.

Galvanostatic deposition of Sn was performed for 1800 seconds using the same electrolyte, RDE rotation speed and temperature [62]. The applied current density ranged from 1.57×10^{-4} A/cm² to 4.7×10^{-4} A/cm². Shiny and smooth Sn deposits were plated when the minimum current density was applied. It was found that smooth and shiny deposits could be achieved at high temperatures, fast RDE rotation rates, or low applied current density. The current efficiency was calculated to be in the range of 85% to 95%. Moreover, no variation on Faradaic efficiency and deposit morphology were observed during the long-term deposition experiments, suggesting the ionic liquid was reasonably stable. However, the deposit nucleation rate in ethaline melt DES was three to four times slower than the one in aqueous solution.

Xing also investigated the electrochemical properties and electroplating process of Sn in ethaline DES system [63]. The cyclic voltammograms of ethaline containing 0.3 M Sn ethaline at brass electrode versus Pt wire at 80°C exhibited a well-defined reduction peak at -0.42 V and oxidation peak at -0.32 V. Potentiostatic deposition of Sn in 0.3 M Sn ethaline was carried out under stagnant condition on brass foil at 80°C using the applied potential ranging from -0.5 V to -0.9 V. It was found that the deposition process could be accelerated by increasing the applied potential. Galvanostatic deposition of Sn under the same conditions were also conducted at various stirring rates. The Faradaic efficiency was found to increase with increasing agitation speed. This was attributed to the improvement of ionic mass transport of tin ions.

The SEM characterization on the galvanostatically plated Sn in ethaline DES from various applied current densities, ranging from 1 to 9 mA/cm², showed that cubic and cuboid-shaped grains could be produced. Lower roughness could also be achieved with higher applied current density, as long as the limiting current density was not exceeded. The results were in agreement with other types of ionic liquids. In addition, it was found that increasing the applied current density could also reduce the grain size and improve the grain coverage on the substrate.

2.2.2 Copper

2.2.2.1 Haloaluminate-based ionic liquids

Cu has been electrodeposited from the haloaluminate based ionic liquids. The electrochemical behaviour of copper in the aluminium chloride-N-alkyl-pyridinium halide room temperature molten salt was investigated by Hussey and co-workers [64]. Cyclic voltammogram based on glassy carbon electrode showed two reduction peaks and two oxidation peaks respectively. Cyclic voltammetry on the tungsten electrode showed similar results, although there was a difference on the peak potentials. These indicated that Cu redox reaction is a two steps electron transfer process: during the cathodic process, Cu (II) was first reduced to Cu (I) before further reduced to Cu. In the anodic process, Cu was initially oxidized to Cu (I), which was further oxidized to Cu (II). They found that the first reduction step of Cu was reversible at both electrodes, and the second reduction step was controlled by the nucleation rate at the beginning of formation of Cu deposit.

Osteryoung and Nanjundiah also studied the electrochemistry of Cu redox system in the butylpyridinium chloride-aluminium chloride ionic liquid [65]. The CV data revealed that Cu (II) underwent two steps for Cu reduction. It was found that the voltammetry could be affected by the molar ratio of aluminium chloride to BuPyCl. When the molar ratio was over 2 or less than 1, there was only one anodic and cathodic peak. When the molar ratio was in the range between 1 and 2 two anodic and cathodic peaks were observed. In

addition, potentiometric measurements showed that $[\text{CuCl}_4]^{3-}$ and $[\text{CuCl}_6]^{4-}$ complexes were found in the basic melts. In the acidic melt, $[\text{Cu}(\text{AlCl}_4)_3]^{2-}$ and $[\text{Cu}(\text{AlCl}_4)_4]^{2-}$ complexes were found to be present.

Copper electrodeposition in chloroaluminate salt was reported by Hussey and co-workers. They plated copper from aluminium chloride and 1-methyl-3-ethylimidazolium chloride (3:2 molar ratio) containing cuprous ions at 40°C [66]. The CV results based on the stationary Pt electrode against Al^{3+}/Al couple showed that there was one reduction peak at 0.85 V and one oxidation peak at approximately 0.7 V, indicating the redox reaction is a one step electron transfer process. The morphology of Cu was found to be changed dramatically with the deposition potential. The deposit produced was dense and of nodular shape at an applied potential of 0.4 V. When the potential was reduced to 0.3 V, the deposit was still dense but the nodular appearance was lost and isolated columnar growth was observed. At 0.2 V, the deposit had a composition of 21% of aluminium and became more dendritic. The deposit became completely dendritic when the applied potential was only 0.1 V. In summary, the morphology of Cu deposit deteriorated under the application of lower potential.

2.2.2.2 Air and water stable ionic liquids

Hirato *et al.* conducted the research on the electrochemical studies of copper in trimethyl-*n*-hexylammonium bis((trifluoromethyl)sulfonyl)amide ([TMHA-Tf₂N]) room temperature molten salt [67]. They reported that the electrochemical window of such electrolyte was 5.6 V at 50°C. Cyclic voltammogram based on Pt electrode versus I⁻/I₃⁻ couple showed that there were three reduction peaks at 0.0 V, 0.6 V and -1.3 V, respectively. Three anodic peaks were observed at 1.3 V, 0.5 V and -0.7 V. The additional peak may be attributed to the impurity such as water. Cyclic voltammetry also indicated that Cu (I) was stable in the electrolyte, but metal Cu was oxidized by Cu (II) species via comproportionation reaction. Moreover, the Faradaic efficiencies of cathodic reaction and anodic dissolution reaction were close to 100%.

Copper plating in 1-butyl-1-methylpyrrolidinium

bis(trifluoromethylsulfonyl)amide ([BMP]Tf₂N) ionic liquid was investigated by the Endres' research group [68]. Cyclic voltammogram of the electrolyte containing 60 mmol/L cuprous ion on the Pt electrode against Pt quasi-reference electrode showed one reduction peak at -0.1 V and one oxidation peak at 0.1 V. The Cu ionic species present in the ionic liquid was Cu (Tf₂N). The reduction potential shifted towards positive with an increase of current density when the temperature increased. The electrodeposition of copper was performed on the gold substrate with a constant potential of -0.25 V for 2

hours at 25°C. SEM micrograph showed that the deposit was dense with smooth crystals and the average grain size was approximately 50 nm.

Nanocrystalline structure was formed without the use of additives. Cu deposit plated at -0.12 V for 2 hours at 100°C exhibited in microcrystalline particulate structure. These deposits were pure metallic copper according to the EDX analysis.

The electrochemical behaviour and electrodeposition of copper was also studied in tri-n-octylmethylammonium chloride room temperature molten salt (TOMAC) by Dhahbi and Assaker [69]. The electrochemical window was measured as 2.4 V and 1.4 V on the Pt and Au substrate versus Ag reference electrode, respectively. Cyclic voltammogram of the electrolyte containing 0.025 M Cu(II) on glassy carbon electrode showed two reduction peaks at 0.25 V and -0.80 V, and the corresponding oxidation peaks at -0.05 V and 0.80 V. Cu was plated on glass doped with ITO substrate at constant potential of -1.2 V for 30 minutes at room temperature. The SEM revealed that the deposit was moderately dense with smooth crystallites, although the substrate surface did not show full coverage of Cu. The average grain size was approximately 1 µm.

Sun and co-workers investigated the electrochemistry of copper in the 1-ethyl-3-methylimidazolium tetrafluoroborate ([EMIM]BF₄) ionic liquid in developing novel electrolyte applied in electrochemical capacitors [70]. One cathodic and one anodic peak were observed at -0.3 V and 0.5 V in the cyclic voltammogram on activated carbon substrate. This indicated the two electrons

transfer reaction between Cu (II) to Cu. Cu (I) was formed as an intermediate and adsorbed state. The charging/discharging processes in the electrochemical capacitor were different compared to the normal mechanism of copper electrodeposition and dissolution reactions, where two reduction and oxidation peaks should be appeared in the CV scan.

The electrodeposition of copper in $[\text{Cu}(\text{CH}_3\text{CN})_n][\text{Tf}_2\text{N}]$ ($n = 2, 4$) ionic liquid was examined by Brooks and his colleague [71]. Cyclic voltammetry showed that there was one oxidation peak at 0.12 V. However no cathodic peak was observed, indicating there was no limiting current density in such electrolyte system. High current density such as 25 A/dm² could be achieved due to the very high mass transport of copper ion. Smooth copper deposit was obtained at a constant current density of 25 A/dm².

Furthermore, they also investigated the electrochemical characters of another two similar types of ionic liquid $[\text{Cu}(\text{MeCN})_n][\text{Tf}_2\text{N}]$ and $[\text{Cu}(\text{PhCN})_n][\text{Tf}_2\text{N}]$ ($n = 2, 4$) [72]. Cu (I) was found to be present in these compounds. Cyclic voltammogram showed that there was no cathodic peak in $[\text{Cu}(\text{MeCN})_n][\text{Tf}_2\text{N}]$, indicating the mass transport of copper ions is not limited by the diffusion process. For $[\text{Cu}(\text{PhCN})_n][\text{Tf}_2\text{N}]$ the cathodic peak was not well-defined. In addition, the current density in $[\text{Cu}(\text{MeCN})_n][\text{Tf}_2\text{N}]$ was significantly higher than $[\text{Cu}(\text{PhCN})_n][\text{Tf}_2\text{N}]$. This is ascribed to the difference in the intermolecular bond's interaction between cuprous ions and acetonitrile or benzonitrile ligands. Rough and dendritic copper deposit was

achieved using $[\text{Cu}(\text{MeCN})_n][\text{Tf}_2\text{N}]$ electrolyte on the Pt substrate under the application of very high current density of 170 A/dm^2 at 90°C . When the current density was applied at 1 A/dm^2 , the morphology of deposit was rough and of nodular shape. The average grain size was higher than $1 \mu\text{m}$. The deposit was in fine cauliflower like morphology when the current density increased to 5 A/dm^2 . When the current density further increased to 25 A/dm^2 , the surface was uniform and wavy with no visible cracks. However, no information is available on the current efficiency from those electrodeposition experiments.

2.2.2.3 Deep eutectic solvents

Abbott *et al.* studied the electrochemical behaviours of Cu from the choline chloride deep eutectic solvents. Cyclic voltammogram were performed on the Pt electrode in 0.1 M cupric chloride dehydrate salt in 1:2 molar ratio of ChCl urea based ionic melt [73]. The results showed two distinct reduction peaks at 0.43 V and -0.45 V , indicating the Cu (II)/Cu (I) and Cu (I)/Cu reactions couple. Two oxidation peaks at -0.12 V and 0.56 V were also observed. The voltammetry on the cupric chloride dehydrate salt in 1:2 molar ratio of ChCl ethylene glycol versus Ag quasi-reference electrode revealed the same results. The diffusion coefficients of copper species were measured as $4.27 \times 10^{-8} \text{ cm}^2/\text{s}$ and $3.01 \times 10^{-7} \text{ cm}^2/\text{s}$ in ChCl urea and ChCl ethylene glycol based melt. The viscosities were determined as 120 cP and 17 cP respectively.

The theoretical Faradaic efficiencies of deposition in both ionic liquids were close to 100% based on the calculation from the charge-mass balance.

The electrochemistry of Cu (II) in ChCl urea deep eutectic solvents was also examined by Popescu and co-workers [74]. The electrochemical window was measured from -1.2 V to 1.2 V versus Ag quasi reference electrode. Three reduction peaks were observed from cyclic voltammogram which was performed on the Pt electrode in a molar ratio of 1:2 ChCl urea melt containing 0.05 M cupric chloride salt. The additional peak was presumably attributed to the water contamination. The results were very similar to the [TMHA-Tf₂N] ionic melt [67]. There were two Cu reduction peaks at 0.20 V and -0.50 V and two Cu oxidation peaks at -0.05 V and 0.65 V, respectively, indicating the Cu (II)/Cu (I) and Cu (I)/Cu redox couples. When the scan rate increased, the reduction peak potential shifted towards negative and the oxidation peak potential shifted towards positive. In addition, it was found that the Cu (I)/Cu couple was quasi-reversible and Cu (II)/Cu (I) was reversible.

Lloyd and his colleague investigated the kinetics of Cu (II)/Cu (I) redox couple in the ChCl ethylene glycol deep eutectic solvents [75]. The UV-Vis spectrum showed that [CuCl₄]²⁻ was the main ionic complex in the Cu (II) solution, and [CuCl₃]²⁻ was the main cationic component in the Cu (I) solution. The diffusion coefficients were measured as 2.7×10^{-7} cm²/s and 1.5×10^{-7} cm²/s for Cu (I) and Cu (II) complexes, respectively. The dynamic viscosity of such electrolyte containing 0.5 mM copper salt was determined as

approximately 41 mPa s. In addition, the reaction rate constant and charge transfer coefficient of Cu (II)/Cu (I) couple were measured as 9.5×10^{-4} cm/s and 0.25, accordingly.

Pollet's group conducted the research on Cu electrodeposition in glyceline 200 (made with ChCl and glycerol) DES [76]. Cyclic voltammetry was performed in glyceline 200 ionic liquid containing 2 g/L cupric chloride on the Pt electrode. Two cathodic peaks were found at 0.460 V and 0.408 V as well as two anodic peaks at -0.217 V and 0.608 V. The diffusion coefficient of Cu (II) was estimated as 7.41×10^{-12} m²/s.

Cu electrodeposition in ChCl ethylene glycol based ionic liquid was studied by Ghosh [62]. The density was measured in the range of 1.11 g/cm³ to 1.15 g/cm³ in a temperature range of 20°C to 55°C with a cupric ion concentration range from 0.01 M to 0.2 M. The conductivity was measured between 4 mS/cm and 25 mS/cm and viscosity was determined between 24 cP and 57 cP. Cyclic voltammetry was carried out using Pt electrode at 25°C with an electrolyte containing 0.1 M cupric chloride dehydrate. There were two reduction peaks at 0.35 V and -0.45 V and two oxidation peaks at -0.18 V and 0.45 V, respectively. It was also found that Cu (II)/Cu (I) reaction was a reversible process, whereas Cu (I) to Cu was not. The diffusion coefficients of Cu (II) and Cu (I) were calculated as 1.22×10^{-7} cm²/s and 2.00×10^{-7} cm²/s. Another set of cyclic voltammetry studies under various agitation were performed. The limiting current density was determined from the scanning

potential after -0.6 V where the second current plateau appeared. Theoretical current efficiency was determined in the range of 98% to 110% by charge calculation from the voltammogram.

The electrodeposition of copper was performed in both potentiostatic and galvanostatic mode. In potentiostatic deposition, the applied potential was set to -0.6 V versus Ag wire at 700 rpm RDE speed. A layer of poor and thin brown copper deposit was obtained in 0.05 M cupric ion concentration. The deposit became homogeneous and in bright pink colour when the cupric ion concentration increased to 0.2 M. In addition, the morphology of Cu deposit was rough when the RDE rotation speed was set to 1300 rpm. When the RDE rotation speed decreased to 700 rpm, the morphology of deposit improved and became more adherent. Moreover, it was reported that high temperature and plating current could lead to rough morphology. The galvanostatic deposition was conducted within mass transfer limit. The plating current density was applied as 4.7×10^{-3} A/cm², which was 78% of limiting current density, and in the condition of 700 rpm RDE rotation speed at 25°C. A layer of dense and homogeneous Cu deposit was achieved with a 97% Faradaic efficiency which was determined using gravimetric method. SEM analysis showed that the average grain size was approximately from 100 nm to 200 nm and it was not affected by the deposit thickness. EDX analysis showed that the composition of Cu was approximately 98% and the remaining 2% came from chlorine and carbon, which could be the result of the electrolyte breakdown.

Xing also investigated Cu electrodeposition in ChCl based deep eutectic solvents [63, 95]. The viscosity of ethaline (ChCl: ethylene glycol in 1:2 molar ratio) containing 1 M cupric chloride dihydrate salt ranged between 10 mPa s and 35 mPa s in a temperature range of 30°C to 100°C. The conductivity was measured in the range of 7.5 mS/cm to 36 mS/cm. For reline (ChCl: urea in 1:2 molar ratio) containing 1 M cupric chloride dihydrate salt, the viscosity ranged between 25 mPa s and 450 mPa s and the conductivity ranged between 2 mS/cm and 24 mS/cm. UV-Vis spectroscopy showed that the $[\text{CuCl}_4]^{2-}$ complexes were present in the ethaline based system and $[\text{Cu}(\text{NH}_3)_4]^{2+}$ complex was the major cationic component in reline based system. Cyclic voltammograms on ethaline with 0.1 M cupric chloride dihydrate revealed that there were two cathodic peaks at -0.25 V and -1.05 V, and two anodic peaks -0.55 V and 0.00 V, respectively, indicating the Cu redox reactions were two steps of electron transfer process.

Cu electrodeposition was performed in ethaline DES and the effects of temperature and cupric concentration were also examined. Based on SEM results, when the temperature increased from 30°C to 80°C, the plated Cu film became more compact and non-porous. The grain size also increased and surface was much smoother. EDX analysis showed that the main component of deposit was copper. Small amount of oxygen was detected and this may be attributed to the partial oxidation of Cu surface. The Faradaic efficiency decreased from 50% to 30% when the temperature increased. Additional sets

of electrodeposition experiments were carried out under various cupric ion concentrations at 80°C. The deposit was in black colour in 0.01 M cupric concentration and became bright when the concentration increased to 1 M.

The effects of pulse current were also investigated in a condition of 0.5 duty cycle, 100 s pulse on-time and 7 mA/cm² peak current density. It was found that the current efficiency drastically increased from 56% to over 90%, by DC plating. This was explained by the replenishment of cupric ions during pulse off-time. Current efficiency tended to increase with higher frequency. In addition, The SEM images showed that finer and more regular grains were formed under the application of pulse current. The side reaction such as hydrogen evolution reaction could be inhibited due to the unique mass transport characteristics of pulse deposition.

2.3 Summary of studies of metal electrodeposition from aqueous solutions using pulse current

2.3.1 Tin

Sn deposition from aqueous electrolytes by pulse plating have been investigated in a number of studies. As previously described, Sn was plated either from alkaline solutions or acidic electrolytes. Very little research has been done on pulse plating of Sn from alkaline baths. Only one comprehensive study was carried out by Hansal and co-workers, who examined the effects of

pulse parameters on the physical and electrochemical properties of Sn deposit from sodium stannate $\text{Na}_2\text{Sn}(\text{OH})_6$ alkaline electrolyte [77]. They found that the electrochemical tin reduction reaction was under mass transport control rather than kinetic control, since the limiting current density was in linear relationship to the reverse of square root of angular velocity based on the Levich plot.

Cyclic voltammetry was performed on the polished steel substrate using 10 mV/s scan rate at 70°C. The data showed that there was one reduction peak at -1300 mV and two oxidation peaks at -1000 mV and -806 mV under stationary condition when the cathodic limit was set to -2000 mV, respectively. The two anodic peaks indicated that oxidation reaction of Sn to Sn (II) and Sn (II) to Sn (IV). However, only one anodic peak was shown at -1000 mV under agitation condition, suggesting the oxidation of Sn (II) to Sn (IV) was not initiated.

Deposit properties of Sn under DC condition were studied via Hull cell tests. Sn deposits were porous and dendritic when the applied current density exceeded the limiting current density, which also lead to solution breakdown and the occurrence of hydrogen evolution reaction. Sn layer was smoother and in matt colour when the applied current density was lower. Another reason for smoother deposits was the slower rate of oxidation process of Sn to Sn (II), which further underwent disproportionation reaction of Sn (II) to Sn and Sn

(IV). However, it was found that the deposit surface became rough and dendritic if the applied current density was very low.

Sn electrodeposition using pulse current was also studied. Powdery tin deposits were reported under high applied current density and low pulse off-time. The results were similar to the ones of using DC plating. However, the quality of Sn deposit significantly improved and became much smoother when the duty cycle was reduced to 10%. The deposit became powdery when the applied current density increased again. The deposit morphology depended on the hydrogen evolution reaction and desorption of hydrogen bubbles from cathode surface. In addition, the duration of pulse off-time was an important parameter for the successful hydrogen desorption process.

Another aspect studied in these electrodeposition experiments was the effect of pulse parameters on current transients. It was reported that current did not relax completely if the pulse on-time was less than 5 ms. The formation of stable plating current and potential could not be established due to the charging and discharging process of electrical double layer at the electrode surface. Therefore, a minimum of 10 ms pulse on-time was suggested for alkaline electrolyte system. However, short pulse on-time could lead to current overshooting and enhanced hydrogen evolution reaction, which disturbed the formation of Sn layers and increased surface roughness.

Sn electrodeposition from an acidic bath was reported by a number of researchers. Lam and co-workers studied the electrochemical behaviours and

deposit morphology under various pulse parameters in the solution containing tin sulphate and sulphuric acid without any additives [78]. They found that the Faradaic efficiency decreased as the duty cycle was lowered, which was ascribed to the charging phenomena of electrical double layer. In addition, the microstructure of tin deposit was related to the pulse parameters and long pulse on-time or DC condition led to dendrite or needle-type deposits. Short pulse on-time with high current density could form smooth deposit with fine crystallinity.

Wouters and his colleagues conducted the research on the effects of organic additives on pulse plating of tin in the acidic electrolyte, which consisted of sulphate and sulphuric acid with various types of organic additives [79]. The polarization curves showed that the deposition potential versus Ag reference electrode shifted from -500 mV to -1050 mV when Culmo, which is a type of commercially available organic additive, was present. Smooth and bright tin deposit was achieved by using the Culmo additive. In comparison, dendritic deposits were formed in the Culmo-free electrolyte. Nodule formation was observed during the plating of tin multilayers due to the deficient adsorption of Culmo additive.

In addition, it was found that the multilayer properties depended on the type of additive. The use of various additive led to differences in smoothness, grain size, deposit compactness and density [80]. Apart from Culmo, a number of commercially available or self-composed additives were tested against the

Culmo additive [79]. It was found that all additives were able to allow the deposition potential shifted towards negative, as similar to Culmo. One of the additives, which contained sodium gluconate, polyethylene, p-anisaldehyde and formaldehyde, could eliminate or minimize nodule formation. Moreover, tin deposit also became significantly smoother by the application of those additives.

Vicenzo *et al.* conducted the studies on pulse plating of matt tin and investigated the influence of pulse parameters on the microstructure from acidic methanesulphonate bath [81]. DC plating was also performed and served as a comparison. They claimed that current efficiencies were approximately 90% when 5 and 10 A/dm² current density applied, and 85% when 20 A/dm² current density applied in DC condition. The SEM results showed that the average grain size decreased from 6.1 μm to 4.6 μm when the current density increased. In addition, increasing the current density could also lead to clear grain boundaries and recesses formation.

Pulse plating experiments were carried out with duty cycle ranging between 5% and 60%, and pulse on-time ranging between 0.3 ms and 600 ms. The selection of these pulse plating parameters was to examine a wide range of pulse conditions. The average current density was fixed as 10 A/dm². Other parameters, such as operating temperature, were kept constant and as the same value as DC condition. It was reported that the Faradaic efficiency decreased with the decrease of duty cycle. In addition, the current efficiency also

decreased with the increase of current density whilst maintaining the same frequency. Current efficiency became significantly lower when pulse on-time was very short. This was attributed to the time needed for the charging of electrical double layer, as was observed in the alkaline solution.

SEM analysis showed that the surface became rougher with the increase of duty cycle. Clear grain boundaries and pores formed at large duty cycles. This was in agreement with the results from DC plating as mentioned above. The average grain size of tin deposit ranged between 4 μm and 6.5 μm . Pulse parameters also affected the grain size. For instance, there was a 25% reduction in grain size when the duty cycle decreased from 60% to 5%, and an approximate 30% reduction on grain size when the frequency increased from 1 Hz to 1000 Hz.

2.3.2 Copper

The application of pulse current in copper plating was initiated firstly in the printed circuit boards (PCB) manufacturing to improve the deposit microstructure and mechanical properties [80]. In 1970, Lamb and his co-workers conducted a comprehensive review on copper electrodeposition including plating by periodic reversal current, which is the same term named as pulse reverse current [82]. It was reported that significant improvements on physical properties of Cu, for instance tensile and yield strengths, were

achieved by using pulse plating. In addition, thicker deposit with increased internal stress was produced with a decrease of grain size. Plating from the sulphate baths showed that the resistivity of deposit was also increased. However no significant effects were observed on the deposit density.

Popov and his colleagues examined the effects of pulse current on the deposit quality in acidic copper sulphate electrolyte system [83]. Experimental plating results were tested and compared to corresponding theoretical models and simulations. They reported that the increase of pulse frequency could lead to lower limiting current density due to the shape deformation of pulse overpotential. The Faradaic efficiencies were found to be approximately 100%. Smoother copper deposit was achieved under the condition of sinusoidal pulse current regime with a frequency of 10^5 Hz at an effective overpotential of 200 mV, and rectangular pulse current regime with a frequency of 10^3 Hz at an effective overpotential of 116 mV. The deposit roughness and porosity were affected by the pulse duty cycle [80]. Smooth and dense deposit was achieved when the duty cycle and pulse time decreased to certain limit, beyond which no improvement on the microstructure was observed. Additionally, the deposit plated by unipolar pulse current was smoother than the one using DC at the same average current density.

The mechanism of pulse plating of copper and its relationship to Faradaic efficiency in acidic cupric sulphate bath were investigated by Tsai *et al* [84]. The pulse period was studied in a range from 0.02 to 200 ms. They

found that the Faradaic efficiency decreased with time shortening in the range of millisecond, this was due to the dissolution of copper adatoms as well as disproportionation reaction of cuprous ion in the charge transfer and surface diffusion-controlled kinetics system. However in the microsecond range, the current efficiency increased with shorter pulses, since adatoms were incorporated into the crystals and the dissolution of copper adatoms or disproportionation reaction of cuprous ions were suppressed.

Yeow and Hibbert examined the mechanism of galvanostatic plating of copper by pulse current from acidic copper halide electrolyte [85]. They reported that cuprous halide was formed due to the comproportionation reaction between copper and cupric halide. It was found that a monolayer of copper was formed during the pulse on-time and dissolved into the solution and formed cuprous halides during the pulse off-time.

White studied the effects of various pulse conditions on Faradaic efficiency in pulse plating of copper from acidic sulphate solution with additives [86]. The current efficiency decreased when the anodic current increased from 0 to 8 A/dm² because of the increase in formation of cuprous ions near the electrode surface. The current efficiency also decreased when the pulse period increased from 1 to 100 ms, since the potential at lower pulse frequencies could not attain the same value achieved when a higher frequency was applied. When polyethylene glycol (PEG) or chloride was added into the electrolyte there was little effect on the current efficiency. However the

Faradaic efficiency decreased significantly when both PEG and chloride were present in the solution. This was attributed to the enhanced stabilization of cuprous ions at the electrode surface by the adsorption of Cl^- to PEG- Cu^+ polymer complexes.

The effect of mass transport on current efficiency in copper pulse electrodeposition were studied by Chene and Landolt [87]. A rotating electrode was used to control the ionic mass transport conditions. The results showed that granular dense deposits were achieved when the applied peak density was lower than the pulse limiting current density. Dendritic deposit was obtained when the pulse limiting current density was exceeded, regardless of the values of pulse parameters. The current efficiency also decreased when the applied peak current density was higher than the pulse limiting current density. In addition, current efficiency increased with the deposit thickness, since the effective surface area became larger.

El-Shazly *et al.* investigated the effects of applying high frequency pulse parameters on deposit microstructure in the electrolyte containing 1.5 M copper sulphate and 0.5 M sulphuric acid [88]. They claimed that columnar crystals deposit was achieved when the pulse frequency was set in the range between 1,000 and 3,000 Hz. Fine equiaxed structure deposit was plated at 10,000 Hz with duty cycles ranged between 0.5 and 0.7. The deposit turned into columnar shape when the duty cycle was reduced into the range of 0.3 to

0.4. When the duty cycle increased to 0.8, the deposit became large equiaxed crystals.

Imaz and co-workers conducted similar research on the influences of pulse parameters on deposit morphology and mechanical properties of copper plating [89]. They found that the deposit plated by DC without additives was compact and smooth. Coarser and rougher needle-shape copper grain was obtained when pulse current was applied at the lowest duty cycle. When the duty cycle increased, the morphology became polyhedric and copper coating became coherent, dense and homogeneous, since the pulse condition with larger duty cycle was similar to DC condition. However, these results seemed in conflict with some of the mentioned literature, which claimed that the pulse plating should be able to improve the deposit microstructure and properties compared to DC condition.

Moreover, they examined the effects of thiourea (TU) and gelatine (GE) additives on the deposit properties and structure [89]. Chloride ions were also added in the solution to improve the levelling effect and adsorption of those additives during copper plating. SEM analysis showed that the morphology turned from polyhedric to dendritic after adding small amount of chloride with TU and GE, suggesting the morphology was not improved with the addition of both additives. EBSD analysis was carried out on the cross section of copper coating and revealed that the deposit had a coarse columnar structure without additives. When the TU additive was present during the

plating process, the structure became distorted. In addition, the increase of TU concentration led to more fibrous microstructure. The deposit changed to equiaxed structure with smaller grain size when GE additive was present. In addition, denser deposit with finer grains could be achieved by either increasing the pulse current density to 30 A/dm² or decreasing the pulse off-time to 5 ms in the GE additive baths.

Natter and Hempelmann studied the effects of citric acid on pulse electrodeposition of Cu [90]. Nano-crystalline copper deposit was obtained using citric acid additive, which played as a role of inhibitor of nuclei growth. The grain size decreased from over 50 nm down to 11 nm when the concentration of citric acid increased from 0 to 100 g/L under 125 A/dm² peak current density, 1 ms pulse on-time and 100 ms pulse off-time pulse conditions. The grain size became larger when the duty cycle became smaller, either by decreasing pulse off-time or increasing pulse on-time, at a constant average current density.

Tao and Li also plated nanocrystalline copper deposit using pulse current from the acidic copper sulphate baths with TU additive [91]. AFM analysis showed that the grain size of deposit plated by DC was approximately 98 nm, and 26 nm for the deposit plated by pulse current. The pulse electrodeposit was smoother with higher throwing power than the deposited plated by DC, since higher instantaneous peak current density could be achieved by pulse plating. They claimed that the growth of nuclei and

crystallites was significantly inhibited when high plating density was applied. Additionally, longer pulse off-time could sufficiently replenish the depleted ions at the electrode surface and the existing crystals were stabilized. On the other hand, the adsorption of TU molecules on the active sites was improved and nuclei growth was even further suppressed.

Roy and Landolt investigated the empirical range of parameters in copper electrodeposition by using pulse reverse current from acidic sulphate baths [92]. They reported that the pulse on-time should be limited in the range of 1 to 1000 ms and duty cycle be smaller than 0.5. The magnitude of cathodic and anodic current density could affect the deposit microstructure. N_m and N_p are two parameters indicating the mass transfer condition. For instance, when the steady state mass transfer number N_m was under 0.3 the deposit was in powders. Dense deposit was obtained when N_m increased to 0.4 to 0.6 with a transient mass transfer number N_p closing to 1. Dendritic, columnar and non-compact deposits was achieved when either N_m or N_p exceeded 1.0.

Pearson and Dennis studied how the structure of copper deposit was affected by pulse reverse current using acidic solutions containing organic additives such as polyether and sulphopropyl sulphides (SSP) [93]. The pulse parameters were set according to the standards utilized in the industrial PCB manufacturing process with a condition of 10 ms pulse on-time, 0.5 ms pulse off-time, 3.7 A/dm² cathodic peak current density and 11.1 A/dm² anodic current density. When no additives were present, the grain size plated by pulse

reverse current was larger than DC. When 75 ppm polyether was added, the grains became more uniform in pulse reverse plating than DC plating, although both groups had smoother deposits. When both SSP and polyether were added, the grain size in DC plating increased and smoother deposit was achieved by pulse reverse plating.

Tantavichet and Pritzker investigated the effect of benzotriazole (BTA) additive in pulse plating of copper [94]. BTA was commonly used as a type of corrosion inhibitor for copper, but also was served as surface brightener in electrodeposition. They found that the addition of chloride ion could eliminate the major beneficial effects of BTA with dull and rough deposit produced. The reason suggested was the mass transport of BTA molecules to the substrate surface was hindered by the introduction of chloride ions.

Pulse plating experiments with BTA were also conducted without the addition of chloride ions [94]. The results showed that plating at low pulse frequency (50 Hz) and small duty cycle (such as 20%) produced smoother and brighter grains, which were similar to the ones plated under DC condition. The deposit has a large grain and rough structure compared to the ones plated without BTA addition. The morphology significantly improved when the duty cycle increased to 50% and 80%. In addition, the grains became denser and smoother when the pulse frequency increased to over 50 kHz compared to the one without BTA, regardless of the duty cycle. In addition, pulse reverse plating was performed under the condition of 6 A/dm² for both cathodic and

anodic current densities with 83.3% duty cycle. Deposit with very rough morphology and large grain size was achieved at 50 Hz pulse frequency. When the pulse frequency increased to over 500 Hz, the deposit became smoother and brighter due to the suppression of dissolution by the electrical double layer effect.

This chapter firstly described the classification of ionic liquids with corresponding electrochemical studies performed by the researchers, followed by the summarization of major studies of metal electrodeposition in DES and pulse plating separately for copper and tin. However, few researches have been conducted while combining the use of DES in pulse deposition except for the preliminary experiments from Xing, and therefore highlights the research gap and the importance of this piece of research. The next chapter would elaborate the fundamental knowledge of electrochemistry and electrodeposition related to the experimental work before the results interpretation.

Reference List

1. Endres F., Abbott A., Macfarlane D. (2017). Electrodeposition from Ionic Liquids. 2nd ed. Wiley-VCH. Germany
2. Kruesi W.H., Fray D.J. (1993). The electrowinning of lithium from chloride-carbonate melts. Metallurgical Transactions B. 24 (4) pp 605-615
3. Fray D.J., Chen G.Z. (2004). Reduction of titanium and other metal oxides using electrodeoxidation. Materials Science and Technology. 20 (3) pp 295-300
4. Grjotheim C., Krohn M., Malinovsky K.M., Thonstad J. (1982). Aluminium Electrolysis. 2nd ed. Aluminium- Verlag. Dusseldorf.
5. Hurley F.H., Wier T.P. (1951). Electrodeposition of metals from fused quaternary ammonium salts. Journal of the Electrochemical Society. 98 (5) pp 203-206
6. Hurley F.H., Wier T.P. (1951). The electrodeposition of aluminium from nonaqueous solutions at room temperature. Journal of the Electrochemical Society. 98 (5) pp 207-212
7. Gale R.J., Gilbert B.G., Osteryoung R.A. (1978). Raman spectra of molten aluminium chloride: 1-butylpyridinium chloride systems at ambient temperatures. Inorganic Chemistry. 17 (10) pp 2728-2729
8. Osteryoung R.A., Robinson J. (1979). An electrochemical and spectroscopic study of some aromatic hydrocarbons in the room

- temperature molten salt system aluminium chloride-n-Butylpyridinium chloride. *Journal of the American Chemical Society*. 101 (14) pp 3776-3779
9. Gale R.J., Osteryoung R.A. (1978). Potentiometric investigation of dialuminum heptachloride formation in aluminium chloride-1-butylpyridinium chloride mixtures. *Inorganic Chemistry*. 18 (6) pp 1603-1605
 10. Wilkes J.S., Levisky J.A., Wilson R.A., Hussey C.L. (1982). Dialkylimidazolium chloroaluminate melts: a new class of room-temperature ionic liquids for electrochemistry, spectroscopy, and synthesis. *Inorganic Chemistry*. 21 (3) pp 1263-1264
 11. Fannin A.A.Jr., Floreani D.A., King L.A., Landers J.S., Piersma B.J., Stoch D.J., Vaughn R.L., Wilkes J.S., Williams J.L. (1983). Properties of 1,3-dialkylimidazolium chloride-aluminium chloride ionic liquids. 2 phase transitions, densities, electrical conductivities, and viscosities. *Journal of Physical Chemistry*. 88 (12) pp 2614-2621
 12. Welton T. (1999). Room-temperature ionic liquids. Solvents for synthesis and catalysis. *Chemical Reviews*. 99 (8), pp 2071-2084
 13. Abbott A.P., Mckenzie K.J. (2006). Application of ionic liquids to the electrodeposition of metals. *Physical Chemistry Chemical Physics*. 8 pp 4265-4279

14. Zell C.A., Endres F., Freyland W. (1998). Electrochemical in situ STM study of phase formation during Ag and Al electrodeposition on Au (111) from a room temperature molten salt. *Physical Chemistry Chemical Physics*. 1 pp 697-704
15. Wilkes J.S., Zaworotko M.J. (1992). Air and water stable 1-ethyl-3-methylimidazolium based ionic liquids. *Journal of the Chemical Society, Chemical Communications*. pp 965-967
16. Wilkes J.S. (2002). A short history of ionic liquids – from molten salts to neoteric solvents. *Green Chemistry*. 4 pp 73-80
17. Smith E.L., Abbot A.P., Ryder K.S. (2014). Deep eutectic solvents (DESS) and their applications. *Chemical Reviews*. 114 pp 11060-11082
18. Fuller J., Carlin R.T., Osteryoung R.A. (1997). The room temperature ionic liquid 1-ethyl-3-methylimidazolium tetrafluoroborate: electrochemical couples and physical properties. *Journal of the Electrochemical Society*. 144 (11) pp 3881-3886
19. Chauvin Y., MuBmann L., Olivier H. (1995). Flussige 1,3-dialkylimidazoliumsalze als losungsmittel fur die katalyse in zweiphasensystemen: durch rhodiumkomplexe katalysierte hydrierung, isomerisierung und hydroformylierung von alkenen. *Angewandte Chemie*. 107 (23) pp 2941-2943
20. Noda A., Hayamizu K., Watanabe M. (2001). Pulsed-gradient spin-echo ^1H and ^{19}F NMR ionic diffusion coefficient, viscosity, and ionic

- conductivity of non-chloroaluminate room-temperature ionic liquids.
Journal of Physical Chemistry B. 105 (20) pp 4603-4610
21. Golding J., Hamid N. MacFarlane D.R., Forsyth M., Forsyth C., Collins C., Huang J. (2001) N-methyl-N-alkylpyrrolidinium hexafluorophosphate salts: novel molten salts and plastic crystal phases. Chemistry of Materials. 13 (2) pp 558-564
 22. Meindersma G.W., Podt A., de Haan A.B. (2006). Ternary liquid-liquid equilibria for mixtures of an aromatic + an aliphatic hydrocarbon + 4-methyl-N-butylpyridinium tetrafluoroborate. Journal of Chemical & Engineering Data. 51 (5) pp 1814-1819
 23. Hagiwara R., Ito Y. (2000). Room temperature ionic liquids of alkylimidazolium cations and fluoroanions. Journal of Fluorine Chemistry. 105 (2) pp 221-227
 24. Carlin R.T., Long H.C.D, Fuller J. Trulove P.C. (1994). Dual intercalating molten electrolyte batteries. Journal of the Electrochemical Society. 141 (7) pp L73-L76
 25. Bonhote P, Dias A.P, Papageorgiou N., Kalyanasundaram K., Gratzel M. (1996). Hydrophobic, highly conductive ambient-temperature molten salts. Inorganic Chemistry. 354 (5) pp 1168-1178
 26. Papageorgiou N., Athanassov Y., Armand M., Bonhote P., Pettersson H., Azam A., and Gratzel M. (1996). The performance and stability of

- ambient temperature molten salts for solar cell applications. *Journal of the Electrochemical Society*. 143 (10) pp 3099-3108
27. Howlett P., MacFarlane D.R., Hollenkamp A.F. (2004). High lithium metal cycling efficiency in a room-temperature ionic liquid. *Electrochemical and Solid-State Letters*. 7 (5) pp A97-A101
28. Chan S.S, Willis C.J. (1968). Trifluoromethyl-substituted fluorophosphates and fluoroarsenates. *Canadian Journal of Chemistry*. 46 (8) pp 1237-1248
29. Schmidt M., Heider U. Kuehner A., Oesten R. Jungnitz M., Ignat'ev N., Sartori P. (2000). Lithium fluoroalkylphosphates: a new class of conducting salts for electrolytes for high energy lithium-ion batteries. *Journal of Power Source*. 97-98 pp 557-560
30. Ignat'ev N.V., Welz-Biermann U. Kucheryna A., Bissky G., Willner H. (2005). New ionic liquids with tris(perfluoroalkyl)trifluorophosphate (FA) anions. *Journal of Fluorine Chemistry*. 126 (8) pp 1150-1159
31. Pringle J.M., Golding J., Forsyth C.M., Deacon G.B., Forsyth M., MacFarlane D.R. (2002). Physical trends and structural features in organic salts of the thiocyanate anion. *Journal of Materials Chemistry*. 12 pp 3475-3480
32. Kumara G.R.A, Shiratsuchi K., Konno A., Tsukahara J., Tennakone K. (2002). Dye-sensitized solid-state solar cells: use of crystal growth

- inhibitors for deposition of the hole collector. *Chemistry of Materials*. 14 (3) pp 954-955
33. Meng Q.B., Takahashi K., Zhang X.T., Sutanto I., Rao T.N., Sato O., Fujishima A. (2003). Fabrication of an efficient solid-state dye-sensitized solar cell. *Langmuir*. 19 (9) pp 3572-3574
34. Nockemann P., Thijs B., Postelmans N., Hecke K.V., Meervelt L.V., Binnemans K. (2006). Anionic rare-earth thiocyanate complexes as building blocks for low-melting metal-containing ionic liquids. *Journal of the American Chemical Society*. 128 (42) pp 13658-13659
35. MacFarlane D.R., Golding J., Forsyth S., Forsyth M., Deacon G.B. (2001). Low viscosity ionic liquids based on organic salts of the dicyanamide anion. *Chemical Communications*. pp 1430-1431
36. MacFarlane D.R., Forsyth S.A., Golding J., Deacon G.B. (2002). Ionic liquids based on imidazolium, ammonium and pyrrolidinium salts of the dicyanamide anion. *Green Chemistry*. 4 pp 444-448
37. Yoshida Y., Muroi K., Otsuka A., Saito G., Takahashi M., Yoko T. (2004). 1-ethyl-3-methylimidazolium based ionic liquids containing cyano groups: synthesis, characterization, and crystal structure. *Inorganic Chemistry*. 43 (4) pp 1458-1462
38. Bessler E., Goubeau J. (1967) Darstellung einiger cyanborverbindungen. *Zeitschrift für Anorganische und Allgemeine Chemie*. 352 pp 67-76

39. Abbott A.P., Capper G., Davies D.L., Rasheed R. (2004). Ionic liquids based upon metal halide/substituted quaternary ammonium salt mixtures. *Inorganic Chemistry*. 43 (11) pp 3447-3452
40. Hsiu S.I., Huang J.F., Sun I.W., Yuan C.H., Shiea J. (2002). Lewis acidity dependency of the electrochemical window of zinc chloride 1-ethyl-3-methylimidazolium chloride ionic liquids. *Electrochimica Acta*. 47 (27) pp 4367-4372
41. Sitze M.S., Schreiter E.R., Patterson E.V., Freeman R.G. (2001). Ionic liquids based on FeCl_3 and FeCl_2 . Raman scattering and ab initio calculations. *Inorganic Chemistry*. 40 (10) pp 2298-2304.
42. Zhang Q.G., Yang J.Z., Lu X.M., Gui J.S., Huang M. (2004). Studies on an ionic liquid based on FeCl_3 and its properties. *Fluid Phase Equilibria*. 226 pp 207-211
43. Xu. W.G., Lu X.M., Zhang Q.G., Gui J.S., Yang J.Z. (2006). Studies on the thermodynamic properties of the ionic liquid BMIGaCl₄. *Chinese Journal of Chemistry*. 24 pp 331-335
44. Yang J.Z., Tian P, He L.L, Xu W.G. (2002). Studies on room temperature ionic liquid InCl_3 -EMIC. *Fluid Phase Equilibria*. 204 pp 295-302
45. Matsumoto K., Hagiwara R., Ito Y. (2002). Room temperature molten fluorometallates: 1-ethyl-3-methylimidazolium hexafluoroniobate (V)

- and hexafluorotantalate (V). *Journal of fluorine chemistry*. 115 (2) pp 133-135
46. Noguera G., Mostany J., Agrifoglio G., Dorta R. (2005). Room temperature liquid salts of Cr and Mo as self-supported oxidants. *Advanced Synthesis & Catalysis*. 347 (2-3) pp 231-234
47. Abbott A.P., Capper G., Davies D.L., Rasheed R.K. (2004). Ionic liquid analogues formed from hydrated metal salts. *Chemistry A European Journal*. 10 (15) pp 3769-3774
48. Wang H.Y, Jing Y, Wang X.H., Yao Y., Jia Y.Z. (2011). Ionic liquid analogous formed from magnesium chloride hexahydrate and its physico-chemical properties. *Journal of Molecular Liquids*. 163 (2) pp 77-82
49. Abbott A.P., Capper G., McKenzie K.J., Ryder K.S. (2007). Electrodeposition of zinc-tin alloys from deep eutectic solvents based on choline chlorides. *Journal of Electroanalytical Chemistry*. 599 (2) pp 288-294
50. Abbot A.P., Capper G., Davies D.L., Rasheed R.K., Tambyrajah V. (2002). Novel solvent properties of choline chloride/urea mixtures. *Chemical Communications*. pp 70-71

51. Abbott A.P., Capper G., Swain B.G. Wheeler D.A. (2013).
Electropolishing of stainless steel in an ionic liquid. Transactions of the
IMF. 83 (1) pp 51-53
52. Abood H.M.A., Abbott A.P., Ballantyne A.D., Ryder K.S. (2011). Do all
ionic liquids need organic cations? Characterisation of $[\text{AlCl}_2 \cdot$
 $n\text{Amide}]^+ \text{AlCl}_4^-$ and comparison with imidazolium based systems.
Chemical Communications. 47 pp 3523-3525
53. Abbott, A.P., Harris R.C., Hsieh Y.T., Ryder K.S., Sun I.W. (2014).
Aluminium electrodeposition under ambient conditions. Physical
Chemistry Chemical Physics. 16 pp 14675-14681
54. Schaltin S., Brooks N.R., Stapper L., Hecke K.V., Meervelt L.V.,
Binnemans K. Fransaer J. (2011). High current density electrodeposition
from silver complex ionic liquids. Physical Chemistry Chemical Physics.
14 pp 1706-1715
55. Xu X.H., Hussey C.L. (1993). The electrochemistry of tin in the
aluminium chloride-1-methyl-3-ethylimidazolium chloride molten salt.
Journal of the Electrochemical Society. 140 (3), pp 618-626
56. Tachikawa N., Serizawa N., Katayama Y., Miura T. (2008).
Electrochemistry of Sn (II) / Sn in a hydrophobic room-temperature ionic
liquid. Electrochimica Acta. 53 (22) pp 6530-6534

57. Huang J.F., Sun I.W. (2003). Electrochemical studies of tin in zinc chloride-1-ethyl-3-methylimidazolium chloride ionic liquids. *Journal of the Electrochemical Society*. 150 (6) E299-E306
58. Deng. M.J., Chang J.K., Leong T.I., Fang S.W., Chen P.Y. Sun I.W. (2008). Electrodeposition of nanostructured Sn in 1-ethyl-3-methylimidazolium dicyanamide room temperature ionic liquid. *Electrochemistry*. 77 (8) pp 588-590
59. Yang W.Z., Cang H., Tang Y.M., Wang T.T., Shi Y.X. (2008). Electrodeposition of tin and antimony in 1-ethyl-3-methylimidazolium tetrafluoroborate ionic liquid. *Journal of the Applied Electrochemistry*. 38 pp 537-542
60. Morimitsu M., Nakahara Y., Iwaki Y., Matsunaga M. (2003). Electrodeposition of tin from EMI • BF₄ • Cl room temperature molten salts. *Journal of Mining and Metallurgy*. 39 (1-2) pp 59-67
61. Martindale B.C.M., Jones S.E.W., Compton R.G. (2009). A comparison of the cyclic voltammetry of the Sn / Sn (II) couple in the room temperature ionic liquids N-butyl-N-methylpyrrolidinium dicyanamide and N-butyl-N-methylpyrrolidinium bis(trifluoromethylsulfonyl)imide: solvent induced changes of electrode reaction mechanism. *Physical Chemistry Chemical Physics*. 12 pp 1827-1833

62. Ghosh S. (2013). Electrodeposition of Cu, Sn and Cu-Sn Alloy from Choline Chloride Ionic Liquid. PhD thesis. School of Chemical Engineering and Advanced Materials. Newcastle University. Newcastle
63. Xing S.J. (2014). Environmentally Friendly Baths for Cu-Sn Co-electrodeposition: Cyanide-free Aqueous Bath and Deep Eutectic Solvents. Department of Industrial Engineering, Universita DeGli Studi Di Trento. Trento
64. Hussey C.L., King L.A., Carpio R.A. (1979). The electrochemistry of copper in a room temperature acidic chloroaluminate melt. *Journal of the Electrochemical Society*. 126 (6) pp 1029-1034
65. Nanjundiah C., Osteryoung R.A. (1983). Electrochemical studies of Cu (I) and Cu (II) in an aluminium chloride-N-(n-butyl)pyridinium chloride ionic liquid. *Journal of the Electrochemical Society*. 130 (6) pp 1312-1368
66. Tierney B.J., Pitner W.R., Mitchell J.A., Hussey C.L., Stafford G.R. (1998). Electrodeposition of copper and copper-aluminium alloys from a room-temperature chloroaluminate molten salt. *Journal of the Electrochemical Society*. 145 (9) pp 3110-3116
67. Hirato T., Murase K., Nitta K., Awakura Y. (2001). Electrochemical behaviour of copper in trimethyl-n-hexylammonium bis((trifluoromethyl)sulfonyl)amide, an ammonium imide-type room

- temperature molten salt. *Journal of Applied Electrochemistry*. 31 (10) pp 1089-1094
68. Abedin S.Z.E., Saad A.Y., Farag H.K., Borisenko N., Liu Q.X., Endres F. (2007). Electrodeposition of selenium, indium and copper in an air- and water-stable ionic liquid at variable temperatures. *Electrochimica Acta*. 52 (8) pp 2746-2754
69. Assaker I.B., Dhahbi M. (2011). Electrochemical study and electrodeposition of copper in the hydrophobic tri-n-octylmethylammonium chloride ionic liquid. *Journal of Molecular Liquids*. 161 (1) pp 13-18
70. Sun G.H., Li K.X., Sun C.G. (2010). Electrochemical performance of electrochemical capacitors using Cu (II)-containing ionic liquid as the electrolyte. *Microporous and Mesoporous Materials*. 128 (1-3) pp 56-61
71. Brooks N.R., Schaltin S., Hecke K.V., Meervelt L.V., Binnemans K., Fransaer J. (2011). Copper (I)-containing ionic liquids for high-rate electrodeposition. *Chemistry a European Journal*. 17 (18) pp 5054-5059
72. Schaltin S. Brooks N.R., Binnemans K., Fransaer J. (2011). Electrodeposition from cationic cuprous organic complexes: ionic liquids for high current density electroplating. *Journal of the Electrochemical Society*. 158 (1) pp D21-D27
73. Abbott A.P. Ttaib K.E., Frisch G., McKenzie K.J., Ryder K.S. (2009). Electrodeposition of copper composites from deep eutectic solvents

based on choline chloride. *Physical Chemistry Chemical Physics*. 11 pp
4269-4277

74. Popoescu A.M., Constantin V., Cojocaru A., Olteanu M. (2011).
Electrochemical behaviour of copper (II) chloride in choline chloride-
urea deep eutectic solvent. *Revista de Chimie*. 62 (2) pp 206-211
75. Llyod D., Vainikka T., Murtomaki L., Kontturi K., Ahlberg E. (2011).
The kinetics of the $\text{Cu}^{2+} / \text{Cu}^{+}$ redox couple in deep eutectic solvents.
Electrochimica Acta. 56 (14) pp 4942-4948
76. Pollet B.G., Hihn J.Y., Mason T.j. (2008). Sono-electrodeposition (20
and 850 kHz) of copper in aqueous and deep eutectic solvents.
Electrochimica Acta. 53 (12) pp 4248-4256
77. Hansal W.E.G., Halmdienst M., Hansal S., Boussaboua I., Darchen A.
(2008). Influence of pulse plating parameters on morphology and
hardness of pure tin deposit. *Transactions of the IMF*. 86 (2) pp 115-121
78. Lam L.T., Ohno I., Saji T., Haruyama S. (1981). Pulse plating of tin in
an acidic bath. *Journal of the Metal Finishing Society of Japan*. 32 (2) pp
64-69
79. Wouters G., Bratoeva M., Celis J.P., Roos J.R. (1995).
Electrocrystallisation of tin in presence of organic additives in view of
the synthesis of NiP/Sn multilayers. *Electrochimica Acta*. 40 (10) pp
1434-1453

80. Wolfgang E., Hansal G., Roy S. (2012). Pulse Plating. Eugen G. Leuze Verlag KG. Germany
81. Vincenzo A., Bonelli S., Cavallotti P.L. (2010). Pulse plating of matt tin: effect on properties. Transactions of the IMF. 88 (5) pp 248-255
82. Lamb V.A., Johnson C.E., Valentine D.R. (1970). Physical and mechanical properties of electrodeposited copper III. Deposits from sulfate, fluoborate, pyrophosphate, cyanide, and amine baths. Journal of the Electrochemical Society. 117 (9) 291C-318C
83. Popov K.I., Keca D.N., Vidojkovic S.I. (1975). Mathematical model and digital simulation of pulsation overpotential copper electrodeposition. Journal of Applied Electrochemistry. 11 (2) pp 239-246
84. Tsai W.C., Wan C.C, Wang Y.Y. (2002). Mechanism of copper electrodeposition by pulse current and its relation to current efficiency. Journal of Applied Electrochemistry. 32 (12) pp 1371-1378
85. Yeow C.W., Hibbert D.B. (1983). Galvanostatic pulse plating of copper and copper (I) halides from acid copper (II) halide solutions. Journal of the Electrochemical Society. 130 (4) pp 786-790
86. White J.R. (1987). Reverse pulse plating of copper from acid electrolyte: a rotating ring disc electrode study. Journal of Applied Electrochemistry. 17 (5) pp 977-982

87. Chene O., Landolt D. (1989). The influence of mass transport on the deposit morphology and the current efficiency in pulse plating of copper. *Journal of Applied Electrochemistry*. 19 (2) pp 188-194
88. El-Shazly M.F., White J.L., Brooman E.W. (1987). High speed deposition using interrupted current. *Plating and Surface Finish*. 74 (5) pp 136-142
89. Imaz N., Garcia-Lecina E., Suarez C., Diez J.A., Rodriguez J., Molina J., Garcia-Navas V. (2009). Influence of additives and plating parameters on morphology and mechanical properties of copper coatings obtained by pulse electrodeposition. *Transaction of the IMF*. 82 (2) pp 64-71
90. Natter H., Hempelmann R. (1996). Nanocrystalline copper by pulsed electrodeposition: the effects of organic additives, bath temperature, and pH. *Journal of Physical Chemistry*. 100 (50) pp 19525-19532
91. Tao S., Li D.Y. (2006). Tribological, mechanical and electrochemical properties of nanocrystalline copper deposits produced by pulse electrodeposition. *Nanotechnology*. 17 pp 65-78
92. Roy S., Landolt D. (1996). Determination of the practical range of parameters during reverse-pulse current plating. *Journal of Applied Electrochemistry*. 27 (3) pp 299-307
93. Pearson T., Dennis J.K. (1990). Effect of pulsed reverse current on the structure and hardness of copper deposits obtained from acidic

electrolytes containing organic additives. *Surface and Coatings Technology*. 42 (1) pp 69-79

94. Tantavichet N., Pritzker M. (2006). Copper electrodeposition in sulphate solutions in the presence of benzotriazole. *Journal of Applied Electrochemistry*. 36 (1) pp 49-61
95. Xing S., Zanella C, Deflorian F. (2014). Effect of pulse current on the electrodeposition of copper from choline chloride-ethylene glycol. *Journal of Solid State Electrochemistry*. 18 pp 1657-1663

Chapter 3. Fundamentals of Electrochemistry and Electrodeposition

Before commencing the investigation of metal electrodeposition in DES by using pulse current, an introduction to the fundamental knowledge of electrochemistry and electrodeposition is essential. This chapter will firstly give a brief description of the mechanism of plating process, followed by the introduction of electrodeposition thermodynamics such as the definition of electrode potentials and Nernst equation. The electrochemical kinetics will then be described including capacitive effects related to the electrical double layer as well as Butler-Volmer and Tafel equations. The ionic mass transport limitation in DC plating system will also be elucidated.

In addition, this chapter will also cover fundamental knowledge of PC plating. Compared to the DC plating system these are similar but more complicated. Both the electrochemical kinetics and the ionic mass transport limitations of pulse plating will be discussed in detail, since these aspects dictate the limitations on experimental pulse parameters selection. Finally, current distribution and deposit growth mechanism will be briefly described.

3.1 Electrodeposition process

As previously mentioned, electroplating is an electrochemical process which a layer of metallic film forms on the designated substrate through reduction of metal ions by using electrical current [1, 2]. Generally, metal deposition proceeds in an electrochemical cell. The simplified electrochemical cell consists of a power supply, cathode, anode and electrolyte. Both electrodes are connected to the power source, which can either provide DC or AC, and are immersed in the electrolyte. The redox reactions are initiated when the power is switched on and applied current is provided to the electrochemical cell. Oxidation reaction occurs at the anode, where the metal atoms are oxidized into ions and dissolve into electrolyte with the release of electrons. At the same time, the reduction reaction occurs at the cathode, where the metal ions in the electrolyte are reduced into metal atoms on the substrate by consuming electrons [3]. The metallic ions migrate from the anode to cathode within the electrolyte, and the electrons are transferred from anode to cathode through the external circuit. The schematic diagram of electrochemical cell in plating process using a soluble metal anode is shown in Figure 3-1.

Theoretically, if the metals ion reduction and oxidation are balanced, depletion of ions due to reduction in the electrolyte are replenished from the anode oxidation reaction. Therefore, the concentration of metal ions in the bulk solution should be uniform throughout the redox process. The electrons

are also balanced as the number of electrons lost at the anode is the same as the number of electrons gained at the cathode. However, in reality often the metal ions are not balanced after the anode and cathode reactions due to the occurrence of side reactions such as hydrogen evolution reaction which is initiated by some of the applied current in the aqueous solution [2]. The simplified electrochemical redox reactions of metal M using soluble metal anode are shown in the equations (3.1) and (3.2).

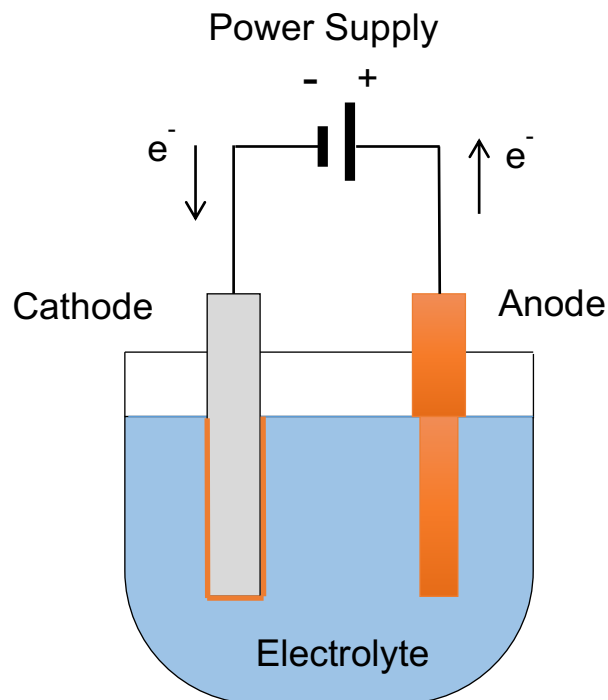
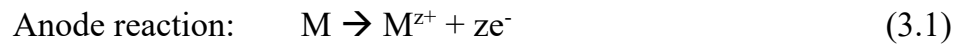


Figure 3-1 Schematic diagram of electrochemical cell in plating process

3.2 Electrodeposition thermodynamics

3.2.1 Nernst equation

When the solid metal M is immersed in the solution containing metal ions M^{z+} without the application of external current, M^{z+} ions are exchanged between the solid-liquid interface. Dynamic equilibrium is established between metal M and M^{z+} after certain period of time and the net flow of M^{z+} across the interface is zero [4]. The reversible electrode potential, or equilibrium potential is defined as the energy released or required in the half-cell reactions during the redox process. However, measurement of such potential is not straightforward. Normally it is measured against another electrode by using a reference electrode [5]. The reference is usually standardized against a standard hydrogen electrode (SHE), which is measured from the redox reaction of hydrogen under the condition of 1 atm atmospheric pressure, 1 mol/L protonic concentration and 298 K temperature. SHE is used to serve as a zero volt reference to determine the reversible electrode potential of metal under standard condition.

The equilibrium potential can be affected by a number of factors such as pressure, concentration of ions and temperature. The Nernst equation is an expression which estimates the equilibrium potential of an electrode which is not under standard state based on the standard electrode potential with the consideration of those deviations [6]. The equation of a simplified redox reaction in metal plating is expressed in equation (3.3).

Redox reaction: $M^{z+} + ze^- \rightleftharpoons M$

$$E_r = E^0 - \frac{RT}{zF} \ln \frac{a_{\text{red}}}{a_{\text{ox}}} = E^0 - \frac{RT}{zF} \ln [c_{M^{z+}}] \quad (3.3)$$

In equation (3.3), [Ox] and [Red] are the oxidized and reduced species, E_r stands for the equilibrium potential of metal M, E^0 is the standard electrode potential referred to SHE, F is Faraday constant, R is gas constant, T is absolute temperature, z is the number of electron transferred in the redox reaction, a is the chemical activity for the species, a_{red} and a_{ox} indicate the activity of the reduced and oxidized species respectively, $c_{M^{z+}}$ is the concentration of metal ion M^{z+} . Taking the Cu reduction process as an example, where Cu^{2+} is reduced to Cu^0 , The Nernst expression is exemplified by equation (3.4).

$$E_r(\text{Cu}) = E_{\text{Cu}}^0 - \frac{RT}{zF} \ln c_{\text{Cu}^{2+}} \quad (3.4)$$

In the equation (3.4), $E_r(\text{Cu})$ is the equilibrium potential of Cu, E_{Cu}^0 is the standard equilibrium potential of Cu and $c_{\text{Cu}^{2+}}$ is the Cu^{2+} ion concentration.

3.2.2 Plating overpotential

The overall metal reduction process is simply presented by equation (3.2). However in the actual case the process undergoes several steps [4]. First is the metal dissolution into the bulk solution and becomes ionic state; second is the convective ionic mass transport from bulk solution to the boundary layer; third is the diffusive ionic mass transport from the boundary layer to the electrode surface; fourth is the adsorption of ionic species on the electrode surface and finally is the deposit formation from the reduction of ionic species.

To initiate the electrodeposition process, additional potential is required to overcome the equilibrium state between the electrode and metal ions. This is defined as overpotential, which is the minimum energy needed to drive the plating reaction [2]. The total overpotential consists of sub-overpotentials which are produced from each step as mentioned. The overall overpotential of reduction process is expressed as follows.

$$\eta = \eta_c + \eta_s + \eta_\Omega \quad (3.5)$$

$$\eta_\Omega = j_p A R_\Omega \quad (3.6)$$

In the equation (3.5) and (3.6), η_c is the concentration overpotential, which indicates the ionic mass transport from bulk solution to the electrode surface, η_s is the surface overpotential, which is caused by the electrochemical reaction

on the electrode surface. η_{Ω} is the ohmic overpotential, which relates to the resistance of ions travelling through the solution. j_p is the peak current density, A is the electrode surface area, R_{Ω} is the resistance of electrolyte between anode and cathode.

In addition, hydrogen evolution could also exist in the plating process in water-based solution. Water molecules break down to proton and hydroxide when the applied potential increases above the limit of electrochemical potential window. The protons may also come from the acidic electrolyte. Hydrogen gas can be formed by those protons when sufficient energy is supplied to overcome the hydrogen potential, the reaction is illustrated by equation (3.7).



Equation (3.7) is indicated as the hydrogen evolution reaction, which occurs in a number of metal electroplating system such as Cu, Pt and Fe. This side reaction could lead to the deterioration of deposit quality and lower plating efficiency. However, hydrogen evolution reaction is unlikely to occur in the DES ionic melt system, which is one of the advantages of using water-free electrolyte.

3.3 Electrodeposition kinetics

When the deposition reaction proceeds in the electrochemical cell, charge separation occurs on the electrode-electrolyte interface [7]. The ionic species in the electrolyte will be attracted to the electrode surface. Therefore, two parallel layers of charge are formed on the boundary between solution and metal. This is indicated as Helmholtz electrical double layers. The model has been further developed by Gouy, Chapman and Stern [8, 9].

Figure 3-2 illustrates the schematic diagram of electrical double layer in the aqueous solution. The reactants firstly travel through the bulk solution and then to both inner and outer layers before reaching the electrode surface, where the electron transfer reaction occurs. The solvent molecules and adsorbed ions are located at the inner layer. Most of the solvated ions are found away from the outer layer.

The case is different in the ionic liquid electrolyte, since the size of ions are larger with higher ionic concentration [10]. Strong interactions are formed between these ions and lead to more complicated interfacial structure, which depends on the type of cation and anion. Ions distribution in ionic melt system is in a multilayer arrangement near the electrode surface because of lattice saturation.

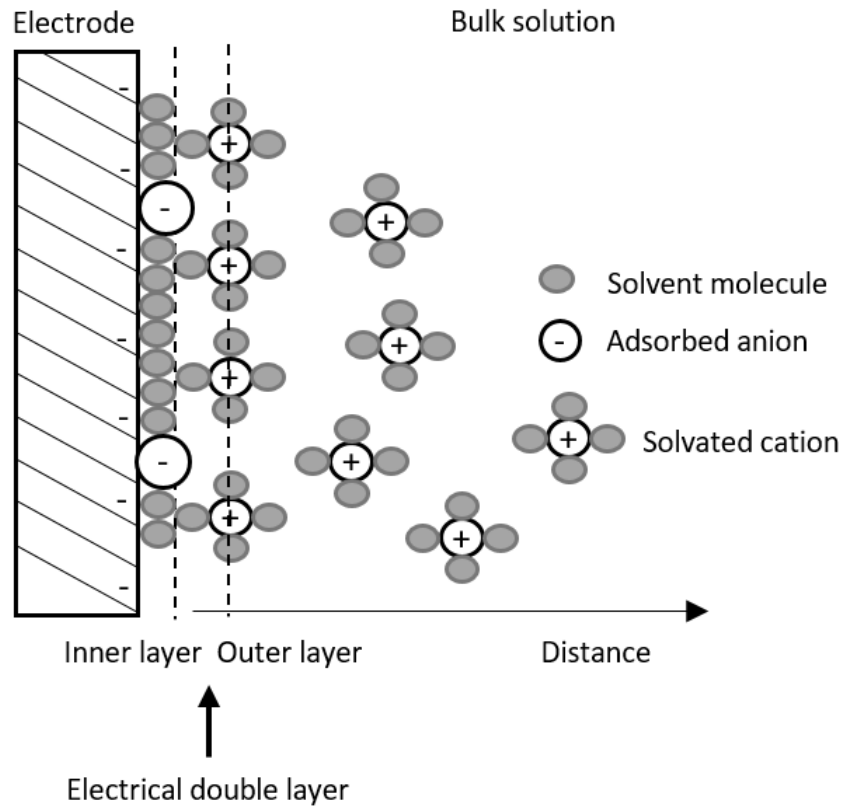


Figure 3-2 Schematic diagram of electrical double layer by Stern model

3.3.1 Faradaic and capacitive currents

The electrical double layer functions as a capacitor in the equivalent circuit, which is shown in Figure 3-3. It undergoes charging when current starts to flow into the electrochemical cell and electrical charges are stored [7]. Therefore, in the initial stage of current application both Faradaic and non-Faradaic current densities exist. The former indicates the charge transfer reaction across the electrode-electrolyte interface and initiates either metal deposition or dissolution reaction. Non-Faradaic current density, which is also

named as capacitive current density, is associated with charging and discharging of the electrical double layer and no charge is transferred across the solid-liquid boundary.

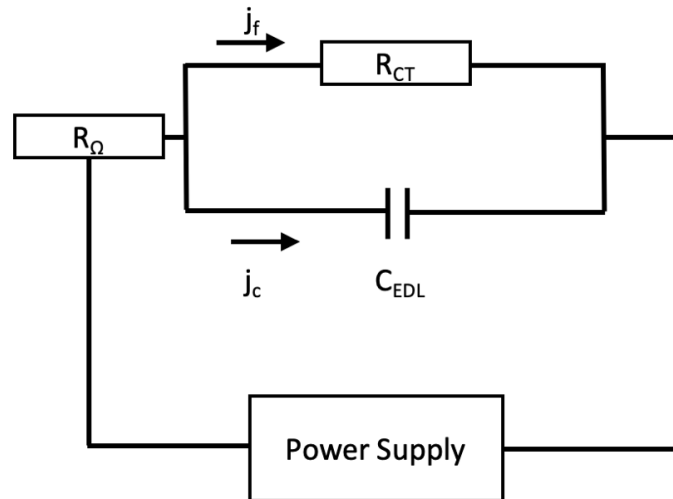


Figure 3-3 Equivalent circuit in the electrodeposition system

Therefore, the peak current density which is applied to the system can be written as follows.

$$j_p = j_f + j_c \quad (3.8)$$

In equation (3.8), j_p stands for the peak current density, j_f is the Faradaic current density or plating current density, j_c is the capacitive current density.

Figure 3-3 illustrates the equivalent circuit in electrodeposition system. In the figure, resistor R_{CT} represents the resistance of charge transfer reaction on the electrode surface. C_{EDL} is the capacitance of the electrical double layer, R_{Ω} stands for the resistance of the electrolyte between anode and cathode, j_f is the Faradaic current density or plating current density, j_c is the capacitive current density or non-Faradaic current density.

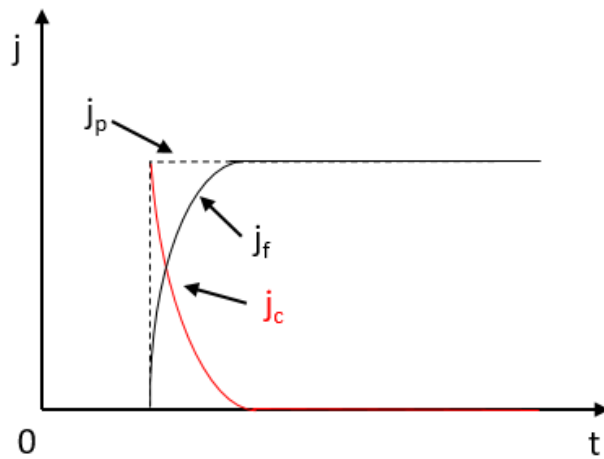


Figure 3-4 Profiles of Faradaic and capacitive current densities in the galvanostatic DC plating

Figure 3-4 shows that at the beginning of DC plating, most of the applied current density is provided to charge the electrical double layer. Later the capacitive current density decreases to zero when the double layer is fully

charged. On the other hand, the Faradaic current density increases from zero gradually to the same magnitude of applied current density.

3.3.2 Overpotential and Butler-Volmer equation

When the current is applied into the electrochemical cell, the electrode potential will change from its equilibrium state, which is defined as the reversible electrode potential. The potential variation between cell potential and reversible electrode potential is defined as overpotential η [7]. The relationship is shown in equation (3.9).

$$\eta = E - E_r \quad (3.9)$$

In the equation (3.9), E stands for the cell potential after the current is applied, E_r is the reversible electrode potential calculated from Nernst equation.

The Faradaic current is assumed under kinetic control and can be expressed by the Butler-Volmer equation, which states how the electrical current which passed through the electrode quantitatively relates to the overpotential in the electrochemical cell [11, 12] and the expression are shown in the equation (3.10) and (3.11).

$$j = j_0 \times \left\{ \exp \left[\frac{\alpha_a z F}{RT} (E - E_r) \right] - \exp \left[\frac{\alpha_c z F}{RT} (E - E_r) \right] \right\} \quad (3.10)$$

$$\text{or } j = j_0 \times \left\{ \exp \left[\frac{\alpha_a z F}{RT} \eta_s \right] - \exp \left[\frac{\alpha_c z F}{RT} \eta_s \right] \right\} \quad (3.11)$$

In equation (3.10) and (3.11), j stands for the electrode current density, j_0 is the exchange current density, which is the current density flow under equilibrium state and describes the rate of oxidation or reduction in a redox system, α_c is cathodic charge transfer coefficient and α_a is the anodic charge transfer coefficient. The charge transfer coefficients are associated with the activation energy of the transition state between reactants and products. η_s is the surface overpotential.

The Butler-Volmer equation indicates that the electrical current density is in exponential relationship to the surface overpotential. In addition, the complexity of Butler-Volmer equation can be simplified depending on the magnitude of surface overpotential [2]. In the practical situation it is very common that large surface overpotential is achieved. Therefore the Butler-Volmer equation is further developed into equation (3.12).

$$\eta_s = \frac{RT}{\alpha z F} \ln \frac{j}{j_0} \quad (3.12)$$

Equation (3.12) can be further developed into Tafel equation under the condition of large surface overpotential. This is shown in equation (3.13), (3.14) and (3.15).

$$\eta_s = a - b \log|j| \quad (3.13)$$

$$a = \frac{2.303RT}{\alpha zF} \log j_0 \quad (3.14)$$

$$b = \frac{2.303RT}{\alpha zF} \quad (3.15)$$

3.3.3 Effect of mass transport limitation in DC plating

The rate of metal plating basically is governed by two variables: kinetics on the electrode and mass transport of ionic species from the electrolyte. The former dictates the rate of charge transfer reaction which proceeds at the electrode-electrolyte interface. The latter indicates how fast of the ions travelling from bulk solution to the interface. The transport limitation of metal ions defines the maximum rate of metal deposition [13]. The approach of the mass transport limitations could lead to the increase of overpotential and energy consumption as well as the change on deposit microstructure [14]. Exceeding the limitations would result in poor deposit microstructure and undesirable physical properties [15, 16].

The mass transfer limitations can be understood by examining the concentration profile of the reactant close to the electrode surface. The concentration profile of metal ions in a DC system is illustrated in Figure 3-5 [7].

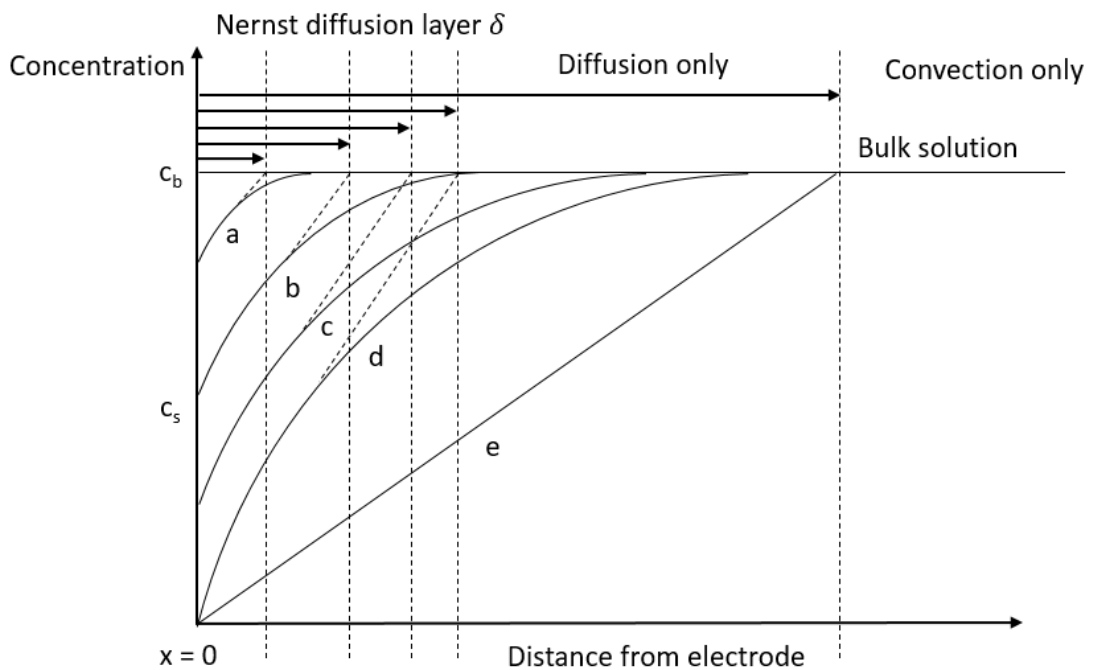


Figure 3-5 Development of concentration profiles and diffusion layer in DC plating

As shown in the figure, the concentration of metal ions on the electrode surface is the same as the one in the bulk solution. After a constant current is applied, metal ions on the electrode surface are consumed and then replenished from the bulk solution. However, the rate of ions depletion is

unmatched to the rate of replenishment. Therefore, the concentration profile and diffusion layer are developed. This occurs in the plating system which has fast electrode kinetics and slow ionic diffusion rate. As can be seen from the time evolution (from curves a to e), the surface concentration continues to decrease with the expansion of diffusion layer boundary. Eventually the metal ions are fully depleted at the electrode surface and its concentration falls to zero, the diffusion layer continues to develop further until a linear concentration gradient is achieved. This is the limit where the maximum current could be applied.

There are three primary mechanisms of mass transport: diffusion, convection and migration. Usually the latter two are neglected near the electrode surface and the model is simplified into diffusion based mass transport control in the electrodeposition process [4]. The flux of reactants is assumed under diffusive mass transport control only. In addition, the limiting current density is corresponding to the reactant which relates to the flux. Therefore, the current density can be expressed in equation (3.16).

$$j = -zFD \left(\frac{dc}{dy} \right) = -zFD \left(\frac{c_b - c_s}{\delta} \right) \quad (3.16)$$

In the equation (3.16), j is the current density, D is the diffusion coefficient, (dc/dy) is the ionic concentration gradient along the diffusion boundary layer,

c_b is the ion concentration in the bulk solution, c_s is the ion concentration at the electrode surface, δ is the thickness of diffusion boundary layer. The ionic concentration at the electrode surface becomes zero under the application of limiting current density, therefore the limiting current density is expressed in below.

$$j_{\text{lim}} = -zFD\left(\frac{c_b}{\delta}\right) \quad (3.17)$$

In the equation (3.17), j_{lim} is the limiting current density. In addition, the rotating disc electrode (RDE) has been widely used in the electrodeposition process to improve the rate of ionic mass transport. The relationship between limiting current density and the mass transport conditions is shown by the Levich equation.

$$j_{\text{lim}} = -0.62zFD^{\frac{2}{3}}\nu^{-\frac{1}{6}}\omega^{\frac{1}{2}}c_b \quad (3.18)$$

In the equation (3.18), ν is the kinematic viscosity, ω is the RDE rotation speed. Combining equation (3.17) and (3.18) gives the expression of δ .

$$\delta = 1.61D^{1/3}\nu^{1/6}\omega^{-\frac{1}{2}} \quad (3.19)$$

As can be seen from equation (3.19), the mass transfer diffusion layer becomes thicker in viscous liquid, which is due to higher value of diffusion coefficient and kinematic viscosity, and the application of lower RDE rotation speed.

3.4 Electrodeposition by pulse current

3.4.1 Definitions of pulse plating and pulse parameters

Direct current plating technique has been extensively used as the conventional method in the metal electrodeposition industry due to its simplicity and low cost [2]. In DC system, a unidirectional current density with fixed magnitude is applied throughout the plating process. Pulse current plating, which the current changes periodically in sequence, is an alternative technique. Compared to DC plating, the fluctuation of applied current density could alter the electrodeposition kinetics and nucleation mechanisms.

Therefore, PC plating offers a number of advantages such as the improvement on the deposit microstructure, enhancement of material physical properties, higher current efficiency and reduction or elimination of additive usage [17, 18, 19]. Another advantage of PC plating is the electroplating process could be optimized by proper manipulation of those pulse parameters, whereas in DC

system the magnitude of applied current density is the only operated parameter [20, 21]. Therefore, the understanding of pulse parameters is crucial for obtaining the desired deposit.

3.4.1.1 Pulse waveform

Generally there are two types of pulse sequences, one is unipolar waveform, which the power is switched on and off periodically, there are only three parameters: pulse on-time t_{on} , pulse off-time t_{off} and applied peak current density j_p . The other type is bipolar waveform, which two opposite directional current densities $j_{cathodic}$ and j_{anodic} alter in sequence, the corresponding plating time are $t_{cathodic}$ and t_{anodic} respectively. The bipolar waveform is also named as pulse reverse current. The schematic diagram of pulse current plating is shown in Figure 3-6.

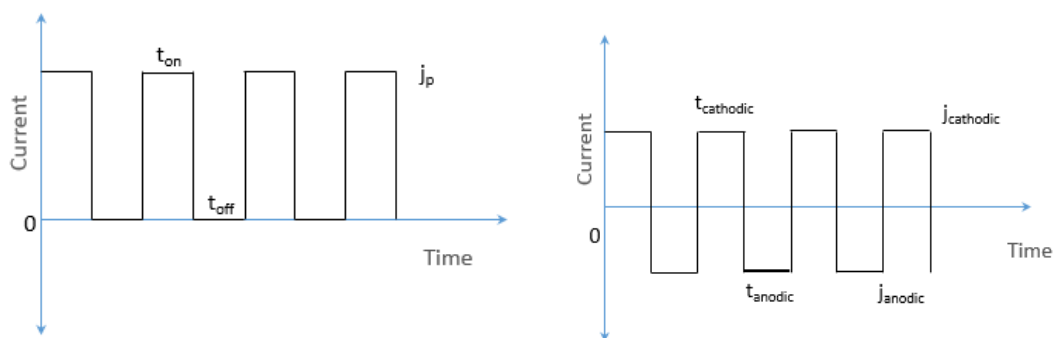


Figure 3-6 Schematic diagram of pulse plating sequence: unipolar (left) and bipolar (right)

In addition, the waveform pattern could be different depending on the current application, for instance square wave pulse, sinusoidal pulse and double cathodic or anodic pulses with various magnitudes [18]. This piece of research work focused only on unipolar square pulse waveform, which will be described in detail in the following section.

3.4.1.2 Duty cycle

Duty cycle θ is one of the important pulse parameters and it is defined as the ratio of pulse on-time t_{on} versus the total pulse time t_{total} , which is the summation of t_{on} and t_{off} . The pulse on-time t_{on} is the duration when current is switched on and t_{off} is the duration when current is switched off. In other words, duty cycle is defined as the proportion of t_{on} in a single pulse. The relationship is expressed in equation (3.20).

$$\theta = \frac{t_{on}}{t_{total}} = \frac{t_{on}}{t_{on} + t_{off}} \quad (3.20)$$

3.4.1.3 Current density

Peak current density j_p is the same as the applied current density during pulse on-time. The average current density j_{av} is defined as the multiplication

of peak current density and duty cycle. The expression is shown in equation (3.21).

$$j_{av} = j_p \times \theta \quad (3.21)$$

3.4.2 Pulse plating kinetics

3.4.2.1 Electrical double layer charging and discharging

In the initial stage of pulse on-time period, the electrical double layer is formed due to charge separation on the electrode-electrolyte interface after the application of peak current, which is the same as in DC plating as stated earlier. When the current is switched off, the electrical double layer undergoes discharging, which releases the capacitive current inside the electrochemical cell [7].

The estimate of the magnitude of capacitive current density and duration of charging discharging process is significant in pulse plating [11, 12]. Generally, the duration of pulse on-time and off-time have to be set considerably longer than the charging and discharging time respectively to eliminate the capacitive effect from non-Faradaic current density. Otherwise, metal electrodeposition would proceed at a varying plating rate due to the variation of Faradaic current density, which is caused by the capacitive

damping effect. As a result, the physical property and microstructure among different deposited layers are not uniform or inconsistent [7].

The relationship between Faradaic and capacitive currents in galvanostatic pulses is shown in Figure 3-7.

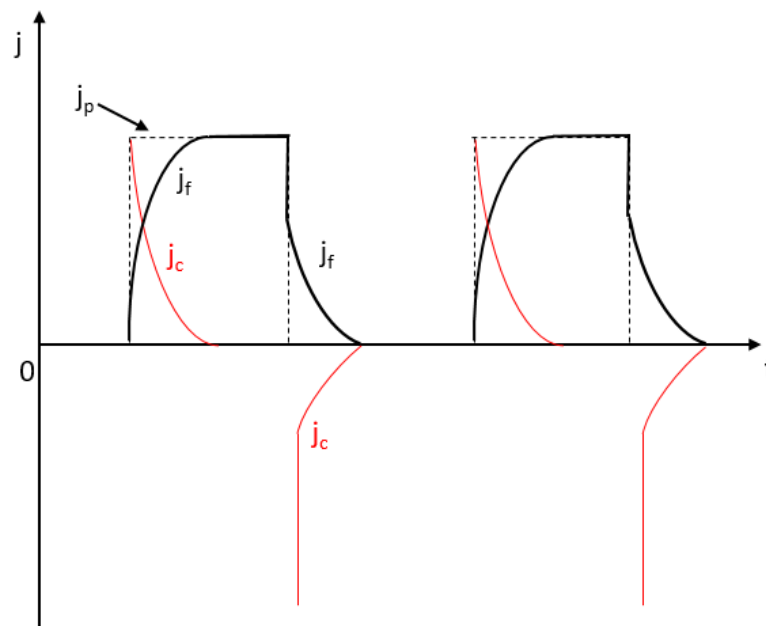


Figure 3-7 Faradaic and capacitive currents profiles in galvanostatic pulse plating

As shown in the figure, after a peak current is applied into the cell, the electrical double layer is charged and non-Faradaic process is dominant. When the double layer is fully charged, the capacitive current density decreases to zero and Faradaic current density reaches 100% of applied peak current

density. During the pulse off-time period when peak current density is switched off, the double layer undergoes discharging process and releases the capacitive charges, which converts to Faradaic current density. The discharging current density equals to the opposite magnitude of charging current density, since the overall net current density is zero due to the charge balance. The relationships between the current densities are shown in equation (3.22) and (3.23).

$$\text{Pulse on-time: } \quad j_p = j_c + j_f \quad (3.22)$$

$$\text{Pulse off-time: } \quad j_f = -j_c \quad (3.23)$$

As the same in DC condition, the Faradaic process is assumed to be kinetically controlled and can be further expressed by the Butler-Volmer equation.

$$j_f = j_0 \times \left\{ \exp \left[\frac{\alpha_a z F}{RT} \eta_s \right] - \exp \left[\frac{\alpha_c z F}{RT} \eta_s \right] \right\} \quad (3.24)$$

Equation (3.24) is a simplified expression and only valid in the single electron transfer process. The surface overpotential η_s is expressed in the

equation (3.12). The capacitive current density j_c is given in the below equation.

$$j_c = d \frac{Q_{EDL}}{dt} = C_{EDL} \left(\frac{d\eta_s}{dt} \right) \quad (3.25)$$

In the equation (3.25), Q_{EDL} and C_{EDL} stand for the charge and capacitance of the electrical double layer. This expression indicates the capacitive current is associated with the change of surface overpotential.

3.4.2.2 Capacitive damping effect of Faradaic current

The capacitive damping effect, which occurs due to the double layer charging, is of great significance in pulse plating. The relationships between charging/discharging time and pulse on/off time are crucial to the development of Faradic current profile in the system. Damping effect can be minimized when the pulse on/off time is much longer than charging/discharging time to ensure that the Faradaic current profile is not affected [12]. However, large damping effect on Faradaic current could occur if the pulse on/off is shorter than charging/discharging time [22, 23]. In this case, undesired deposit properties may be achieved and the advantages of pulse plating are eliminated. The damping effect on Faradaic current profiles is illustrated in Figure 3-8.

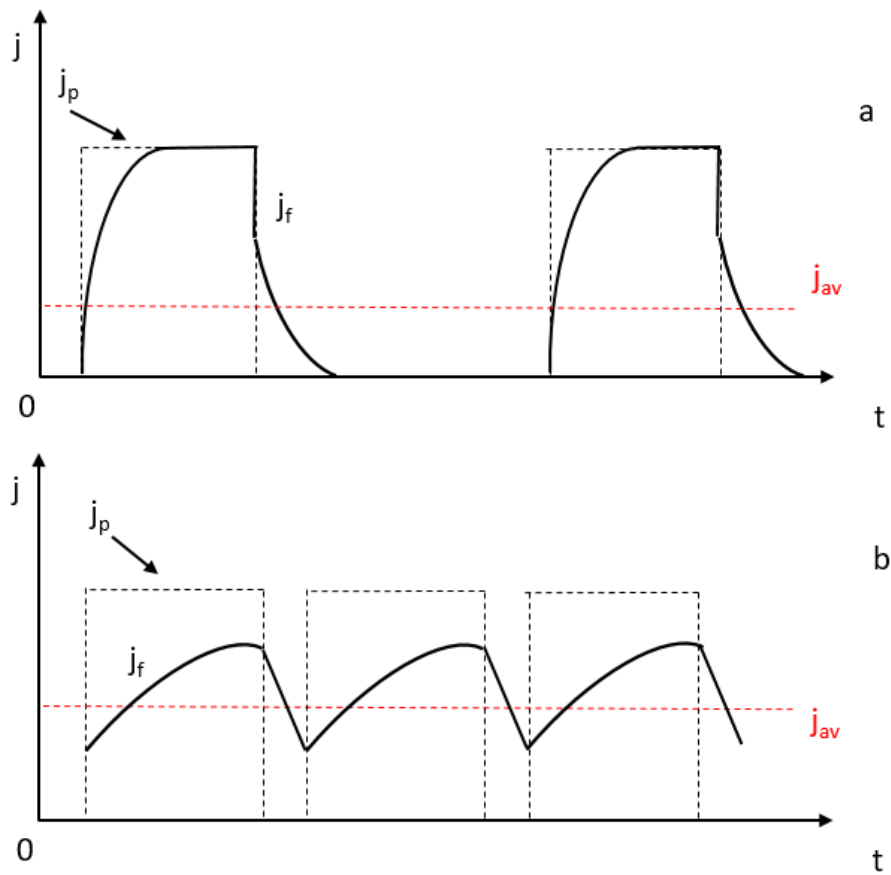


Figure 3-8 Damping effect of Faradaic current due to electrical double layer charging (a) small damping effect with $t_{on} > t_c$ and $t_{off} > t_d$ (b) large damping effect with $t_{on} < t_c$ and $t_{off} < t_d$

The extent of damping effect Δ can be quantitatively measured as the degree of flattening, which is expressed in equation (3.26).

$$\Delta = \frac{j_p t_{on} - \int_0^{t_{on}} j_f dt}{j_{av} t_{off}} \quad (3.26)$$

Equation (3.26) shows that the degree of flattening depends on the pulse parameters including peak current density, pulse on-time and off-time and average current density, which relates to pulse duty cycle. Normally the magnitude of Δ ranges between 0 and 1 and lower value indicates stronger damping effects. When $\Delta = 1$ the damping effect is eliminated and there are no charging and discharging processes. This is the ideal condition of pulse plating where capacitive effect does not occur. When $\Delta = 0$ the damping effect is maximum and the Faradaic current density becomes constant. In this case it is equivalent to DC condition.

3.4.3 Effect of mass transport limitations on pulse plating

3.4.3.1 Concentration profiles and dual diffusion layers

As previously described in DC plating, a reactant concentration diffusion layer is formed due to the limitation of mass transport of ions when the power is switched on. This limitation also exists in pulse plating, however the mass transport condition and development of concentration diffusion layer is much more complicated.

The mechanism is exemplified in a bipolar pulse system and demonstrated in Figure 3-9 (a) and (b). After the pulse current is applied, the reacting species are consumed at the electrode surface [7]. During the pulse on-time period, the reactants are consumed with the establishment of

concentration gradient. As a result, the boundary layer increases throughout the time (curve t_1 to t_3). In the duration of pulse off-time, the current is switched off and no electrochemical reactions occur at the electrode, the reacting species are replenished from the bulk solution and its concentration gradually recovers (curve t_3 to t_6). Eventually, the concentration will be fully recovered if the duration of pulse off-time is sufficiently long. The process will be replicated in the following pulse cycles.

During the development of concentration gradient, dual diffusion layers are formed in pulse plating system [12]. The concentration change is confined in the region which is close to the electrode surface (approximately 1 to 10 μm). This is also designated as inner diffusion or pulse diffusion layer (δ_p), which is mainly governed by diffusion. The thickness of inner pulsating layer depends on the pulse on-time and diffusion coefficient. Beyond this layer the concentration basically remains unaffected. This is designated as the outer diffusion layer or outer stagnant layer (δ_s).

The outer diffusion layer plays an important role in controlling the rate of mass transfer from bulk solution to the electrode surface. The reaction rate can not be maintained if the reaction species are not supplied sufficiently. Therefore the maximum reaction rate are controlled by both inner and outer diffusion layers. Similar to the DC condition, the mass transport limitations in pulse plating can not be exceeded to avoid the adverse effect on the deposit uniformity and quality.

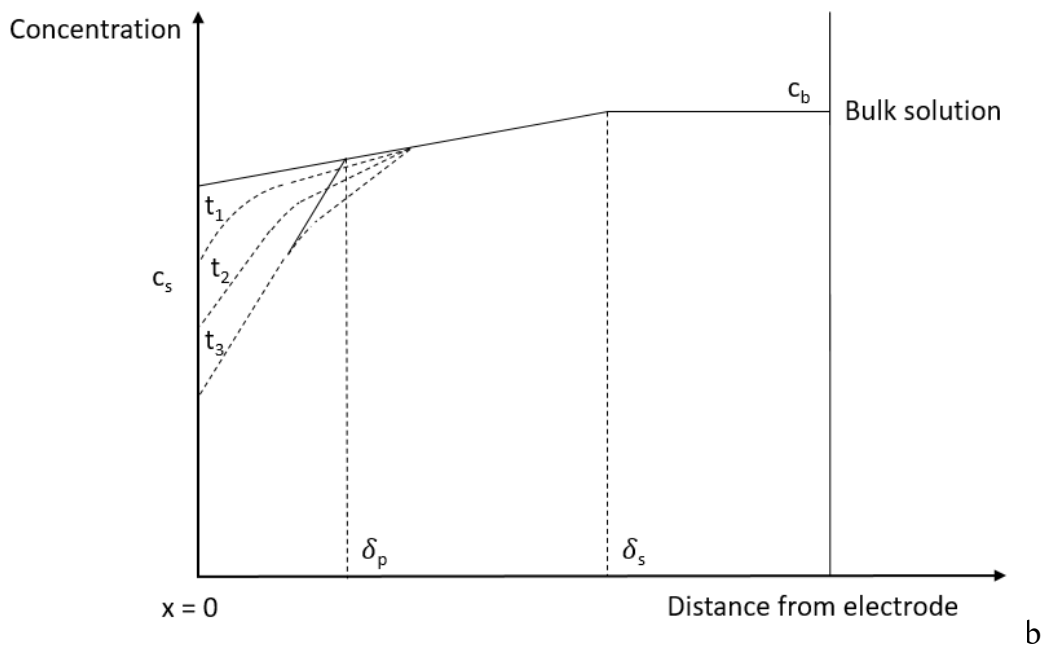
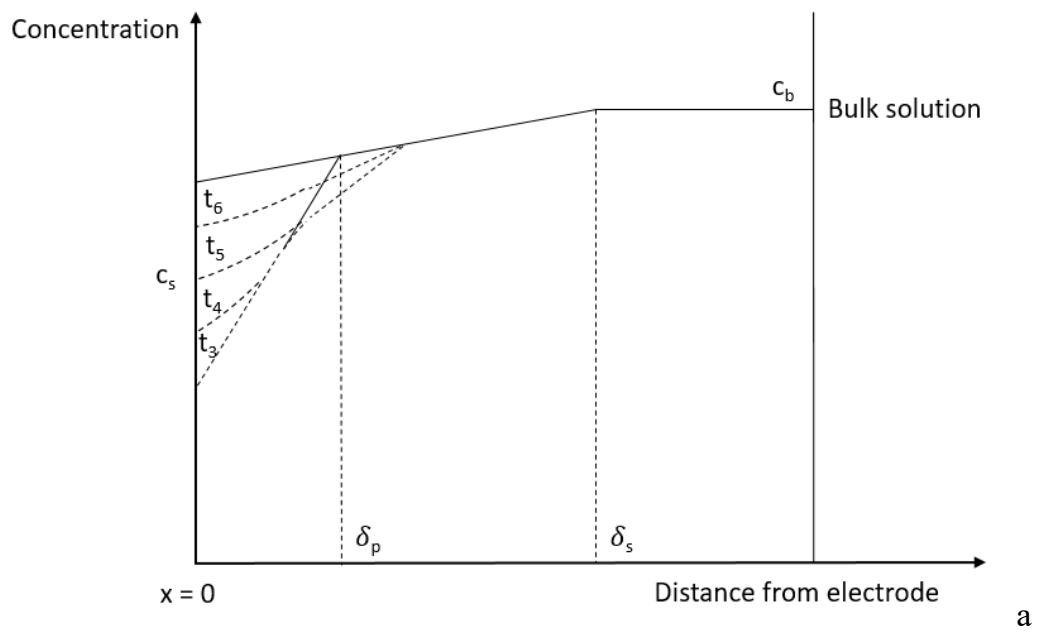


Figure 3-9 Schematic diagram of concentration profiles in pulse plating (a)

pulse on-time ($t_1 < t_2 < t_3$) (b) pulse off-time ($t_3 < t_4 < t_5 < t_6$)

3.4.3.2 Maximum plating rate in pulse plating

The maximum plating rate in electrodeposition is defined as the reduction rate when the reactants are fully depleted at the electrode surface [13, 25]. This definition is valid in DC plating system. Due to the mass transport limitation from bulk solution, the deposition reaction rate can not increase any further once the concentration of reacting species decreases to zero [7]. DC limiting current density, which is defined as the maximum current density could be applied without exceeding the mass transport limitations. It also indicates the maximum deposition rate which can be performed.

However, this definition is not adequate for pulse plating system. When the peak current is applied, the rate of concentration changes at the cathode is related to the peak current density. The mass transport limitation is to be achieved soon if a higher peak current density is applied. On the other hand, the ionic concentration at the electrode surface will gradually recover in the pulse off-time period. The concentration could not recover back to the initial condition if the duration of off-time is not long enough. As a result, the profile of surface concentration will be different in the next pulse cycle. To achieve such quasi steady state condition, it is important that the surface processes, such as the change of concentration profiles, reaction rates and current densities, should be replicated in every pulse cycle [7]. This implies that the mass transport limitation in pulse plating system depends on both pulse on-

time and off-time. The pulse limiting current density is defined as the maximum current density that could be applied, in the condition of the surface concentration of reacting species reaches zero at the end of pulse on-time, and is fully recovered back to the bulk solution at the end of pulse off-time.

As previously mentioned, exceeding the pulse limiting current condition could lead to poor and undesired deposit quality. The pulse limiting current was found to be dependent on the direct current limiting current and other pulse parameters such as duty cycle [26-29]. The calculation of pulse limiting current density was shown in equation (3.27) to (3.29).

$$\frac{j_{plim}}{j_{lim}} = \frac{1}{1 - 2t^* \sum_{m=1}^{\infty} \frac{\exp[\lambda_m(1-\theta)] - 1}{\lambda_m[\exp(\lambda_m) - 1]}} \quad (3.27)$$

$$t^* = \frac{Dt_{total}}{\delta^2} \quad (3.28)$$

$$\lambda_m = \pi^2 t_{total} (m - 0.5)^2 \quad (3.29)$$

In the equation (3.27), (3.28) and (3.29), j_{plim} is the pulse limiting current density, t^* is dimensionless time, λ_m is the summation term, m is the summation variable.

3.5 Nucleation mechanism of metal deposit

There are three primary mechanisms of nucleation growth during the formation of metal deposit [7]. The first mechanism is charge transfer with surface diffusion, which the adsorbed atom (ad-atom) is formed after the metal ion is discharged near the electrode surface. These ad-atom then diffuses towards the next available growing site on the electrode surface. The second mechanism is charge transfer without diffusion. The ad-atom, which is formed by the discharging of metal ions, directly incorporated into the available growing site on the electrode surface without the diffusion process. The third mechanism is charge transfer with new nuclei, which the ad-atom forms a new nucleus rather than incorporating into the existing nuclei on the electrode surface. Figure 3-10 illustrates the schematic diagram of three nucleation mechanisms.

Compared to DC plating process, pulse plating technique allows grain refinement and the formation of nano-crystalline electrodeposit layers by promoting the growth of new nuclei over the existing crystals [30]. In addition, pulse deposition can also control the composition and microstructure of metal deposit [7]. The nucleation rate and deposit morphology mainly depend on the pulse parameters including the duration of pulse time and off-time, peak current density and the waveform pattern [31-36]. High peak current density with short pulse time is in favour of nucleation process, which leads to the reduction of grain size [7]. Other aspects such as electrical double

layer charging time, ionic mass transport phenomena and overpotential could also have strong influence [7, 35].

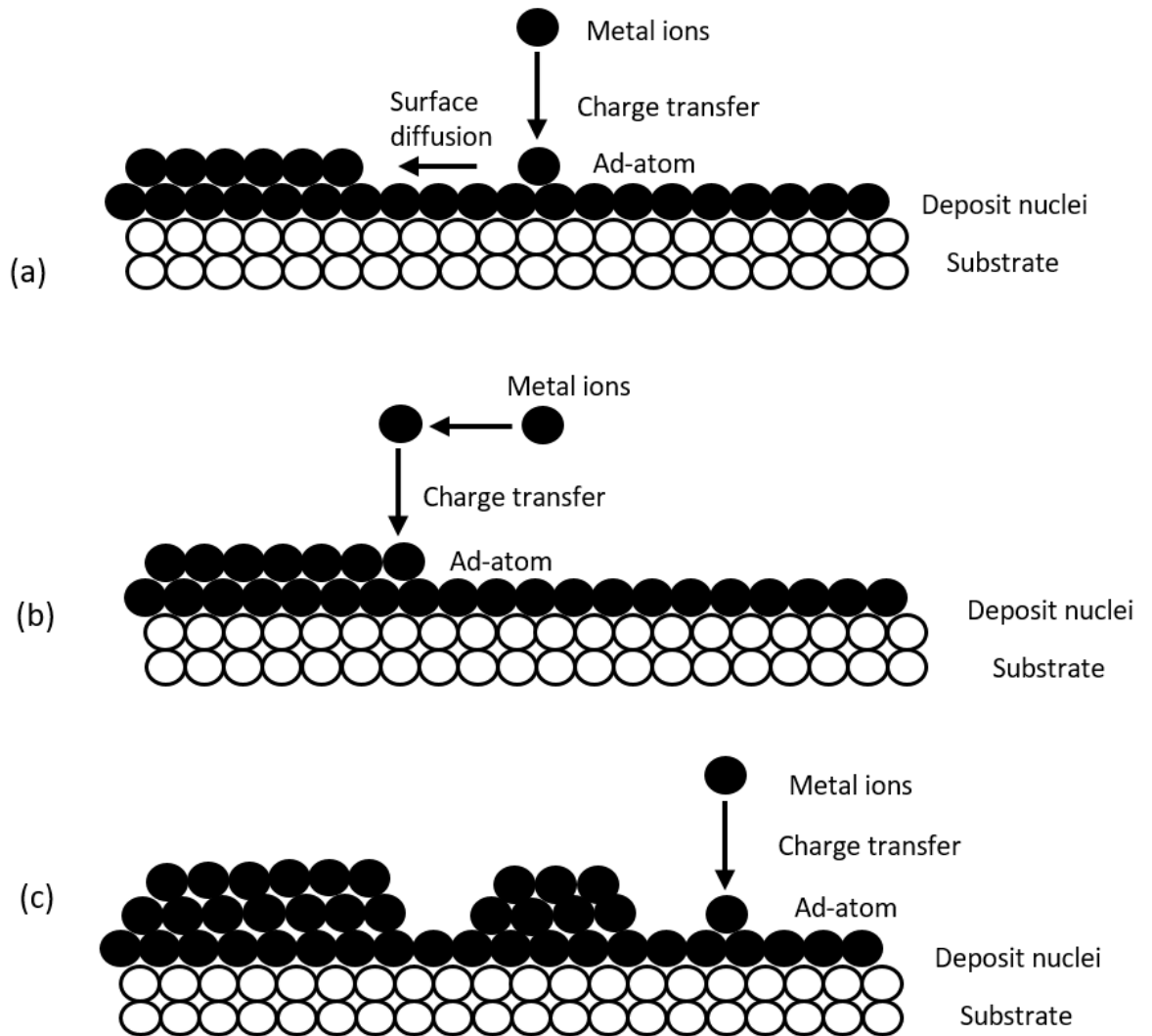


Figure 3-10 Schematic diagram of nucleation mechanism (a) charge transfer with surface diffusion (b) charge transfer without surface diffusion (c) charge transfer forming a new nucleus

3.6 Current distribution

Current distribution is another important parameter in galvanic electrodeposition [7]. The current density is defined as the peak current applied on the electrode surface divided by the surface area. In the ideal condition, the current density is uniform across the electrode-solution interface and metal deposit with homogenous thickness could be achieved. However, in reality the current density is not uniform and varies with the location of substrate. The current density on the edge of electrode surface is higher than the one at the centre, which is ascribed to the formation of non-uniform deposit thickness.

In general, there are three types of current distribution. The first one is primary current distribution, which is under the condition when ohmic resistance of electrolyte is much higher than the polarization resistance of the electrode. In this case the effects of overpotential and mass transport limitations could be neglected. The current distribution only depends on the geometry of electrochemical cell. The secondary current distribution mainly depends on the charger transfer reaction which occurs at the electrode surface. The polarization resistance of the electrode could not be neglected. The effect of mass transport is negligible, since the current density applied is lower than the limiting current density. The tertiary current distribution is determined by mass transfer limitations. The influences of polarization resistance and ohmic resistance are neglected.

Wagner number is used as an indicator of estimating the secondary current distribution. The formula is shown in below.

$$Wa = \frac{\kappa RT}{\alpha FL_c j_p} \quad (3.30)$$

In the equation (3.30), Wa is the Wagner number, κ is the specific conductivity of the electrolyte, α is charge transfer coefficient, L_c is the characteristic length. A Wagner number which is much higher than unity suggests a uniform deposit thickness. Poor uniformity is produced if the Wagner number is much smaller than unity:

$Wa > 1$, uniform deposit thickness across the electrode surface

$Wa < 1$, non-uniform deposit thickness across the electrode surface

Equation (3.30) suggests that uniform current distribution could be achieved under the condition of using electrolytes with high conductivity, high operating temperature, small electrode surface area and low peak current density. It is expected that the current distribution in the pulse system is worse than DC condition, which is attributed to the application of higher peak current density.

This chapter firstly has demonstrated the theoretical knowledge in electrochemistry, followed by the various aspects in electroplating process such as thermodynamics, kinetics, mass transport in both DC and PC plating techniques. The deposit nucleation mechanism and current distribution have also been briefly described. The understanding of these fundamentals is crucial in the subsequent chapters of results analysis and interpretation. The next chapter would describe the experimental procedure as well as methodologies of calculation and programming related to this piece of research work.

Reference List

1. Nasser. K. (2004). Electroplating-basic principles, processes and practice. Elsevier Ltd. Berlin
2. Pena E.M.B.D. (2017). Electrodeposition of copper using additive-containing low metal ion concentration electrolytes for EnFace applications. PhD thesis. University of Strathclyde. Glasgow
3. Eyring H. (1970). Electrochemistry. Newness. London
4. Dini D., Synder D. (2010). Modern electroplating. 5th ed, edited by Mordechay. S, Milan, P. Wiley, New York.
5. Bard A.J., Faulkner L.R. (1980). Electrochemical methods: fundamentals and applications. 2nd ed. Wiley. New York
6. West A.C. (2012). Electrochemistry and electrochemical engineering: an introduction. Columbia University. New York
7. Wolfgang E., Hansal G., Roy S. (2012). Pulse Plating. Eugen G. Leuze Verlag KG. Germany
8. Schmickler W. (1996). Interfacial electrochemistry. Oxford University Press. Oxford
9. Hamman, C.H., Hamnett A, Vielstich W. (2007) 2nd ed. Wiley-VCH. Weinheim
10. Ghosh S. (2013). Electrodeposition of Cu, Sn and Cu-Sn Alloy from Choline Chloride Ionic Liquid. PhD thesis. School of Chemical Engineering and Advanced Materials. Newcastle University. Newcastle

11. Puippe J.Cl., Ibl N. (1980). Influence of charge and discharge of electric double layer in pulse plating. *Journal of Applied Electrochemistry*. 10 (6) pp 775-784
12. Ibl N. (1980). Some theoretical aspects of pulse electrolysis. *Surface Technology* 10 (2), pp 81-104
13. Yeager E., Borkris J.O'M, Conway B.E., Sarangapani S., Ibl N. (1983). *Comprehensive treatise of electrochemistry*. Plenum Press. New York
14. Newman J., Aleya K. (2004), *Electrochemical systems*. 3rd ed. John Wiley & Sons. New Jersey
15. Ibl N, Javet P.H., Stahel F. (1972). Note on the electrodeposits obtained at the limiting current. *Electrochimica Acta*. 17 (4) pp 733-739
16. Winand R. (1991). *Electrocrystallization: fundamental considerations and application to high current density continuous steel sheet plating*. *Journal of Applied Electrochemistry*. 21 (5) pp 377-385
17. Rointan F.B. (1994). *Handbook of deposition technologies for films and coatings: science, technology and applications*. 2nd ed. William Andrew Publication, United States
18. Chandrasekar M.S., Pushpavanam M. (2008). Pulse and pulse reverse plating-conceptual, advantages and applications. *Electrochimica Acta*. 53 (8) pp 3313-3322
19. Osero N. (1986). An overview of pulse plating. *Plating and Surface Finishing*. 73 (3) pp 20-22

20. Piuppe J.C., Leaman F. (1987). Theory and practice of pulse plating.
Amer Electroplater Soc. United States
21. Yung E.K., Romankiw L.T., Alkire R.C. (1989). Plating of copper into through-holes and vias. *Journal of the Electrochemical Society*. 136 (1) pp 206-215
22. Holmbom G., jacobsson B.E. (1988). Through-hole plating of Cu by modulated current deposition. *Surface and Coating Technology*. 35 (3-4) pp 333-341
23. Tsai W.C., Wan C.C., Wang Y.Y. (2003). Frequency effect of pulse plating on the uniformity of copper deposition in plated through holes. *Journal of the Electrochemical Society*. 150 (5) C267-C272
24. Datta M., Landolt D. (1985). Experimental investigation of mass transport in pulse plating. *Surface Technology*. 25 (2) pp 97-110
25. Selman J.R., Tobias C. (1978). *Advances in chemical engineering*. Edited by Drew T. Academic Press. New York
26. Roy S., Landolt D. (1997). Determination of the practical range parameters during reverse-pulse current plating. *Journal of Applied Electrochemistry* 27 (3) pp 299-307
27. Cheh H.Y. (1971). Electrodeposition of gold by pulsed current. *Journal of the Electrochemical Society*. 118, pp 551-557
28. Cheh H.Y. (1971). The limiting rate of deposition by P-R plating. *Journal of the Electrochemical Society*. 118, pp 1132-1134

29. Budevski E., Staikov G., Lorenz W.J. (1996). Electrochemical phase formation and growth. VCH Publishers. New York
30. Landolt D., Marlot A. (2003). Microstructure and composition of pulse-plated metals and alloys. *Surface and Coating Technology*. 169-170, pp 8-13
31. Holmbom L.G., Jacobson B.E. (1987). Effects of bath temperature and pulse-plating frequency on growth morphology of high-purity gold. *Plating and Surface Finish*. 74, pp74-79
32. Halmdienst M., Hansal W.E.G., Kaltenhauser G., Kautek W. (2007). Pulse plating of nickel: influence of electrochemical parameters and composition of electrolyte. *Transaction of the IMF*. 85 pp 22-26
33. El-Sherik A.M., Erb U., Page J. (1997). Microstructural evolution in pulse plated nickel electrodeposits. *Surface and Coating Technology*. 88 (1-3) pp 70-78
34. Kollina C., Spyrellis N., Amblard J., Froment M., Maurin G. (1990) Nickel plating by pulse electrolysis: textural and microstructural modifications due to adsorption/desorption phenomena. *Journal of Applied Electrochemistry*. 20 (6), pp 1025-1032
35. Chene O., Landolt D. (1989). The influence of mass transport on the deposit morphology and the current efficiency in pulse plating of copper. *Journal of Applied Electrochemistry*. 19 (2) pp 188-194

36. Ibanez A., Fatas E. (2005). Mechanical and structural properties of electrodeposited copper and their relation with the electrodeposition parameters. *Surface and Coating Technology*. 191 (1) pp 7-16

Chapter 4. Experimental Procedure

This chapter describes experimental procedure and methodology applied in this research project. It includes the details of calculation process used to determine pulse parameters, which consider electrical double layer charging and mass transport limitations that provide the practical range for operation [1]. The preparation methods of electrolyte and electrodes needed are described later, followed by the setup procedure of electrochemical cell for the deposition and metal dissolution experiments. Material characterization employed in this study, for example scanning electron microscopy (SEM) and energy-dispersive X-ray spectroscopy (EDX), are also described with the method of microstructural classification.

4.1 Determination of pulse parameters

4.1.1 DC and pulse limiting current densities

As described in the previous chapter, DC limiting current density (j_{lim}) and the thickness of diffusion layer in DC system (δ) needed to be calculated first in order to determine the pulse limiting current density j_{plim} by using equation (4.1) and (4.2).

$$j_{lim} = -0.62zFD\frac{2}{3}v^{-\frac{1}{6}}\omega^{\frac{1}{2}}c_b \quad (4.1)$$

$$\delta = 1.61D^{1/3}v^{1/6}\omega^{-\frac{1}{2}} \quad (4.2)$$

Once j_{lim} and δ were known, the next step was to determine the pulse limiting current density j_{plim} . The corresponding expressions are shown in equation (4.3), (4.4) and (4.5).

$$\frac{j_{plim}}{j_{lim}} = \frac{1}{1-2t^* \sum_{m=1}^{\infty} \frac{\exp[\lambda_m(1-\theta)]-1}{\lambda_m[\exp(\lambda_m)-1]}} \quad (4.3)$$

$$t^* = \frac{Dt_{total}}{\delta^2} \quad (4.4)$$

$$\lambda_m = \pi^2 (t_{on} + t_{off}) (m - 0.5)^2 \quad (4.5)$$

The applied peak current density j_p was set to 80% of j_{plim} to ensure the plating condition does not exceed the mass transport limitations. In addition, it was found that the desirable granular deposit can only be achieved when both dimensionless number N_m (ratio of average current density to DC limiting current density) is smaller than N_p (ratio of peak current density to pulse limiting current density) [2]. Also j_{av} and j_p need to be smaller than j_{lim} and j_{plim} respectively. N_p was fixed as 0.8 in this research work and the relationship between both dimensionless numbers is shown in equation (4.6).

$$N_m < N_p = (j_{av} / j_{lim}) < (j_p < j_{plim}) < 1 \quad (4.6)$$

The limiting current densities and corresponding plating parameters, such as applied peak current and total deposition time, could either be calculated manually or using Matlab software. In this work, Matlab was used to calculate all parameters for the plating experiments. The programming codes are shown in Figure C-1 and Figure C-2 in the Appendix section.

As shown in the figures, the first part of code is the input parameters including the pulse parameters, the properties of electrolyte and plated metal, and plating system. The second part of this code is the calculation procedure which integrates the equations by programming. The final part provides with the parameters that need to be set up into potentiostat software and the results of both dimensionless numbers. In the copper electrodeposition experiment, four pulse on-times (10 ms, 50 ms, 100 ms and 200 ms) and four duty cycles (0.2, 0.3, 0.5 and 0.67) formed the plating matrix of a total 16 different pulse conditions. The corresponding pulse parameters, which are able to plate a nominal thickness of 5 μm deposit assuming with 100% Faradaic efficiency are shown in the Table C-1.

In the table DLCD and PLCD stand for DC limiting current density j_{lim} and pulse limiting current density j_{plim} respectively. These parameters were calculated based on the condition of 700 rpm RDE rotation speed, 25°C

operating temperature, 1.26 cm effective diameter of RDE surface and 0.2 mol/L cupric concentration. In addition, DC deposition experiment was also necessary to be performed in the purpose of comparison to pulse plating experiments. The table shows that the j_{lim} is fixed as 6.2 mA/cm² in all pulse conditions and j_{plim} varies from 8.6 mA/cm² to 45.4 mA/cm² depending on the specific pulse condition.

Similar conditions were also applied to the tin electrodeposition experiments. Four pulse on-times (10 ms, 50 ms, 100 ms and 200 ms) and four duty cycles (0.1, 0.2, 0.5 and 0.67) formed a matrix of 16 pulse plating conditions. In addition, the concentration of Sn²⁺ in the DES was 0.1 mol/L, the settings of RDE rotation speed, operating temperature, substrate and desirable deposit thickness were the same as the copper pulse deposition experiments. Table C-2 shows the pulse parameters for the tin electroplating experiment. The DC limiting current density of tin plating experiment was fixed as 4.9 mA/cm² and N_p was fixed as 0.8. The pulse limiting current density varied from 6.7 mA/cm² to 34.4 mA/cm² depending on the specific pulse condition.

In addition, the total charge applied during the electrodeposition process was calculated by equation (4.7).

$$Q_{dep} = j_p A \theta t_{dep} \quad (4.7)$$

In the equation (4.7), Q_{dep} is the total deposition charge and t_{dep} is the total plating time. Q remains constant in whatever the pulse condition, since the deposit thickness is the same. Based on the calculation, Q_{dep} for Cu and Sn were 16.9 coulomb and 7.4 coulomb, respectively.

Using these pulse parameters ensures that the metal plating is always performed below the mass transfer limit and their microstructure, as far as possible, is not influenced by solution side diffusion limitations.

4.1.2 Electrical double layer capacitive effect

As mentioned earlier, the selected pulse on-time and pulse off-time should be configured considerably longer than the charging and discharging time of electrical double layer in order to obtain uniform metal deposit [1]. When the electrical double layer undergoes charging at the initial stage of t_{on} , peak current density j_p is portioned into Faradaic current density j_f and capacitive current density j_c .

$$j_p = j_f + j_c \quad (4.8)$$

j_f can be expressed in the form of Butler-Volmer equation [3, 4].

$$j_f = j_o \times \left\{ \exp \left[\frac{\alpha_a z F}{RT} \eta_s \right] - \exp \left[\frac{\alpha_c z F}{RT} \eta_s \right] \right\} \quad (4.9)$$

In the equation (4.9), j_o is the exchange current density, α_a and α_c are the anodic and cathodic charge transfer coefficients respectively, R is the gas constant, η_s is the surface overpotential, T is the absolute temperature. The equation of j_c can be expressed by the differentiation of surface overpotential.

$$j_c = d \frac{Q_{EDL}}{dt} = C_{EDL} \left(\frac{d\eta_s}{dt} \right) \quad (4.10)$$

In the equation (4.10), Q_{EDL} and C_{EDL} are the charge and capacitance of electrical double layer respectively. The double layer discharges when the current is switched off. The Faradaic current density is the same as the charging current density since the net current is zero, as indicated in equation (4.11).

$$j_f = -j_c \quad (4.11)$$

Due to the calculation complexity, both charging time t_c and discharging time t_d were determined by Matlab software, which can integrate all the equations. However, the calculation loop would be infinite in theory since j_c never actually reaches zero. Therefore, both parameters need to be properly defined with certain limitations: t_c is defined as the time when j_f has reached 99% of j_p and t_d is defined as the time when j_f has fallen to 1% of j_p . In addition, the double layer damping effect can be determined by the degree of flattening Δ using Matlab software. The programming code is listed in the Figure C-3 and C-4.

The Matlab programming code was developed based on Pearson's model [5]. The first part of code is the parameters list, among which the plating system parameters are either empirically determined or configured based on assumption. The second part is the calculation of t_c and t_d by loop control, as well as the degree of flattening Δ . The code reveals that the charging and discharging process mainly depends on the pulse parameters including pulse on-time, duty cycle and peak current density. The corresponding parameters of copper and tin pulse electrodeposition are listed in the Table C-3 and Table C-4.

The parameters of plating system for the calculation of charging and discharging time were adopted from the literature [6]. Therefore the results were only estimated values. As can be seen from the table that the duration of pulse on-time and off-time is set to be much longer than the charging and

discharging time for the deposition experiments, indicating the electrical double layer capacitive effect on the pulse plating process is very limited.

4.2 Material preparation

4.2.1 Electrolyte formulation

The DES electrolyte was formed by mixing choline chloride and ethylene glycol with a copper metal salt. To prepare the copper ethaline melt DES, firstly the ethaline melt was prepared by mixing choline chloride ($\geq 98\%$, Sigma-Aldrich) with ethylene glycol ($\geq 99\%$, Sigma-Aldrich) in a molar ratio of 1:2. Choline chloride powder was added into a beaker, followed by the addition of ethylene glycol. The mixture was kept on a thermostatic heater up to 70°C with stirrer until colourless liquid was observed. Then the copper (II) chloride dihydrate (ACS, Reag.Ph Eur, Merck) was added into a volumetric flask, after which the ethaline melt was added. The flask was kept on a thermostatic heater at 70°C with stirrer until all metal salt was dissolved and the colour of solution changed from colourless to light brown, as shown in the Figure 4-1. To make up 250 ml of 0.2 mol/L of this melt, 1 mole of choline chloride (139.62 g), 2 moles of ethylene glycol (124.14 g) and 0.05 mole of copper (II) chloride dehydrate (8.52 g) are needed.

The preparation of tin ethaline DES electrolyte was prepared in a similar fashion. Tin (II) chloride dihydrate salt (Analytical reagent grade,

Fisher Scientific) was added to the ethaline melt before filling up the required amount of melt in the volumetric flask. The flask was then kept heated with stirrer until all metal salt was dissolved. To make up 250 ml of 0.1 mol/L of this melt, 1 mole of choline chloride (139.62 g), 2 moles of ethylene glycol (124.14 g), and 0.025 mol of tin (II) chloride dihydrate (5.64 g) are needed. The electrolytes were stored at ambient conditions, and crystallization or phase separations were not observed.



Figure 4-1 Virgin cupric ethaline melt DES electrolyte (left) and tin ethaline melt DES electrolyte (right)

4.2.2 Electrode preparation

Three types of electrodes were used in the research project. The working electrode, which is served as the substrate for metal being plated on,

was made of steel (Fe 71.2%, Cr 13.4%, Ni 9.9%). The counter electrode was a copper rod (Alfa Aesar, 3.18 mm, 99.999%) or a tin rod (Alfa Aesar, 3.2 mm, 99.95%). The reference electrode was a piece of silver wire (Aldrich, 1.0mm, $\geq 99.99\%$) dipped in the ethaline melt DES, as shown in the Figure 4-2. This is a quasi-reference electrode since it was reported to provide stable potential and avoid water contamination by the conventional reference electrode [7]. All electrodes were polished using grit 1200 and 4000 SiC paper before being washed and dried by blowed N_2 gas. The working electrode was fitted into a holder and the polishing was performed on the Struers Dap-7 polishing machine with 125 rpm rotation speed for approximately five minutes on each SiC paper.



Figure 4-2 Working electrode (left), counter electrode (middle) and reference electrode (right)

In most of the cases, the working electrode was mounted to the rotating disc by a tip holder assembly. As shown in Figure 4-3, the assembly is composed of working electrode, tip holder, a bolt and a holder cap. The

working electrode was inserted into the bottom of tip holder, followed by placing the bolt on the back of the electrode centre, and then the holder cap was tightened with the tip holder. The diameter of the exposed area to the DES electrolyte was measured as 1.26 cm.



Figure 4-3 Working electrode tip holder assembly and components

4.3 Electrochemical cell

The electrochemical cell was assembled as illustrated in the Figure 4-4. The working electrode tip assembly was mounted to the RDE rotor, which was connected to a rotation speed control unit (Radiometer analytical, model CTV101, 0-5000 rpm). The default rotation speed was 700 rpm. Then the cell was connected to an AutoLab PGSTAT30 potentiostat, which is the power source to apply current density into the cell. A water recirculation unit was connected to the cell to keep the reaction system under constant temperature control. The plating procedure and parameters settings were programmed through the NOVA (Version 2.0.2) software which had been installed on a desktop computer. The potential transient and current were measured by potentiostat. In addition, both cyclic and linear sweep voltammetry

experiments were corrected by IR compensation. The impedance was measured by the PStace (Version 5.5) software using Palmsens Palmsens4 potentiostat.

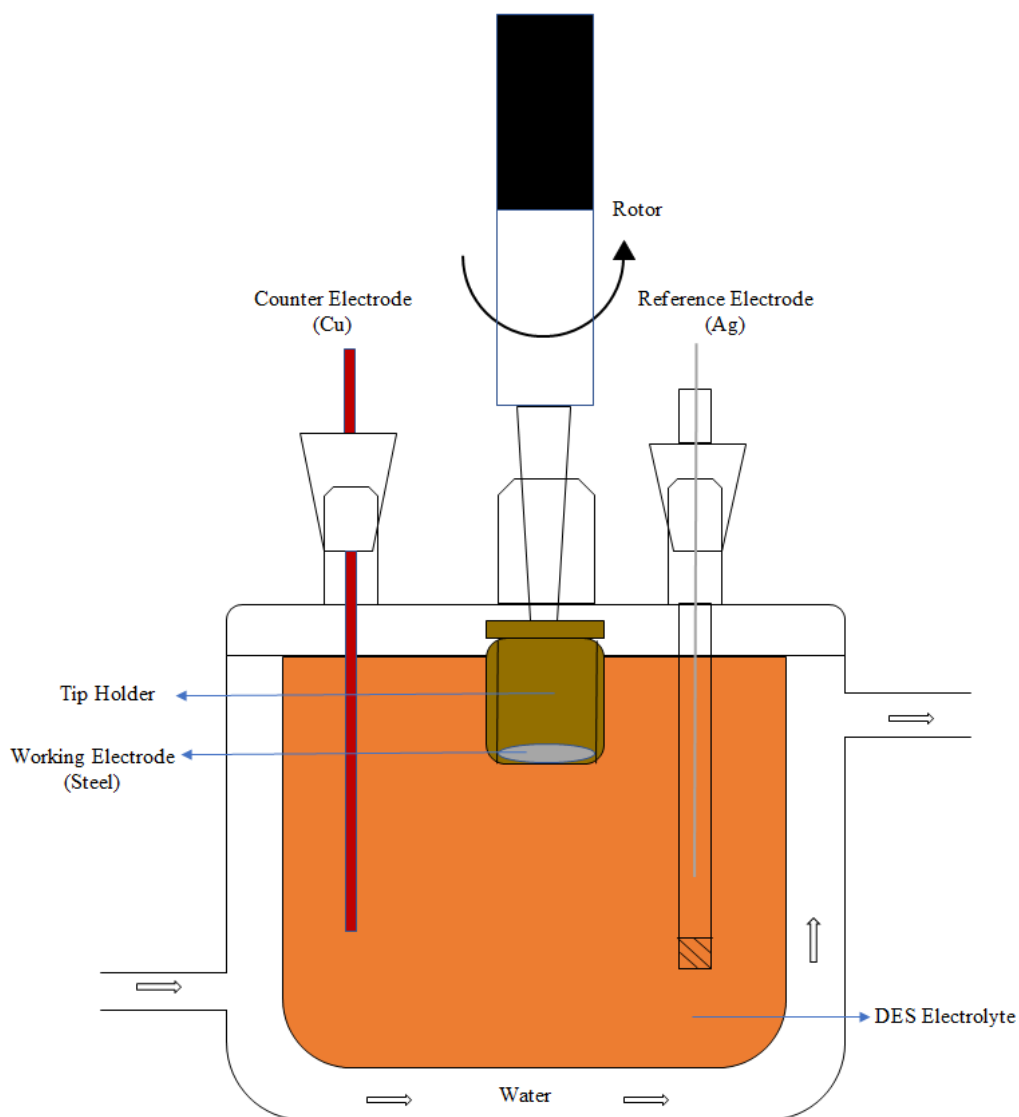


Figure 4-4 Schematic diagram of electrochemical cell in metal electrodeposition experiment

4.4 Metal plating experiments

Metal deposition was operated in galvanostatic mode, in which the magnitude of applied current was fixed along the entire process in order to plate a uniform layer of deposit. In addition, it could achieve more precise measurement and high stability of transient potential of the working electrode, as well as suppressing passivation of metal surface. Therefore, galvanostatic plating has been used widely in the pulse plating industry. To obtain a nominal 5 μ m thickness of copper deposit, the deposition time lasted from 47 to 78 minutes depending on the specific pulse condition.

The apparatus setup for tin electrodeposition experiment was similar to the copper except that tin rod was used as the counter electrode instead of copper. In addition, other experiments including polarization test, cyclic voltammetry and linear sweep voltammetry scanning measurements, the apparatus setup was nearly the same apart from the settings on the programming procedures on the NOVA software. The plating time for tin deposition lasted from 26 to 73 minutes.

4.5 Metal dissolution experiment

During the pulse plating of copper experiment, it was found that plated copper dissolved into the electrolyte. In addition, the electrolyte colour turned dark and precipitates were found at the bottom of cell after the electrolyte had

been used for some time. Therefore a number of metal corrosion experiments were undertaken to investigate these issues under both stationary and agitated conditions.

4.5.1 Stagnant metal immersion experiment

The aim of this experiment is to examine whether Cu and steel could dissolve in the DES solution and any change on the solution appearance. Basically one piece of copper sheet and steel disc were dipped inside the ethaline melt with and without the metal salt, as well as with and without benzotriazole (BTA) additive for 410 hours. The top of the beaker was sealed by parafilms to prevent the water absorption.

4.5.2 Agitated metal dissolution experiment using RDE

The electrochemical cell apparatus setup was similar to the plating experiments except that no current was passed. The electrolyte was the same as the plating solution and the electrodes preparation were also the same. The experiment duration lasted from 10 to 60 minutes under various RDE rotating speeds depending on the specific case. Both copper and steel substrates were tested in the dissolution experiments.

4.6 Deposit appearance observation and gravimetric measurement

After the plating or metal dissolution experiment was finished, the electrode was disassembled from the tip holder and washed by deionized water, followed by drying with N₂ gas or oven at approximately 70°C. A photograph of the electrode showing the general appearance of the deposit was taken by phone camera to ensure that an early observation was made. These observations were needed to determine if the deposit was adherent so that meaningful current efficiency calculations could be carried out.

In addition, the weight of tip was measured before and after the experiment by using using Kern ABS 220-4N balance (accuracy of 0.1 mg). The difference in weight was used to calculate the Faradaic efficiency in the plating experiments, and also the rate of metal dissolution during the investigation of corrosion behaviour. The expressions are shown in equation (4.12) and (4.13).

$$\varepsilon = \frac{m_{\text{actual}}}{m_{\text{theoretical}}} \times 100\% \quad (4.12)$$

$$r_{\text{dis}} = \frac{m_a - m_b}{t} \quad (4.13)$$

In above equations, $m_{\text{theoretical}}$ is the theoretical weight gain of metal deposit and m_{actual} is the actual weight gain of metal deposit, r_{dis} is the rate of

dissolution, m_a and m_b are the weight of substrate after and before the dissolution experiment, t is the experiment time.

The theoretical weight gain $m_{\text{theoretical}}$ was calculated by the Faraday's law of electrolysis, which is a quantitative method to estimate the amount of metal plated based on the quantity of provided electricity charge [8]. The expression is shown in equation (4.14).

$$m_{\text{theoretical}} = \frac{QM}{Fz} = \frac{jAtM}{Fz} \quad (4.14)$$

In the equation (4.14), Q is the total electrical charge, F is the Faraday constant, M is the molar mass of metal, z is the ionic charge, j is the current density, A is the surface area of electrode, t is the plating time.

4.7 Material characterization

4.7.1 Scanning electron microscopy (SEM)

The topography and morphology of metal deposit was characterized by scanning electron microscopy (SEM) [9]. SEM offers a number of unique advantages including the ease of operation, minimal sample treatment and preparation, provision of high quality images, high specimen capacity, highly effective data collection and analysis, and could perform concurrent other

types of characterization techniques such as EDX, which could provide with the information of sample elemental composition [10].

The working principle of SEM is shown in the Figure 4-5. The electron gun emits a stream of high energy electron beams, which later hit the sample and produce various signals such as back scattered electrons, secondary electrons, photons, characteristic X- rays, visible light and heat. Among of those the back scattered electrons and secondary electrons are very important and collected by detectors for image production. The secondary electron signals are produced from the specimen surface atoms therefore could reveal the material surface features.

4.7.2 Energy-dispersive X-ray spectroscopy (EDX)

Under stationary condition, ground stated electrons are located in their specific electron shell surrounding the sample's atom nucleus. An electron hole is created after the electron in the inner shell of atom is excited and ejects from its electron shell. The electron from outer shell containing higher energy fills in the electron hole by emitting radiation energy in the form of X-ray, which is then collected and analysed by EDX instrument. The elemental composition is measured from the X-ray signals by the distinct characters of the energy difference between atomic electron shells. Figure 4-6 demonstrates the EDX working principles.

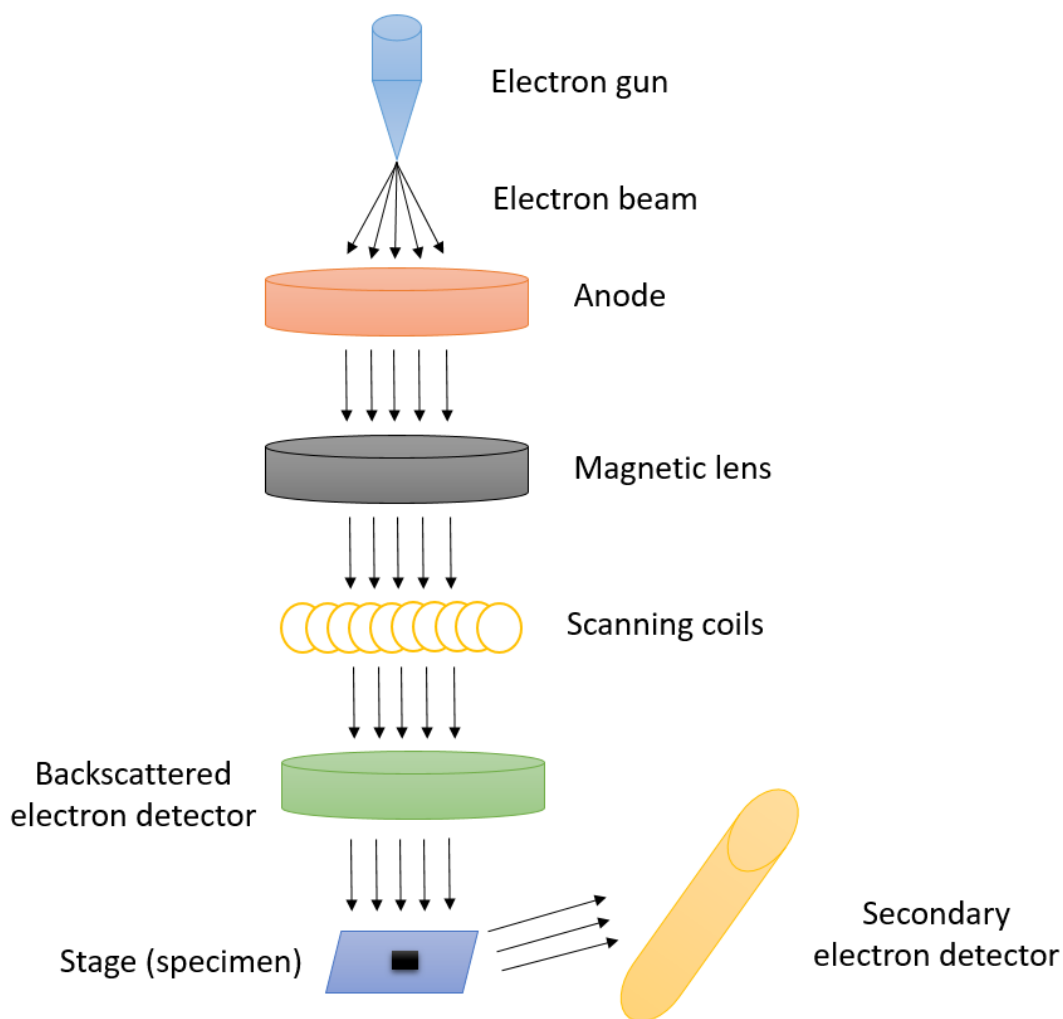


Figure 4-5 Schematic diagram of working principle of SEM

Tin deposit sample was characterized using the Philips/FEI XL30 ESEM environmental scanning electron microscope, which attaches an Oxford Instruments Energy 250 energy dispersive spectrometer system), provided by the chemistry department of the University of Glasgow. Two magnification modes 2,500x and 5,000x were adopted to observe the deposit microstructure.

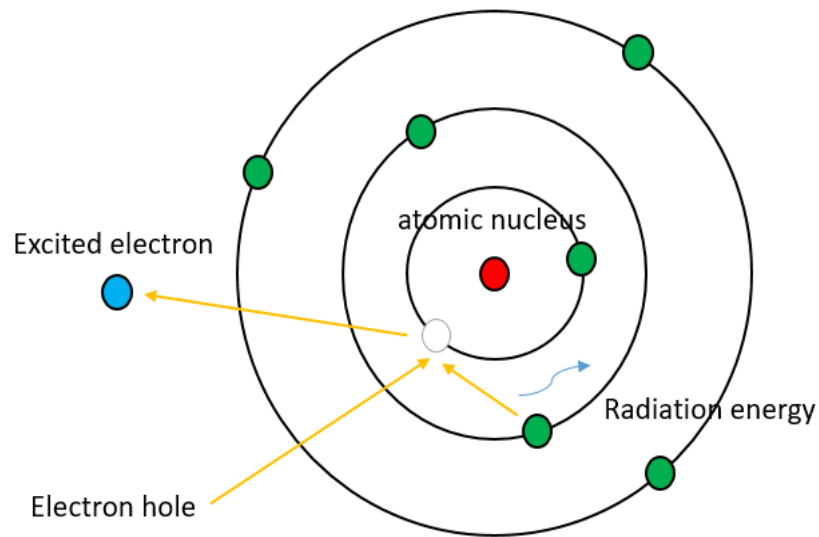


Figure 4-6 Schematic diagram of working principle of EDX

4.8 Microstructural classification

It was reported that the deposit microstructure was strongly affected by mass transport phenomena [9]. The deposit morphology is related to both dimensionless number N_m , which is the ratio of average current density to DC limiting current density, and N_p that is the ratio of peak current density to pulse limiting current density. They stand for steady-state and transient mass transfer limitations respectively [2]. The electro-crystallization behaviours are interpreted from the quantification of mass transport limitation using the plot of N_p versus N_m , as shown in Figure 4-7.

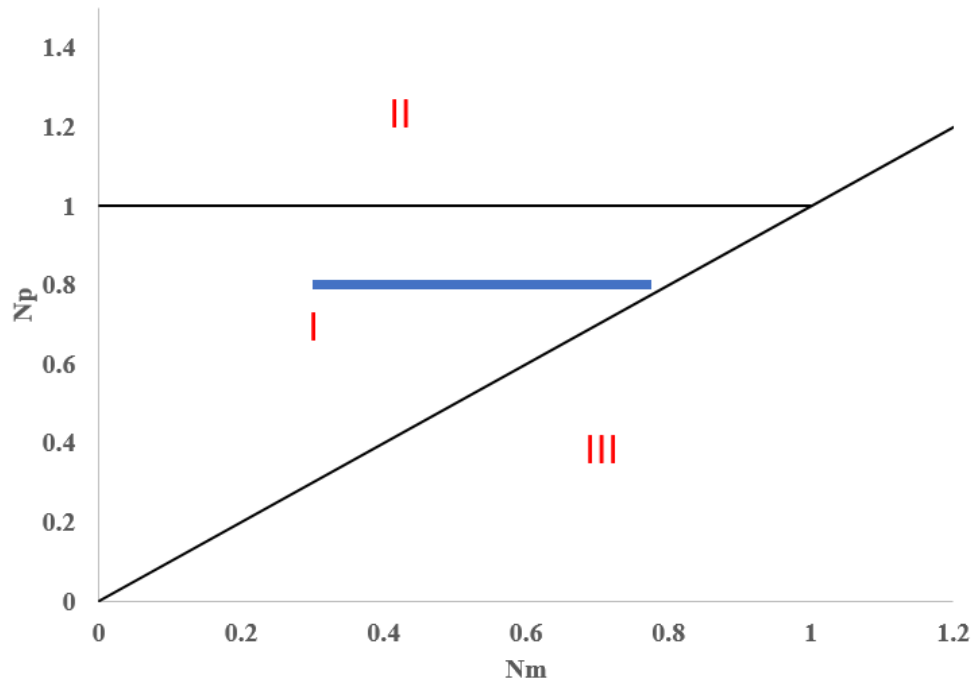


Figure 4-7 Deposit microstructure classification based on steady state and transient mass transfer limitations

There are three regions in the plot of N_p versus N_m . The condition of Region III is not reachable since N_m could not exceed N_p empirically. Region II is the situation where the limiting current density is exceeded. The deposit morphology becomes dendritic and nodular with a reduction on the Faradaic efficiency. Region I corresponds to the condition where the mass transport limitations are not exceeded and granular deposit is achieved. When N_m is constant, the increase of N_p lead to the transition of deposit morphology from granular to dendritic.

The range of deposit microstructure can also be quantitatively categorized from the Figure 4-7 [11]. For instance, smooth and compact deposit could be achieved with measured deposit grain size smaller than 60 nm when both N_m and N_p are smaller than 0.5. The deposit becomes looser and rougher when N_p is in the range of 0.5 to 0.7. The corresponding deposit grain size is in the range between 60 nm to 150 nm. When N_p is larger than 0.7 the deposit grain size is larger than 150 nm with a rough surface morphology.

The blue region in the figure indicates the range of N_m and N_p of the pulse parameters in this piece of research. As shown in the Table C-1 and Table C-2, N_p was fixed as 0.8. The range of N_m for copper was from 0.47 to 0.79 and from 0.28 to 0.78 for tin. All the pulse conditions are located in region I, indicating that the plating process is under mass transfer limitations. Therefore, it is expected that granular and smooth deposit should be achieved.

This chapter has illustrated the details of calculation methods on determination of pulse parameters. The experimental setup and procedure for metal deposition and dissolution experiments were also elaborated, followed by the working principles of SEM and EDX characterization as well as deposit microstructural classification. The next two chapters will demonstrate the experimental results with interpretations on metal plating of copper and tin, respectively.

Reference List

1. Wolfgang E., Hansal G., Roy S. (2012). Pulse Plating. Eugen G. Leuze Verlag KG. Germany
2. Chene O., Landolt D. (1989). The influence of mass transport on the deposit morphology and the current efficiency in pulse plating of copper. *Journal of Applied Electrochemistry*. 19 (2) pp 188-194
3. Ibl N. (1980). Some theoretical aspects of pulse electrolysis. *Surface Technology*. 10 (2) pp 81-104
4. Puipe J.Cl., Ibl N. (1980). Influence of charge and discharge of electric double layer in pulse plating. *Journal of Applied Electrochemistry*. 10 (6) pp 775-784
5. Pearson T. (2005). Modelling of Faradaic current profiles during pulse reverse plating. *Transactions of the Institute of Metal Finishing*. 83 (4) pp 171-180
6. Puipe J.Cl., Ibl N. (1980). Influence of charge and discharge of electric double layer in pulse plating. *Journal of Applied Electrochemistry*. 10 pp 775-784
7. Endres F., Abbott A., Macfarlane D. (2017). Electrodeposition from ionic liquids. 2nd ed. Wiley-VCH. Germany

8. Bard A.J., Faulkner L.R. (1980). Electrochemical methods: fundamentals and applications. 2nd ed. Wiley. New York
9. Pena E.M.B.D. (2017). Electrodeposition of copper using additive-containing low metal ion concentration electrolytes for EnFace applications. PhD thesis. University of Strathclyde. Glasgow
10. Goldstein J, Newbury D.E, Joy D.C, Lyman C.E, Echlin P, Lifshin E, Sawyer L, Michael J.R. (2003) .Scanning Electron Microscopy and X-ray Microanalysis, 3rd Ed Springer-Verlag. New York. USA
11. Wolfgang E., Hansal G., Roy S. (2012). Pulse Plating. Eugen G. Leuze Verlag KG. Germany

Chapter 5. Results and Discussions: Electrodeposition of Copper and the Investigation of Metal Dissolution Behaviour

This chapter describes the experimental results obtained from pulse plating of Cu using DES electrolyte and discusses their implications in detail. The chapter is divided into five primary sections: first is the study of electrochemical behaviour of DES solution by cyclic voltammetry and linear sweep voltammetry. The second part is the electrochemical analysis of Cu deposit plated from DES solution using pulse current based on deposit visual appearance, Faradaic efficiency and potential transients. The third section is the examination of metal dissolution behaviour, which was observed during the electrodeposition experiment, followed by the establishment of mathematical model revealing the relationship between metal dissolution and pulse parameters. The final part is the investigation of inhibition effect of benzotriazole in deposition and dissolution experiments.

5.1 Electrochemical study of DES electrolyte

The electrochemical properties of DES electrolyte need to be studied first. As mentioned in the previous chapter, the determination of limiting current density provides the practical operation range for deposition experiments to ensure that the mass transport limitations are not exceeded. The

theoretical DC and pulse limiting current densities were calculated based on the electrolyte properties, such as diffusion coefficient and kinematic viscosity, which were reported in the earlier electrochemical studies. The results could be compared and validated experimentally from the polarization experiments. In addition, the understanding of electrochemical behaviour of DES electrolyte provides useful information for the forthcoming analysis of deposition and metal dissolution experiments, as well as development of mathematical corrosion model.

The cyclic voltammetry study of 0.2 M Cu ethaline was performed on Pt working electrode. In these experiments, a Cu rod counter electrode and an Ag wire quasi reference electrode were used. The temperature was 25°C and a scan rate ranging between 10 mV/s and 50 mV/s was applied. The potential scan range was from -0.70 V to 0.70 V. The data was corrected for ohmic drop by applying IR compensation into the programming in NOVA software, as shown in Figure 5-1.

The figure shows two reduction peaks E_{pc1} and E_{pc2} were observed during the cathodic process from the voltammogram, indicating the reduction process of Cu^{2+} species to Cu. The CV diagram confirms that the Cu reduction process involves two steps, Cu^{2+} species firstly is reduced to Cu^+ species before further reduced to Cu. Similar results were reported from earlier CV studies on Cu in aqueous solution, DES electrolyte and other types of ionic liquids [1-6]. The first and second reduction potential was shown at +0.45 V

and -0.35 V. The result is in agreement with the literature which showed that the two cathodic peaks at approximately +0.50 V and -0.40 V [7, 8].

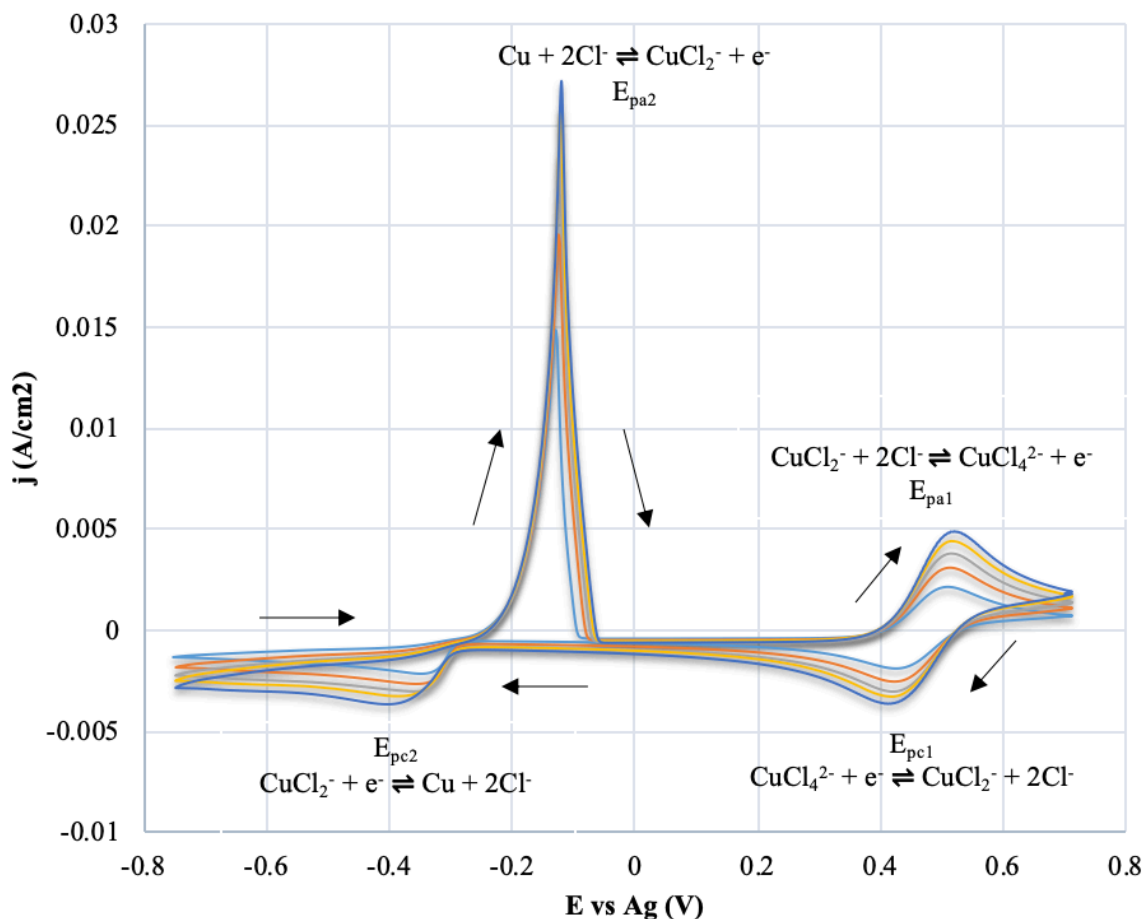
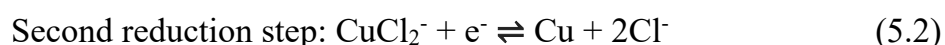
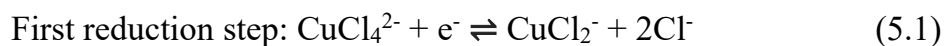
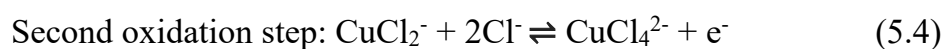
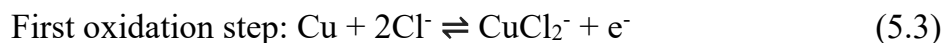


Figure 5-1 Cyclic voltammetry of ethaline melt containing 0.2 M CuCl_2 on Pt electrode under 700 rpm RDE rotation speed at 25°C temperature with various scan rates (—) 10 mV/s (—) 20 mV/s (—) 30 mV/s (—) 40 mV/s (—) 50 mV/s

The primary cupric ionic species existing in the CuCl₂ ethaline electrolyte has been identified as CuCl₄²⁻ complex [9, 10]. Therefore the corresponding reduction reactions are suggested as in equation (5.1) and (5.2).



Two oxidation peaks E_{pa1} and E_{pa2} were observed during the anodic process at -0.12 V and +0.52 V, indicating the oxidation process of Cu to Cu⁺ species and Cu⁺ species to Cu²⁺ species respectively. The corresponding reactions are shown in equation (5.3) and (5.4).



The Cu²⁺ / Cu⁺ redox is a quasi-reversible electron transfer reaction couple, since the ratio of anodic and cathodic peak current density j_{pa1} / j_{pc1} is in the range of 1.05 to 1.30. The ratio of j_{pa2} / j_{pc2} is much greater than 1, indicating the Cu⁺ / Cu redox process is non-reversible. Literature showed

similar reversibility of $\text{Cu}^{2+} / \text{Cu}^+$ couple in aqueous solution and DES electrolyte containing CuCl_2 [1, 8, 11].

The limiting current densities of Cu reduction process in DES solution were studied by linear sweep voltammetry, which was carried under various RDE rotating speeds from 300 rpm to 1200 rpm on Pt substrate at 25°C. The potential range scanned from +0.56 V, which was measured as the open circuit potential, to -1.2 V with 5 mV / s scan rate. Ohmic drop was corrected by applying IR compensation. The voltammogram was shown in Figure 5-2.

As shown in the figure, two cathodic peaks at +0.4 V and -0.4 V are observed from the voltammetry, indicating the two steps redox process of Cu^{2+} to Cu. The measured open circuit potential is similar to the literature, which reported the values were in the range of +0.5 V to +0.6 V [11, 12]. The current densities $j_{\text{lim}1}$ and $j_{\text{lim}2}$ indicate the limiting current density of Cu^{2+} and Cu^+ reduction reaction, while j_{lim} is the DC limiting current density of Cu^{2+} stripping reaction to Cu ($j_{\text{lim}} = j_{\text{lim}1} + j_{\text{lim}2}$). The value of j_{lim} was determined as 7.2 mA / cm² from the second current plateaux at -1.15 V on the 700 rpm curve. The measured j_{lim} is slightly higher than the theoretical value 6.2 mA / cm² and literature, which reported the value was in the range between 6.0 mA / cm² and 6.5 mA / cm² under the same experimental conditions [7, 12]. The reason could be attributed to the use of soluble Cu anode in the voltammetry rather than insoluble anode in the reported studies.

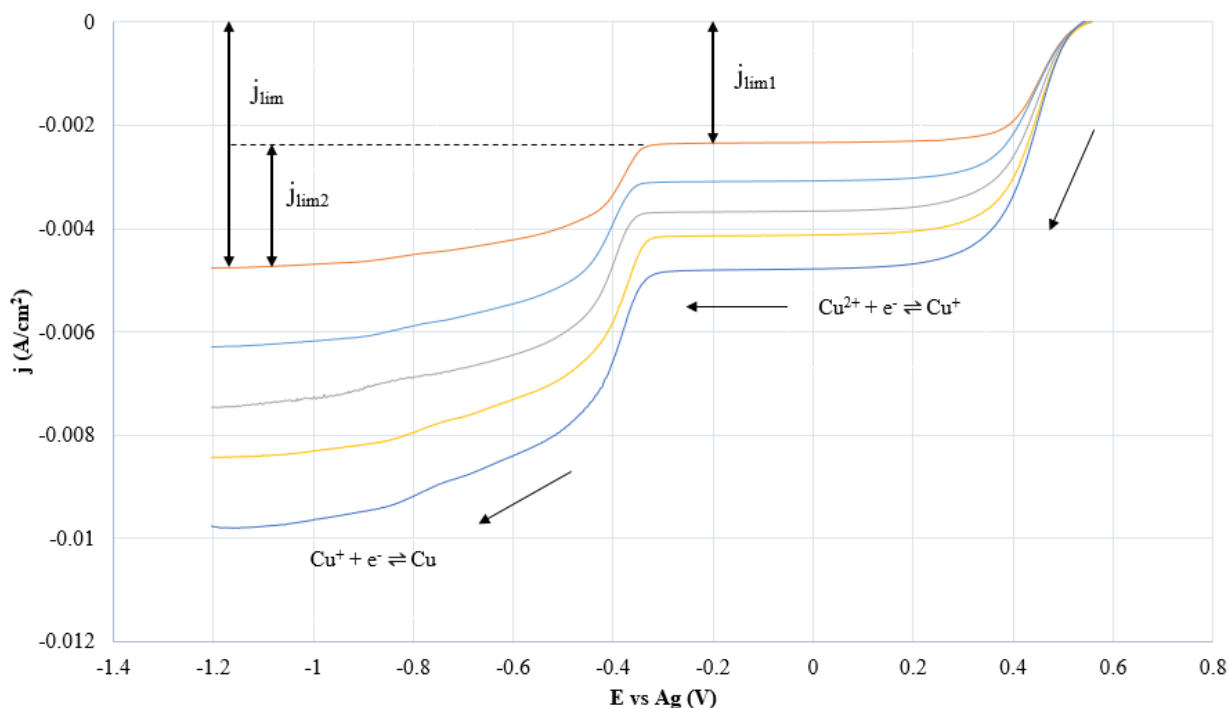


Figure 5-2 Linear sweep voltammetry of ethaline melt containing 0.2 M CuCl_2 on Pt electrode 25°C temperature with 5 mV/s at various RDE rotation speed
 (—) 300 rpm (—) 500 rpm (—) 700 rpm (—) 900 rpm (—) 1200 rpm

In addition, it was reported that the DC limiting current density from the aqueous electrolyte containing the same concentration of CuCl_2 was measured as approximately $96.7 \text{ mA} / \text{cm}^2$, which is more than 13 times larger than the one measured in DES system [12]. This is because of the higher viscosity of aqueous solution compared to the DES electrolyte.

The diagram also illustrates the relationship between limiting current density and the strength of agitation. Both limiting current densities become more negative as the RDE rotation speed increases, indicating higher current

densities are achieved with increased agitation condition. The results confirm that the Cu reduction reactions from DES electrolyte were under mass transport control, which also coincide with previous studies [11].

5.2 Electrochemical characterization of Cu deposition

The pulse deposition of Cu experiments in DES electrolyte were carried out after the study of electrochemical behaviour. The peak current density was applied as 80% of pulse limiting current density, which was calculated from the DC limiting current density. In this case, the mass transport limitations are not exceeded to avoid the formation of rough and dendritic Cu deposit [13, 14]. A matrix of 16 pulse conditions consisting of four duty cycles (0.2, 0.3, 0.5 and 0.67) and four pulse on-times (10 ms, 50 ms, 100 ms and 200 ms) was applied. The galvanostatic deposition was performed on steel substrate with Cu soluble counter electrode and Ag quasi-reference electrode in the 0.2 M CuCl₂ ethaline DES. The temperature and RDE rotation speed were fixed at 25°C and 700 rpm respectively. The setting of plating time in each pulse condition aimed to achieve a nominal 5 µm thickness Cu deposit.

In the forthcoming sections, the visual appearance of Cu deposit is illustrated with its implications from the analysis of Faradaic efficiency and potential profiles.

5.2.1 Visual appearance

After the deposition experiment was finished, the steel substrate was washed by deionized water and dried by blowing nitrogen gas. The appearance of Cu deposits under various pulse on-time (t_{on}) and duty cycle (θ) conditions were shown in the Figure 5-3.

As shown in the figure, plated Cu deposit was shown in reddish orange colour and the grey regions are those of exposed steel substrate. Some of the deposits have water stain which was formed during drying process. Cu only partially covers the substrate under certain pulse conditions, where copper is visible at the edge of substrate and steel is exposed at the centre. This annulus appearance becomes more prominent for lower duty cycle and longer pulse on-time conditions. No Cu is observed in the pulse condition of 200 ms duty cycle and 0.1 duty cycle. This plating pattern was compared to the Cu deposit plated under DC condition where Cu fully covered the electrode [12]. The reasons are further investigated from the analysis of Faraday efficiency.

5.2.2 Faradaic (current) efficiency

The Faradaic efficiency was calculated to show the comparison between the quantity of plated Cu deposit and the theoretical value where no Faradaic loss is accounted. The calculation method has been described in the

equation (4.12) and (4.14) [15, 16]. The current efficiencies under various pulse conditions are shown in the Table 5-1.

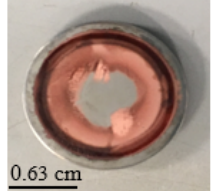






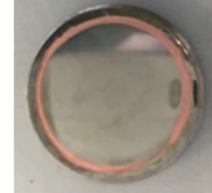

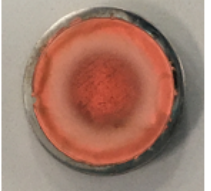


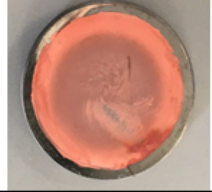
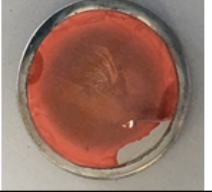

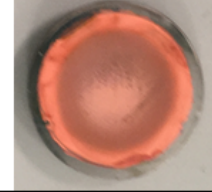
	$t_{on} = 10 \text{ ms}$	$t_{on} = 50 \text{ ms}$	$t_{on} = 100 \text{ ms}$	$t_{on} = 200 \text{ ms}$
$\theta = 0.2$				
$\theta = 0.3$				
$\theta = 0.5$				
$\theta = 0.67$				

Figure 5-3 Results from pulse deposition of Cu in 0.2 M Cu ethaline under various pulse conditions

As shown in the table, the Faradaic efficiency in the pulse plating matrix is in the range of -23.3% to 61.1% with 3.5% error. In general, current efficiency tends to be higher when duty cycle increases under the same pulse on-time condition and becomes lower when the period of pulse on-time is

longer with fixed duty cycle. In the pulse condition of 200 pulse on-time and 0.2 duty cycle the Faradaic efficiency becomes negative, indicating the weight loss of the steel substrate after plating. These results correspond to the Cu coverage on the steel substrate from the previous visual observations. The current efficiency tends to be higher with larger Cu coverage. Such behaviour has not been reported during the pulse deposition in aqueous solution, or DC plating using DES electrolyte. As a comparison, the Faradaic efficiencies using pulse current are lower than the one obtained under DC condition, which was measured as 78.0% using the same electrolyte. Lower Faradaic efficiency values from 50% to 60% were reported from DC plating under CuCl₂ ethaline DES system [12, 15, 16]. The Faradaic efficiency of pulse deposition of Cu in aqueous solution was reported to be over 90% under certain pulse conditions [17, 18].

	t_{on} = 10 ms	t_{on} = 50 ms	t_{on} = 100 ms	t_{on} = 200 ms
θ = 0.2	40.7 %	21.2 %	9.2 %	-23.3 %
θ = 0.3	44.4 %	30.0 %	13.7 %	-1.7 %
θ = 0.5	57.5 %	53.2 %	45.6 %	30.4 %
θ = 0.67	61.1 %	57.4 %	56.2 %	45.9 %

Table 5-1 Faradaic efficiency from pulse deposition of Cu in 0.2 M Cu ethaline DES under various pulse conditions

5.2.3 Potential profiles

One important method monitoring the Cu pulse deposition process is to investigate the change of potential change at the electrode surface. As depicted in the chapter 3, the overall cell potential E equals the addition of equilibrium potential E_r and overall overpotential η , which is the summation of surface overpotential (η_s), concentration overpotential (η_c) and ohmic overpotential (η_Ω) [75]. The corresponding equation is illustrated below.

$$E = E_r + \eta_s + \eta_c + \eta_\Omega \quad (5.5)$$

In the equation (5.5), the concentration overpotential could be neglected if the electrolyte is in well-agitated condition [20]. The surface overpotential and ohmic overpotential could be expressed in equation (3.6) and (3.12) respectively. E_r equals to the open circuit potential, which was measured as +0.56 V previously.

The potential transient of a single pulse was recorded after one thousand pulses due to the storage limitation of potentiostat instrument. Figure 5-4 illustrates the potential diagram of one pulse condition of 200 ms pulse on-time and 0.5 duty cycle with 10.6 mA/cm² applied peak current density. The charging time t_c is 0.49 ms and discharging time t_d is 0.58 ms.

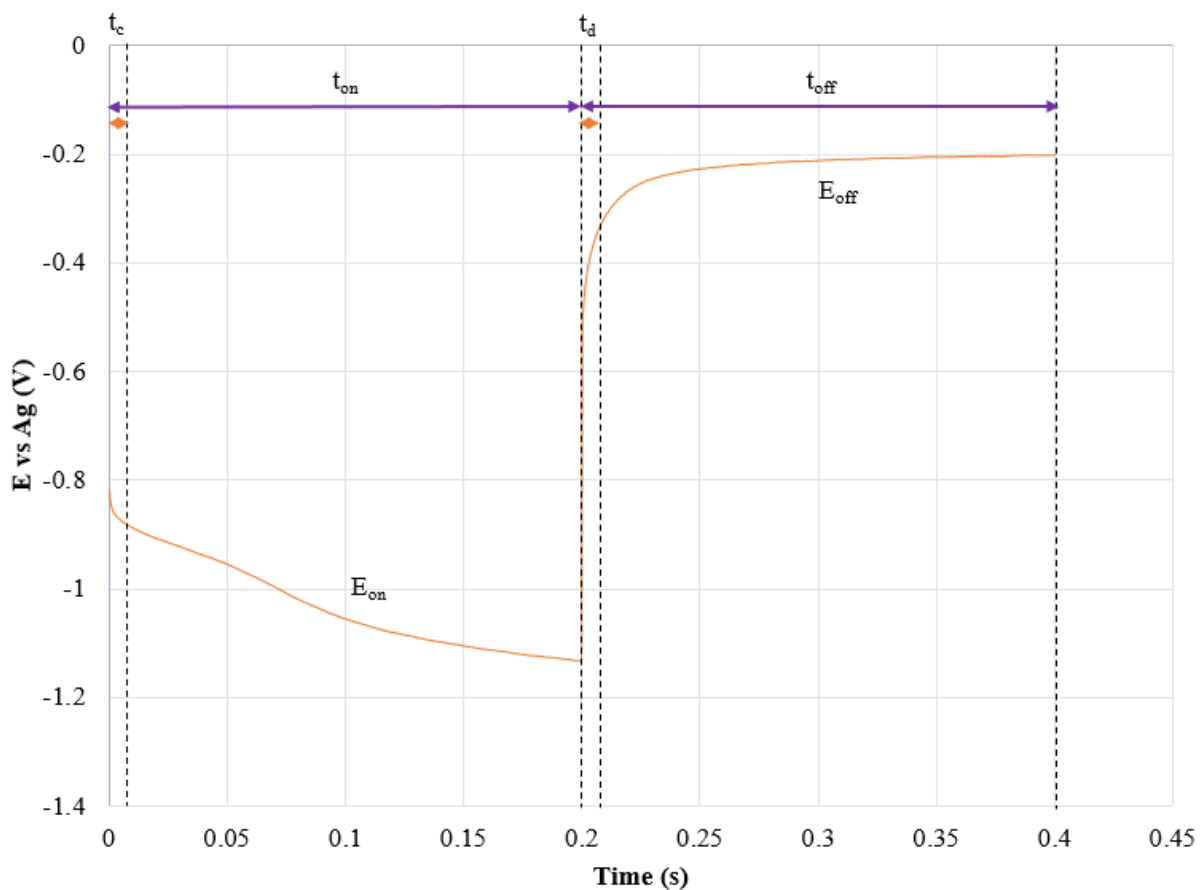


Figure 5-4 Potential profile in single pulse in pulse electrodeposition of Cu with the condition of $t_{on} = 200$ ms and $\theta = 0.5$

The diagram shows the entire electrochemical reaction process in one pulse of Cu electrodeposition. When the current is switched on, the electrical double layer undergoes charging and part of the electrical charges are stored in the duration of charging time. During this process, the overall potential becomes more negative due to the increase of surface overpotential and ohmic overpotential when the charging (capacitive) current density decreases. The

electrochemical reduction reaction of Cu proceeds with 100% peak current density after the electrical double layer is fully charged. Cell potential continues to fall from -0.85 V to -1.15 V, indicating the Cu^+ reduction process (equation 5.2) on the surface of steel substrate.

When the power is switched off, the double layer discharges and the stored charges are released in the form of current density. Cell potential rises significantly due to the decrease of overall current density in the system. After the discharging period, the overall overpotential is zero and cell potential should be equal to the equilibrium potential only, if no other electrochemical reactions take place. However, the diagram shows that the cell potential gradually increases to -0.2 V at the end of pulse, indicating the occurrence of other electrochemical reactions during the pulse off-time. The potential diagrams of Cu deposition in other pulse conditions are shown in the appendix section.

The trends found from visual observation of Cu deposit and Faradaic efficiency correspond to the potential diagram. Three potential profiles in a single pulse of 200 ms pulse on-time with 0.2, 0.3 and 0.67 duty cycles are compared in Figure 5-5. Full Cu coverage was found on the substrate at 0.67 duty cycle condition, partial Cu coverage at 0.3 duty cycle condition and no copper coverage was found at 0.2 duty cycle condition. During pulse on-time period, the cell potential becomes more negative with lower duty cycle due to the larger overall overpotential, since higher peak current density is applied. In

pulse off-time period, the potential at 0.67 duty cycle condition remains constant at -0.21 V at the end of pulse cycle. The potential at 0.3 duty cycle firstly reaches -0.25 V and then continues to rise. The potential at 0.2 duty cycle reaches at -0.30 V at the beginning before rising gradually to a constant potential of -0.08 V in the end.

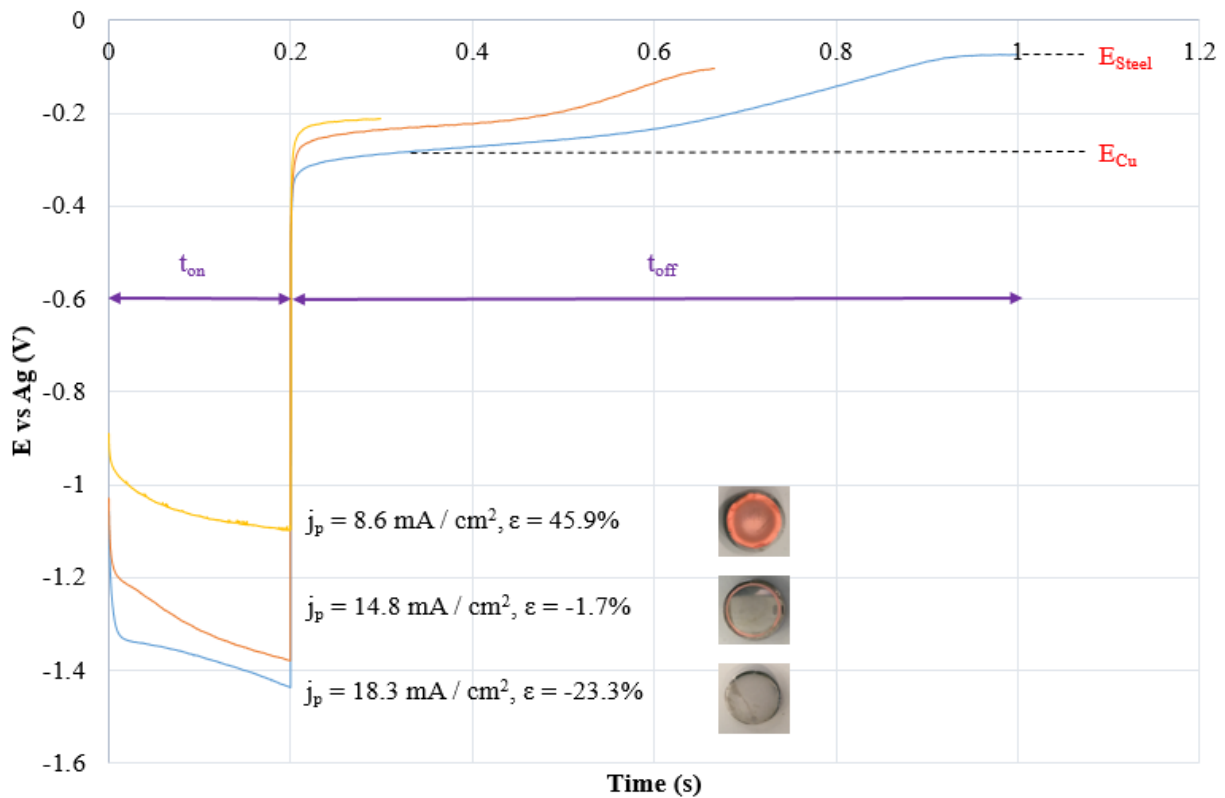


Figure 5-5 Potential profile of single pulse in pulse plating of Cu, $t_{on} = 200$ ms,
 (—) $\theta = 0.2$ with no Cu coverage (—) $\theta = 0.5$ with partial Cu coverage (—) $\theta = 0.67$ with full Cu coverage

These results confirm the occurrence of side reactions during the pulse off-time period. Lower Faradaic efficiency and lower Cu coverage were observed with the increase of pulse off-time. Based on these findings, it is reasonable to suggest the Cu is dissolved and started to be removed from the electrode surface when power is switched off with a corresponding corrosion potential E_{Cu} , which is indicated as the dissolution potential of copper. After that the rise of potential indicates the process where Cu is removed off from the centre of electrode, until to the point of E_{Steel} when Cu is fully removed from the electrode surface of steel substrate, which also suffers from dissolution. E_{steel} is the dissolution potential of steel. Based on these findings metal dissolution is suggested and would be investigated in the next section.

5.3 Examination of metal dissolution behaviour

Metal dissolution was proposed during the off-time period in the experiment of Cu pulse deposition using $CuCl_2$ ethaline DES electrolyte. A series of experiments were therefore undertaken to test this hypothesis in both qualitative and quantitative methods.

5.3.1 Metal dissolution under stagnant and agitation condition

At first, metal dissolution experiments were performed to test whether both Cu and steel could dissolve in the DES solution without agitation. A

piece of Cu sheet and steel disc was added into a beaker containing approximately 30 ml ethaline melt electrolyte with and without 0.2 M cupric chloride salt respectively and left for 410 hours. The weight of Cu sheet and steel disc was measured before and after the experiment. The colour of ethaline melt without and with CuCl_2 is transparent and light brown respectively, as shown in Figure 4-1. Figure 5-6 shows the appearance of pure ethaline after the soaking experiment.

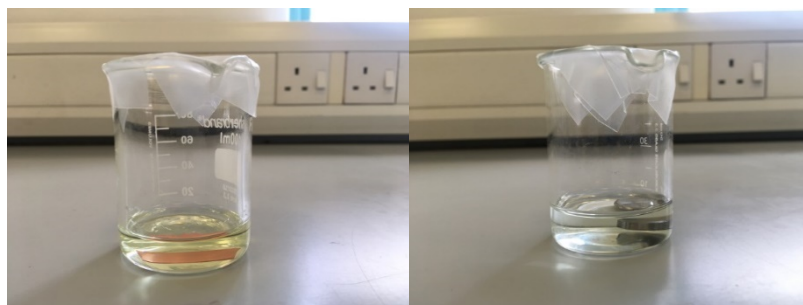


Figure 5-6 Appearance of ethaline DES after 410 hours soaking experiment with Cu sheet (left) and steel disc (right)

The figure shows that the colour of ethaline containing Cu sheet turns to light yellow but still remains transparent. No appearance change was observed in the soaking experiment of steel disc.

Figure 5-7 reveals the appearance of ethaline containing cupric chloride salt after the soaking experiment. Major appearance changes were observed in both groups. The solution containing Cu sheet turns dark with a colour of light

green. The solution containing steel disc also becomes dark with slight yellow colour.

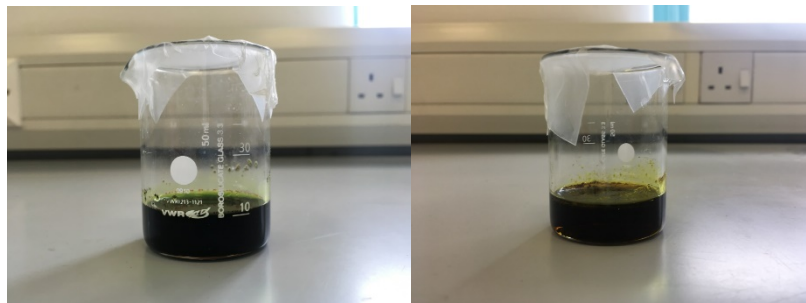


Figure 5-7 Appearance of CuCl_2 ethaline DES after 410 hours soaking experiment with Cu sheet (left) and steel disc (right)

The weight change and rate of change of Cu sheet and steel disc were shown in Table 5-2. The negative sign indicates the weight loss after the soaking experiment. It shows that metal dissolution in pure ethaline is a very slow process. However, the weight loss increases dramatically for both Cu sheet and steel disc after CuCl_2 was added into ethaline. It implies that the interaction between metal and the cupric ionic complex is much stronger than pure ethaline.

The examination of metal dissolution was further tested under agitation condition. For these experiments, a layer of Cu was plated on the steel substrate under DC condition to ensure Cu entirely covers the substrate surface. Then the substrate was mounted to the RDE rotor and remained

spinning with 700 rpm RDE rotation speed in the CuCl₂ ethaline DES electrolyte for 15 minutes without any applied external peak current density.

Metal	Solution	Weight Change (mg)	Rate (mg / cm² h)
Cu (sheet)	Pure ethaline	- 0.6	- 3.27×10^{-4}
Cu (sheet)	0.2 M CuCl ₂ ethaline	- 110.6	- 0.058
Steel (disc)	Pure ethaline	- 0.2	- 1.53×10^{-4}
Steel (disc)	0.2 M CuCl ₂ ethaline	- 47.2	- 0.037

Table 5-2 List of weight change and rate of change of Cu sheet and steel disc in ethaline with and without CuCl₂

Figure 5-8 shows the appearance of steel substrate before and after the experiment. Cu is removed from the centre of substrate and steel is exposed. The rate of weight loss was calculated as 0.32 mg/cm² h, which is approximately 5.5 times higher than the rate measured under stagnant condition. Therefore, the increase of mass transport condition can accelerate the rate of metal dissolution. These studies have clearly verified the proposed hypothesis that both Cu and steel could dissolve in the CuCl₂ ethaline DES electrolyte.



Figure 5-8 Plated Cu deposit on steel substrate before (left) and after (right) 15 minutes dissolution experiment in 0.2 M Cu ethaline under 700 rpm RDE rotation speed

5.3.2 Further investigation of metal dissolution process

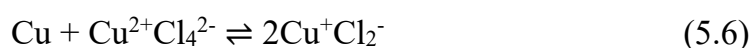
An early study reported the extremely slow corrosion rate of steel immersed in pure ethaline melt, which was in agreement with the obtained results [21]. However, corrosion behaviour was found in a number of DES electrolyte and other type of ionic liquids containing chloride ions. For instance, Cu was corroded by Cu (II) species in the trimethyl-n-hexylammonium bis((trifluoromethyl)sulf-onyl)amide (TMHA-Tf₂N) ionic liquid and Cu(I) was formed via comproportionation reaction, which was reported to be thermodynamically favourable [22, 23].

The corrosion behaviour in other metals was also observed in the chloride-containing DES electrolyte. It was found that Cr anode was corroded in the CrCl₃ ethaline DES electrolyte [24]. In addition, the corrosion of Fe

anode was reported via comproportionation reaction between Fe^{3+} and Fe in the FeCl_3 DES electrolyte [25, 26].

In addition, Cu corrosion was reported in the aqueous solution containing chloride. Cu was etched in the CuCl_2 -HCl-KCl water based solution, which is an important procedure during the PCB manufacturing process [27]. Corrosion was also observed in the galvanostatic Cu deposition from acidic cupric halide electrolyte during the pulse off-time period [28]. Moreover, such behaviour was also revealed from the study of pulse plating Cu alloys [29, 30].

Based on the previous studies and reports it can be concluded that the electrolyte containing chloride ions is metal corrosive both in aqueous solution and DES electrolyte. The comproportionation reaction of Cu dissolution during the pulse off-time is suggested as follows.



The deposit layer thickness across the electrode surface was studied in Cu deposition using CuCl_2 ethaline DES electrolyte under DC condition [12]. The applied peak current density was 4.68 mA/cm^2 and the Wagner number was calculated to be 0.17, indicating a non-uniform deposit thickness [31]. It was also reported that the current density on the edge of working electrode was

much higher than the one on the centre, indicating thicker Cu deposit is plated far from the centre of electrode surface. Similar experimental conditions were undertaken in the Cu pulse deposition. The Wagner number of each pulse condition was calculated and shown in Table 5-3.

On time (ms)	Duty cycle	Wagner number
10	0.2	0.0036
10	0.3	0.0051
10	0.5	0.0080
10	0.67	0.0106
50	0.2	0.0042
50	0.3	0.0056
50	0.5	0.0084
50	0.67	0.0109
100	0.2	0.0046
100	0.3	0.0059
100	0.5	0.0087
100	0.67	0.0110
200	0.2	0.0053
200	0.3	0.0065
200	0.5	0.0090
200	0.67	0.0112

Table 5-3 Wagner number of each pulse condition for copper deposition

As can be seen from the table, the calculated Wagner number in pulse plating ranges between 0.0036 and 0.011 depending on the pulse condition, indicating a non-uniform deposit layer thickness across the surface of steel substrate [31]. The applied peak current density is much higher than DC condition. Therefore, the current distribution for pulse plating is expected to be worse compared to DC condition, since the Wagner number is much lower.

Therefore the layer of Cu deposit on the edge of electrode is much thicker than the one on the centre of electrode surface.

Since the comproportionation reaction proceeds during the pulse off-time, more copper is dissolved when the duration of off-time is longer. Cu at the electrode centre is removed first and the dissolution of Cu at the electrode edge takes longer time to dissolve, which explains the formation of annulus pattern of Cu deposit under certain pulse condition. When the duration of off-time is sufficiently longer, Cu both at the edge and at the centre of electrode is completely removed from the surface of steel substrate.

5.3.3 Determination of dissolution rate and current density

The occurrence of metal dissolution in CuCl_2 ethaline DES electrolyte has been identified. The next step is to quantitatively determine the rate of reaction and test whether the dissolution process is under mass transport control. Pure Cu disc was used in these experiments. The weight change was measured before and after the experiment by using gravimetric method. The dissolution current density j_{dis} was calculated from the dissolution rate r_{dis} , which is defined as the mass loss of metal per unit time per unit area. The expression is illustrated in equation (5.7).

$$r_{\text{dis}} = \frac{m_{\text{dis}}}{tA} \quad (5.7)$$

In equation (5.7), m_{dis} is the metal mass loss, t is the time, and A is the surface area. m_{dis} can be further expressed by the Faraday's law.

$$m_{\text{dis}} = \frac{Q_{\text{dis}}M}{Fz} \quad (5.8)$$

In equation (5.8), M is the metal molar mass, F is the Faraday constant, z is the ionic charge, Q_{dis} is the dissolution charge and can be expressed in terms of dissolution current density j_{dis} .

$$Q_{\text{dis}} = \frac{j_{\text{dis}}t}{A} \quad (5.9)$$

In equation (5.9), j_{dis} is the dissolution current density. The relationship between dissolution current density and dissolution rate is shown by combining the equations of (5.7), (5.8) and (5.9).

$$j_{\text{dis}} = \frac{zFr_{\text{dis}}}{M} \quad (5.10)$$

The duration of experiment was fixed at 20 minutes with 25°C temperature, RDE rotation speed ranged from 300 rpm to 1200 rpm. The

surface area of Cu substrate was measured as 1.25 cm². The rate of dissolution was shown in Table 5-4.

RDE (rpm)	Mass Loss (mg)	r_{dis} (mg min⁻¹cm⁻²)	j_{dis} (mA cm⁻²)
300	2.2	0.088	2.23
500	2.8	0.112	2.84
700	3.4	0.136	3.45
900	3.8	0.152	3.86
1200	4.5	0.180	4.57

Table 5-4 Dissolution rate and current density with varying RDE rotation speed for Cu disc

As can be seen from Table 5-4, the corrosion current density is in the range of 2.23 mA/cm² to 4.57 mA/cm², depending on the agitation condition. In addition, the current density is in linear relationship to the square root of RDE rotation speed, suggesting the dissolution process is under mass transport control, as shown in Figure 5-9.

5.3.4 Dissolution potential

The electrochemical behaviour of metal dissolution was also monitored by measuring the dissolution potentials during the dissolution process. The corrosion potential profile of Cu disc was measured independently under various RDE rotation speeds for 10 minutes, as shown in the Figure 5-10.

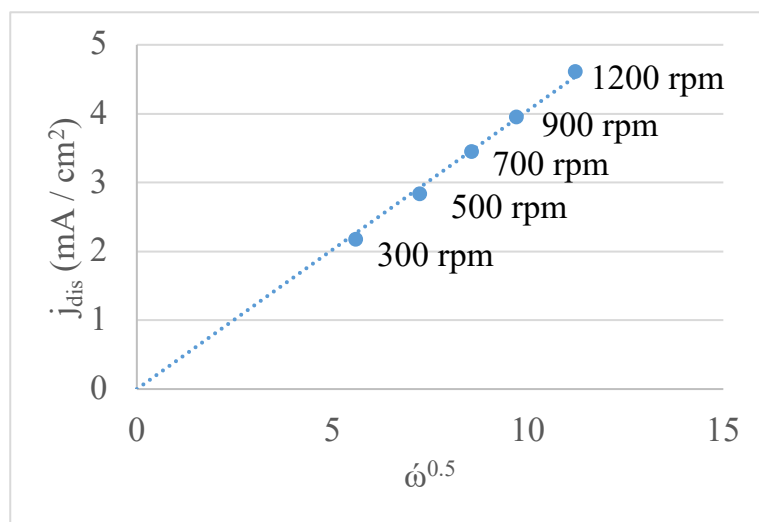


Figure 5-9 Relationship between dissolution current density and square root of RDE rotation speed (regression equation $y = 0.81x$ with $R = 0.99$)

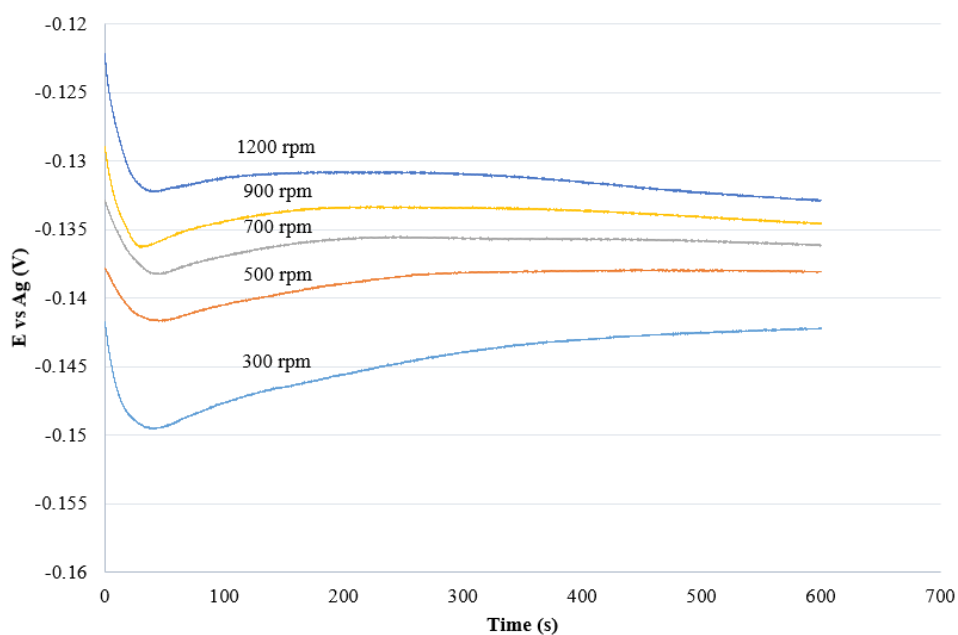


Figure 5-10 Dissolution potential profiles of Cu substrate under various RDE rotation speeds (—) 300 rpm (—) 500 rpm (—) 700 rpm (—) 900 rpm (—) 1200 rpm

Figure 5-10 shows that the dissolution potential falls at the beginning and gradually rises later before remaining constant nearly at the end of experiment. This may contribute to the microstructure change at the substrate surface during the dissolution process. It is noted that when the dissolution potential is shifting towards positive with the increase of agitation, the dissolution current density is also increasing.

Based on visual observation, the appearance of Cu disc is smooth and shiny in a mirror-like before the experiment, and it becomes rough and non-reflecting after dissolution experiment, as shown in Figure 5-11. In addition, the corrosion potential become more positive when the RDE rotation speed increases from 300 rpm to 1200 rpm, implying the effect of mass transport condition.



Figure 5-11 Visual appearance of Cu disc before (left) and after the dissolution experiment (right)

However, the dissolution potential data measured separately is not very reproducible and variance could occur in some cases. Therefore, the dissolution potentials were measured in one experiment while changing the RDE rotation speed from 300, 500, 700, 900 and until to 1200 rpm every 15 minutes, which is illustrated in Figure 5-12.

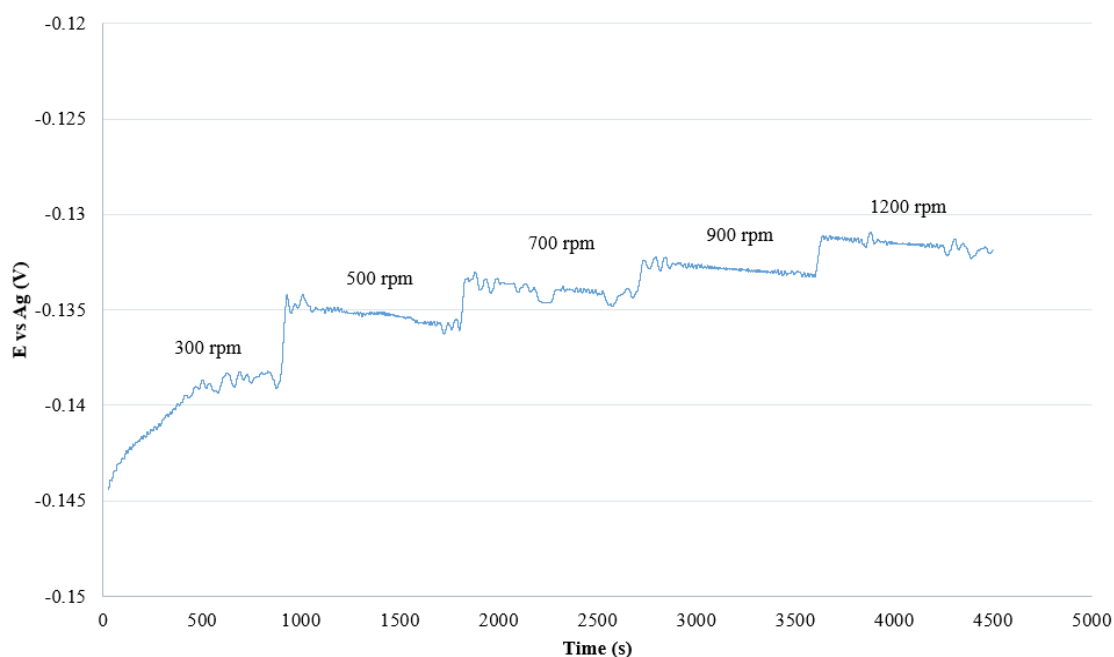


Figure 5-12 Dissolution potential of Cu disc with varying RDE rotation speeds

The figure shows that the dissolution potential shifts towards positive with the increase of RDE rotation speed. The trend is similar to the results which were obtained separately. The potential slightly falls when RDE rotation speed is constant except for the 300 rpm agitation condition, and the

reason may be attributed to the microstructure change during the experiment but it has not been fully understood yet. In addition, the data noise is more prominent, probably because of the poor contact of RDE rotor damaged by the infiltrated corrosive DES electrolyte.

The dissolution current density can be related to dissolution potential from the polarization curve, which is shown in Figure 5-13. During the pulse on-time, Cu deposition is achieved from the reduction reaction of Cu^+ ionic species. During the pulse off-time, Cu dissolution occurs due to the comproportionation reaction between Cu and Cu^{2+} ionic species. The anodic current density j_{anodic} , which is also indicated as dissolution current density j_{dis} , is the same as cathodic current density with opposite sign at the dissolution potential E_{dis} . The dissolution current density increases dramatically as the corrosion potential shifts towards positive.

In addition, the net current density in the electrolyte is zero during pulse off-time. Therefore, the relationship between the anodic and cathodic current density is shown in equation (5.11)

$$j_{\text{dis}} = j_{\text{anodic}} = -j_{\text{cathodic}} \quad (5.11)$$

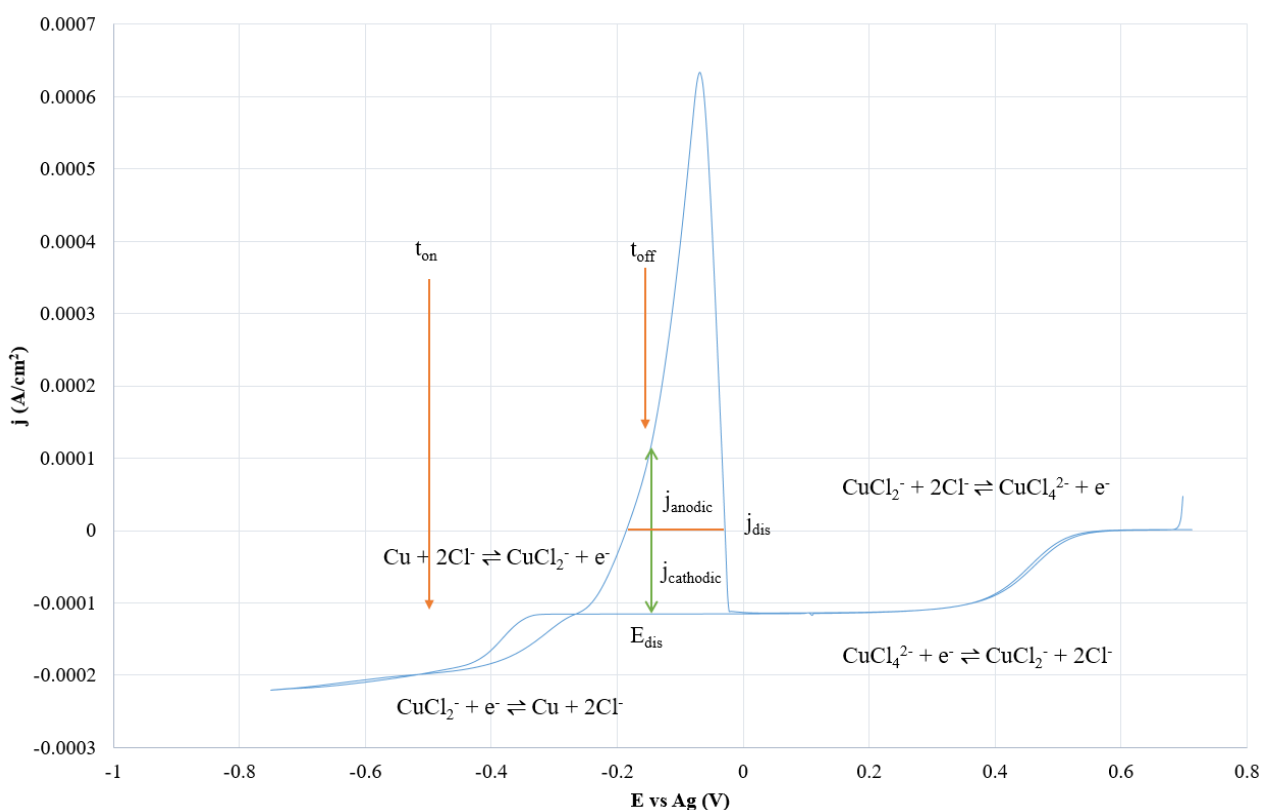


Figure 5-13 Polarization diagram of 0.2 M CuCl₂ ethaline DES on Pt electrode under 700 rpm at 25°C

5.3.5 Examination of solution aging effect

As been described in the soaking experiment of Cu sheet under stagnant condition, the colour of ethaline DES electrolyte containing CuCl₂ changed from transparent light brown to dark. Similar behaviour was also observed after performing a number of electrodeposition experiments without replacing the electrolyte. In addition, dark red precipitate was found at the bottom of electrochemical cell. The solution was in light blue colour after deionized water was added, as was shown in Figure 5-14.

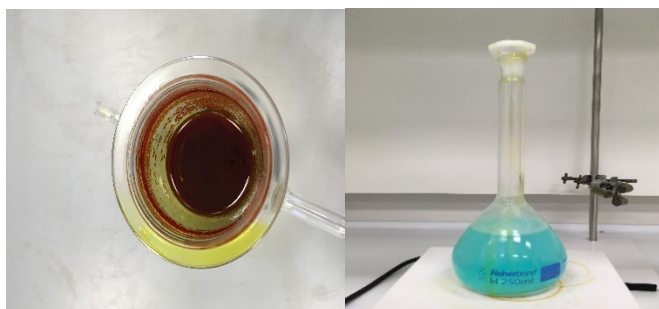


Figure 5-14 Dark red precipitate in the aging DES solution (left) and its dissolution in water (right)

Repeated Cu pulse deposition experiments, which are in a pulse condition of 10 ms and 0.67 duty cycle, were undertaken in the same solution to study how the solution aging phenomena affect the Faradaic efficiency. It was found that the Faradaic efficiency slightly increased from approximately 60% to 70% after performing seven repeated experiments under the same pulse condition, which is shown in Figure 5-15. Similar behaviour was also observed in the preliminary pulse deposition experiments, where the Faradaic efficiency using aged solution was higher than the one using fresh solution. In some cases the current efficiency was reported over 100%.

During the pulse off-time period, both Cu anode and Cu plated on the steel substrate are dissolved into the DES electrolyte due to corrosion. Therefore, the concentration of Cu^+ ionic species increases in an aged solution. This give rise to the increase of Faradaic efficiency, since Cu can be formed

by one electron transfer process from Cu^+ species, instead of the normal two electrons transfer process from Cu^{2+} species. Therefore, more Cu was formed when the provision of electrical charge is still the same. The colour change of electrolyte may be ascribed to the increase of Cu ionic concentration.

However, the exact reasons are not fully understood yet and need to be further investigated.

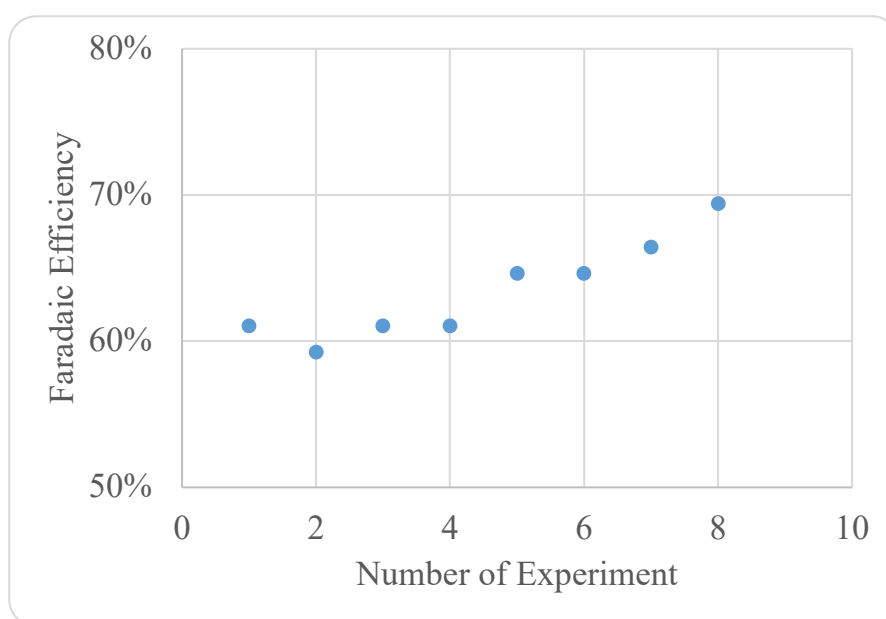


Figure 5-15 Faradaic efficiency of consistent repeated pulse deposition of Cu under the pulse condition of 10 ms pulse on-time and 0.67 duty cycle

5.4 Mathematical model for pulse deposition and dissolution

The relationships among Faradaic efficiency, pulse parameters and dissolution could be established in mathematical expressions. During the pulse

on-time period, cathodic peak current density is applied with a deposition efficiency ε_d due to Faradaic loss. During the pulse off-time the dissolution reaction of Cu proceeds. The remaining amount of Cu deposit at the end of electrodeposition is determined from the difference between Cu weight gain during pulse on-time and the weight loss during pulse off-time. The Faradaic efficiency ε_f is calculated by the remaining amount of Cu deposit versus the one under theoretical circumstance, where the deposition efficiency is 100% without the occurrence of Cu dissolution. Therefore the Faradaic efficiency is expressed in below.

$$\varepsilon_f = \frac{m_{\text{theoretical}}\varepsilon_d - m_{\text{dis}}}{m_{\text{theoretical}}} = \varepsilon_d - \frac{m_{\text{dis}}}{m_t} \quad (5.12)$$

In equation (5.12), ε_f is the observed Faradaic efficiency, m_t is the theoretical weight gain, m_{dis} is the total weight loss by dissolution during the pulse off-time, ε_d is the actual deposition efficiency. During the reduction reaction of Cu^{2+} to Cu two electrons are transferred. However only one electron needs to be transferred during the dissolution process of Cu. Both weight gain and weight loss could be expressed by Faraday's law.

$$m_{\text{theoretical}} = \left(\frac{j_p A t_{\text{on}}}{F}\right) \left(\frac{M}{z_p}\right) \quad (5.13)$$

$$m_{\text{dis}} = \left(\frac{j_{\text{dis}} A t_{\text{off}}}{F} \right) \left(\frac{M}{z_{\text{dis}}} \right) \quad (5.14)$$

In the equation (5.13) and (5.14), j_p and j_{dis} are the applied peak current density and dissolution current density, A is the surface area of metal deposit. M is metal molar weight, z_p and z_{dis} indicates the number of electrons transferred in plating and dissolution process respectively. In the case of Cu, z_p is 2 and z_{dis} is 1, since two electrons are transferred in deposition process and one electron transferred in dissolution. Combine the equation (5.12), (5.13) and (5.14) gives equation (5.15).

$$\varepsilon_f = \varepsilon_d - \frac{2j_{\text{dis}}t_{\text{off}}}{j_p t_{\text{on}}} \quad (5.15)$$

The relationship between pulse on-time t_{on} , pulse off-time t_{off} and duty cycle θ are shown below.

$$\theta = \frac{t_{\text{on}}}{t_{\text{on}} + t_{\text{off}}} \quad (5.16)$$

Combine equation (5.15) and (5.16) gives (5.17):

$$\varepsilon_f = \varepsilon_d - \frac{2j_{\text{dis}}(1-\theta)}{j_p\theta} \quad (5.17)$$

Equation (5.17) reveals that the Faradaic efficiency depends on the pulse parameters (j_p and θ) and dissolution rate. The main purpose of testing this mathematical model is trying to find out if the dissolution data obtained in the chapter 5.3 can be well integrated into the electrodeposition experiments.

5.4.1 Constant dissolution current density model

The model can be simply tested by fitting the data of Faradaic efficiency and pulse parameters (j_p and θ) in a linear relationship, assuming the dissolution current density is constant. Figure 5-16 illustrates the model which includes the results obtained from every pulse condition. The gradient and intercept indicate the value of dissolution current density and deposition efficiency. The deposition efficiency is in the range of 70.4% to 77.8%, which generally is in agreement with 78.0% that was determined from DC plating experiment. R^2 values ranges between 0.93 and 0.99, indicating the data generally fit the model. However, the values of dissolution current density are in the range of 0.93 mA/cm² and 1.75 mA/cm², which is against the assumption of constant dissolution current density. Therefore the model based on constant dissolution current density is inadequate.

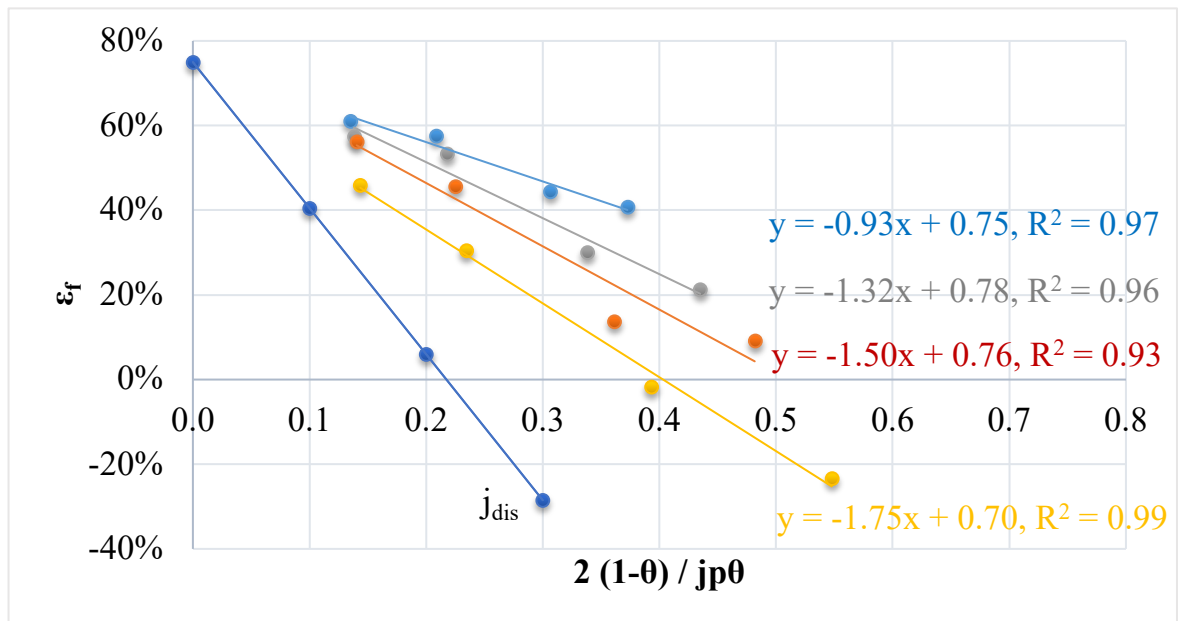


Figure 5-16 Relationship of ϵ_f vs $[2(1-\theta) / j_p\theta]$ derived from pulse plating of Cu experiment (•) 10 ms pulse on-time (•) 50 ms pulse on-time (•) 100 ms pulse on-time (•) 200 ms pulse on-time (•) j_{dis}

In addition, the dissolution current density increases with longer pulse period [32]. However, these dissolution current densities are lower than 3.45 mA/cm², which was determined from the separate Cu dissolution experiment. Another problem is that this mathematical model only considers Cu dissolution. However, only half of the data meet this condition with full Cu coverage based on the results of visual observation of Cu deposit. The corrosion of steel substrate is involved for the remaining data. The dissolution potential and current density of steel substrate are different from those of Cu,

suggesting that the dissolution current densities shown from the mathematical model are the results determined by both Cu and steel dissolution.

5.4.2 Varying dissolution current density model

Based on the results obtained from plating and dissolution experiments it is concluded that the dissolution current density is not constant in the corrosion process. Instead, the dissolution current density or corrosion reaction rate increases with time. In this case, the dissolution current density can not be determined using equation (5.17). Another approach of calculating the dissolution current density can be achieved from its relation to dissolution potential based on polarization curve, which is shown in Figure 5-13. Figure 5-5 illustrates the potential change during the entire pulse off-time period. But it should be noted that the corrosion reaction only takes place in the range of -0.265 V and 0 V. The average dissolution current density can be calculated by integrating the dissolution charges divided by the time. The corresponding equation is shown below:

$$j_{\text{dis (vr)}} = \frac{\int_{E=-0.265}^{E=E_{\text{off}}} j}{t_{\text{dis}}} \quad (5.18)$$

In the equation (5.22), $j_{\text{dis(vr)}}$ is the average dissolution current density calculated using varying dissolution current density mathematical model, E_{off} is the potential when reaching the end of pulse off-time. t_{dis} is the total dissolution time (s). The relationship between the dissolution current density and dissolution potential is shown in Figure 5-17. The corresponding trend line can be expressed as $y = 2.44 \times 10^6 x^5 + 2.62 \times 10^6 x^4 + 1.11 \times 10^6 x^3 + 2.34 \times 10^5 x^2 + 2.49 \times 10^4 x + 1.10 \times 10^3$, where y is dissolution corrosion current density and x is dissolution potential.

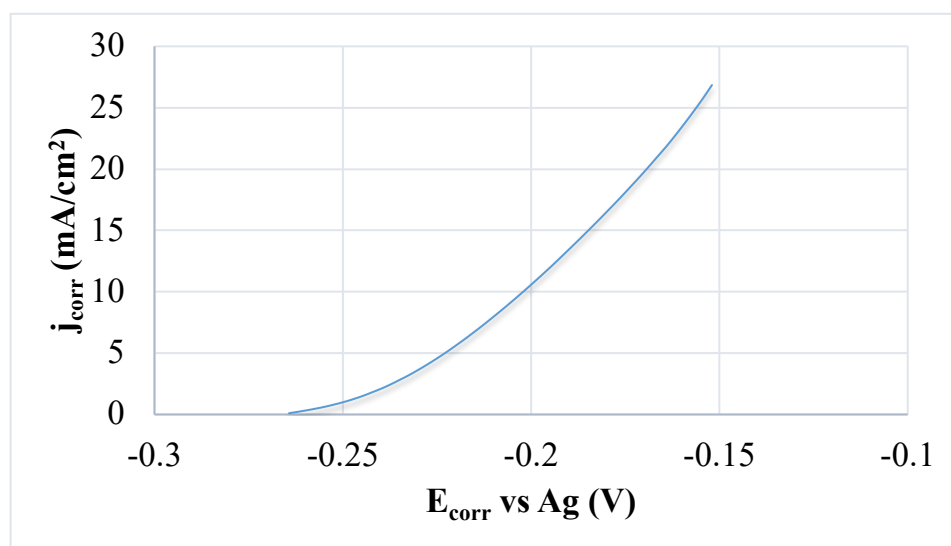


Figure 5-17 Relationship between dissolution current density and potential derived from the polarization curve (0.2 M CuCl_2 ethaline DES, 700 rpm RDE rotation speed, Pt electrode)

The average dissolution current density can also be calculated directly from equation (5.17) as a comparison to the data obtained from the mathematical model, assuming 78.0% of deposition efficiency. The results derived from all direct calculation, constant dissolution current density model and varying dissolution current density model are shown in Table 5-5.

θ	t_{on} (ms)	$j_{dis(c)}$ (mA/cm ²)	$j_{dis(vr)}$ (mA/cm ²)	$j_{dis(cr)}$ (mA/cm ²)
0.2	10	1.00	1.44	0.93
0.3	10	1.10	3.13	0.93
0.5	10	0.98	-	0.93
0.67	10	1.25	-	0.93
0.2	50	1.31	5.25	1.32
0.3	50	1.42	6.83	1.32
0.5	50	1.14	1.85	1.32
0.67	50	1.49	2.00	1.32
0.2	100	1.43	12.82	1.50
0.3	100	1.78	9.06	1.50
0.5	100	1.44	2.52	1.50
0.67	100	1.55	4.17	1.50
0.2	200	1.85	7.58	1.75
0.3	200	2.03	7.49	1.75
0.5	200	2.03	7.70	1.75
0.67	200	2.24	5.47	1.75

Table 5-5 List of dissolution current density determined from different approaches

The dissolution current density determined from calculation ($j_{\text{dis(c)}}$), varying corrosion rate model ($j_{\text{dis(vr)}}$) and constant corrosion rate model ($j_{\text{dis(cr)}}$) for all pulse conditions are demonstrated in the table. The blue font indicates the pulse condition where steel corrosion is involved. The values of $j_{\text{dis(c)}}$ are generally close to the $j_{\text{dis(cr)}}$ and are smaller than the $j_{\text{dis(vr)}}$, indicating the mathematical model of varying corrosion current density also could not fit the data very well. One of the reasons is due to the potential range selection for integration. In some cases, the dissolution current density is much higher than 3.45 mA/cm^2 that was measured from the independent dissolution experiment, since the dissolution current density of copper significantly increases when dissolution potential shifts toward positive, as indicated from the polarization curve. However, steel corrosion is still not considered in this model. $j_{\text{dis(vr)}}$ is calculated mostly within the range of Cu dissolution and no similar calculation was performed on the steel substrate, of which the polarization data is not available. Moreover, it is difficult to identify the point where steel corrosion starts to get involved, which could lead to errors on estimating the dissolution current density. For instance, very high corrosion current density is observed at -0.10 V from Cu polarization curve, whereas in reality Cu is fully removed from the substrate surface at that potential. However, it may suggest that the dissolution current density of steel substrate is possibly much smaller than Cu, based on the results that the dissolution rate of steel is slower than copper from the stagnant metal dissolution experiments.

It is also noted that for $j_{\text{dis(vr)}}$ can not be calculated on the pulse condition of 100 ms on-time with 0.5 and 0.67 duty cycles, since the corrosion potentials are lower than -0.265 V. This is attributed to the polarization curve used for calculation was performed on the Pt electrode rather than steel substrate. Based on preliminary tests it was found that the polarization curve on steel electrode was not well defined, which is not suitable for the forthcoming analysis. This is another limitation of this mathematical model.

In addition, the errors of the model may be ascribed to the “dead time theory”, which Cu dissolution reaction takes time to initiate. As a result, the actual dissolution time becomes shorter and the range of dissolution potential which is used for integration calculation shrinks. Therefore, the integrated average dissolution current density is expected to be lower. This proposal could be investigated in the future.

5.5 Study of the effect of benzotriazole additive (BTA)

Previous experiments have shown the Cu dissolution due to the corrosive property of CuCl₂ ethaline DES. The addition of BTA additive into the electrolyte was attempted to suppress the metal dissolution. According to the literature, numerous types of additive have been investigated for the corrosion protection [33]. The inorganic additives, such as copper nickel alloy, phosphates and phosphoric acid, zinc adatoms can effectively inhibit the Cu

corrosion and decrease the dissolution rate [34-36]. A number of organic additives and their derivatives, for instance the compounds containing amino acid, amines or azole group, were reported to be effective to suppress copper corrosion [37-39]. It was observed that the hetero atoms in the molecules of organic additives, such as phosphorus, sulphur and nitrogen, could improve the efficiency of corrosion inhibition [33].

BTA is a type of heterocyclic organic compound and known as an effective additive in the corrosion inhibition of copper and its alloys [40]. The schematic diagram of BTA structure is shown in Figure 5-18. It was found that the mechanism of the inhibition of copper dissolution by BTA is due to the formation of polymeric Cu-BTA complex barrier layer on the surface of copper when immersed in the solution [33, 41, 42]. In addition, the formation of CuO and Cu₂O layers were also reported along with the Cu-BTA complex in the solution containing chloride ions and BTA in alkaline, neutral and acidic conditions [43, 44].

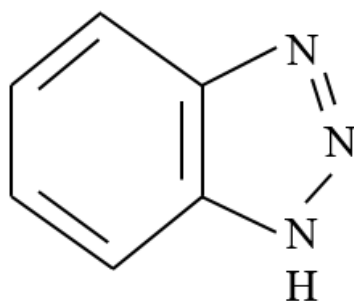


Figure 5-18 Schematic diagram of BTA structure

The inhibiting effect of BTA and its derivative on copper dissolution was reported from a number of studies in the aqueous electrolyte [33, 45, 46]. Therefore, it was proposed that BTA could be used to suppress the corrosion process in the DES electrolyte. The pulse plating and metal dissolution experiments with similar conditions were performed with the addition of BTA. The inhibition behaviour was examined with the comparison of the results obtained with and without the presence of BTA.

5.5.1 Voltammetry of Cu ethaline DES electrolyte with BTA

The influence of BTA on the electrochemical behaviour of Cu ethaline DES electrolyte was studied first from the cyclic voltammetry. In this experiment, the electrolyte was 0.2 M CuCl_2 ethaline DES containing 10 mM BTA, Pt was used as working electrode, Cu rod as counter electrode and Ag wire as quasi-reference electrode. The scan rate was fixed as 5 mV/s with 700 rpm RDE rotation speed at 25°C temperature. The voltammetry is shown in Figure 5-19 and compared against the one which has no BTA addition. The ohmic drop was corrected by applying IR compensation.

It is shown that the general profile of voltammetry with 10 mM BTA group is similar to the one without BTA. There are two cathodic and anodic peaks respectively, indicating the two steps redox reactions between Cu^{2+} ionic complex and Cu. The major difference is that the BTA has lower

cathodic current density than the non-BTA. In addition, the Cu stripping peak of BTA shifts towards negative and the peak current density becomes smaller. The voltammogram reveals that the addition of BTA does not significantly alter the redox process of Cu, however the magnitude of current density is observed to be slightly different. The limiting current densities for both Cu reduction steps are also lowered by when BTA is added.

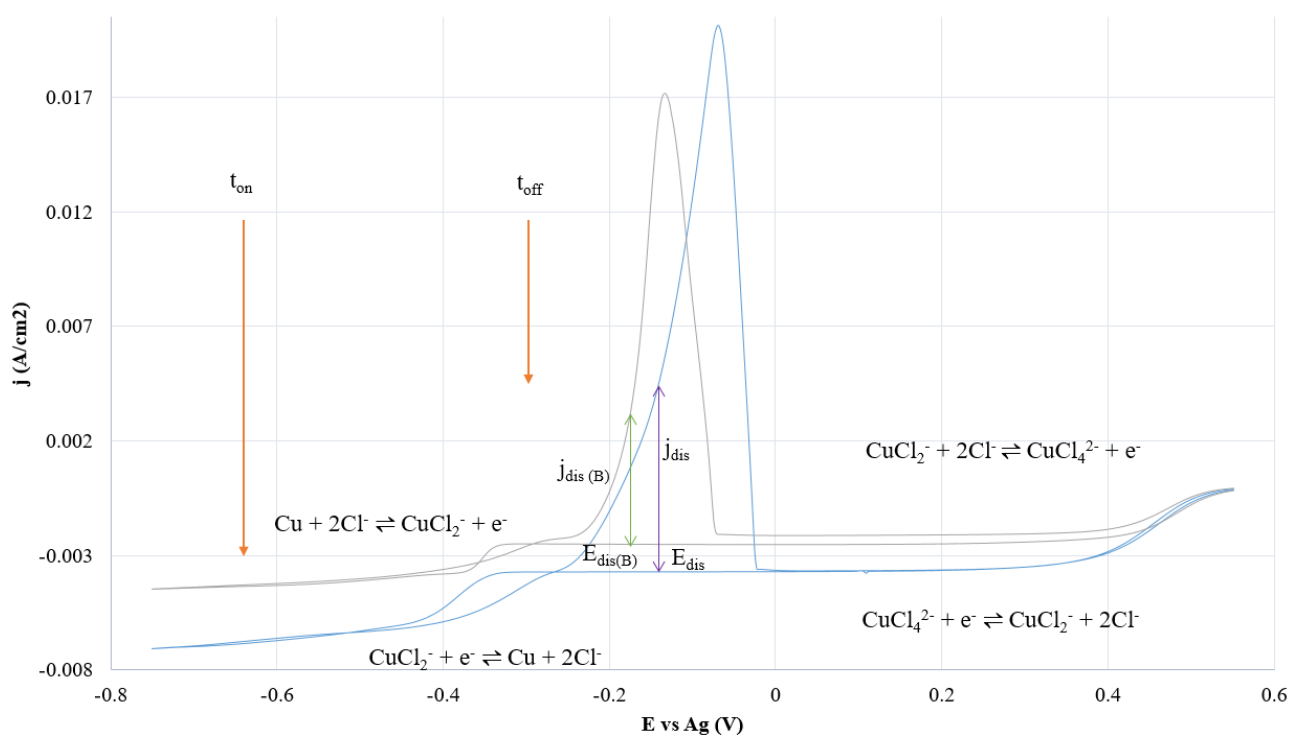


Figure 5-19 CV diagram of 0.2M Cu ethaline containing on Pt electrode under 700 rpm RDE rotation speed (—) No BTA (---) 10 mM BTA

5.5.2 The effect of BTA on Cu pulse electrodeposition in DES

The Cu pulse electrodeposition experiments were undertaken in the 0.2 M CuCl₂ ethaline DES with the addition of 10 mM BTA. The electrochemical equipment setup was exactly the same as those that have been performed without BTA. Cu plating was carried out under the pulse condition of 10 ms and 100 ms pulse on-times and 0.2, 0.3, 0.5 and 0.67 duty cycles. The visual appearance of plated Cu deposit is shown in Table 5-6.

The plated Cu deposits are illustrated in dark red colour compared to the light reddish colour of the ones obtained without BTA. It is shown from Figure 5-18 that the DC limiting current density of BTA is approximately 4.45 mA/cm², which is lower than 7.04 mA/cm² which was measured without the presence of BTA. Therefore the pulse limiting current density for BTA is expected to be lower. On the other hand, the applied peak current density was applied as the same for the purpose of comparison. Therefore, the values of N_p and N_m are higher than the ones without BTA addition. The results are shown in Table 5-7.

As shown in the table, N_p is fixed as 1.12 and N_m ranges between 0.70 and 1.10 depending on the pulse condition. For the non-BTA group, N_p is fixed as 0.80 and N_m ranges between 0.47 and 0.79. This indicates that the mass transport limitations of BTA group were exceeded in the plating process. Therefore, the deposit microstructure would change from granular to dendritic.

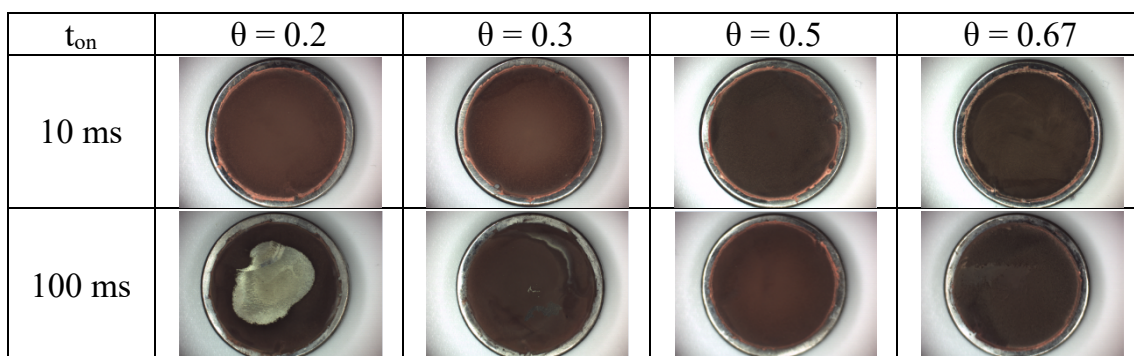


Table 5-6 Plating results from pulse deposition of Cu in 0.2 M CuCl_2 ethaline

DES containing 10 mM BTA under various pulse conditions

On time (ms)	Duty cycle	N_m	N_p
10	0.2	0.97	1.12
10	0.3	1.03	1.12
10	0.5	1.08	1.12
10	0.67	1.10	1.12
50	0.2	0.83	1.12
50	0.3	0.93	1.12
50	0.5	1.03	1.12
50	0.67	1.07	1.12
100	0.2	0.75	1.12
100	0.3	0.87	1.12
100	0.5	1.00	1.12
100	0.67	1.06	1.12
200	0.2	0.66	1.12
200	0.3	0.80	1.12
200	0.5	0.96	1.12
200	0.67	1.03	1.12

Table 5-7 N_m and N_p values for pulse condition with BTA addition

In addition, the coverage of Cu plated improves after BTA is added.

However, the adherence of Cu grain become worse that the plated Cu is prone to be removed from the substrate, which is exemplified in the plating result

with pulse condition of 100 ms pulse on-time and 0.2 duty cycle. The reason could be explained by the result of exceeding mass transport limitations.

The results of Faradaic efficiency from Cu electrodeposition experiments using BTA are shown in Table 5-8. The tendency of current efficiency change is similar compared to non-BTA. The Faradaic efficiency tends to be higher with the increase of duty cycle and shorter pulse on-time. Under the same pulse condition, BTA group shows a dramatic increase of current efficiency compared to the non BTA group and the magnitude increases from 30% up to 50%. These results indicate that BTA is assumed to suppress the corrosion reaction in the electrodeposition process.

T_{on}	$\theta = 0.2$	$\theta = 0.3$	$\theta = 0.5$	$\theta = 0.67$
10 ms	$\varepsilon = 70.75\%$ (40.68%)	$\varepsilon = 76.37\%$ (44.40%)	$\varepsilon = 87.18\%$ (57.54%)	$\varepsilon = 91.57\%$ (61.05%)
100 ms	$\varepsilon = 58.63\%$ (9.16%)	$\varepsilon = 66.82\%$ (13.71%)	$\varepsilon = 78.35\%$ (45.55%)	$\varepsilon = 87.07\%$ (45.86%)

Table 5-8 Faradaic efficiencies from Cu pulse deposition in 0.2 M CuCl_2

ethaline DES with (black font) and without 10 mM BTA (red font) under various pulse conditions

5.5.3 The effect of BTA on Cu dissolution in DES electrolyte

The influence of BTA in Cu corrosion process was also studied. First the stagnant metal dissolution experiment was performed using 0.2 M CuCl₂ ethaline DES containing 10 mM BTA. Both Cu sheet and steel disc were immersed in the solution for 410 hours.

As can be seen from Figure 5-20, the solution turned dark from reddish colour, the appearance is similar to the ones which both Cu sheet and steel disc are immersed in the same DES electrolyte without BTA. The weight change of metal samples and their rates of change are summarized in the Table 5-9 with the comparison to non-BTA group.

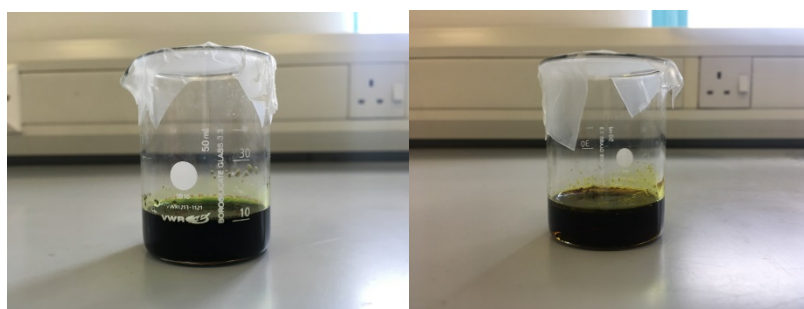


Figure 5-20 Appearance of 0.2 M CuCl₂ ethaline DES and 10 mM BTA after 410 hours soaking experiment with Cu sheet (left) and steel disc (right)

Table 5-9 shows that the weight loss of both Cu and steel with and without BTA from the stagnant dissolution experiment. The rate of dissolution

of Cu significantly decreases with the addition of BTA. For steel the dissolution rate becomes slightly slower when BTA is added into the solution.

Metal	Solution	Weight Change (mg)	Rate (mg/cm² h)
Cu sheet	0.2 M CuCl ₂ ethaline + 10 mM BTA	- 64.6	- 0.036
Cu sheet	0.2 M CuCl ₂ ethaline	- 110.6	- 0.058
Steel disc	0.2 M CuCl ₂ ethaline + 10 mM BTA	- 40.3	- 0.031
Steel disc	0.2 M CuCl ₂ ethaline	- 47.2	- 0.037

Table 5-9 List of weight change and rate of change of Cu sheet and steel disc in CuCl₂ ethaline DES with and without BTA

The metal dissolution experiments on Cu disc were also undertaken with 5 mM and 10 mM BTA concentration under agitation condition. The dissolution time was set as 20 minutes under various RDE rotation speeds ranging from 300 rpm up to 1200 rpm. The rate of dissolution and dissolution current density are shown in Table 5-10.

Table 5-10 shows there is no evident correlation between the dissolution current density and RDE rotation speeds for both 5 mM and 10 mM BTA group, indicating that the dissolution process is not under mass transport control when BTA is added. In addition, the dissolution rate is very stable in both groups. The dissolution current density is in the range of 1.22 mA/cm² to 1.42 mA/cm², and 0.91 mA/cm² to 1.12 mA/cm² for 5 mM BTA and 10 mM BTA group respectively. As a comparison, the dissolution current

density without BTA is in the range of 2.23 mA/cm² to 4.57 mA/cm². These results reflect the inhibition effect of corrosion behaviour of BTA. Moreover, better inhibition could be achieved by increasing the concentration of BTA.

	RDE (rpm)	Weight Loss (mg)	r_{dis} (mg min⁻¹cm⁻²)	j_{dis} (mA cm⁻²)
5 mM BTA	300	1.2	0.048	1.22
	500	1.2	0.048	1.22
	700	1.4	0.056	1.42
	900	1.3	0.052	1.32
	1200	1.2	0.048	1.22
10 mM BTA	300	0.9	0.036	0.91
	500	1.0	0.400	1.01
	700	1.1	0.044	1.12
	900	1.1	0.044	1.12
	1200	1.1	0.044	1.12

Table 5-10 Dissolution rate and current density with varying RDE rotation speeds Cu disc with 5 mM and 10 mM BTA addition

Figure 5-21 illustrates the dissolution potentials of non BTA, 5 mM BTA and 10 mM BTA under varying agitation conditions from the separate measurement. The dissolution potential is under mass transport control when no BTA is added and in the range of -0.167 V to -0.144 V with increasing RDE rotation speed. For BTA group their dissolution potentials are close to -0.2 V and they are not affected by mass transport control. The dissolution potentials on 10 mM BTA are slightly lower than the 5 mM BTA group. These results are also correlated to the dissolution current densities.

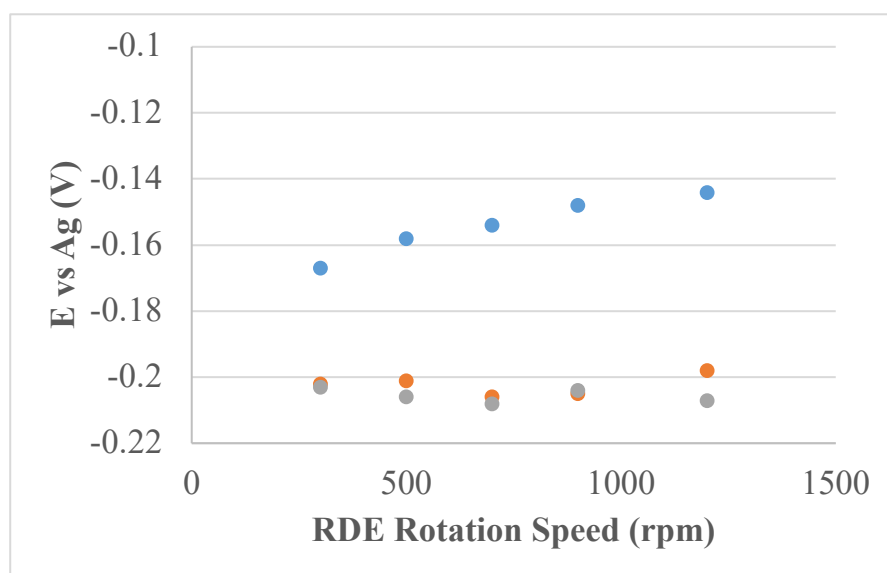


Figure 5-21 Dissolution potential with varying RDE rotation speeds in 0.2 M CuCl_2 ethaline DES electrolyte (•) without BTA (•) 5 mM BTA (•) 10 mM BTA

The change of dissolution current density and potential by BTA could be reflected from the cyclic voltammogram, which is shown in Figure 5-22. In the diagram j_{dis} and E_{dis} stand for the dissolution current density and potential without BTA, $j_{\text{dis(B)}}$ and $E_{\text{dis(B)}}$ are the dissolution current density and potential with 10 mM BTA. During the pulse off-time period, the comproportionation reaction takes place between Cu^{2+} species and Cu. The measured dissolution potential of BTA is more negative than the one without BTA. Therefore the dissolution current density is lower, which is shown from the CV diagram. Based on the results from deposition and dissolution experiments, it could be concluded that BTA is an effective additive to inhibit Cu dissolution process.

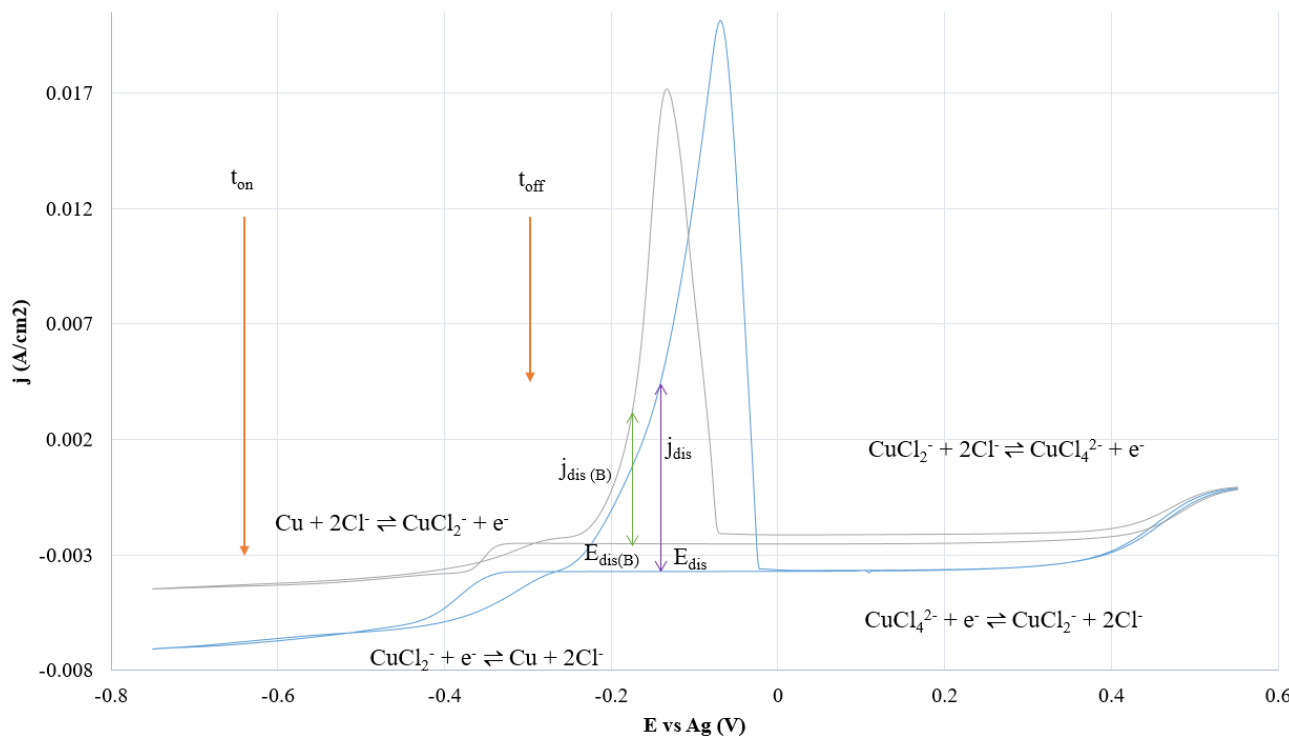


Figure 5-22 Polarization diagrams of 0.2 M CuCl_2 ethaline DES on Pt electrode under 700 rpm at 25°C (—) No BTA (—) 10 mM BTA

5.5.4 The effect of BTA on the mathematical model

The data of Cu pulse deposition in DES containing BTA additive could be tested by the mathematical models which have been purposed in the previous section. The constant corrosion current density model with the integration of BTA data is shown below with the comparison to the non-BTA group is shown in Figure 5-23.

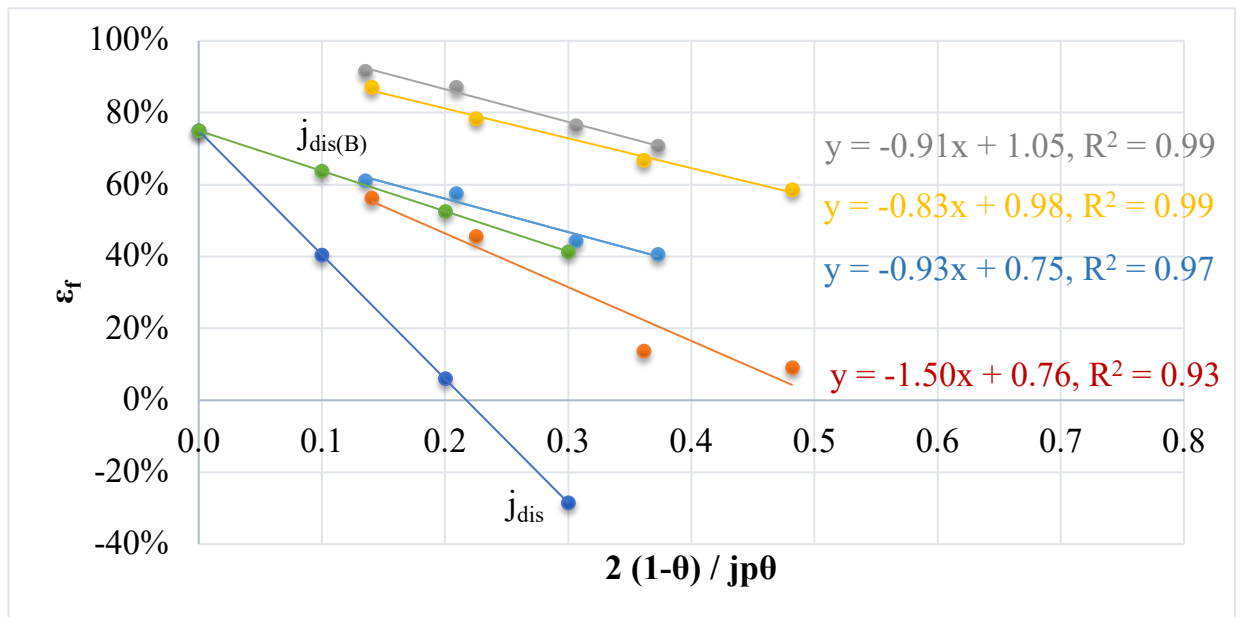


Figure 5-23 Relationship of ϵ_f vs $[2(1-\theta) / jp\theta]$ derived from pulse plating of Cu experiment (•) 10 ms pulse on-time (•) 50 ms pulse on-time (•) 10 ms pulse on-time with BTA (•) 100 ms pulse on-time with BTA (•) j_{dis} (•) $j_{dis(B)}$

It is shown from Figure 5-23 that the Faradaic efficiency is in linear relationship with the pulse parameters for BTA group. The dissolution current density was measured as 0.91 mA/cm^2 and 0.83 mA/cm^2 for 10 ms and 100 ms pulse time group with the addition of BTA. The values are smaller compared to the ones measured from separate dissolution experiment, which is 1.12 mA/cm^2 . Very little difference on the dissolution current density is found between the BTA and non-BTA for the 10 ms pulse on-time group. The results indicate the limited inhibition effect of BTA, which contradicts to the results obtained from the dissolution experiments, where noticeable reduction of dissolution current density was observed. In addition, the deposition efficiency

of BTA group is shown to be approximately 100% rather than 75% for non-BTA. These results indicate that the constant corrosion density model poorly reflect the BTA data.

The dissolution current density determined from direct calculation and varying dissolution current density model are shown in Table 5-11.

θ	t_{on} (ms)	$j_{dis(e)}$ (mA/cm ²)	$j_{dis(vr)}$ (mA/cm ²)	$j_{dis(cr)}$ (mA/cm ²)
Non-BTA				
0.2	10	1.00	1.44	0.93
0.3	10	1.10	3.13	0.93
0.5	10	0.98	-	0.93
0.67	10	1.25	-	0.93
0.2	100	1.43	12.82	1.50
0.3	100	1.78	9.06	1.50
0.5	100	1.44	2.52	1.50
0.67	100	1.55	4.17	1.50
BTA				
0.2	10	0.79	0.75	0.91
0.3	10	0.77	0.51	0.91
0.5	10	0.61	-	0.91
0.67	10	0.62	-	0.91
0.2	100	0.86	2.21	0.83
0.3	100	0.92	0.97	0.83
0.5	100	0.96	0.78	0.83
0.67	100	0.92	-	0.83

Table 5-11 List of dissolution current density determined from different approaches with and without BTA

It can be seen that generally the dissolution current density is lower with the addition of BTA under the same pulse condition. The results of BTA group which were determined using three different approaches are very close. The dissolution current density for BTA with full Cu coverage is in the range of 0.5 mA/cm^2 to 1.0 mA/cm^2 . One large discrepancy takes place at the 100 ms pulse on-time and 0.2 duty cycle pulse condition possibly because Cu is partially plated and steel corrosion also involves. No clear trend is found between dissolution current density and pulse parameters in the BTA group.

The varying corrosion current density mathematical model of BTA also shares similar limitations with non-BTA group. The results calculated from the model only consider Cu dissolution and no data on steel substrate is available. In addition, the polarization data was obtained on Pt electrode rather than steel substrate. The dissolution current density of some pulse conditions could not be determined, since the potential is beyond the range of initiate point of corrosion process. Overall, the data of BTA does not vary too much compared to the one without the BTA.

This chapter has illuminated the interpretation of experimental results from pulse deposition of copper in DES. The electrochemical characteristics of copper ethaline were examined via voltammetry measurement firstly, followed by the investigations on various aspects in the electrochemical characterization of copper deposit, where metal dissolution was observed and further studied through a number of corrosion experiments. Two mathematical

models which describe the relationship among pulse parameters, plating data and corrosion data were developed afterwards. The inhibition effect of BTA additive was tested in a similar approach as mentioned above. The next chapter would elaborate the results with corresponding analysis on pulse deposition of tin.

Reference List

1. Leon C. P. D. and Walsh F. C. (2003). Research and development techniques 1: potentiodynamic studies of copper metal deposition. Transactions of the Institute of Metal Finishing. 81 (5) pp B95-B100.
2. Boxall, L. G., Jones H. L. and Osteryoung R. A. (1974). Electrochemical studies on Ag, Fe, and Cu species in AlCl_3 -NaCl melts. Journal of the Electrochemical Society. 121 (2) pp 212-219.
3. Anders U. and Plambeck J. A. (1969). Electrochemistry of copper, silver, gold, gallium, indium and thallium in fused AlCl_3 -NaCl-KCl eutectic. Canadian Journal of Chemistry, 47 (16) pp 3055-3060.
4. Endres F., Schweizer A. (2000). The electrodeposition of copper on Au (111) and on HOPG from the 66/34 mol% aluminium chloride/1-butyl-3-methylimidazolium chloride room temperature molten salt: an EC-STM study. Physical Chemistry Chemical Physics. 2 pp 5455-5462
5. Sun G.H., L. K.X., Sun C.G. (2010). Electrochemical performance of electrochemical capacitors using Cu(II)-containing ionic liquid as the electrolyte. Microporous and Mesoporous Materials. 128 (1-3) pp 56-61
6. Xing S.J. (2014). Environmentally friendly baths for Cu-Sn co-electrodeposition: cyanide-free aqueous bath and deep eutectic solvents. Department of Industrial Engineering. Universita Degli Studi Di Trento. Italy
7. Ghosh S. and Roy S. (2014). Electrochemical copper deposition from an ethaline- $\text{CuCl}_2 \cdot 2\text{H}_2\text{O}$ DES. Surface and Coatings Technology. 238 pp 165-173

8. Abbott A.P., Ttaib K.E., Frisch G., Mckenzie K.J. and Ryder K.S. (2009). Electrodeposition of copper composites from deep eutectic solvents based on choline chloride. *Physical Chemistry Chemical Physics*. 11 pp 4269-4277
9. Hartley J.M., Ip C.M., Forrest G.C., Singh K., Gurman S.J., Ryder K.S., Abbott A.P., Frisch G. (2014). EXAFS study into the speciation of metal salts dissolved in ionic liquids and deep eutectic solvents. *Inorganic Chemistry*. 53 pp 6280-6288
10. Vreese P.D., Brooks N.R., Hecke K.V., Meervelt L.V., Matthijs E., Binnemans K., Deun R.V. (2012). Speciation of copper(II) complexes in an ionic liquid based on choline chloride and in choline chloride/water mixtures. *Inorganic Chemistry*. 51: pp 4972-4981
11. Ghosh S. (2013). Electrodeposition of Cu, Sn and Cu-Sn alloy from choline chloride ionic liquid. PhD thesis. School of Chemical Engineering and Advanced Materials. Newcastle University. Newcastle
12. Armas P.E.V. (2019). Effect of water on copper electrodeposition from water – containing deep eutectic solvents. Department of Chemical and Process Engineering. University of Strathclyde. Glasgow
13. Landau U. (1982). Landau U., Yeager E. Kortan D. eds. *Electrochemistry in Industry*. Plenum Press. New York.

14. Barkey D.P., Muller R.H. and Tobias C.W. (1989). Roughness development in metal electrodeposition. *Journal of the Electrochemical Society*. 136 (8) pp 2199-2207
15. Xing S.J., Zanella C. Deflorian F. (2014). Effect of pulse current on the electrodeposition of copper from choline chloride-ethylene glycol. *Journal of Solid State Electrochemistry*. 18 pp 1657-1663
16. Bernasconi R., Zebarjadi R., Magagnin L. (2015). Copper electrodeposition from a chloride free deep eutectic solvent. *Journal of Electroanalytical Chemistry*. 758 pp 163-169
17. Tsai W.C., Wan C.C, Wang Y.Y. (2002) Mechanism of copper electrodeposition by pulse current and its relation to current efficiency. *Journal of Applied Electrochemistry*. 32 (12) pp 1371-1378
18. Chene O., Landolt D. (1989). The influence of mass transport on the deposit morphology and the current efficiency in pulse plating of copper. *J Journal of Applied Electrochemistry*. 19 (2) pp 188-194
19. Bockris J.O.M., Reddy A.K.N. (1970). *Modern electrochemistry*. Plenum Publishing Corporation. New York
20. Newman J. (1966). Current distribution on a rotating disc below the limiting current. *Journal of the Electrochemical Society*. 113 (12) pp 1235-1241

21. Abbott A.P., Al-Bassam A.Z.M., Goddard A., Harris R.C., Jenkin G.R.T., Nisbet F.J., Wieland M. (2017). Dissolution of pyrite and other Fe-S-As minerals using deep eutectic solvents. *Green Chemistry*. 19 pp 2225-2233
22. Murase K., Nitta K., Hirato T., Awakura Y. (2001). Electrochemical behaviour of copper in Trimethyl-n-hexylammonium bis((trifluoromethyl)sulf-onyl)amide, an ammonium imide-type room temperature molten salt. *Journal of Applied Electrochemistry*. 31 (10) pp 1089-1094
23. Lloyd D., Vainikka T., Murtomaki L, Kontturi K., Ahlberg E. (2011). The kinetics of the $\text{Cu}^{2+} / \text{Cu}^{+}$ redox couple in deep eutectic solvents. *Electrochimica Acta*. 56 pp 4942-4948
24. Fischer J., Nagel E., Mann M. (2012). Investigations concerning chromium plating from electrolytes containing chromium-III chloride and ionic liquid. Report No. 120808. University of North Dakota, United States
25. Lloyd D., Vainikka T., Roinkainen M., Kontturi K. (2013). Characterisation and application of the Fe (II) / Fe (III) redox reaction in an ionic liquid analogue. *Electrochimica Acta*. 109 pp 843-851
26. Miller M.A., Wainright J.S., Savinell R.F. (2017). Iron electrodeposition in a deep eutectic solvent for flow batteries. *Journal of the Electrochemical Society*. 164 (4) pp A796-A803

27. Georgiadou M., Alkire R. (1993). Anisotropic chemical etching of copper foil. *Journal of the Electrochemical Society*. 140 (5) pp 1340-1347
28. Yeow C.W. and Hibbert D.B. (1983). Galvanostatic pulse plating of copper and copper (I) halides from acid copper (II) halide solution. *Journal of the Electrochemical Society*. 130 (4) pp 786-790
29. Roy S., Matlosz M. and Landolt D. (1994). Effect of corrosion on the composition of pulse-plated Cu-Ni alloys. *Journal of the Electrochemical Society*. 141 (6) pp 1509-1517
30. Roy S. (1998). Electrodeposition of compositionally modulated alloys by an electrodeposition-displacement reaction method. *Surface and Coatings Technology*. 105 pp 202-205
31. Wolfgang E., Hansal G., Roy S. (2012). *Pulse Plating*. Eugen G. Leuze Verlag KG. Germany
32. Green T., Su X., Roy S. (2017). Pulse plating of copper from deep eutectic solvents. *ECS Transactions*. 77 (11) pp 1247-1253
33. Milic S.M., Antonijevic M.M. (2009). Some aspects of copper corrosion in presence of benzotriazole and chloride ions. *Corrosion Science*. 51 pp 28-34
34. Munoz A.I., Anton J., Guinon J.L., Herranz V.P. (2004). Comparison of inorganic inhibitors of copper, nickel and copper-nickels in aqueous lithium bromide solution. *Electrochimica Acta*. 50 (4) pp 957-966

35. Edwards M., Hidmi L., Gladwell D. (2002). Phosphate inhibition of soluble copper corrosion by-product release. *Corrosion Science*. 44 (5) pp 1057-1071
36. Hourani M., Wedian F. (2000). The effect of adatoms on the corrosion rate of copper. *Corrosion Science*. 42 (12) pp 2131-2144
37. Matos J.B. Pereira L.P., Agostinbo S.M.L, Barcia O.E., Cordeiro G.G.O, Elia E.D. (2004). Effect of cysteine on the anodic dissolution of copper in sulphuric acid medium. *Journal of Electroanalytical Chemistry*. 570 (1) pp 91-94
38. Ma H., Chen S., Niu L., Zhao S., Li S., Li D. (2002). Inhibition of copper corrosion by several Schiff bases in aerated halide solutions. *Journal of Applied Electrochemistry*. 32 (1) pp 65-72
39. Lalitha A., Ramesh S., Rajeswari S. (2005). Surface protection of copper in acid medium by azoles and surfactants. *Electrochimica Acta*. 51 (1) pp 47-55
40. Finsgar M. and Milosev I. (2010) Inhibition of copper corrosion by 1,2,3-benzotriazole: a review. *Corrosion Science*. 52 pp 2737-2749
41. Antonijevic M.M., Milic S.M., Serbula S.M., Bogdanovic G.D. (2005). The influence of chloride ions and benzotriazole on the corrosion behaviour of Cu₃₇Zn brass in alkaline medium. *Electrochimica Acta*. 50 (18) pp 3693-3701

42. Rlkina M.V., Didik M.V. (2007). Inhibition of the early depassivation of α -brass in neutral chloride electrolytes. *Protection of Metals*. 43 (2) pp 179-185
43. Modestov A.D., Zhou G.D., Ge H.H., Loo B.H. (1994). A study of copper electrode behaviour in alkaline solutions containing benzotriazole-type inhibitors by the photocurrent response method and intensity modulated photocurrent spectroscopy. *Journal of Electroanalytical Chemistry*. 375 (1-2) pp 293-299
44. Modestov A.D., Zhou G.D., Wu Y.P., Notoya T., Schweinsberg D.P. (1994). A study of the electrochemical formation of Cu (I)-BTA films on copper electrodes and the mechanism of copper corrosion inhibition in aqueous chloride/benzotriazole solutions. *Corrosion Science*. 36 (11) pp 1931-1946
45. Prasad Y.N., Ramanathan S. (2007). Chemical mechanical planarization of copper in alkaline slurry with uric acid as inhibitor. *Electrochimica Acta*. 52 (22) pp 6353-6358
46. Ravichandran R., Rajendran N. (2005). Electrochemical behaviour of brass in artificial seawater: effect of organic inhibitors. *Applied Surface Science*. 241 (3-4) pp 449-458

Chapter 6. Results and Discussions: Electrodeposition of Tin

The objective of this chapter is to describe and discuss the results obtained from pulse plating of Sn in ethaline based DES electrolyte. There are three primary sections in this chapter: first is the study of electrochemical behaviour of SnCl₂ ethaline DES solution by cyclic voltammetry and linear sweep voltammetry, followed by the analysis of results from Sn electrodeposition under various pulse conditions based on the visual appearance, Faradaic efficiency and potential profiles of metal deposit. The third part is the material characterization of plated Sn, including the study of deposit microstructure and grain size by using scanning electron microscopy (SEM), as well as the elemental composition analysis from energy-dispersive X-ray spectroscopy (EDX).

6.1 Electrochemical study of Sn ethaline DES

The electrochemical properties of DES electrolyte were investigated before the plating experiments, since the understanding of electrochemical behaviour of electrolyte is important for the analysis of results obtained from metal electrodeposition. In addition, the DC limiting current density can be determined from the electrochemical study. As has been described in the previous chapter, the limiting current density is the key information that

ensuring the plating process is below mass transport limitations. The theoretical limiting current densities were calculated based on the physical properties of electrolyte. The calculation method has been described in the experimental section and the results can be validated from the experiment.

6.1.1 Cyclic voltammetry of Sn ethaline DES

The cyclic voltammetry study of 0.2 M Sn ethaline DES electrolyte was performed to investigate the redox reactions of Sn. In these experiments, Pt substrate was the working electrode, Sn rod was the counter electrode and Ag wire was served as quasi reference electrode. The temperature was 25°C and a scan rate ranging between 10 mV/s and 50 mV/s was applied. The potential scan range between -1.0 V to -0.0 V was used. The data was corrected for IR compensation. The cyclic voltammogram is shown in Figure 6-1.

The voltammogram shows there is one cathodic peak at -0.55 V and two peaks at -0.35 V and -0.25 V in the forward sweep respectively. The cathodic peak at -0.55 V indicates the reduction process of Sn^{2+} species to Sn. The first peak at -0.35 V in the forward scan reflects the oxidation reaction of Sn to Sn^{2+} ionic complex. The second peak at -0.25 V may suggests the occurrence of side reaction rather than the oxidation process of Sn^{2+} to Sn^{4+} , otherwise it is expected that an additional cathodic peak would appear during the reverse sweep in the following scan. It was reported that the Sn^{4+} oxidation

reaction is unlikely to occur, since Sn^{4+} with chloride ionic species was not stable in the non-basic electrolyte [1].

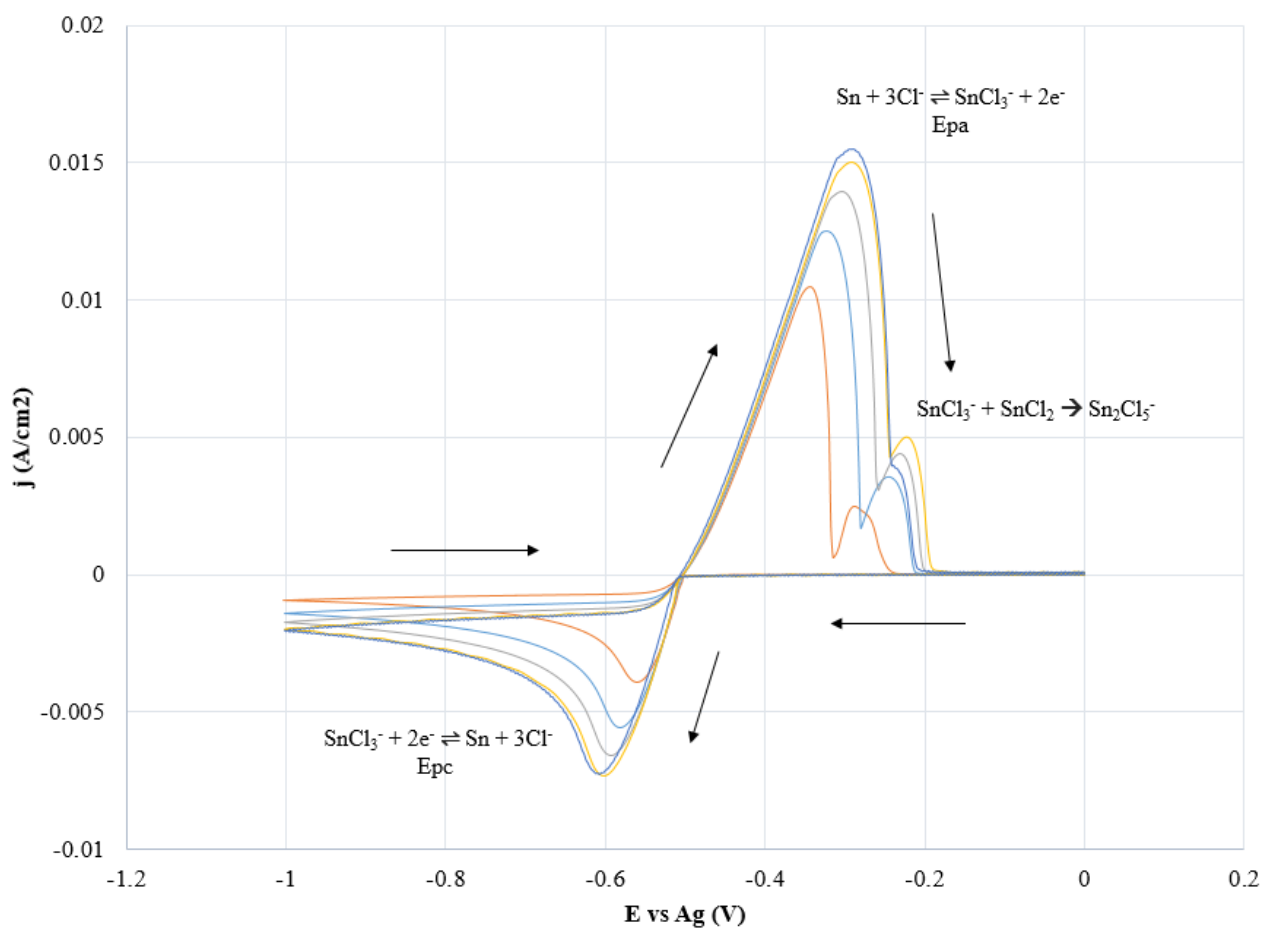
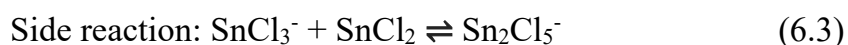
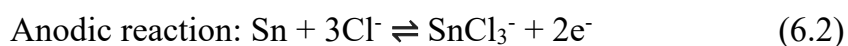
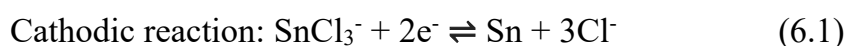


Figure 6-1 Cyclic voltammetry of 0.1 M SnCl_2 ethaline melt containing on Pt electrode under 700 rpm RDE rotation speed at 25°C temperature with various scan rates (—) 10 mV/s (—) 20 mV/s (—) 30 mV/s (—) 40 mV/s (—) 50 mV/s

According to the study, the second peak indicates that $[\text{Sn}_2\text{Cl}_5]^-$ species was formed by the reaction of SnCl_2 and $[\text{SnCl}_3]^-$ species when the ionic concentration of Sn exceeded 0.07 M [1]. Only one stripping peak was observed when the metal salt concentration was under 0.07 M. The double peaks in the forward scan were also reported from the electrochemical study of 1-alkyl-3-methylimidazolium chloride ionic liquids [2], which stated the formation of various Sn ionic species in the electrolyte. Although the formation of Sn^{4+} species from the additional peak was reported in the 1-ethyl-3-methylimidazolium dicyanamide ionic liquid [3]. It was found that the distance between two oxidation peaks was approximately 1.2 V, which is much larger than 0.1 V as shown in this experiment. Therefore, it is suggested that the second peak indicates the formation of a different Sn^{2+} ionic species rather than the oxidation to Sn^{4+} species in this experiment.

Most of the literature reported the formation of one cathodic peak and one anodic during the investigation of electrochemical properties of Sn in other types of ionic liquid. For instance, Miura and his colleagues found one reduction peak at -0.6 V and -0.4 V in the 1-n-butyl-1-methylpyrrolidinium bis(trifluoromethylsulfonyl)imide ionic melt [4]. Similar results were achieved by Yang's research group that the peaks were at -0.68 V and -0.75 V in the 1-ethyl-3-methylimidazolium tetrafluoroborate ionic liquid [5]. The single redox peak was also reported to be -0.43 V and -0.23 V in the N-butyl-N-methylpyrrolidinium dicyanamide electrolyte [6].

In addition, the Sn^{2+}/Sn redox couple is an irreversible two electrons single electron transfer reaction, since the ratio of anodic and cathodic peak current density j_{pa}/j_{pc} is much larger than unity. The single electron transfer mechanism was reported in the electrochemical studies of 1-n-butyl-1-methylpyrrolidinium bis(trifluoromethylsulfonyl)imide and 1-methyl-3-ethylimidazolium ionic melts [4, 7]. The corresponding electrochemical reactions of 0.1 M Sn ethaline DES electrolyte are suggested in equation (6.1), (6.2) and (6.3).



6.1.2 Linear sweep voltammetry of Sn ethaline DES

Linear sweep voltammetry was performed to determine the DC limiting current density of Sn reduction process in DES electrolyte. The experiment was carried out using various RDE rotating speeds ranging from 300 rpm to 900 rpm on Pt substrate at 25°C. The potential was scanned between -0.4 V and -0.7 V with 5 mV/s scan rate. The data was corrected by IR compensation. The voltammogram is shown in Figure 6-2.

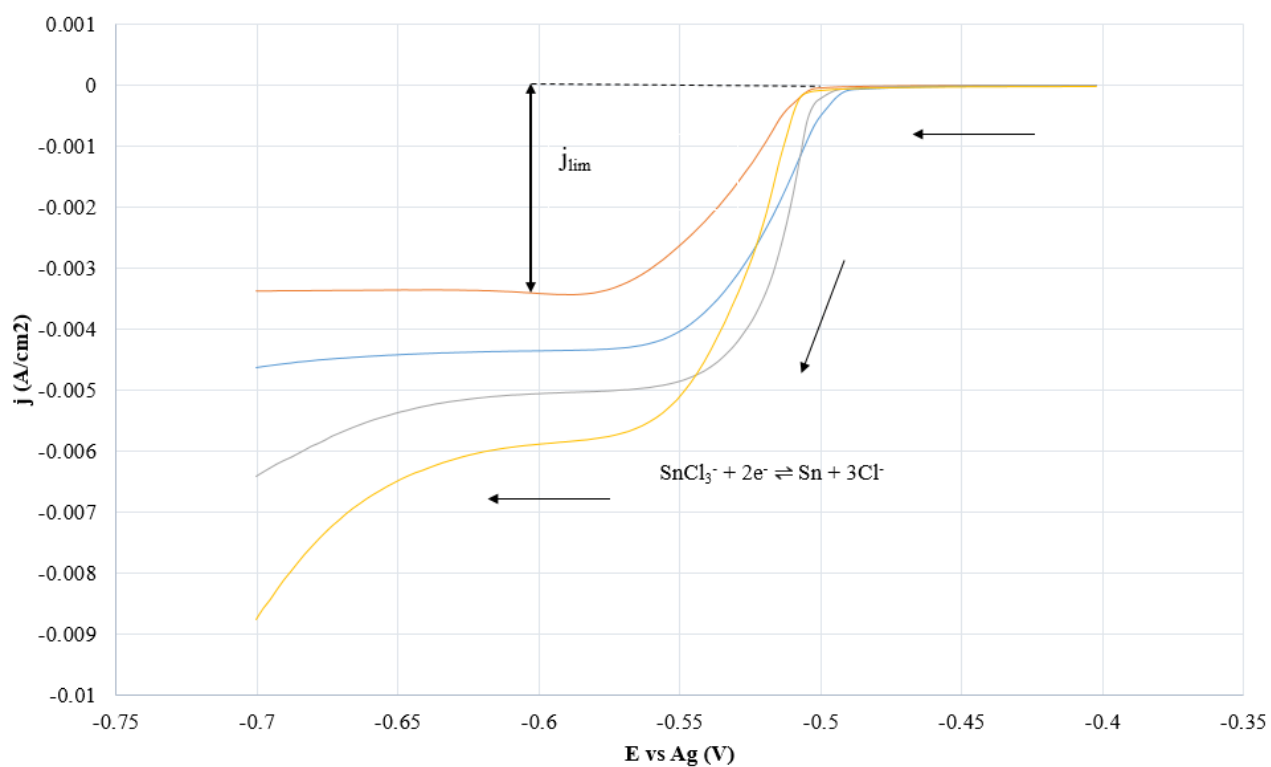


Figure 6-2 Linear sweep voltammetry of 0.1 M SnCl_2 ethaline DES electrolyte on Pt electrode 25°C temperature with 5 mV/s at various RDE rotation speed
 (—) 300 rpm (—) 500 rpm (—) 700 rpm (—) 900 rpm

A single cathodic peak at approximately -0.55 V is observed from the voltammogram, indicating the reduction reaction of Sn^{2+} ionic species to Sn. The DC limiting current density is determined from the flat plateau region following the reduction peak. The limiting current density becomes more negative along with the increase of RDE rotating speed, which means the Sn reduction reaction is under mass transport control. In addition, the flat plateau

region shrinks when the agitation condition becomes stronger. The decrease of current density after -0.6V for 700 and 900 rpm indicates the electrolyte breakdown.

The DC limiting current density under 700 rpm is determined as 5.06 mA/cm² from the linear sweep voltammetry, which is very close to 4.90 mA/cm² based on the theoretical calculation. Literature showed that the DC limiting current density was measured at approximately 0.7 mA/cm², 1.2 mA/cm², 2.4 mA/cm² at 0.01 M, 0.025 M and 0.04 M SnCl₂ ethaline DES on Pt electrode at 25°C, indicating the DC limiting current density increases with the ionic concentration [8]. Therefore both DC limiting current densities at 0.1 M determined from experimental and calculation are in agreement with the earlier study.

6.2 Electrochemical characterization of Sn deposition

Tin pulse electrodeposition experiments in ethaline based DES electrolyte were performed after the study of electrochemical behaviour. A matrix of 16 pulse conditions consisting of four duty cycles (0.1, 0.2, 0.5 and 0.67) and four pulse on-times (10 ms, 50 ms, 100 ms and 200 ms) was used. The peak current density was applied as 80% of pulse limiting current density to ensure that the mass transport limitations are not exceeded to avoid the formation of rough and dendritic deposits [9, 10]. Plating was performed

under galvanostatic mode so the applied current was fixed in the deposition process. Sn was plated on the steel substrate with soluble Sn counter electrode against Ag quasi-reference electrode in the 0.1 M SnCl₂ ethaline DES electrolyte. The temperature and RDE rotation speed were fixed at 25°C and 700 rpm respectively. The setting of plating time in each pulse condition aimed to achieve a nominal 5 μm thickness Sn deposit.

6.2.1 Visual appearance

The appearance of Sn deposits under various pulse on-time (t_{on}) and duty cycle (θ) pulse conditions as well as DC condition are shown in the Figure 6-3. It could be seen that the Sn deposit generally shows grey in colour. However there is colour variation on the deposit so parts of the surface are darker or brighter under some pulse conditions. It could be seen that the surface smoothness is related to the pulse parameters. For instance, the surface of Sn deposit looks rougher with the increase of duty cycle under the same pulse on-time. The DC sample is the roughest compared to the ones prepared by pulse plating. When the duty cycle is fixed, the substrate surface looks smoother with the increase of pulse on-time, although the trend is not very clear. One of the reasons causing the surface roughness is possibly due to poor adhesion of Sn deposit on the steel substrate so that Sn deposit is easily removed from the substrate.

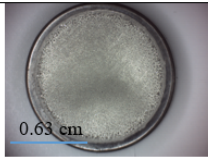
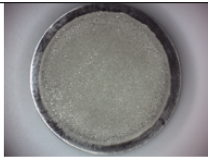
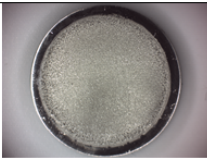
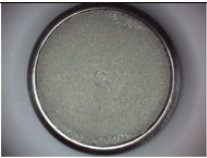
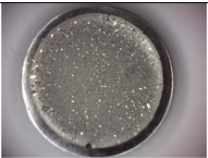
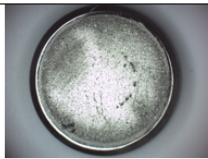
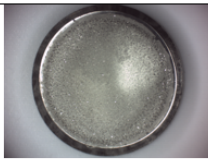
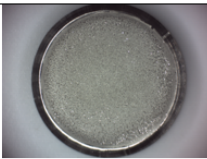
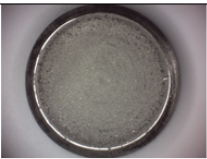
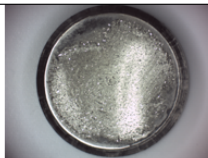

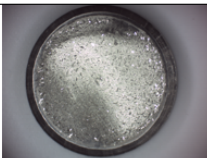
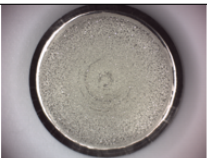
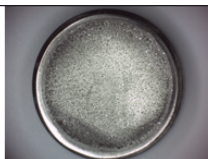
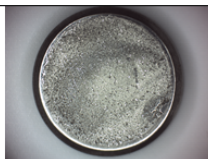
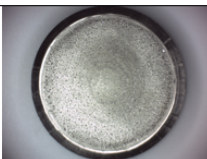

	$t_{on} = 10 \text{ ms}$	$t_{on} = 50 \text{ ms}$	$t_{on} = 100 \text{ ms}$	$t_{on} = 200 \text{ ms}$	DC
$\theta = 0.1$	 $\varepsilon = 105.3 \%$	 $\varepsilon = 102.8 \%$	 $\varepsilon = 99.3 \%$	 $\varepsilon = 95.2 \%$	 $\varepsilon = 98.5 \%$
$\theta = 0.2$	 $\varepsilon = 103.8 \%$	 $\varepsilon = 104.7 \%$	 $\varepsilon = 102.7 \%$	 $\varepsilon = 103.9 \%$	
$\theta = 0.5$	 $\varepsilon = 101.1 \%$	 $\varepsilon = 103.9 \%$	 $\varepsilon = 96.5 \%$	 $\varepsilon = 98.9 \%$	
$\theta = 0.67$	 $\varepsilon = 96.0 \%$	 $\varepsilon = 103.8 \%$	 $\varepsilon = 99.09 \%$	 $\varepsilon = 94.5 \%$	

Figure 6-3 Visual appearance and Faradaic efficiency from Sn pulse electrodeposition in 0.1 M SnCl_2 ethaline DES under various pulse conditions

6.2.2 Faradaic (current) efficiency

The Faradaic efficiency was calculated to determine the percentage of the quantity of actual plated Sn deposit to the theoretical value based on provided electrical charge. The corresponding calculation equations are shown in the equation (4.12) and (4.14) from the previous section [11, 12].

The Faradaic efficiencies under various pulse conditions and DC condition are shown in the Figure 6-3. The current efficiency of Sn from DC

plating is 98.5%, and ranges between 95% and 105% for pulse plating, depending on the pulse condition. There is no relationship or clear trend between the Faradaic efficiency and pulse parameters, considering a measurement error of $\pm 5\%$. It is shown that the electrodeposition both from DC and pulse current achieves a current efficiency close to 100%. The results are in agreement with the literature which reported that the current efficiency for Sn deposition in DC condition using the same electrolyte was in the range between 93% and 97% [8]. In addition, the Faradaic efficiency of Sn deposition for other types of room temperature ionic liquids, for instance 1-ethyl-3-methylimidazolium chloride, 1-ethyl-3-methylimidazolium dicyanamide and N-butyl-N-methylpyrrolidinium dicyanamide, were reported in the range between 82% to 100% [3, 12, 14]. The current efficiency from the aqueous solution like acidic methanesulphonate bath was reported in the range between 75% and 95% [11, 15].

6.2.3 Potential profiles

The Sn pulse deposition process can be analysed from the examination of potential change at the electrode surface. As has been described in the previous chapter, the overall cell potential E consists of potential E_r and overpotential η , which is the summation of surface overpotential (η_s), concentration overpotential (η_c) and ohmic overpotential (η_Ω). The concentration overpotential could be neglected if the electrolyte is in well-

agitated condition [16]. The surface overpotential and ohmic overpotential could be expressed in equation (3.6) and (3.12) respectively. E_r equals to the open circuit potential, which is approximately -0.40 V measured from the linear sweep voltammetry.

The potential transient of a single pulse was recorded after every thousand pulses due to the storage limitation of potentiostat. Figure 6-4 illustrates the potential diagram of one pulse condition of 50 ms pulse on-time and 0.5 duty cycle. The applied peak current density is 8.9 mA/cm². The charging time t_c is 0.54 ms and discharging time t_d is 0.66 ms. This diagram is served as an example, the potential diagrams under other pulse conditions are listed in the appendix section.

The figure shows the surface potential through the entire Sn plating process. When the current is switched on, the electrical double layer undergoes charging and part of the electrical charges are stored during the charging time t_c . The overall potential becomes more negative due to the increase of surface overpotential and ohmic overpotential when the charging (capacitive) current density decreases. The electrochemical reduction reaction of Sn proceeds with 100% peak current density after double layer is fully charged. Cell potential continues to fall until to -1.19 V and the Sn plating still proceeds until to the end of pulse on-time.

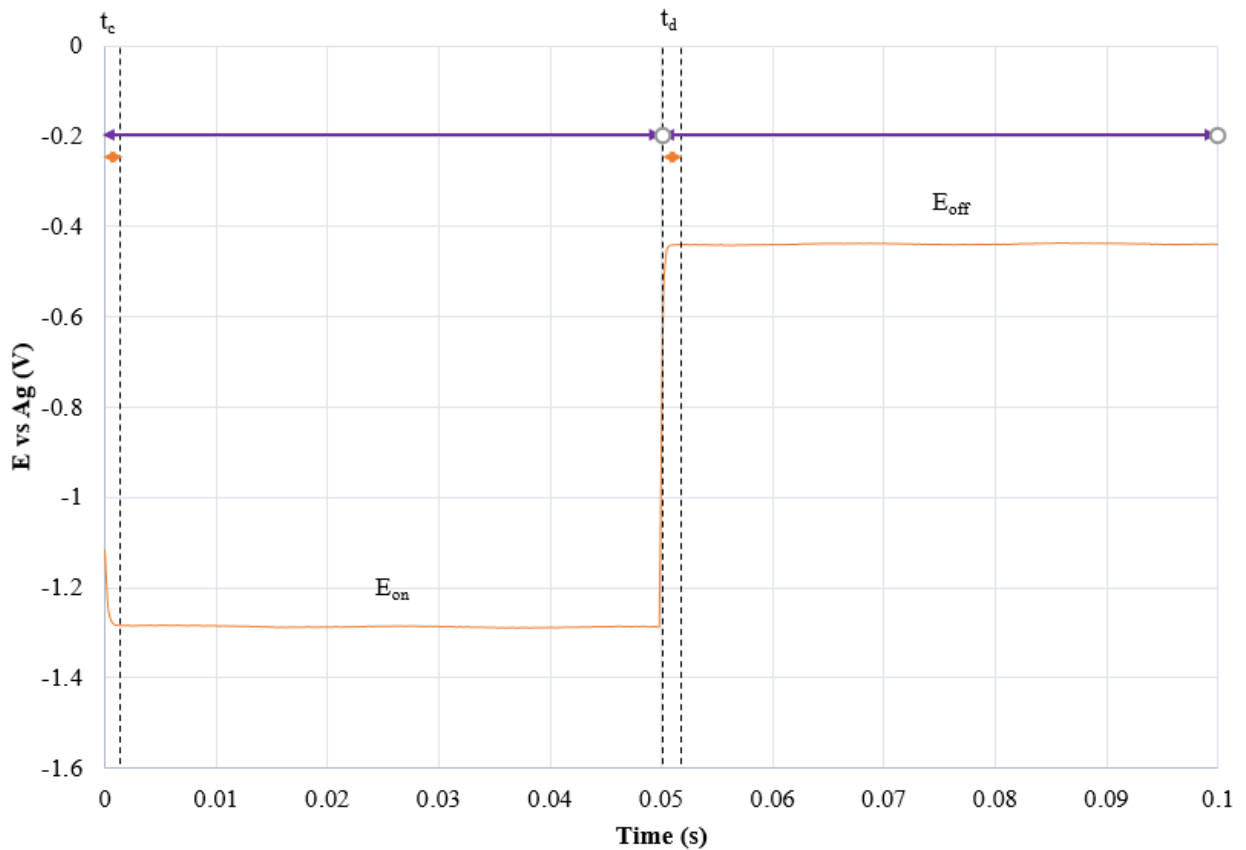


Figure 6-4 Potential profile in a single pulse in pulse electrodeposition of Sn with the pulse condition of $t_{\text{on}} = 50 \text{ ms}$ and $\theta = 0.5$

When the current is switched off, the double layer discharges and the stored charges are released in the form of current density. Cell potential shifts towards positive due to the decrease of overall current density. After the discharging period, the overall overpotential becomes zero and the cell potential rises to approximately -0.4V , which is the same as the measured open circuit potential. This indicates that side electrochemical reaction, such as metal dissolution reaction which took place in Cu pulse deposition, does not

occur during Sn pulse deposition. The reason is the comproportionation reaction is not feasible in Sn plating process. The potential remains constant until to the end of pulse off-time.

The relationship between cell potential and pulse parameters is investigated by the comparison of potential profiles under various pulse conditions, as shown in Figure 6-5 and 6.6.

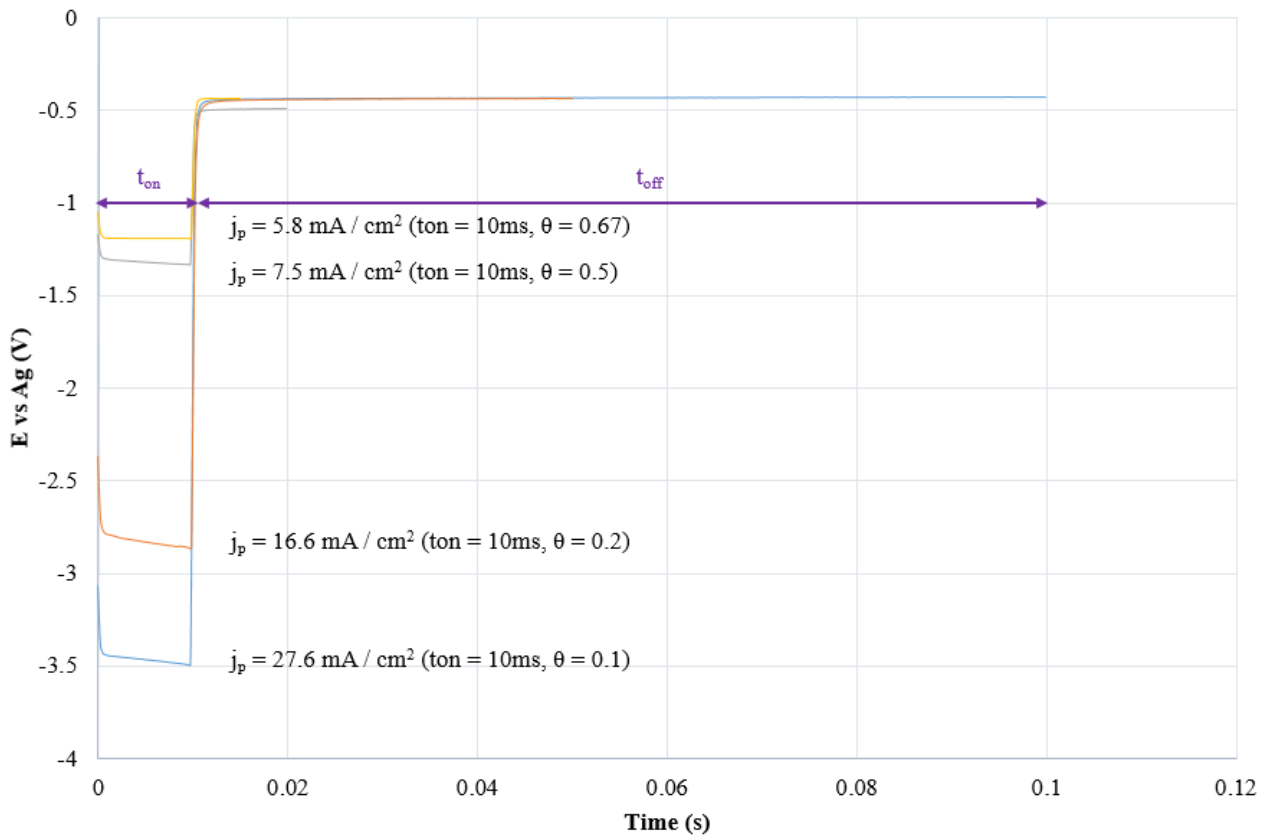


Figure 6-5 Potential profiles comparison of Sn deposition with 10 ms t_{on} with

(—) $\theta = 0.1$ (—) $\theta = 0.2$ (—) $\theta = 0.5$ (—) $\theta = 0.67$

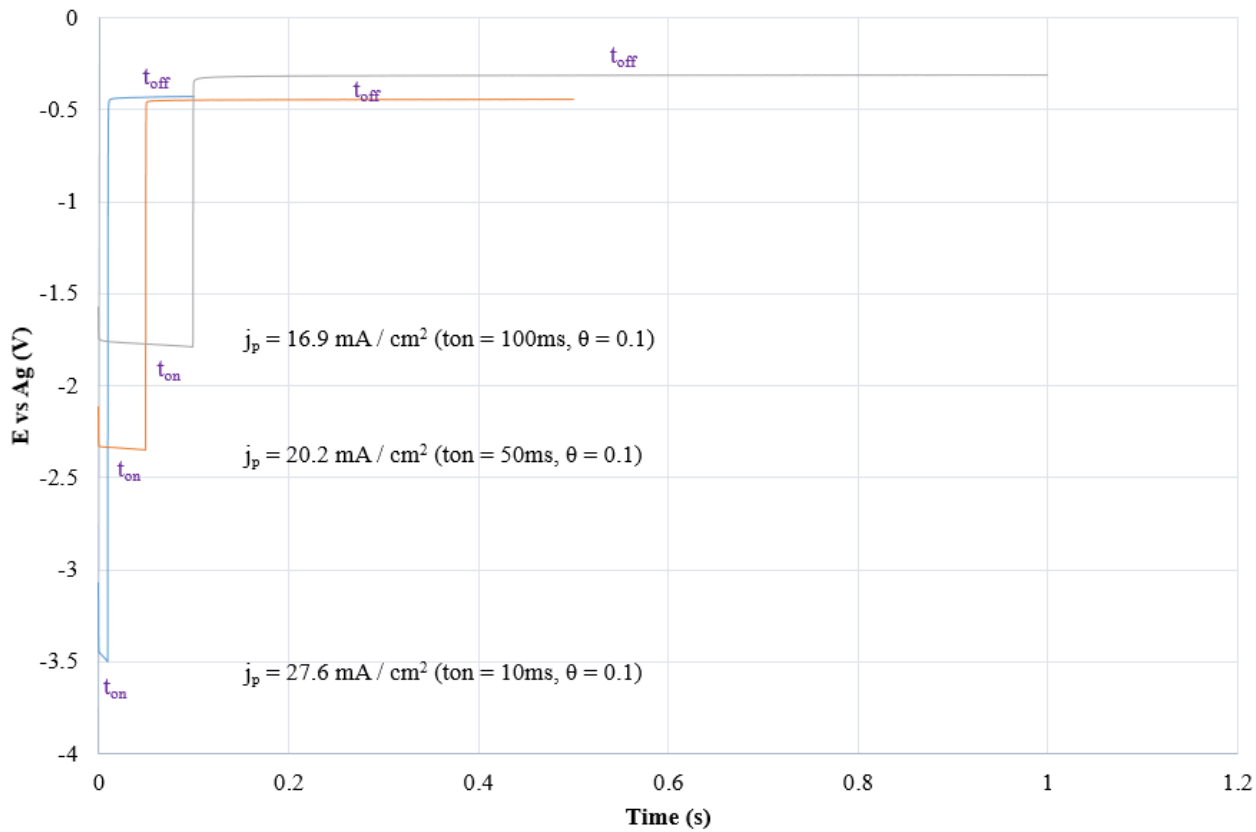


Figure 6-6 Potential profiles comparison of Sn deposition with 0.1 duty cycle
 θ with (—) $t_{on} = 10$ ms (—) $t_{on} = 50$ ms (—) $t_{on} = 100$ ms

Figure 6-5 and 6-6 show that during pulse on-time period, cell potential becomes more negative with lower pulse on-time and lower duty cycle, in which higher applied peak current is applied. Therefore both the surface overpotential and ohmic overpotential become larger. During pulse off-time period, the cell potentials are close to the equilibrium potential, in which no peak current density is applied.

6.3 Material characterization of Sn deposit

6.3.1 SEM analysis

The plated Sn deposits were characterized by the SEM to examine the microstructure and grain size. Seven samples were prepared by pulse electrodeposition with pulse condition of 10 ms pulse on-time group and 0.5 duty cycle group. One sample was prepared by DC plating. 1,000x, 2,500x and 5,000x three magnifications were adopted. The deposit microstructure at both the centre and edge of substrate was characterized from the samples plated under the pulse condition of 100 ms pulse on-time with 0.5 duty cycle, and 200 ms pulse on-time with 0.5 duty cycle.

Figure 6-7 shows the SEM results of Sn deposit. All Sn samples exhibit a granular morphology, indicating that the mass transport limitations are not exceeded. Deposits plated by DC do not have a dense film. Generally pulse plated deposits are denser than DC condition. Some of the deposits, such as the one plated under the pulse condition of $t_{on} = 10$ ms, $\theta = 0.67$, show full coverage of Sn grain, although no clear trends between grain coverage and pulse parameters are found. Some of the deposits such as the sample plated under pulse condition of $t_{on} = 10$ ms, $\theta = 0.1$ show clear grain boundary. The sample plated under pulse condition of $t_{on} = 10$ ms, $\theta = 0.67$ shows full grain coverage, where grain boundaries have merged.

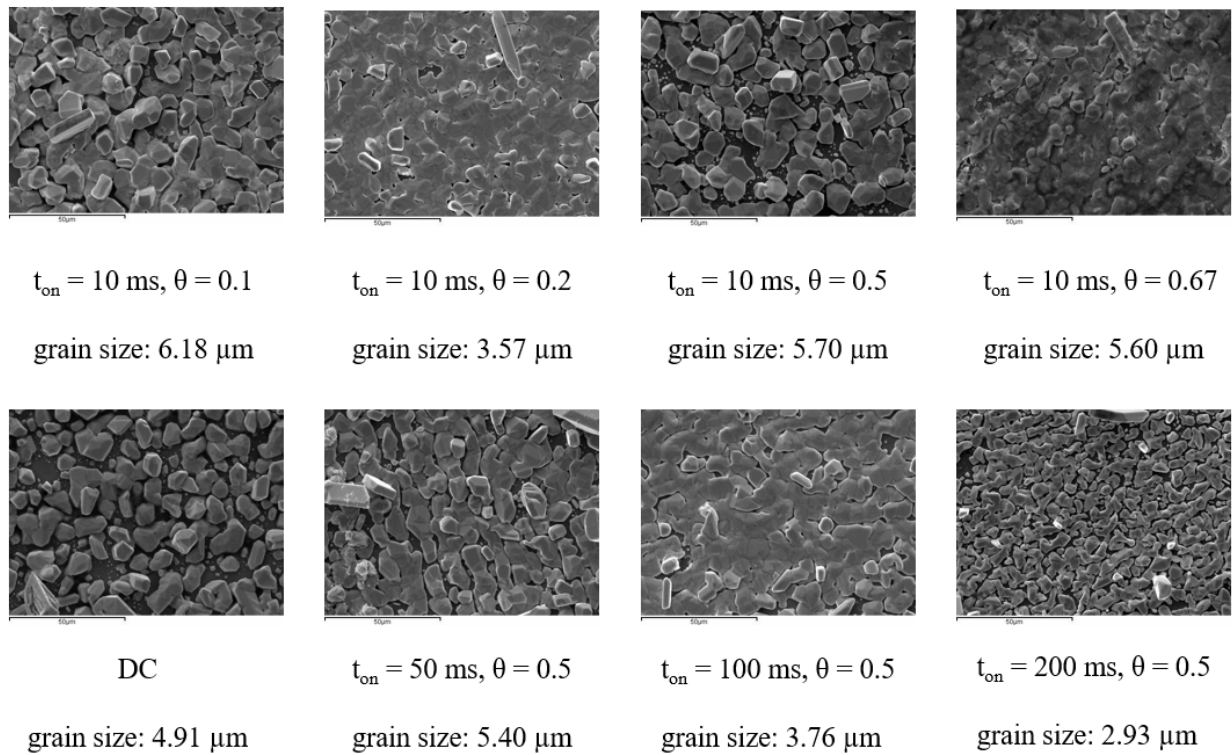


Figure 6-7 The microstructure and grain size of Sn deposit from pulse plating and DC plating in 1000x magnification from SEM characterization

The average grain size of Sn deposit was determined by line intercept method using ImageJ software. Firstly a random straight line was drawn on the micrograph and the scale needed to be calibrated. After then the number of intersections between the straight line and deposit grain were counted. The average grain size was determined by the scaled length of straight line divided by the number of intersections, which the expression is shown in the equation (6.4). The sample grain size was calculated by the average value from ten

intercept lines, which consist of five horizontal and five vertical lines on the micrograph, to ensure the result is as accurate as possible.

$$\text{Particle grain size} = \frac{\text{Scaled length of straight line}}{\text{Number of interceptions}} \quad (6.4)$$

The grain size of Sn deposit plated from DC condition is 4.91 μm and in the range of 2.93 μm to 6.18 μm by pulse plating, depending on the pulse condition. This means pulse deposition could achieve smaller grain size than DC condition if the pulse parameters are chosen suitably. There is no clear relationship between grain size and pulse duty cycle, but it is found that grain size becomes smaller with longer pulse on-time. The variation of the deposit microstructure and grain size may be contributed to the poor adhesion of Sn particle on the steel substrate. The uncertainty of particle size ranges from 0.11 to 0.60 μm , calculated from the standard deviation of the mean.

Figure 6-8 shows that the microstructure of Sn deposit on the edge and centre of substrate is very different. For the sample plated in 100 ms pulse on-time and 0.5 duty cycle condition, the deposit at the substrate centre has good adhesion and is dense. The deposit at the edge is loose and particles have various grain size. For the sample plated in 200 ms pulse on-time and 0.5 duty cycle condition, the deposit at the substrate edge is dense but in dendritic shape compared to the one plated at the substrate centre. The reason is likely

ascribed to the poor current density distribution across the electrode surface, which the case is similar to Cu deposition.

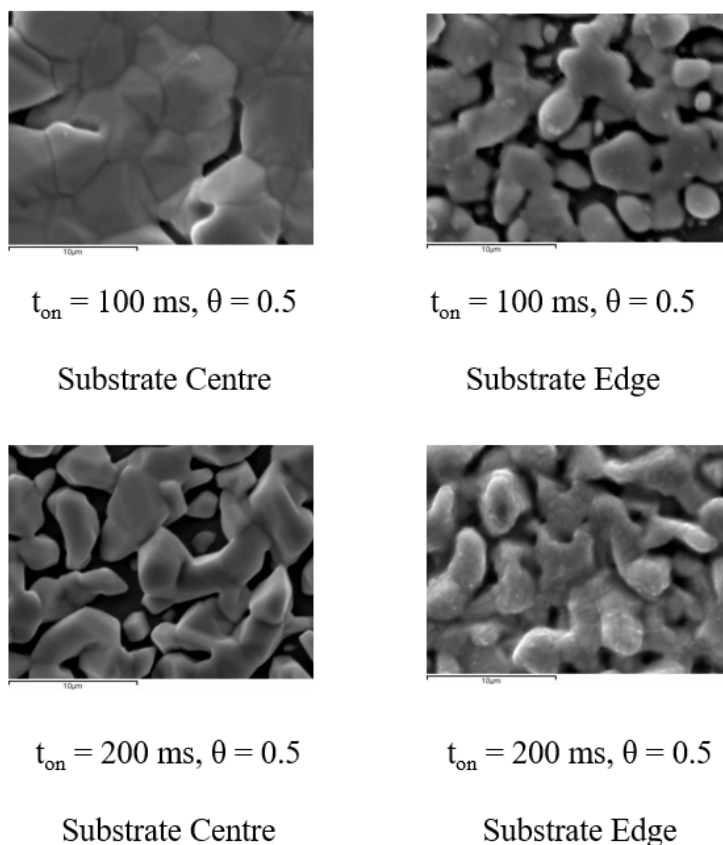


Figure 6-8 The microstructure of Sn deposit from pulse plating at the edge and centre of substrate under 5000x magnification from SEM characterization

The uneven growth of Sn grain was reported during Sn deposition using 0.05 M SnCl_2 ethaline DES under DC condition with 1.57 mA/cm^2 peak

current density, which is in agreement some of the results in this experiment [8]. Irregular cubic and cuboid-shaped crystals were reported from 0.3 M SnCl₂ ethaline DES under DC condition using 3 mA/cm² and 7 mA/cm² current density on brass electrode [17]. This also coincides with some of the plating results. The grain size of Sn deposit plated using 1-methyl-3-ethylimidazolium electrolyte was reported ranged between 2 to 5 μm under DC condition [7]. The grain size of Sn obtained from aqueous solution by pulse plating ranged from 4 μm to 6 μm depending on the pulse condition [15].

The morphology of Sn deposit from ethaline DES electrolyte was also reported by other researchers. Non-regular and dendritic Sn particles were reported with plating on the Pt electrode [18]. Silva's research group reported the formation of ill-defined crystallites with few of the parallelepiped particles with a grain size less than 1 μm using the glassy carbon electrode [19]. Net-like and porous Sn deposit with an average grain size of 200 nm to 300 nm was achieved on Cu foil substrate by Gu and his co-workers [20]. Therefore, it is suggested that the grain size of Sn deposit may depend on the choice of plating substrate.

6.3.2 EDX analysis

The elemental composition of Sn deposits was characterized by the EDX analysis. The samples prepared were exactly the same as the ones characterized by the SEM test. The results are shown in the Table 6-1.

Condition	Sn%	O%	Fe%	Cl%	N%	Cr%
DC	98.57%	0.00%	0.71%	0.72%	0.00%	0.00%
$t_{on} = 10 \text{ ms}, \theta = 0.1$	86.44%	12.01%	1.30%	0.26%	0.00%	0.00%
$t_{on} = 10 \text{ ms}, \theta = 0.2$	98.44%	0.00%	0.77%	0.00%	0.80%	0.00%
$t_{on} = 10 \text{ ms}, \theta = 0.5$	87.23%	10.02%	1.05%	0.00%	1.71%	0.00%
$t_{on} = 10 \text{ ms}, \theta = 0.67$	66.95%	30.36%	1.65%	1.05%	0.00%	0.00%
$t_{on} = 50 \text{ ms}, \theta = 0.5$	83.71%	14.45%	0.48%	0.00%	1.37%	0.00%
$t_{on} = 100 \text{ ms}, \theta = 0.5$	92.66%	4.55%	0.00%	0.00%	2.79%	0.00%
$t_{on} = 200 \text{ ms}, \theta = 0.5$	93.70%	4.76%	1.54%	0.00%	0.00%	0.00%

Table 6-1 Elemental composition of Sn deposits characterized by EDX analysis

The elemental composition shown in the table is in weight percentage. The instrument uncertainty is $\pm 0.005\%$. It could be seen from the table that generally Sn is the primary element in the deposit which can take 67.0% to 98.6%, oxygen comes to the second and the elemental percentage ranges from 0.0% to 30.4%. The remaining elements such as Fe, Cl, N and Cr only take less than 3%. DC plating achieves the highest percentage of Sn than pulse plating in all pulse conditions. The reading of 0.00% indicates no element was detected. There is no clear relationship between the Sn percentage and duty cycle. However, it shows that the Sn percentage could be higher when the pulse on-time becomes longer, except for the discrepancy of 50 ms pulse on-time and 0.5 duty cycle pulse condition.

The trend of oxygen percentage is opposite to the Sn percentage. DC plating and one pulse condition achieves zero percent of oxygen in the deposit. The oxygen percentage decreases when the pulse on-time becomes longer. The highest oxygen content is achieved in the condition of 10 ms pulse on-time and 0.67 duty cycle, which the deposit shows merged grain boundary. The incorporation of oxygen into the deposit has never been found in the other earlier studies of Sn plating using non-aqueous electrolyte. The oxygen may come from the water originated from the hydrate ions in metal salt or incorporation of water molecules from the air into the electrolyte, since DES has good tolerance of water uptake. Another source of oxygen content could

come from the drying process, which Sn deposit was placed in the oven at 70°C after washed by deionized water.

Minor Fe and Cr elements originate from the steel substrate. Small amount of N and Cl element are also detected. An earlier study reported the incorporation of small amount of Cl into the deposit due to the breakdown of ethaline occurring below -0.7 V [1, 13]. Chlorinated compounds were reported to be formed by the breakdown of such electrolyte [21]. Sn plated using 1-methyl-3-ethylimidazolium ionic liquid was reported to have pure Sn without any other elements such as boron, fluoride and chloride [22].

Based on the SEM and EDX analysis, it could be concluded that Sn deposition in DES using pulse current does not provide prominent advantages compared to the conventional methods in term of grain size and microstructure. Instead, the deposit quality deteriorates due to the oxygen incorporation. The exact reason is unclear at this moment and further investigation on wider range of pulse condition needs to be carried out in the future. Besides, the homogeneity of tin deposit remains unknown and needs to be investigated to obtain more reliable results.

This chapter has described the results as well as interpretation of pulse deposition of tin. The electrochemical behaviour of tin ethaline DES was studied in the first place, followed by the investigation of various aspects in the electrochemical characterization of tin deposit. The results from SEM and

EDX analysis were also discussed in detail. The final chapter will summarize all the experimental results with indications as well as purposed future work.

Reference List

1. Ghosh S., Roy S. (2014). Characterization of tin films synthesized from ethaline deep eutectic solvent. *Materials Science and Engineering B*. 190 pp 104-110
2. Currie M., Estager J., Licence P., Men S, Pockermann P., Seddon K.R., Swadzba-Kwasny M., Terrade C. (2013). Chlorostannate (II) ionic liquids: speciation, Lewis acidity, and oxidative stability. *Inorganic Chemistry*. 52 (4) pp 1710-1721
3. Leong T.L, Hsieh Y.T., Sun I.W. (2011). Electrochemistry of tin in the 1-ethyl-3-methylimidazolium dicyanamide room temperature ionic liquid. *Electrochimica Acta*. 56 (11) pp 3941-3946
4. Tachikawa N., Serizawa N., Katayama Y., Miura T. (2008). Electrochemistry of Sn (II) / Sn in a hydrophobic room-temperature ionic liquid. *Electrochimica Acta*. 53 (22) pp 6530-6534
5. Yang W.Z., Cang H., Tang Y.M., Wang T.T., Shi Y.X. (2008). Electrodeposition of tin and antimony in 1-ethyl-3-methylimidazolium tetrafluoroborate ionic liquid. *Journal of the Applied Electrochemistry*. 38 pp 537-542
6. Martindale B.C.M., Jones S.E.W., Compton R.G. (2009). A comparison of the cyclic voltammetry of the Sn / Sn(II) couple in the room temperature ionic liquids N-butyl-N-methylpyrrolidinium dicyanamide and N-butyl-N-methylpyrrolidinium bis(trifluoromethylsulfonyl)imide: solvent induced

- changes of electrode reaction mechanism. *Physical Chemistry Chemical Physics*. 12 pp 1827-1833
7. Xu X.H., Hussey C.L. (1993). The electrochemistry of tin in the aluminium chloride-1-methyl-3-ethylimidazolium chloride molten salt. *Journal of Electrochemical Society*. 140 (3) pp 618-626
8. Ghosh S. (2013). Electrodeposition of Cu, Sn and Cu-Sn alloy from choline chloride ionic liquid. PhD thesis. School of Chemical Engineering and Advanced Materials. Newcastle University. Newcastle
9. Landau U. (1982). Landau U., Yeager E. Kortan D. eds. *Electrochemistry in Industry*. Plenum Press. New York.
10. Barkey D.P., Muller R.H. and Tobias C.W. (1989). Roughness development in metal electrodeposition. *Journal of the Electrochemical Society*. 136 (8) pp 2199-2207
11. Schlesinger M., Paunovic M. (ed) (2010) *Modern Electroplating*, 5th ed, John Wiley and Sons Inc, New York.
12. Bard A.J., Faulkner L.R. (1980). *Electrochemical Methods: Fundamentals and Applications*. 2nd ed, Wiley, New York
13. Huang J.F., Sun I.W. (2003). Electrochemical studies of tin in zinc chloride-1-ethyl-3-methylimidazolium chloride ionic liquids. *Journal of the Electrochemical Society*. 150 (6) E299-E306

14. Martinadale B.C., Jones S.E.W., Compton R.G. (2010). A comparison of the cyclic voltammetry of the Sn / Sn (II) couple in the room temperature ionic liquids N-butyl-N-methylpyrrolidinium dicyanamide and N-butyl-N-methylpyrrolidinium bis(trifluoromethylsulfonyl)imide: solvent induced changes of electrode reaction mechanism. *Physical Chemistry Chemical Physics*. 12 pp 1827-1833
15. Vincenzo A., Bonelli S., Cavallotti P.L. (2010). Pulse plating of matt tin: effect on properties. *Transactions of the IMF*. 88 (5) pp 248-255
16. Landau U. (1982). Landau U., Yeager E. Kortan D. eds. *Electrochemistry in Industry*. Plenum Press. New York.
17. Xing S.J. (2014). Environmentally friendly baths for Cu-Sn co-electrodeposition: cyanide-free aqueous bath and deep eutectic solvents. PhD Thesis. Department of Industrial Engineering. Universita Degli Studi Di Trento. Italy
18. Anicai L, Petica A., Costovici S., Prioteasa P., Visan T. (2013). Electrodeposition of Sn and NiSn alloys coatings using choline chloride based ionic liquids-evaluation of corrosion behaviour. *Electrochimica Acta*. 114 pp 868-877
19. Salome S., Pereira N.M., Ferreira E.S., Pereira C.M., Silva A.F. (2013). Tin electrodeposition from choline chloride based solvent: Influence of the hydrogen bond donors. *Journal of Electroanalytical Chemistry*. 703 pp 80-87

20. Gu C.D., Mai Y.J., Zhou J.P., You Y.H., Tu J.P. (2012). Non-aqueous electrodeposition of porous tin-based film as an anode for lithium-ion battery. *Journal of Power Sources*. 214 pp 200-207
21. Haerens K., Matthijs E., Binnemans K., Bruggen B.V.D. (2009). Electrochemical decomposition of choline chloride based ionic liquid analogues. *Green Chemistry*. 11 pp 1357-1365
22. Yang W.Z., Cang H., Tang Y.M., Wang T.T. Shi Y.X. (2008). Electrodeposition of tin and antimony in 1-ethyl-3-methylimidazolium tetrafluoroborate ionic liquid. *Journal of Applied Electrochemistry*. 38 pp 537-542

Chapter 7. Conclusions and Future Studies

7.1 Conclusions

According to the previous studies, DES electrolyte and pulse plating method have shown superior advantages compared to the conventional aqueous solution and direct current plating. However, very few studies attempted to apply the pulse plating technique in the DES electrolyte system. Therefore, the primary objective of this study is to fill in this research gap and investigate the effects of combining both approaches in the electrodeposition process.

Plated copper and tin are two important metals used in a variety of industries such as automotive, decorative, electronic, and microelectronics. While they can also be deposited from aqueous system, here they are used as ‘model’ systems for the purpose of comparison. Studies of DC and pulse plating of copper and tin from aqueous solutions are relatively common, and this provides a useful way of benchmarking the present study.

The electrochemical characteristics of copper ethaline DES electrolyte was examined in the first place. Two cathodic peaks and two anodic peaks were shown in the cyclic voltammogram, indicating the copper redox reaction is a two-step single electron transfer process. $\text{Cu}^{2+} / \text{Cu}^{+}$ was a quasi-reversible redox couple and $\text{Cu}^{+} / \text{Cu}$ was non-reversible redox couple. In addition, The

DC limiting current density was determined empirically as 7.20 mA/cm² under 700 rpm RDE rotation speed.

The deposition process was further studied from the electrochemical characterization of copper deposit. The plated copper was appeared in a light reddish orange colour. Partial or no copper coverage on the substrate was observed under some pulse conditions, especially in the case of long pulse off-time period. It was speculated that this was possibly due to the corrosion effect occurring during the pulse off-time. The Faradaic efficiency was determined ranging from -23.3% to 61.1%. Higher current efficiency was achieved under the pulse condition of high duty cycle and long pulse on-time.

The study of plating potential profiles was followed and showed that the potential in pulse off-time was nowhere equal to the OCP as measured. Transition of potential was also found when Cu was being removed from the electrode surface when pulse off-time becomes longer. Cell potential shifted towards negative with higher peak current density due to the increase of system overpotential. These results indicated that side reaction occurs during the pulse off-time.

Copper dissolution during pulse off-time was further verified from the evidence demonstrated in the separate metal soaking experiments under stagnant and agitation condition. The comproportionation reaction between Cu and Cu²⁺ species was proposed: $\text{Cu} + [\text{Cu}^{2+}\text{Cl}_4^{2-}] \rightleftharpoons 2[\text{Cu}^+\text{Cl}_2^-]$. In addition,

the separate metal dissolution experiments tests revealed that pure ethaline does not cause prominent metal dissolution in DES electrolyte, whereas the solvent became corrosive when copper salt was added. This result was in support of the proposed hypothesis. In the case of partial coverage of copper on the substrate, annulus shape of deposit was found. This was caused by poor plating current density distribution on the electrode surface, since the calculated Wagner number was much smaller than unity.

The process of metal corrosion was investigated in detail afterwards. Copper dissolution current density was determined in the range of 2.23 to 4.57 mA/cm² depending on the agitation condition. The corresponding dissolution potential was found in the range of -0.13 V to -0.15 V. It was revealed that the dissolution process was under mass transport control. Stronger agitation could lead to higher dissolution current density and more positive dissolution potential. In addition, the colour of DES solution turned dark and dark red precipitate was found at the bottom of cell after the electrolyte became aged. The Faradaic efficiency increased when plating was performed using aged solution. The reason of aging effect could possibly be attributed to the increase of Cu concentration.

Two mathematical models were developed to explain the relationship among metal deposition, dissolution effects and pulse parameters. The first model assumed a constant corrosion rate in the pulse off-time, whose magnitude reflected the corrosion rate determined earlier in metal dissolution

experiments under steady-state conditions. A second model assumed a varying corrosion rate in the pulse off-time, as the potential in the off time suggested that the corrosion rate was not constant. Both models qualitatively explained the dissolution effect, but there were some discrepancies and the data did not fit very well, since they had two major limitations: one was the electrode used in the electrodeposition is different from the one used in the electrochemical study. In addition, both mathematical models did not take consideration of steel corrosion, of which no information was available for analysis.

The inhibition effect of BTA additive was later investigated in a similar approach as described above, aiming to suppress the copper dissolution process. The redox process with BTA addition was similar to non-BTA group, DC limiting current density was determined to be 4.45 mA/cm^2 . Copper deposits plated using DES containing BTA were shown in dark red colour with poor adhesion. The current efficiency was found to be at least 30% higher on average compared to the original group, yet the mass transport limitations were exceeded. The effects of pulse parameters on Faradaic efficiency were also similar to the non-BTA group.

The inhibition effect of BTA was also demonstrated in the dissolution experiments. The dissolution current density was determined to be in the range of 0.91 to 1.42 mA/cm^2 , which was smaller than the ones obtained without BTA addition. The dissolution potential shifted towards more negative values to approximately -0.20 V with very small variations on the change of agitation

condition. The data obtained by BTA was also integrated to the established mathematical models and tested. The calculated dissolution current density of BTA was in the range of 0.5 to 1.0 mA/cm² from three different approaches, which was close to the ones measured from the empirical dissolution experiments. However, the BTA data also did not fit the models very well with the same reasons aforementioned.

Similar to the approach adopted in copper electrodeposition. The electrochemical behaviours of tin ethaline DES electrolyte were studied firstly. In contrast to copper, the Sn redox reaction occurred in a single two electrons transfer process. One cathodic and two peaks in the forward sweep were illustrated from the cyclic voltammogram. According to the previous study, the second peak might indicate the formation of a different Sn²⁺ species rather than the oxidation of Sn⁴⁺ species. The DC limiting current density was later determined to be 5.06 mA/cm².

The experiments of pulse plating of tin in DES were carried out afterwards. The plated tin deposit showed in poor adhesion on steel substrate, the Faradaic efficiency was found to be in the range of 95% to 105%, yet the effects of pulse parameters were not observed. The potential profiles showed that there was no side reaction during pulse off-time period, since the potential during pulse off-time was similar to the measured OCP. It was found that the overall potential becomes more negative with shorter pulse on-time and shorter duty cycle during pulse on-time.

The microstructure of tin deposit was examined by SEM analysis, which showed that pulse plated tin was in granular shape and denser than the ones plated by DC. The grain size of pulse deposit was in the range of 2.93 to 6.18 μm , compared to 4.91 μm in DC. Smaller grain size was achieved when pulse on-time is longer. No clear relationship between grain size and pulse duty cycle was found and no trends were observed between the microstructure and pulse parameters. The deposit at the substrate edge was more dendritic compared to the one at the substrate centre due to poor current density distribution.

The elemental composition of tin deposit was characterized by EDX analysis, which showed that Sn had a percentage of 67.0% to 99.6%, and oxygen was incorporated into some of the deposits. No clear relationship was found between the percentage of Sn and pulse parameters. The exact reasons of oxygen incorporation remained unknown at present. Other elements such as Fe, Cl, N and Cr, which came from the breakdown of electrolyte and steel substrate, were also detected under some pulse conditions.

In summary, this piece of research work has fulfilled all the objectives purposed in the first chapter. The results showed that it is feasible to plate both copper and tin from deep eutectic solvents using pulse current. Currently they do not demonstrate superior advantages in terms of deposit quality and microstructure compared to the conventional methods. Issues such as occurrence of corrosion reaction in copper

deposition, and oxygen incorporation in tin deposit were detected and need to be addressed in the future optimization. Nevertheless, the studies of both corrosive (Cu) and non-corrosive (Sn) DES electrolyte system could provide valuable insights on the electrodeposition of other metals such as Cr, Zn and Mg in the similar approach. It is reasonable to assume that metal dissolution could occur when comproportionation reaction is feasible between metal and metal ions with different valences.

7.2 Future studies

There are a number of suggestions which either could improve the experiment or provide further understanding in this subject. Firstly, although the addition of BTA exhibits an increase of faradic efficiency in copper plating due to its inhibition effect, the mass transport limitations were exceeded by using the same pulse parameters. The CV data showed that the DC limiting current density BTA was lower than the non-BTA group. Therefore, the pulse parameters in plating experiment using BTA additive should be adjusted accordingly to ensure the mass transport condition remained the same as the non-BTA group. It was expected that the copper plated under such experimental conditions is expected to provide better results.

In addition, the aging effect of DES electrolyte was found in the electroplating process and needs to be further investigated. The analytes in the

solution could be identified by using ultraviolet-visible spectroscopy (UV-Vis) characterization technique. The relationship between the change of Cu concentration with time of usage should also be determined. This could reveal more insights on the process of metal corrosion.

In the metal plating experiments, low Faradaic efficiency was observed due to metal dissolution during pulse off-time. Applying the bipolar pulse waveform, which is also named as pulse reverse current plating technique, is expected to counteract the metal dissolution behaviour caused by the comproportionation reaction of Cu without the need of using inhibitors such as BTA. This could eliminate the drawbacks of additives which complicate the electrochemical process.

Due to the limitations exhibited in both mathematical models purposed in this research. More complex model should be established to explain the results with better fitted data. Firstly, polarization and cyclic voltammetry of copper ethaline on steel substrate needs to be performed, the results are expected to be more reliable when using the same substrate with metal plating, though the voltammogram based on steel substrate may be ill-defined. Secondly, the dissolution of steel experiment in DES needs to be performed and the data should be integrated into the model with copper dissolution. Finally, the purposed “dead time” theory also needs to be test quantitatively.

As described in the thesis, it was reported that metal corrosion behaviour was observed in the DES and other types of ionic liquids containing

chloride not only just in copper but also in other metals such as Cr and Fe. It is reasonable to assume that chloride plays a crucial role in the initiation of comproportionation reactions. Therefore, the pulse deposition experiments of copper can be performed in a non-chloride DES electrolyte system, such as the use of choline nitrate and choline citrate to replace choline chloride, to prevent from the occurrence of metal dissolution.

During the study of electrochemical characterization of tin deposition, only one pulse on-time group and one duty cycle pulse condition group were tested as preliminary results in this research. However, no clear trends or implications were found. To investigate further the entire range of pulse conditions should be explored by the same approach applied in copper deposition. Better picture of the results is expected to be achieved.

The elemental composition of tin deposit should be further examined by EDX, which multiple areas on the deposit surface need to be detected to show the homogeneity. In addition, the crystal structure and atomic arrangement of Sn deposit could be revealed by using X-ray diffraction technique, which is able to identify the orientation of Sn crystal and provide information on unit cell dimensions. The thickness of Sn film can also be determined using such characterization method.

Appendix

Appendix A: Potential profiles of Cu deposition in ethaline DES under various pulse conditions.

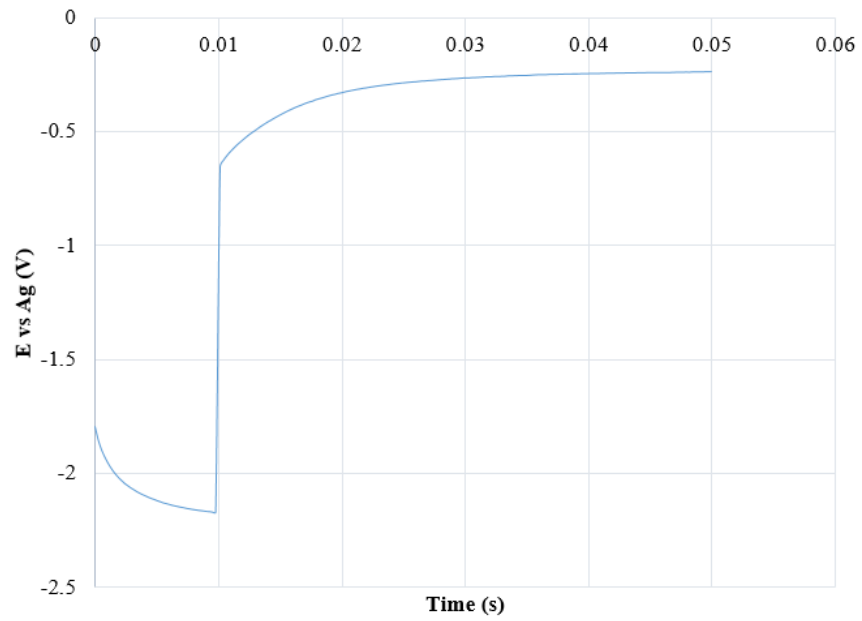


Table A-1 Potential profile in a single pulse in pulse electrodeposition of Cu with the condition of $t_{\text{on}} = 10 \text{ ms}$ and $\theta = 0.2$

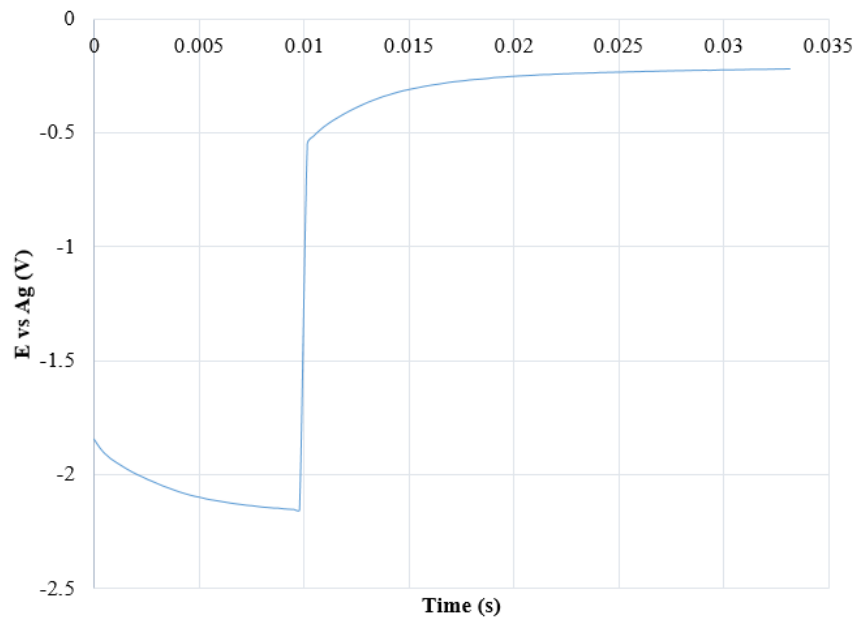


Table A-2 Potential profile in a single pulse in pulse electrodeposition of Cu with the condition of $t_{on} = 10$ ms and $\theta = 0.3$

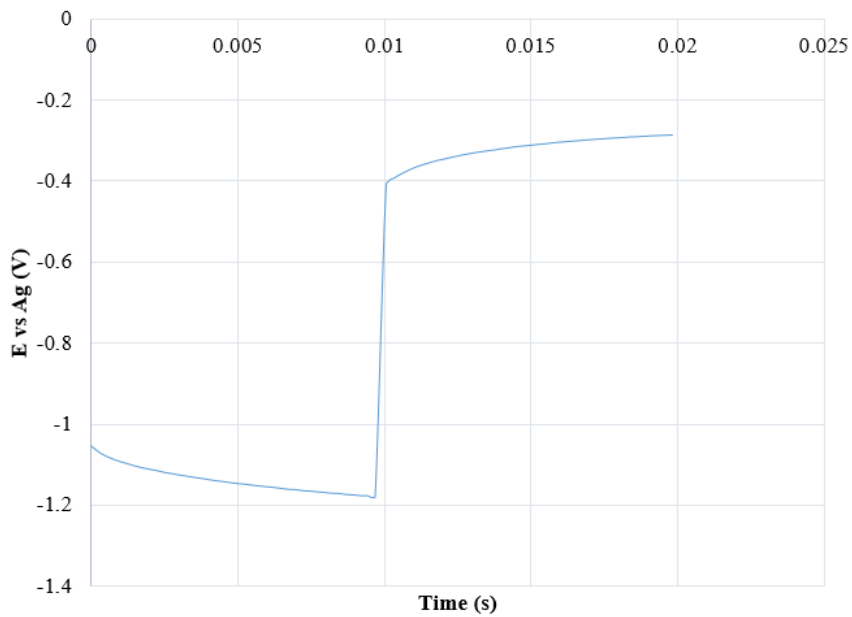


Table A-3 Potential profile in a single pulse in pulse electrodeposition of Cu with the condition of $t_{on} = 10$ ms and $\theta = 0.5$

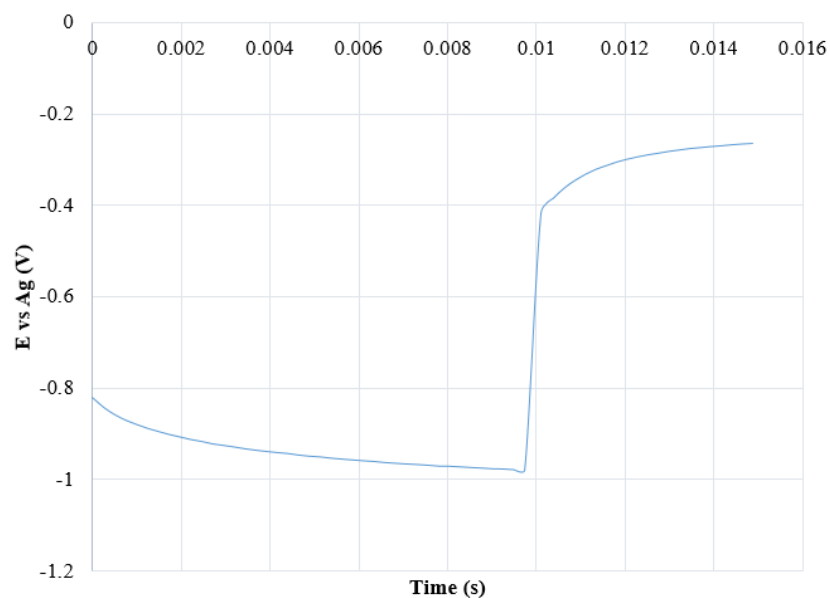


Table A-4 Potential profile in a single pulse in pulse electrodeposition of Cu with the condition of $t_{on} = 10$ ms and $\theta = 0.67$

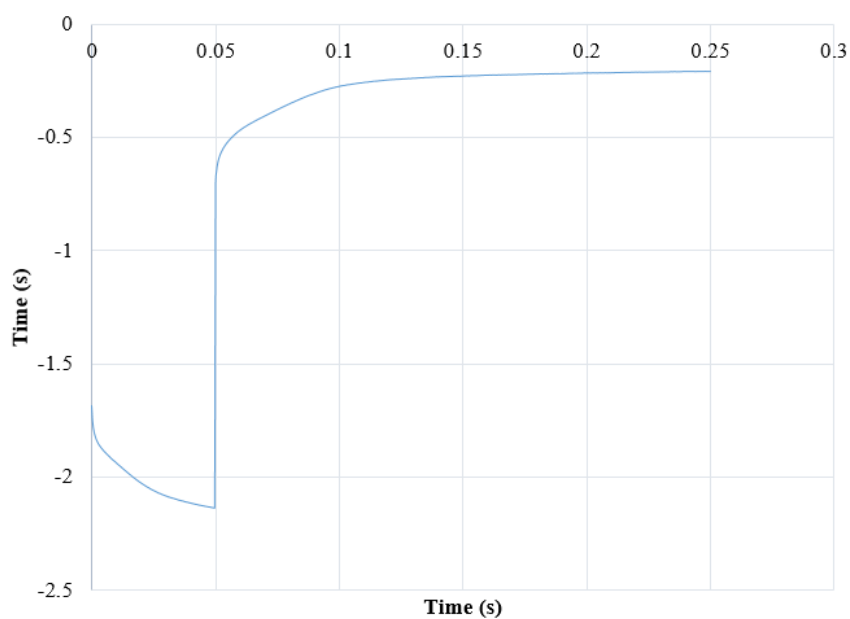


Table A-5 Potential profile in a single pulse in pulse electrodeposition of Cu with the condition of $t_{on} = 50$ ms and $\theta = 0.2$

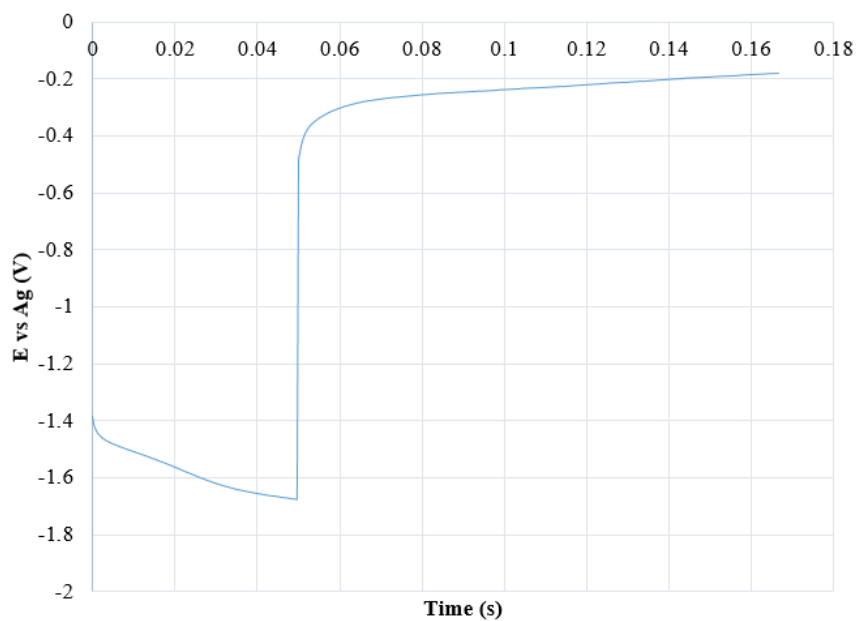


Table A-6 Potential profile in a single pulse in pulse electrodeposition of Cu with the condition of $t_{on} = 50$ ms and $\theta = 0.3$

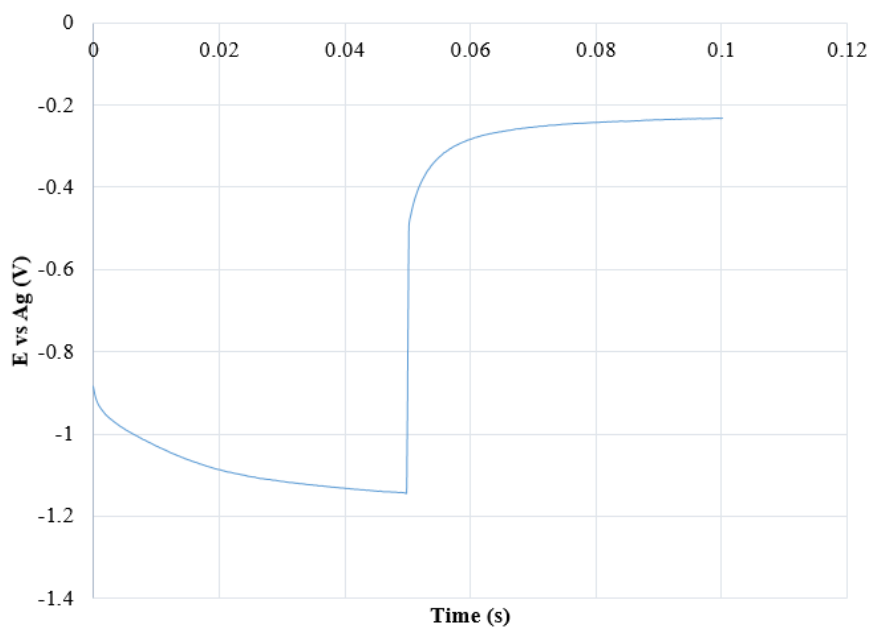


Table A-7 Potential profile in a single pulse in pulse electrodeposition of Cu with the condition of $t_{on} = 50$ ms and $\theta = 0.5$

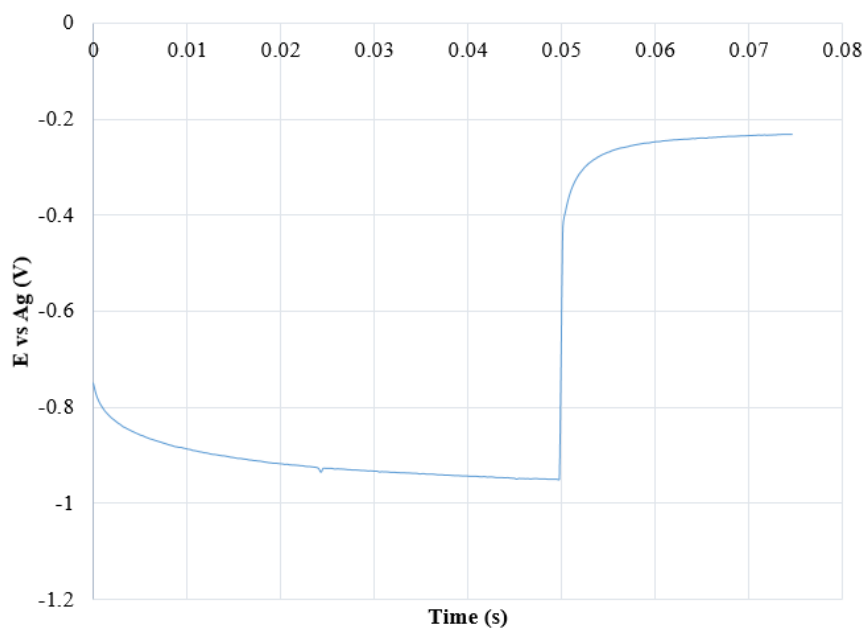


Table A-8 Potential profile in a single pulse in pulse electrodeposition of Cu with the condition of $t_{on} = 50$ ms and $\theta = 0.67$

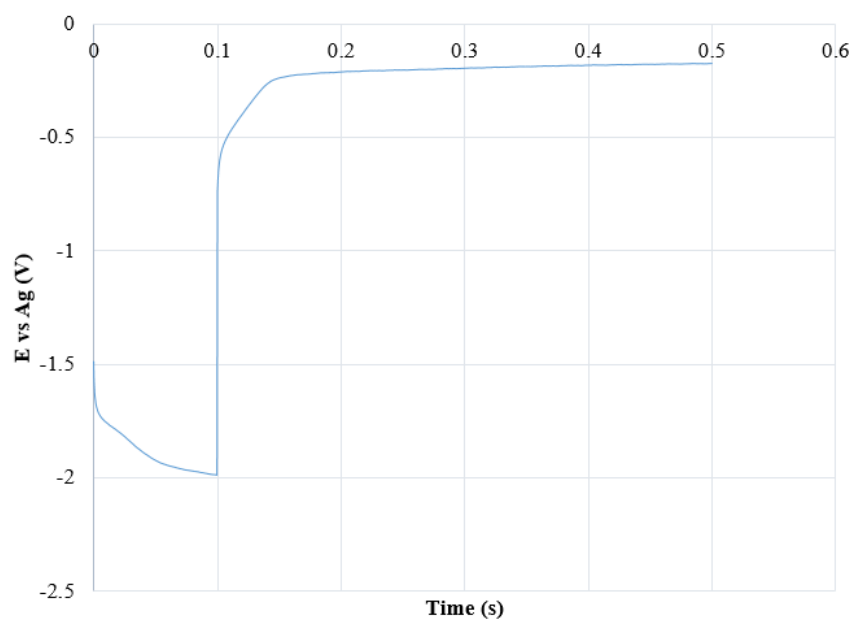


Table A-9 Potential profile in a single pulse in pulse electrodeposition of Cu with the condition of $t_{on} = 100$ ms and $\theta = 0.2$

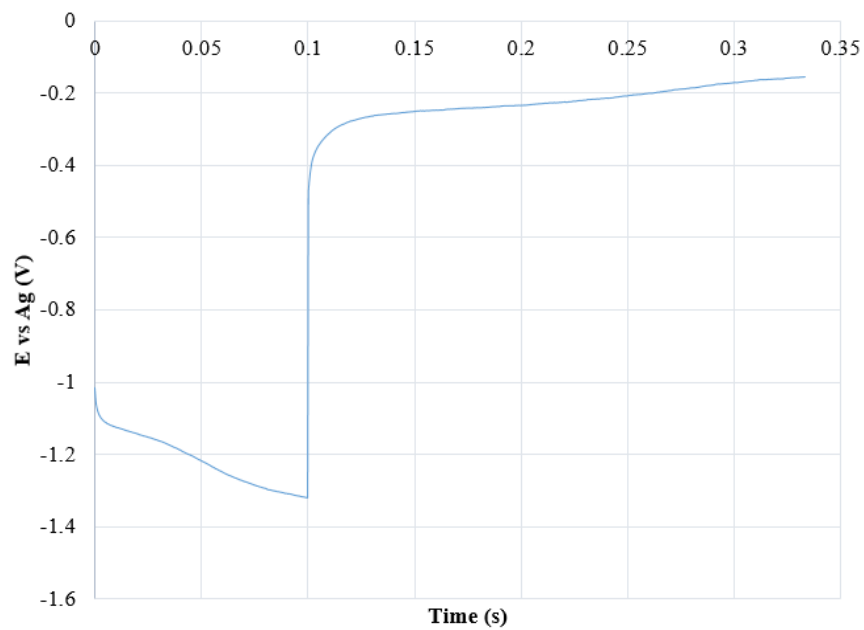


Table A-10 Potential profile in a single pulse in pulse electrodeposition of Cu with the condition of $t_{on} = 100$ ms and $\theta = 0.3$

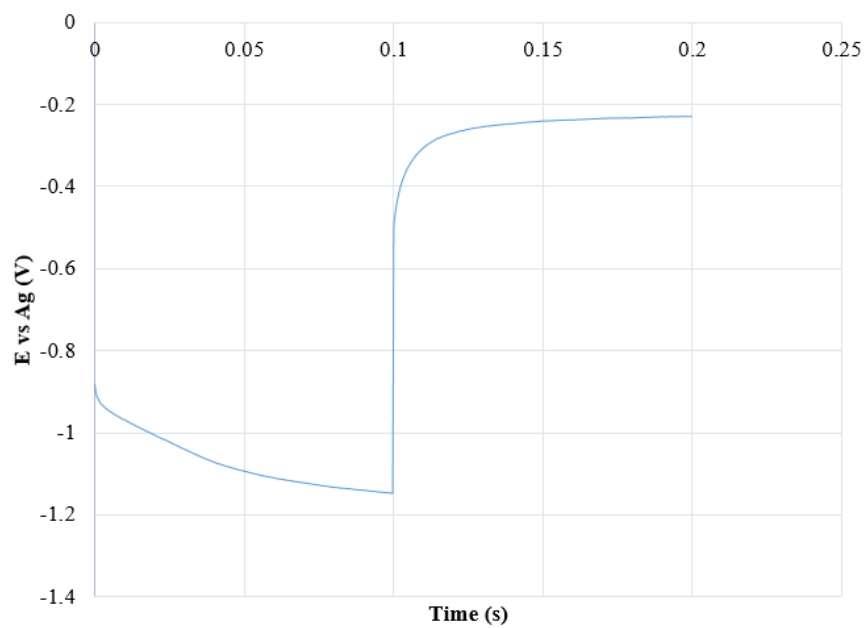


Table A-11 Potential profile in a single pulse in pulse electrodeposition of Cu with the condition of $t_{on} = 100$ ms and $\theta = 0.5$

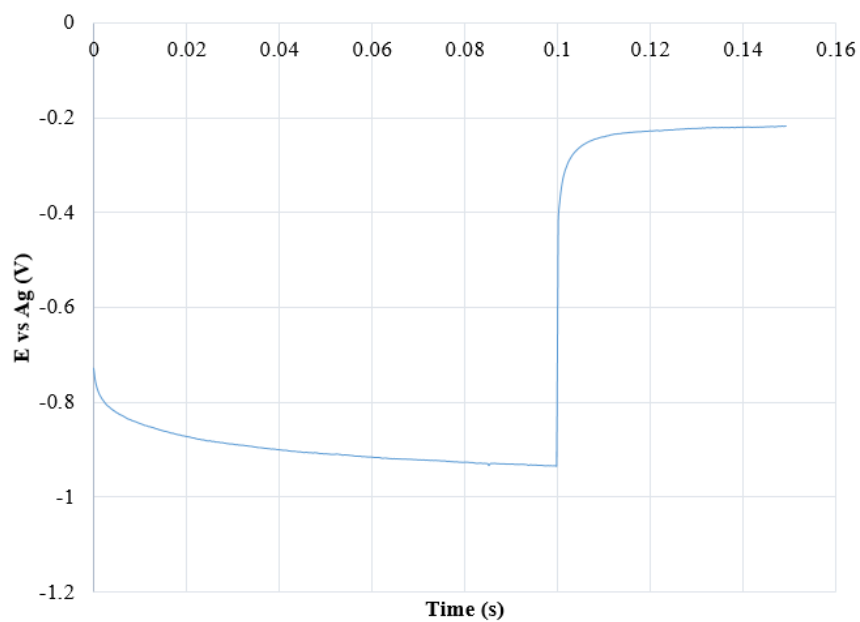


Table A-12 Potential profile in a single pulse in pulse electrodeposition of Cu with the condition of $t_{\text{on}} = 100$ ms and $\theta = 0.67$

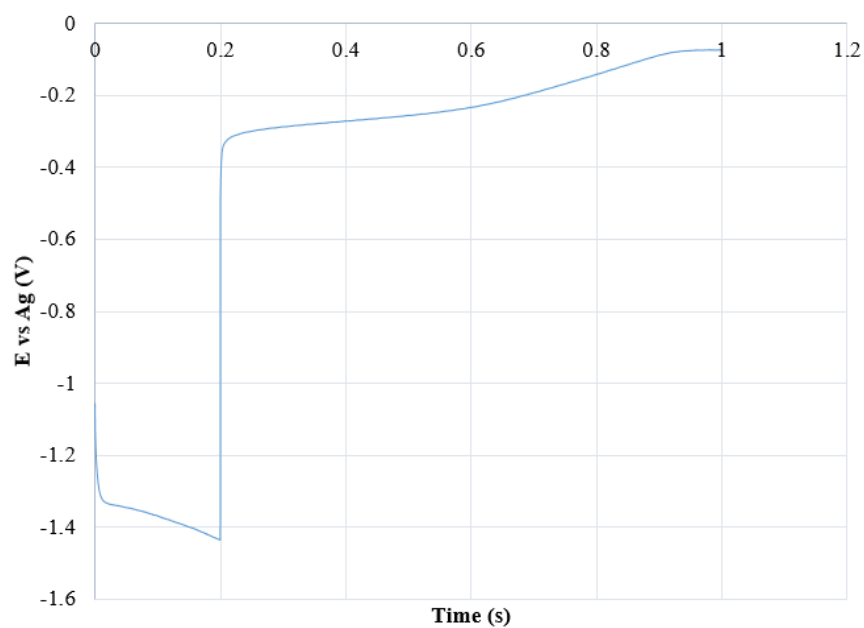


Table A-13 Potential profile in a single pulse in pulse electrodeposition of Cu with the condition of $t_{\text{on}} = 200$ ms and $\theta = 0.2$

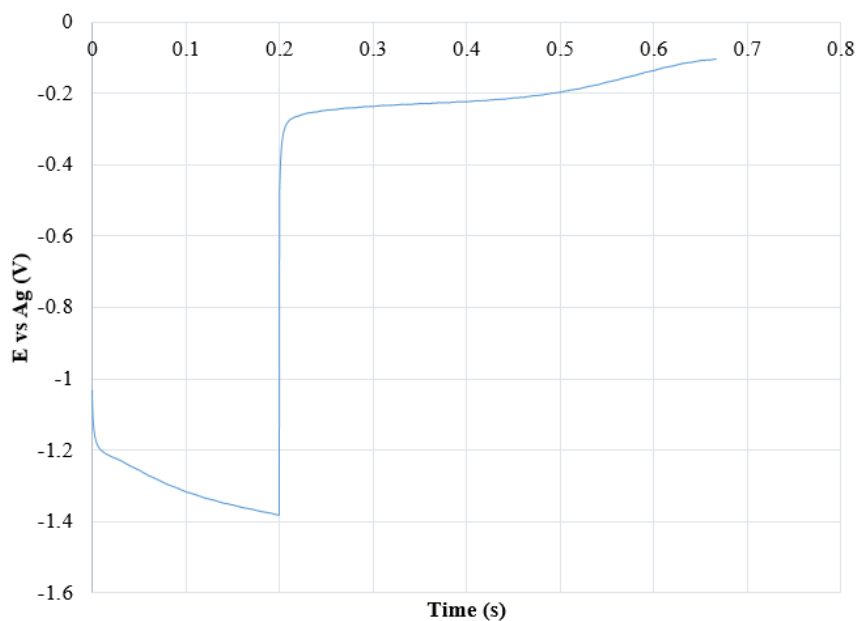


Table A-14 Potential profile in a single pulse in pulse electrodeposition of Cu with the condition of $t_{on} = 200$ ms and $\theta = 0.3$

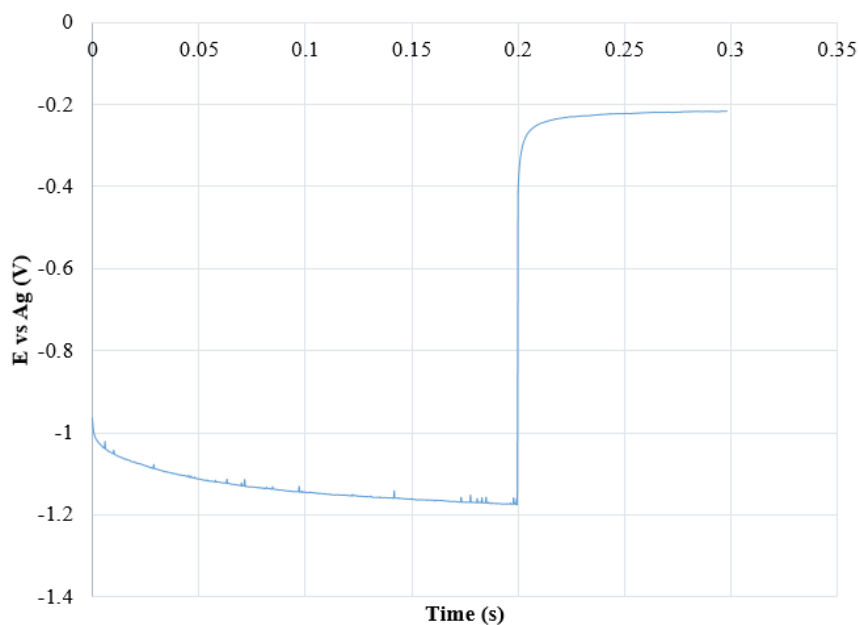


Table A-15 Potential profile in a single pulse in pulse electrodeposition of Cu with the condition of $t_{on} = 200$ ms and $\theta = 0.67$

Appendix B: Potential profiles of Sn deposition in ethaline DES under various pulse conditions.

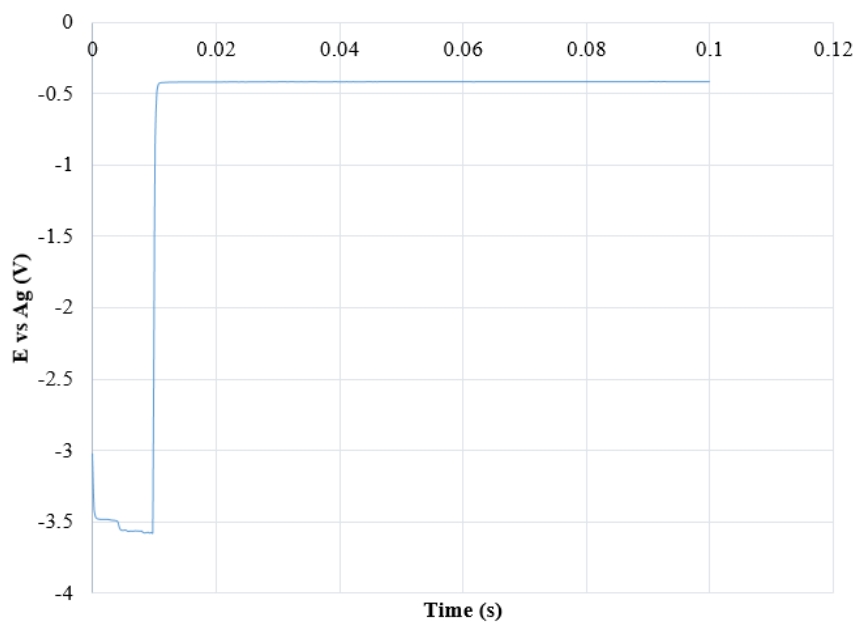


Table B-1 Potential profile in a single pulse in pulse electrodeposition of Sn with the condition of $t_{\text{on}} = 10$ ms and $\theta = 0.1$

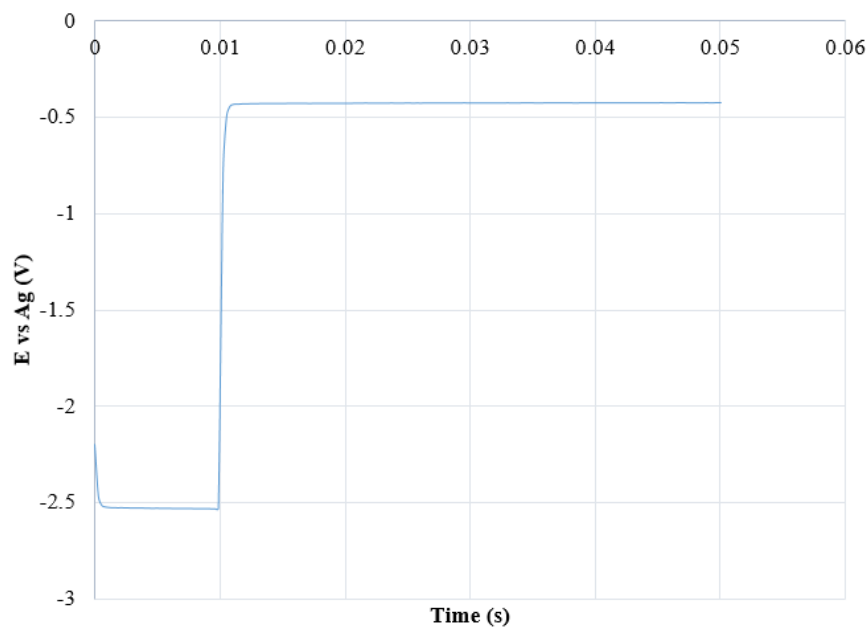


Table B-2 Potential profile in a single pulse in pulse electrodeposition of Sn with the condition of $t_{on} = 10$ ms and $\theta = 0.2$

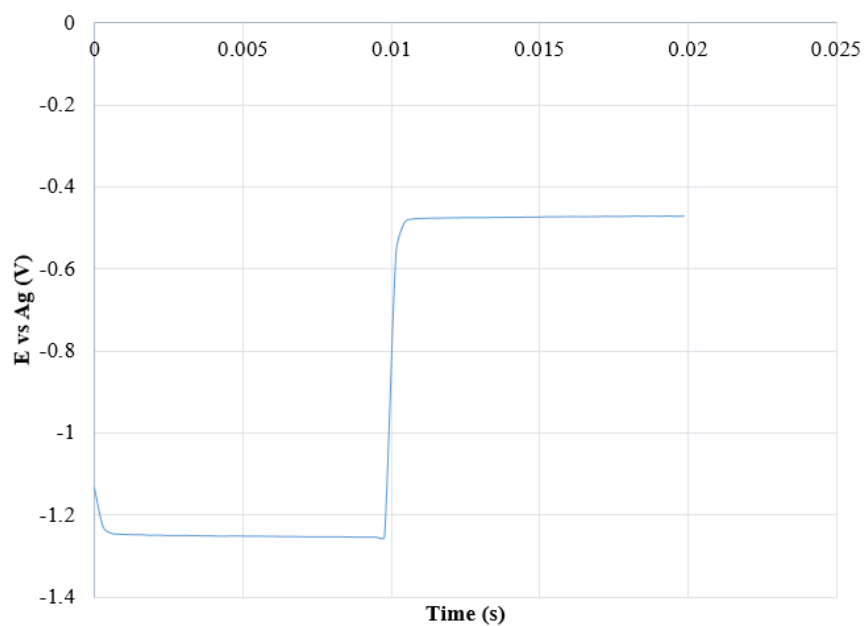


Table B-3 Potential profile in a single pulse in pulse electrodeposition of Sn with the condition of $t_{on} = 10$ ms and $\theta = 0.5$

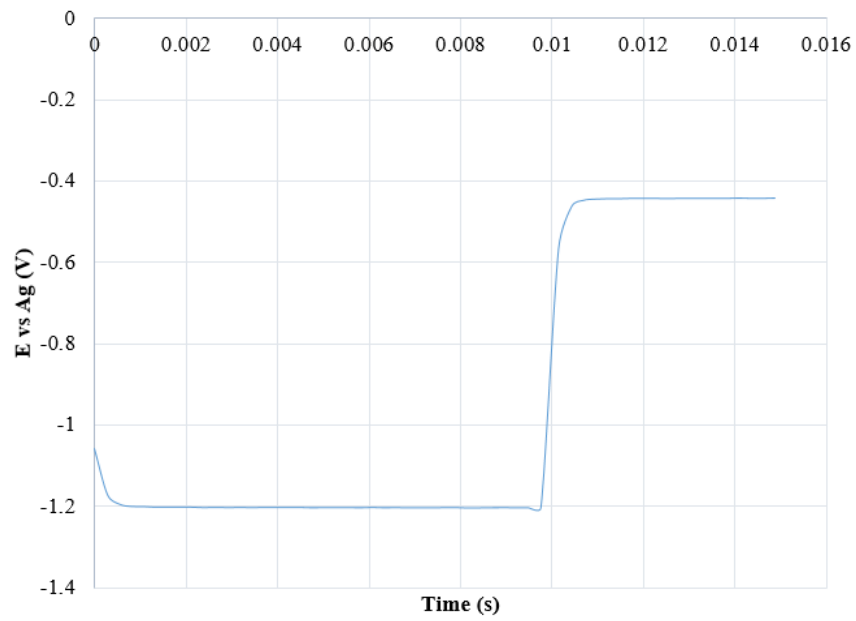


Table B-4 Potential profile in a single pulse in pulse electrodeposition of Sn with the condition of $t_{on} = 10 \text{ ms}$ and $\theta = 0.67$

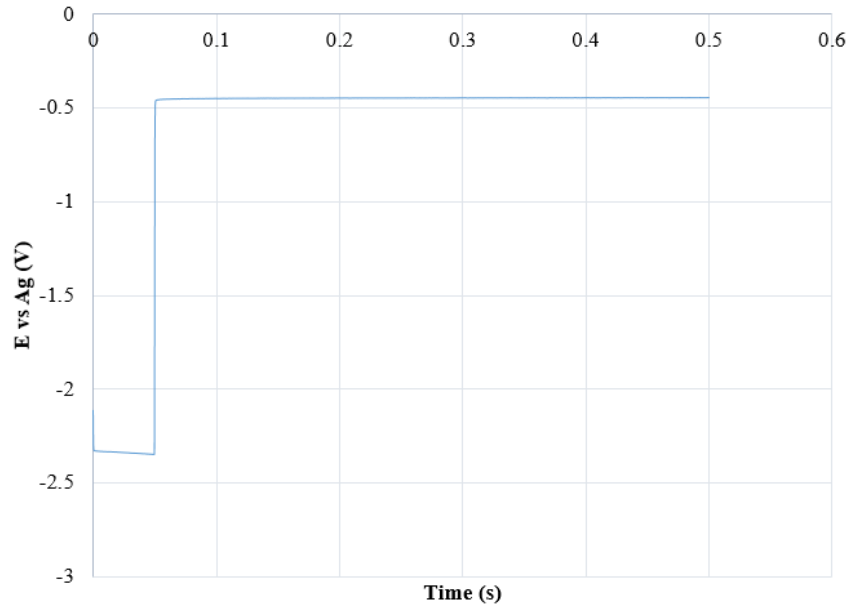


Table B-5 Potential profile in a single pulse in pulse electrodeposition of Sn with the condition of $t_{on} = 50 \text{ ms}$ and $\theta = 0.1$

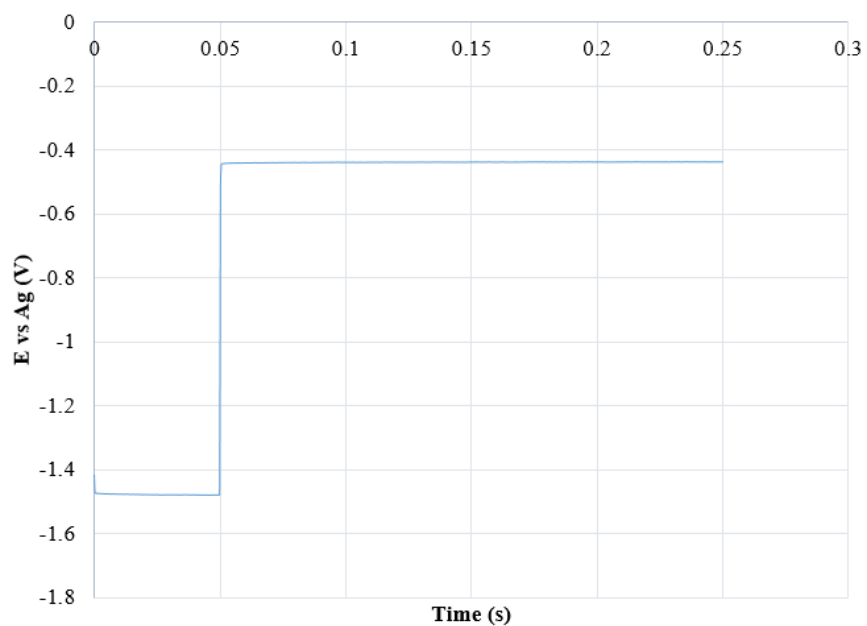


Table B-6 Potential profile in a single pulse in pulse electrodeposition of Sn with the condition of $t_{\text{on}} = 50$ ms and $\theta = 0.2$

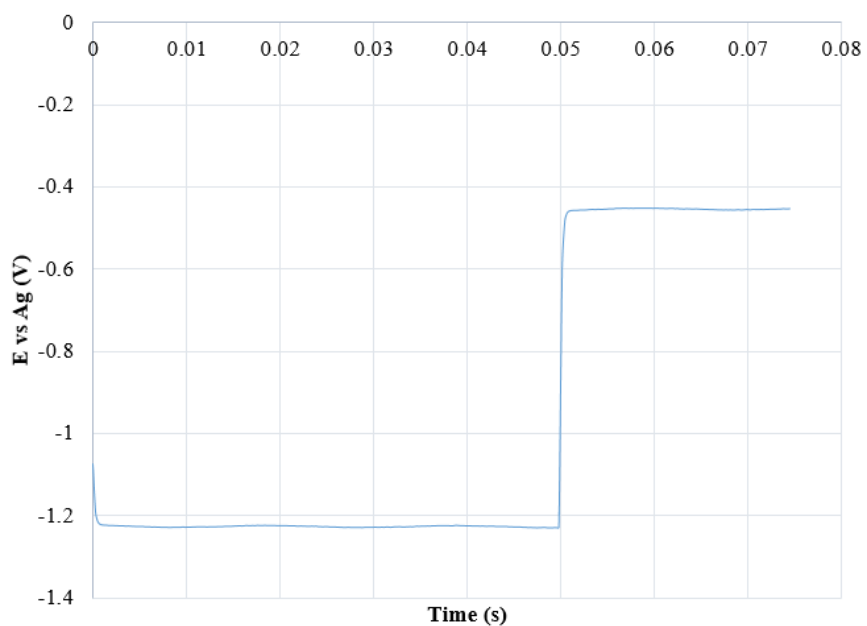


Table B-7 Potential profile in a single pulse in pulse electrodeposition of Sn with the condition of $t_{\text{on}} = 50$ ms and $\theta = 0.67$

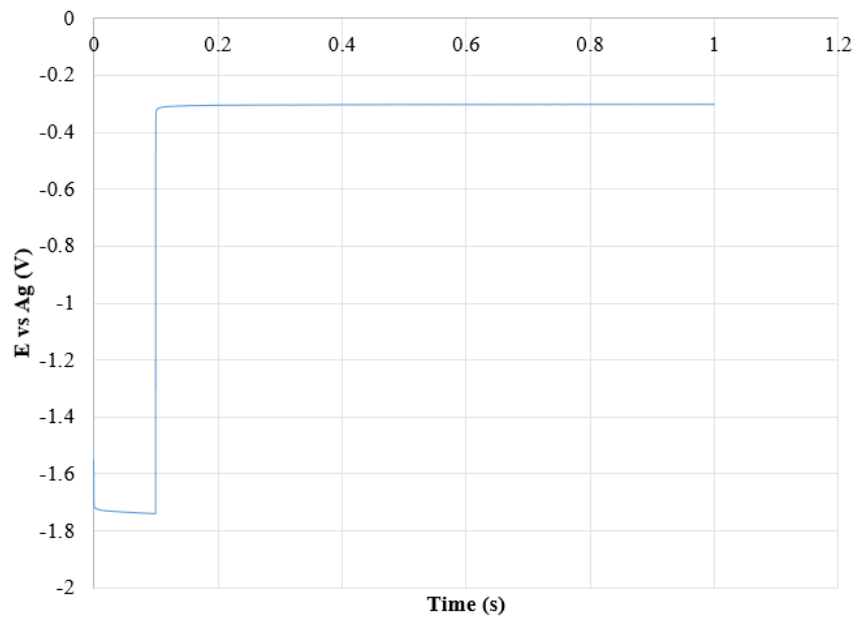


Table B-8 Potential profile in a single pulse in pulse electrodeposition of Sn
with the condition of $t_{on} = 100$ ms and $\theta = 0.1$

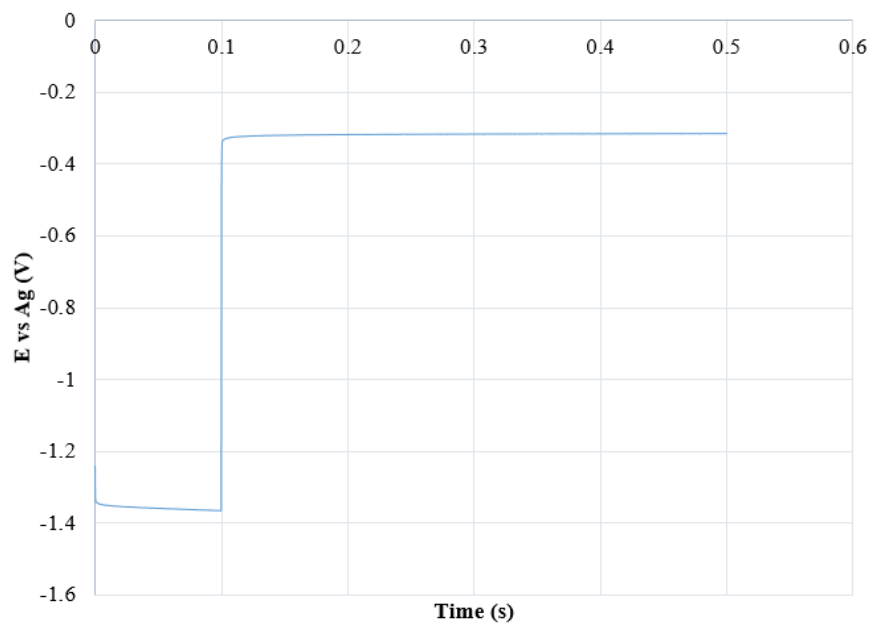


Table B-9 Potential profile in a single pulse in pulse electrodeposition of Sn
with the condition of $t_{on} = 100$ ms and $\theta = 0.2$

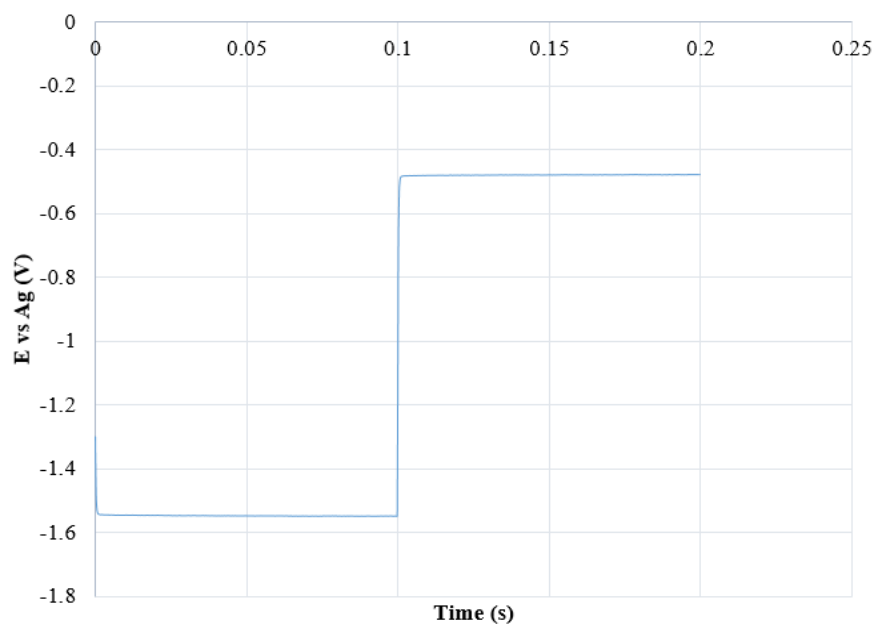


Table B-10 Potential profile in a single pulse in pulse electrodeposition of Sn with the condition of $t_{on} = 100$ ms and $\theta = 0.5$

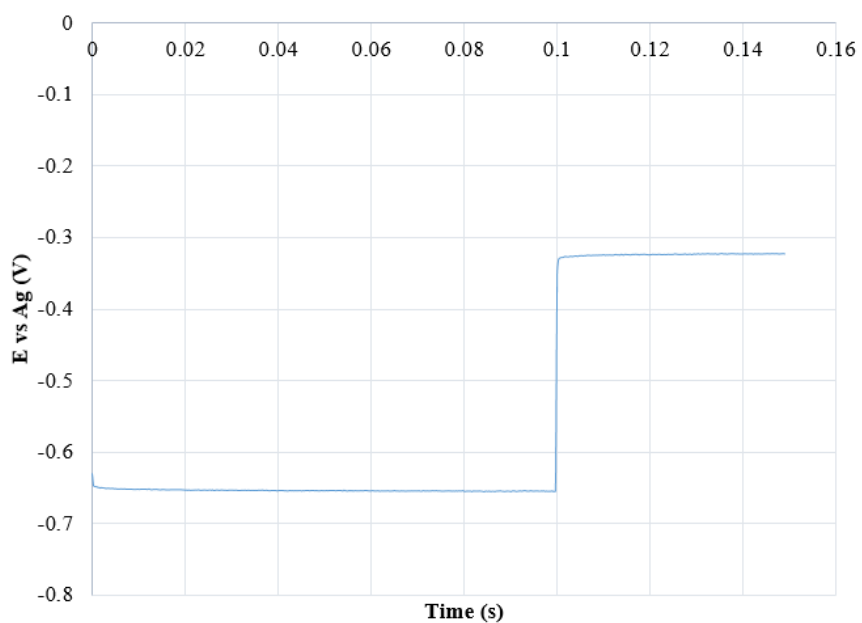


Table B-11 Potential profile in a single pulse in pulse electrodeposition of Sn with the condition of $t_{on} = 100$ ms and $\theta = 0.67$

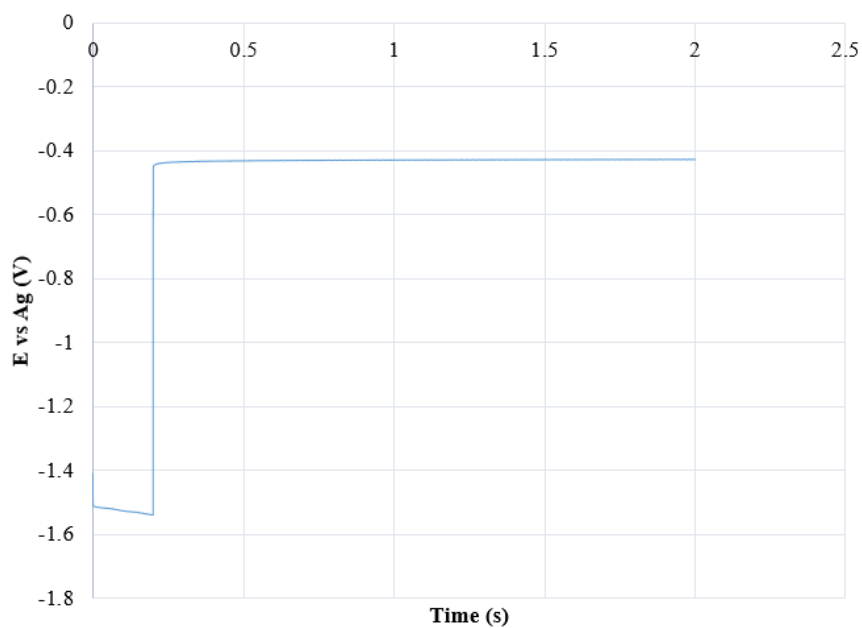


Table B-12 Potential profile in a single pulse in pulse electrodeposition of Sn with the condition of $t_{on} = 200$ ms and $\theta = 0.1$

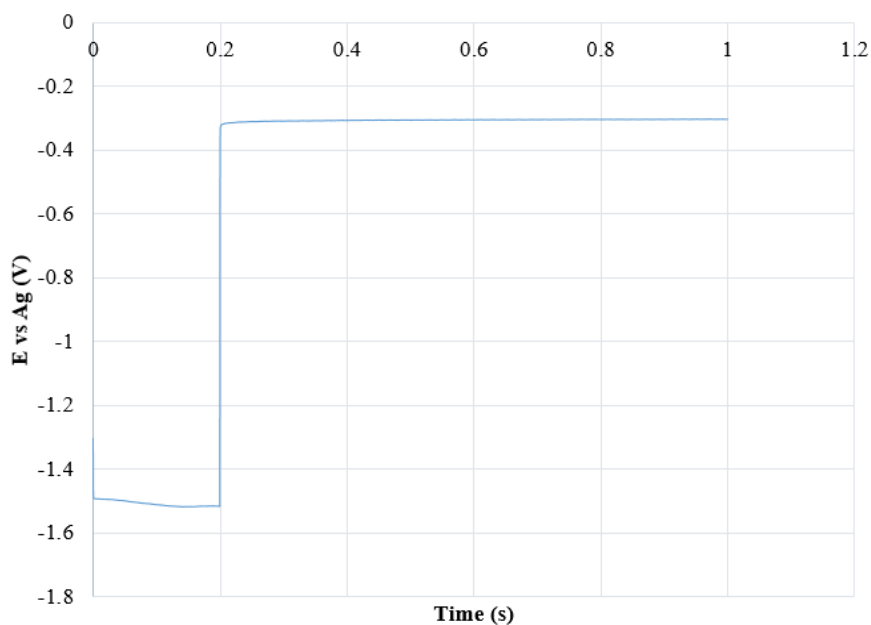


Table B-13 Potential profile in a single pulse in pulse electrodeposition of Sn with the condition of $t_{on} = 200$ ms and $\theta = 0.2$

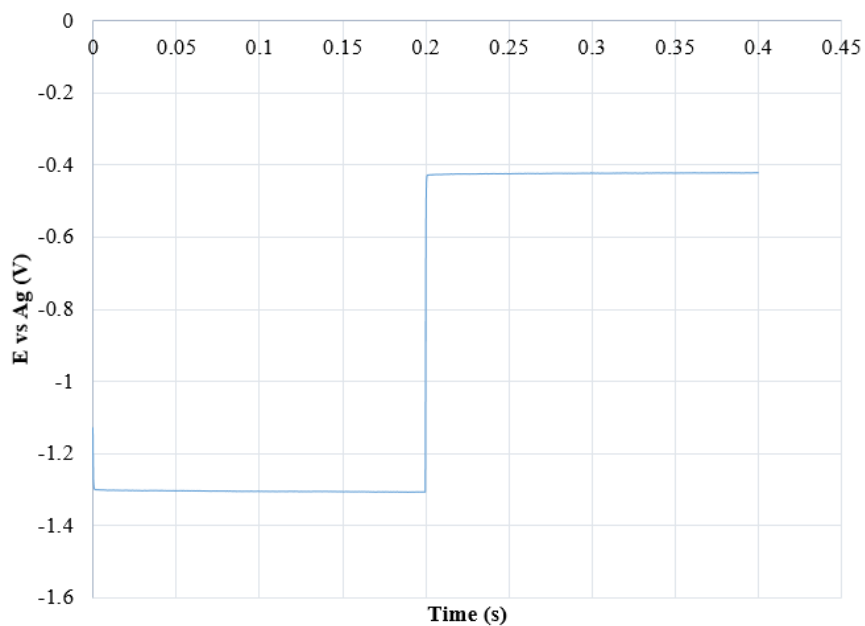


Table B-14 Potential profile in a single pulse in pulse electrodeposition of Sn with the condition of $t_{\text{on}} = 200 \text{ ms}$ and $\theta = 0.5$

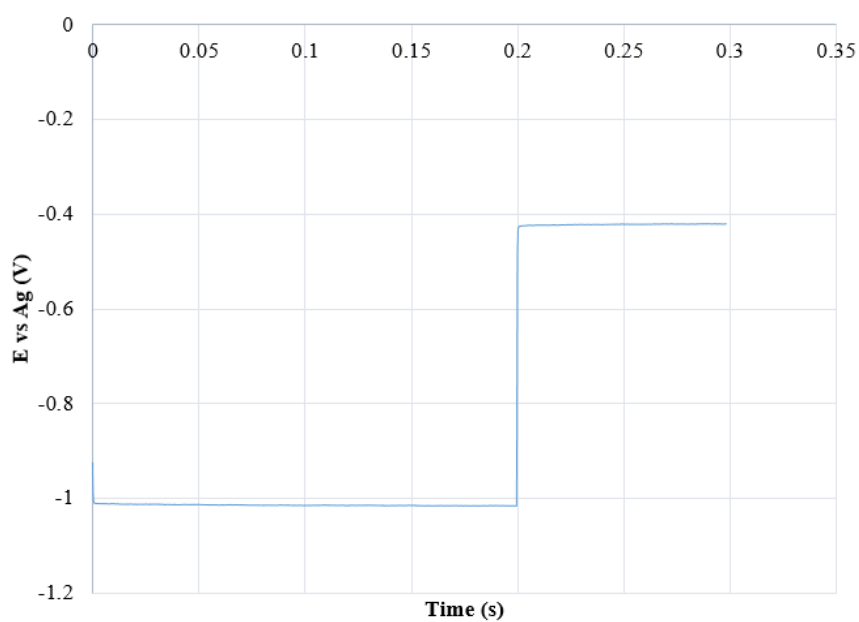


Table B-15 Potential profile in a single pulse in pulse electrodeposition of Sn with the condition of $t_{\text{on}} = 200 \text{ ms}$ and $\theta = 0.67$

Appendix C: List of Experimental parameters and programming codes

```
1
2 % Constants
3
4 F=96485; % Faraday constant (C/mol)
5
6 % Plating system parameters
7
8 % Electrolyte
9
10 D=1.4*10^-7; % Electrolyte diffusion coefficient (cm2/s)
11 v=0.5; % Kinematic viscosity (cm2/s)
12 cb=0.2; % Electrolyte bulk concentration (mol/L)
13
14 % Rotating disc electrode (RDE)
15
16 w=700; % RDE rotating speed (rpm)
17 d=1.26; % Effective Diameter of RDE surface (cm)
18
19 % Metal properties
20
21 M=63.55; % Metal molar mass (g/mol)
22 p=8.96; % Metal density (g/cm3)
23 h=5; % Metal deposit thickness (um)
24 z=2; % Ionic charge
25
26 % Input pulse parameters
27
28 t1=input('Pulse on time (ms)='); % Pulse on time (ms)
29 DC=input('Pulse duty cycle='); % Pulse duty cycle
30 jrev=0; % Pulse reverse current density (A/cm2)
31
32 % Parameters unit conversion and DC limiting current density calculation
33
34 ton=t1/1000; % Pulse on-time (s)
35 w1=w*pi/30; % RDE rotating speed (rad/s)
36 Ld=1.61*D^(1/3)*v^(1/6)/(w1^0.5); % Length of DC Diffusion layer (cm)
37 c1=cb/1000; % Electrolyte concentration (mol/cm3)
38 jlim=z*F*c1*D*1000/Ld; % DC limiting current density (mA/cm2)
39
40 % Calculation of Dimensionless time and reverse current density
```

Figure C-1 Matlab programming code for determination of limiting current densities and plating parameters (part 1/2)

```

41
42 - t=ton/DC;           % Total pulse time (s)
43 - td=D*t/(Ld*Ld);   % Dimensionless pulse time
44 - jd=jrev/jlim*1000; % Dimensionless reverse current density
45
46 % Calculation of pulse limiting current density by using Roy's equation
47
48 - syms m
49 - S=symsum((exp((pi^2*td*(m-0.5)^2)*(1-DC))-1)/((pi^2*td*(m-0.5)^2)*(exp(pi^2*td*(m-0.5)^2)-1)),m,1,Inf);
50 - S1=double(S);
51
52 - S2=1+2*td*jd*S1;
53 - S3=1-2*td*S1;
54 - jratio=S2/S3;
55 - jplim=jlim*jratio % Pulse limiting current density (mA/cm2)
56 - A=pi*(d/2)^2;    % Surface area of RDE electrode (cm2)
57 - Iplim=jplim*A;   % Pulse limiting current (mA)
58
59 % Average current density check versus direct limiting current density
60
61 - jp=0.8*jplim;    % Peak current density (mA/cm2)
62 - jav=jp*DC;      % Average current density (mA/cm2)
63
64 - if jav<jlim
65 -     disp('jav < jlim, parameters are ok');
66 - else
67 -     disp('jav > jlim, paramters need to be reviewed or reset');
68 - end
69
70 % Calculation of input parameters for potentiostat programming
71
72 - Ip=jp*A;         % Applied peak current (mA)
73 - toff=t-ton;     % Pulse off-time (s)
74 - DR=jav*M*600000/(1000*z*F*p); % Deposition rate (um/min)
75 - DepositionTime=h/DR*60; % Total plating time (s)
76
77 % Nm and Np
78 - Nm=jav/jlim;
79 - Np=jp/jplim;

```

Figure C-2 Matlab programming code for determination of limiting current densities and plating parameters (part 2/2)

```

1      % Constants
2
3      R=8.314;           % Gas constant
4      F=96485;          % Faraday constant
5      Int=0.0001;       % Interval of potential change
6
7      % Initial set parameters
8
9      jf=0;              % Faradaic current density at interval n
10     jf1=0;             % Faradaic current density at interval n+1
11     P=0.01;           % Potential at interval n
12     P1=0;             % Potential at interval n+1
13     ChargeTime=0;     % Integrated double layer charge time(us)
14     DischargeTime=0;  % Integrated double layer discharge time(us)
15     Current=0;        % Integrated Faradaic current(uC/cm2)
16     Delta=0;          % Degree of flattening
17
18     % Plating system parameters
19
20     C=50;              % Double layer capacitance(uF/cm2)
21     z=2;               % Ionic charge of reducing species
22     A=0.5;             % Transfer coefficient
23     T=25;              % Temperature(C)
24     ECD=0.005;        % Exchange current density(A/cm2)
25
26     % Input pulse parameters
27
28     jpo=input('Peak current density(mA/cm2)='); % Input peak current density(mA/cm2)
29     ton=input('Pulse on-time(ms)=');          % Input pulse on-time(ms)
30     DC=input('Pulse duty cycle=');            % Input pulse duty cycle
31
32     % Pre-loop definition and calculations
33
34     toff=(ton/DC)-ton; % Pulse off-time(ms)
35     T1=ton/1000;      % Pulse on-time(s)
36     T2=toff/1000;    % Pulse off-time(s)
37     jp=jpo/1000;     % Peak current density (A/cm2)
38     jc1=jp;          % Capacitative current density at pre-loop
39     TC=R*(T+273);    % Temperature coefficient
40
41     % Charge time calculation
42
43     while jf<0.99*jp
44
45         % The charge time is defined as the time elapsing before jf is 99% of jp
46         % When jf>=0.99*jp the loop ends and calculation stops
47
48         AC1=(A*z*F*P)/TC;
49         AC2=(-(1-A)*z*F*P)/TC;
50         jf=ECD*(exp(AC1)-exp(AC2));
51         jc=jp-jf;

```

Figure C-3 Matlab programming code for the calculation of electrical double layer charging time, discharging time and degree of flattening (part 1/2)

```

52 - TN=C*((P-P1)/(jf-jf1))*log(jc1/jc);
53 - ChargeTime=ChargeTime+TN;
54 - Current=Current+(jf*TN);
55
56 - % The calculation of charging time for a single loop is listed above
57
58 - P1=P;
59 - P=P+Int;
60 - jf1=jf;
61 - jc1=jc;
62
63 - % Above parameters are reset for the preparation of next loop
64 - end
65 - ChargeTime % Final integrated charging time
66
67 - % Discharge time calculation
68
69 - P1=P;
70
71 - while jf>0.01*jp;
72
73 - % The discharge time is defined as the time elapsing from jf=0.999jp to jf=0.01jp
74 - % When jf<0.99*jp the loop ends and calculation stops
75
76 - AC1=(A*z*F*P)/TC;
77 - AC2=(-(1-A)*z*F*P)/TC;
78 - jf=ECD*(exp(AC1)-exp(AC2));
79 - jc=jf;
80 - TN=C*((P-P1)/(jf-jf1))*log(jc1/jc);
81 - DischargeTime=DischargeTime+TN;
82
83 - % The calculation of discharging time for a single loop is listed above
84
85 - P1=P;
86 - P=P-Int;
87 - jf1=jf;
88 - jc1=jc;
89
90 - % Above parameters are reset for the preparation of next loop
91
92 - end
93 - DischargeTime % Final integrated discharging time
94
95 - % Calculation of degree of flattening
96
97 - jAV=jp*DC;
98 - Num=(jp*T1)-(Current/1000000)-jp*((T1-(ChargeTime/1000000)));
99 - Den=jAV*T2;
100 - Delta=Num/Den;
101
102 - Delta % Calculated degree of flattening

```

Figure C-4 Matlab programming code for the calculation of electrical double layer charging time, discharging time and degree of flattening (part 2/2)

Duty Cycle	On-Time (ms)	DLCD (mA/cm ²)	PLCD (mA/cm ²)	N _m	N _p	Applied Current (mA)	Plating Time (s)
0.2	10	6.2	26.8	0.69	0.80	26.8	3167
0.3	10	6.2	19.0	0.73	0.80	19.0	2981
0.5	10	6.2	12.0	0.77	0.80	12.0	2839
0.67	10	6.2	9.1	0.79	0.80	9.1	2787
0.2	50	6.2	23.0	0.59	0.80	22.9	3697
0.3	50	6.2	17.3	0.67	0.80	17.2	3282
0.5	50	6.2	11.5	0.74	0.80	11.4	2964
0.67	50	6.2	8.9	0.77	0.80	8.9	2847
0.2	100	6.2	20.8	0.54	0.80	20.7	4094
0.3	100	6.2	16.2	0.62	0.80	16.1	3508
0.5	100	6.2	11.1	0.72	0.80	11.1	3057
0.67	100	6.2	8.8	0.76	0.80	8.8	2892
0.2	200	6.2	18.3	0.47	0.80	18.2	4656
0.3	200	6.2	14.8	0.57	0.80	14.8	3827
0.5	200	6.2	10.7	0.69	0.80	10.6	3189
0.67	200	6.2	8.6	0.74	0.80	8.6	2956

Table C-1 Pulse parameters for copper electrodeposition experiment

Duty Cycle	On-Time (ms)	DLCD (A/cm²)	PLCD (A/cm²)	N_m	N_p	Applied Current (mA)	Plating Time (s)
0.1	10	4.9	34.5	0.56	0.80	34.4	2146
0.2	10	4.9	20.8	0.68	0.80	20.7	1781
0.5	10	4.9	9.4	0.77	0.80	9.4	1575
0.67	10	4.9	7.2	0.78	0.80	7.2	1542
0.1	50	4.9	25.3	0.41	0.80	25.2	2931
0.2	50	4.9	17.5	0.57	0.80	17.5	2115
0.5	50	4.9	9.0	0.73	0.80	8.9	1654
0.67	50	4.9	7.0	0.76	0.80	7.0	1580
0.1	100	4.9	21.1	0.34	0.80	21.0	3519
0.2	100	4.9	15.7	0.51	0.80	15.6	2365
0.5	100	4.9	8.7	0.71	0.80	8.6	1713
0.67	100	4.9	6.9	0.75	0.80	6.9	1609
0.1	200	4.9	17.1	0.28	0.80	17.0	4343
0.2	200	4.9	13.6	0.44	0.80	13.6	2719
0.5	200	4.9	8.3	0.67	0.80	8.2	1796
0.67	200	4.9	6.7	0.73	0.80	6.7	1649

Table C-2 Pulse parameters for tin electrodeposition experiments

Duty Cycle	On-Time (ms)	Off-Time (ms)	Charging Time (ms)	Discharging Time (ms)	Degree of Flattening
0.1	10	90	0.23	0.48	0.0077
0.2	10	40	0.32	0.54	0.0108
0.3	10	23.3	0.42	0.58	0.0137
0.5	10	10	0.48	0.59	0.0199
0.67	10	4.9	0.52	0.66	0.0283
0.1	50	450	0.29	0.53	0.0018
0.2	50	200	0.37	0.56	0.0023
0.3	50	116.7	0.43	0.57	0.0028
0.5	50	50	0.52	0.59	0.0040
0.67	50	24.6	0.53	0.65	0.0056
0.1	100	900	0.32	0.54	0.0009
0.2	100	400	0.38	0.55	0.0012
0.3	100	233.3	0.42	0.57	0.0014
0.5	100	100	0.49	0.59	0.0020
0.67	100	49.3	0.55	0.65	0.0028
0.1	200	1800	0.37	0.56	0.0005
0.2	200	800	0.40	0.58	0.0006
0.3	200	466.7	0.44	0.56	0.0007
0.5	200	200	0.49	0.58	0.0009
0.67	200	98.5	0.61	0.65	0.0014

Table C-3 Electrical double layer parameters on Cu pulse deposition

Duty Cycle	On-Time (ms)	Off-Time (ms)	Charging Time (ms)	Discharging Time (ms)	Degree of Flattening
0.1	10	90	0.29	0.51	0.0087
0.2	10	40	0.37	0.55	0.0117
0.5	10	10	0.60	0.66	0.0189
0.67	10	4.9	0.70	0.63	0.0238
0.1	50	450	0.33	0.53	0.0020
0.2	50	200	0.43	0.57	0.0024
0.5	50	50	0.54	0.66	0.0037
0.67	50	24.6	0.55	0.63	0.0046
0.1	100	900	0.37	0.55	0.0010
0.2	100	400	0.45	0.57	0.0012
0.5	100	100	0.57	0.65	0.0018
0.67	100	49.3	0.57	0.63	0.0022
0.1	200	1800	0.42	0.57	0.0005
0.2	200	800	0.48	0.61	0.0006
0.5	200	200	0.55	0.65	0.0009
0.67	200	98.5	0.59	0.62	0.0011

Table C-4 Electrical double layer parameters on Sn pulse deposition

Appendix D: List of publications

Green T., Su X., Roy S. (2017). Pulse plating of copper from deep eutectic solvents. ECS Transactions. 77 (11) pp 1247-1253.

Su X., Green T., Roy S. Copper electrodeposition and corrosion in deep eutectic solvents using pulse current. In preparation. (Corresponding to chapter 5)

Su X., Green T., Roy S. Pulse plating of tin from deep eutectic solvents. In preparation. (Corresponding to chapter 6)

Appendix E: List of attended conferences and activities

2019 SCI Electrochemistry Postgraduate Conference. Oral presentation.

May 2019. University of Newcastle, United Kingdom.

2018 Electrochem. Oral presentation. September 2018. University of

Lancaster, United Kingdom.

2018 SCI Electrochemistry Postgraduate Conference. Oral presentation.

May 2018. University of Strathclyde, United Kingdom.

2017 ChemEngUKDay. Poster presentation. Mar 2017. University of

Birmingham. United Kingdom

2016 Research Celebration Day: Chemical and Process Engineering. Oral

presentation. December 2016. University of Strathclyde, United Kingdom

2016 Faculty of Engineering Research Presentation Day. Poster

presentation. June 2016. University of Strathclyde. United Kingdom

2016 Research Celebration Day: Chemical and Process Engineering.

Poster presentation. April 2016. University of Strathclyde, United Kingdom